AD-A144 311 ENCAPSULATED MULTIFUNCTION CORROSION INHIBITIVE PRIMER 1/4
(U) GULF SOUTH RESEARCH INST NEW ORLEANS LA
D V GUPTA ET AL. NOV 83 AFWAL-TR-83-4123
UNCLASSIFIED F33615-79-C-5061 F/G 11/3 NL

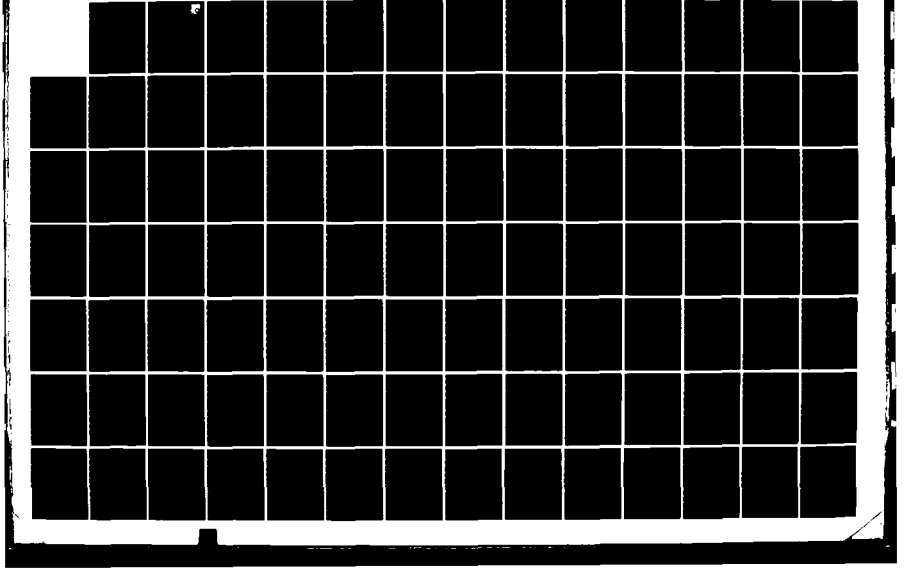

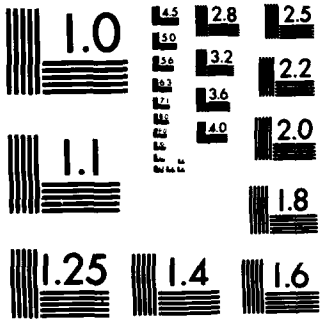

AFWAL-TR-83-4123

ENCAPSULATED MULTIFUNCTION CORROSION INHIBITIVE PRIMER

DR ISRAEL CABASSO

D. V. GUPTA

DR JOHN GRAWE

FERREL BOWEN

GULF SOUTH RESEARCH INSTITUTE
P. O. BOX 26518
NEW ORLEANS, LA 70186

NOVEMBER 1983

FINAL REPORT FOR PERIOD SEPTEMBER 1979 TO JANUARY 1983

MATERIALS LABORATORY
AIR FORCE WRIGHT AERONAUTICAL LABORATORIES
AIR FORCE SYSTEMS COMMAND
WRIGHT-PATTERSON AIR FORCE BASE, OH 45433

NOTICE

When Government drawings, specifications, or other data are used for any purpose other than in connection with a definitely related Government procurement operation, the United States Government thereby incurs no responsibility nor any obligation whatsoever; and the fact that the government may have formulated, furnished, or in any way supplied the said drawings, specifications, or other data, is not to be regarded by implication or otherwise as in any manner licensing the holder or any other person or corporation, or conveying any rights or permission to manufacture use, or sell any patented invention that may in any way be related thereto.

This report has been reviewed by the Office of Public Affairs (ASD/PA) and is releasable to the National Technical Information Service (NTIS). At NTIS, it will be available to the general public, including foreign nations.

This technical report has been reviewed and is approved for publication.

Sgd/ Halliwell

M. J. HALLIWELL
Project Engineer

B.O. McConnell

B. D. McCONNELL, Chief
Nonstructural Materials Branch
Nonmetallic Materials Division

FOR THE COMMANDER

F. D. Cherry

F. D. CHERRY, Chief
Nonmetallic Materials Division

"If your address has changed, if you wish to be removed from our mailing list, or if the addressee is no longer employed by your organization please notify AFWAL/MLBT W-PAFB, OH 45433 to help us maintain a current mailing list".

Copies of this report should not be returned unless return is required by security considerations, contractual obligations, or notice on a specific document.

UNCLASSIFIED

SECURITY CLASSIFICATION OF THIS PAGE

AD-A144311

REPORT DOCUMENTATION PAGE

1a. REPORT SECURITY CLASSIFICATION UNCLASSIFIED	1b. RESTRICTIVE MARKINGS N/A
2a. SECURITY CLASSIFICATION AUTHORITY N/A	3. DISTRIBUTION/AVAILABILITY OF REPORT Approved for public release; distribution unlimited.
2b. DECLASSIFICATION/DOWNGRADING SCHEDULE N/A	
4. PERFORMING ORGANIZATION REPORT NUMBER(S) AFWAL-TR-83-4123	5. MONITORING ORGANIZATION REPORT NUMBER(S) Same as Block 4.
6a. NAME OF PERFORMING ORGANIZATION Gulf South Research Institute 6b. OFFICE SYMBOL (If applicable) P.O. Box 26518, New Orleans, LA 70186	7a. NAME OF MONITORING ORGANIZATION Materials Laboratory, AF Wright Aeronautical Laboratories, Air Force Systems Command
6c. ADDRESS (City, State and ZIP Code) Same as Block 6a.	7b. ADDRESS (City, State and ZIP Code) AFWAL/MLBT Wright-Patterson AFB, OH 45433
8a. NAME OF FUNDING/SPONSORING ORGANIZATION Same as Block 7b. 8b. OFFICE SYMBOL (If applicable)	9. PROCUREMENT INSTRUMENT IDENTIFICATION NUMBER F33615-79-C-5061
8c. ADDRESS (City, State and ZIP Code)	10. SOURCE OF FUNDING NOS. PROGRAM ELEMENT NO. 62102F; PROJECT NO. 2422; TASK NO. 02; WORK UNIT NO. 03
11. TITLE (Include Security Classification) Encapsulated Multi-functional Corrosion Inhibitive Primer	
12. PERSONAL AUTHOR(S) Drs Israel Cabasso, John Grawe, Messrs J. K. Smith, D. V. S. Gupta, H. Ferrel Bowen	
13a. TYPE OF REPORT Final 13b. TIME COVERED FROM 15Sep79 TO 15Jan83	14. DATE OF REPORT (Yr., Mo., Day) November 1983 15. PAGE COUNT 336
16. SUPPLEMENTARY NOTATION	
17. COSATI CODES FIELD / GROUP / SUB. GR.	18. SUBJECT TERMS (Continue on reverse if necessary and identify by block number) inhibitor; corrosion, coating; capsules; microcapsules; water soluble; aluminum; steel, microencapsulation controlled release; nylon; polyurea; epoxy.

19. ABSTRACT (Continue on reverse if necessary and identify by block number)

Air Force Contract F33615-79-C-5061 investigates the possibility of using highly water soluble corrosion inhibitors as an aircraft primer as a replacement primer for hexavalent chromium primers which have been under attack for toxicity. The difficult problem of coating blistering which has made water soluble inhibition little used in primers is approached with the use of microencapsulation of the inhibitors and control release polymers to obtain controlled release. Additionally direct incorporation in the primer matrix with controlled pigment volume concentration to control internal pressures and other methods are shown. Steel inhibition showed promise as well as release polymers for corrosion protection. Some state-of-the-art corrosion pigments showed promise for aluminum and steel but none of the inhibitors performed as well as chromate inhibitors currently being used on Air Force aircraft.

20. DISTRIBUTION/AVAILABILITY OF ABSTRACT UNCLASSIFIED/UNLIMITED ☒ SAME AS RPT. ☐ DTIC USERS ☐	21 ABSTRACT SECURITY CLASSIFICATION UNCLASSIFIED
22a. NAME OF RESPONSIBLE INDIVIDUAL MICHAEL HALLIWELL	22b TELEPHONE NUMBER (Include Area Code) (513)255-7377 22c OFFICE SYMBOL AFWAL/MLBT

DD FORM 1473, 83 APR EDITION OF 1 JAN 73 IS OBSOLETE

UNCLASSIFIED

SECURITY CLASSIFICATION OF THIS PAGE

PREFACE

This report is submitted in fulfillment of contract No. F33615-79-C-5061. The work was performed by Gulf South Research Institute as GSRI No. 325-946-11. The institute appreciates the contributions of principal investigators, Israel Cabasso, D.V. Gupta, John Grawe and J.K. Smith. Ferrel Bowen, Bill Eggert, Brenda Zimny and Joe Smith provided the day-to-day support that produced the results reported. Ferrel Bowen's contribution in accumulation and analysis of data for the final report is especially appreciated. Credit and acknowledgment are referenced, as appropriate throughout the report for information gathered from other sources.

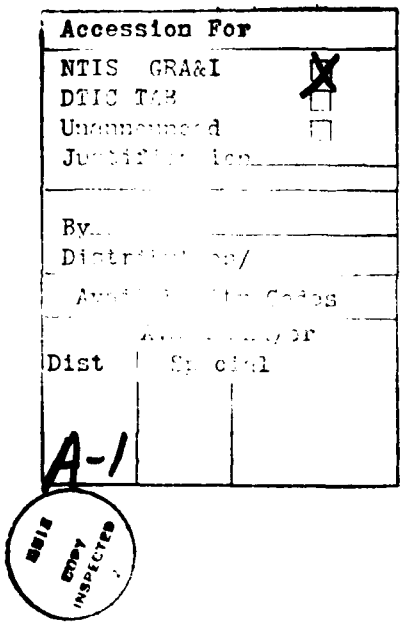

CONTENTS

LIST OF TABLES

LIST OF ILLUSTRATIONS

I. INTRODUCTION

A. Background

The corrosion of military aircraft is a serious and costly problem for the Air Force, and can pose a hazard not only from the standpoint of material failure of metallic structural elements, but also to the safety of personnel involved. Even though the metallic structures are covered with protective surface coatings, corrosion may still occur from a myriad of causes. Improperly cleaned and prepared metal surfaces, film defects during application, abrasion or other mechanical damage, environmental stress, weathering, and aging of the protective coating may all lead to corrosive attack of metal structures. When corrosion occurs, it is not uncommon for several of these mechanisms to occur simultaneously, and on different time scales. Therefore, the requirements that a surface coating must meet to insure substrate integrity under field conditions are very stringent. Chromate corrosion inhibitors are used extensively with great success, but have the disadvantage of being toxic.

The recent EPA/OSHA concern of the toxicity of chromate salts has caused the initiation of this investigation of replacement of hexavalent chromates currently used in the primer formulation applied to military aircraft, meeting MIL-P-23377D. Preferably, the new pigment would be an advanced, multifunctional, corrosion-inhibitive combination capable of providing an equivalent range of protective responses as the chromate inhibitor. Gulf South Research Institute (GSRI) has studied several concepts for aircraft primer systems for improved corrosion resistance. These studies focused on techniques for the incorporation of multifunctional, nontoxic inhibitors with extended protection by limiting rates of solution thus providing a reservoir of protection while limiting undesirable blistering of the coating.

The primary method of corrosion protection for aircraft surfaces employed by the Air Force is an epoxy-polyamide primer (MIL-P-23377D) containing $SrCrO_4$ as the corrosion inhibitive pigment and topcoated with an aliphatic polyurethane (MIL-C-83286B). This coating system provides only limited protection against corrosion resulting from film defects, mechanical damage, and localized crack growth. A possible solution would be to replace

the $SrCrO_4$ with a combination of multifunctional inhibitors for both anodic and cathodic processes, in the hope that increased corrosion protection could be achieved.

Furthermore, if these inhibitors could somehow be entrapped or encapsulated within the primer, then the release of inhibitor action would occur only as required, in a manner controlled by the formulator. These multifunctional corrosion inhibitors must be incorporated into the primer so that corrosion protection is provided for the lifetime of the primer-topcoat system. The target period for functional corrosion inhibition is currently five years.

Since the chromate-containing inhibitive pigment is now suspected of being a toxicologically active agent, there exist health hazards in all work phases with this material. Therefore, several promising nontoxic, multifunctional inhibitors were developed and studied by the Air Force, specifically for protection of high strength aluminum and steel.

One formulation of interest to the Air Force is the rinse inhibitor system developed for use at the automated rinse facility at MacDill AFB. This material (termed AFIF, for Air Force Inhibitor Formulation) is a nontoxic, multifunctional blend of inhibitors which has provided good protection against crack growth enhancement under stress corrosion and corrosion fatigue conditions. This inhibitor formulation was evaluated in the research effort performed by GSRI.

B. General Approach and Rationale

The objective of this research program was to perform a pilot study on the development of a paint-protective system containing a nontoxic, multifunctional corrosion inhibitor, providing corrosion protection equivalent to or greater than the chromate-containing system currently in use. A brief overview of the general technical approach and rationale applied to the solution of this problem is given in this section. In-depth discussions of each stage are presented later in the report.

Initially, a state-of-the-art survey of nonchromate corrosion inhibitors was performed to access the current literature and to avoid duplication of research already in published form. Also, any current, novel strategies for use of these corrosion inhibitors were sought.

Then, evaluation of the various corrosion inhibitor systems was performed via potentiodynamic anodic polarization studies on a Princeton 350 Corrosion Measurement System under different conditions of concentration and pH. This procedure was applied in order to select the best corrosion inhibitor system meeting our requirements.

Once the candidate corrosion inhibitor was identified, three technical approaches were implemented. Each approach had the aim of incorporating the corrosion inhibitor within the primer matrix. Each of these methods represented a different approach for delivering the corrosion inhibitor in an active state, and each method displayed a set of technical problems which were peculiar to the methods and concepts involved.

The first technical approach was the microencapsulation of the corrosion inhibitor system by means of interfacial polymerization. An aqueous solution of the corrosion inhibitor, a surfactant, and one of the reactant monomers was emulsified in an immiscible organic phase, containing an additional surfactant. A water-in-oil emulsion was thus formed. To the continuous phase of this emulsified system was added the other reactant monomer. The polymerization reaction occurs at the interface between the discrete H_2O phase and the continuous organic phase, depositing the polymer product around each of the water drops. Thus, the corrosion inhibitor was effectively encapsulated within the surrounding polymer wall. The inhibitor system used in the majority of these studies was the basic AFIF mixture. Initially, a nylon 6,10 polymer membrane was used in microencapsulation, although the polymer of interest later in the study was a polyurea formed from toluene-2,4-diisocyanate and hexane-1,6-diamine. The average diameter of these microcapsules was approximately 6 microns.

The second technical approach involved the attachment of corrosion inhibitors as pendant groups along a polymeric backbone. In principle, these modified polymers would then be incorporated into the primer matrix prior to application. Release of the inhibitor group would occur by hydrolysis, as water penetrated into the primer matrix. The corrosion inhibitors used in this part of the study were the borate and cinnamate anions. The polymers used for the backbone in pendant group attachment were polyvinyl alcohol and methyl cellulose.

The third technical approach involved the direct physical entrapment of the corrosion inhibitor within the primer matrix. The material was added to

the polyamide component of the primer system and jar milled to the appropriate fineness of grind. The primers formulated with the corrosion inhibitor were then sprayed out on metal test panels and tested by the standard methods for salt spray, 100% relative humidity, and wet (tape) adhesion. The primer composition was optimized to provide the best possible response to the battery of test procedures.

II. LITERATURE SURVEY OF CORROSION INHIBITORS

This research project was a pilot study for development of a nontoxic, corrosion-inhibitive, epoxy-polyamide primer suitable for use on military aircraft, providing approximately five years of protection against corrosion. The currently used corrosion inhibitor is $SrCrO_4$, which is toxic to both personnel and the environment. Therefore, the need to identify and evaluate novel, nontoxic, corrosion inhibitors as potential chromate replacements is, and remains, paramount.

This section deals with the general classification of corrosion inhibitors and the requirements for their effective use, as a prelude to the literature survey for these materials.

A. General Comments on Organic Coatings

The primary functions of an organic coating are protective and decorative, although the protective aspect is the main concern with military aircraft primers. Decorative functions are usually more prevalent for coatings systems used in commercial applications, although the two functions are never entirely separated in any application. Perhaps the main feature of an organic coating is that it serves as a type of membrane, or barrier, interposed between the metal substrate and the environment. However, it is not impervious to the environment, since water, oxygen, and many ionic species, such as chloride anion, may penetrate through the coating matrix to the metal surface (1-4). The driving forces in these cases may be simply diffusion or those due to osmotic pressure gradients. It is inevitable that any coating will be permeated by such chemical species, given enough time and a source of the penetrants. Even coating systems designed to exclude such deleterious molecules will eventually fail through mechanical damage, weathering, and aging. Thus, the art and science of paint formulation reside in developing a coating which forestalls this eventual failure, through the judicious choice of paint raw materials, solvent vehicles, and the use of scientific principles and techniques in every phase of the endeavor.

There are several general requirements that a paint should meet if it is to provide protection against corrosion (5). It should form an effective

barrier to vapor transmission and have a low permeability to small molecules. This is best achieved through the use of multiple coating applications, which seal off pores and other film defects. Furthermore, the diffusion path within the paint can be greatly increased through the addition of pigments and extenders. Pigment geometry is also a consideration; flakes of such particles which orient parallel to the metal surface are especially effective for this purpose. The pigment chosen for the prime coat should also be an effective corrosion inhibitor, in addition to its function of hiding the metal surface. The requirement for pigment water solubility is very specific; the pigment must be soluble enough to supply the minimum effective concentration of inhibitor at the metal surface, but not so soluble that it will leach out of the coating.

It must also be mentioned that the surface treatment of the metal prior to coating application, as well as the film thickness, are as important to the performance of the system as the paint formulation.

B. Classification of Corrosion Inhibitors

In a typical corrosion process there are two coupled electrochemical reactions occurring simultaneously: the anodic and cathodic reactions. The anodic reaction is the metal oxidation reaction, which involves the loss of electrons (e^-) by the metal (M°) to form the metal ions (M^{n+}), with subsequent increase in its oxidation state,

$$M^\circ \rightarrow M^{n+} + ne^-.$$

The cathodic reaction can be any one of many reactions and has the net result of accepting the electrons made available in the anodic reaction. The two most common reactions of this type are:

(1) reduction of hydrogen ions (H^+) in the electrolyte to form hydrogen gas (H_2):

$$2H^+ + 2e^- \rightarrow H_2;$$ and

(2) reduction of oxygen in the electrolyte to form hydroxyl ions (OH^-):

$$O_2 + 2H_2O + 4e^- \rightarrow 4OH^-.$$

The corrosion process takes place when at least one anodic and one cathodic reaction occur simultaneously. For example, rusting of steel involves the oxidation of iron to ferrous and ferric ions which react with available oxygen or hydroxide to form ferrous and ferric oxides or hydroxides. Corrosion of aluminum alloys occurs by a similar mechanism which involves oxidation of Al and the formation of aluminum oxide or hydroxide as the corrosion product. It should be emphasized that these corrosion products when first formed are thin, amorphous, physico-chemical barriers to further corrosion. They are called "passive layers" at this stage. However, their continued growth into crystalline, permeable layers renders them ineffective as anti-corrosion barriers (5,6).

The control of corrosion can be achieved by modifying the anodic or cathodic reaction, or both (6). Of the methods available for corrosion control, the use of inorganic and organic substances as inhibitor additives is widespread. Inhibitors which are effective in controlling both the cathodic and anodic reactions of the metal are called multifunctional inhibitors.

Corrosion inhibitors can be divided into three groups based on the general mechanism of action: (1) anodic corrosion inhibitors, (2) cathodic corrosion inhibitors, and (3) chelating agents.

1. Anodic Corrosion Inhibitors

The inhibitors which retard the anodic reaction are termed anodic inhibitors. These materials are generally oxidizing agents and promote passivation of the metal surface through the formation of metal oxide layers. They directly enhance anodic passivation through shielding part of the anodic surface by (a) adsorption of the oxidizing agent by the metal surface or (b) chemical oxidation of the metal surface. Examples of anodic inhibitors are phosphates, chromates, polyphosphates, alkalis, silicates, borates, benzoates, cinnamates, nitrates, nitrites, sulfates, perrhenates, permanganates, tungstates, and pertechnetates (1,5,6). In addition to the oxidizing anions listed above, some cationic species may also act as passivators, such as Ca^{2+}, Fe^{3+}, and Ce^{4+} (7). It should be noted that some of these oxidizing inhibitors (e.g. borate) function as such only in the presence of oxygen (5,6).

2. Cathodic Corrosion Inhibitors

The cathodic corrosion inhibitors retard corrosion by accelerating the cathodic process, thus shifting the overall potential of the system to more positive potentials corresponding to the onset of passivity (6-8). This shift is produced by increasing the effectiveness of cathodic depolarization. Higher valence metallic cations may be considered inhibitors of this type; in acidic media, many oxidizing ions of the type MeO_4^{n-} and nitrates can also be considered as such inhibitors.

There is an intermediate class of inhibitors which inhibit the anodic process as well as enhance the cathodic process. It is also possible that a given anodic inhibitor, depending on conditions, can function by different mechanisms. For example, in near-neutral media, chromates do not increase the effectiveness of the cathodic process, and their strong inhibiting effect for iron/steel is completely determined by direct anodic inhibition (9). The same chromates in acid media are good cathodic depolarizers and must be considered as inhibitors which retard the anodic process indirectly by accelerating the cathodic process.

3. Chelating Inhibitors

A category of corrosion inhibitors currently attracting considerable attention are the chelating agents. Chelating agents have been studied for possible use as corrosion inhibitors for steel, zinc, and aluminum in various environments (10-14).

The chelating agents of interest are organic molecules with at least two polar functional groups capable of binding to a metal cation. The functional groups may be either Lewis bases, such as $-NH_2$, or Lewis acids, for example, -COOH.

Protection of the metal surface by chelation occurs through two main mechanisms. In the first type, the chelate either interacts with metal ions which are locked into the metal lattice, or interacts with metal ions in the surface oxide film. In the second type, the surface metal ions dissolve and immediately react with the chelating agent at the metal interface, forming a high molecular weight, low solubility complex which deposits as a barrier film on the surface.

Examples of chelating inhibitors are sarcosine-type compounds, alizarin, α-mercaptoacetic acid compounds, and 8-hydroxyquinoline.

C. Novel Nontoxic Inhibitors

This section is a description of a wide spectrum of chromate-free nontoxic inhibitor formulations developed since 1975.

1. Phosphonocarboxylic Acid Compositions

One method for preventing corrosion consists of using an inhibition system based on phosphonocarboxylic acids (PCA) or their salts and other synergistically active substances (15). Polyphosphates inhibit corrosion by oxygen scavenging. But these are not stable over wide temperature ranges and are hydrolyzed relatively easily into orthophosphates; thus, their corrosion-inhibiting effect is impaired. The inhibitory action can be enhanced by adding to the PCA about 5-500 percent by weight of the phosphonocarboxylic acid, a synergistic agent from the group consisting of a benzimidazole derivative, polyacrylamide, polyethyleneimine, polyvinylpyrrolidone, and lignin sulfonate. The effect of the corrosion-preventing system can be further enhanced by addition of phosphonic acid and phosphates. It was shown that a system, containing 40 ppm by weight phosphonobutane-1,2,4-tricarboxylic acid, 15 ppm H_3PO_4 and 1 ppm 2-(ε-aminopentyl)-benzimidazole, reduced the corrosion rate of St 35 carbon steel from 21 g/m^2/day at room temperature to 0.4 g/m^2/day.

A similar formulation (16) uses a compound selected from a group of

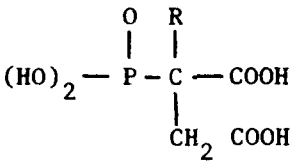

or a corresponding water-soluble salt. R may be hydrogen, C_{1-4} alkyl, or alkenyl; phenyl; C_{3-6} cycloalkyl; benzyl; phenethyl or

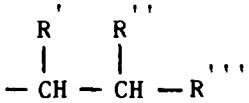

where R' is hydrogen or C_{1-4} alkyl group or carboxyl;
R'' is hydrogen or methyl group;
R''' is carboxyl group.

These phosphonocarboxylic acids are distinguished by their low phosphorous content, resistance to hydrolysis, and thermal stability compared with conventional polyphosphates. The effectiveness of these compounds can be improved by the addition of phosphonic acid or phosphates which have a distinct synergistic effect.

A similar inhibitive effect was found using 1-phosphonopropane-1,2,3-tricarboxylic acid; 2,3-diphosphonopropionic acid; 2 methyl-3-phosphonopropionic acid; 3-phosphonobutanoic acid; and 2-phosphonohexanoic acid (17).

2. Polyphosphate-phosphonic-polyacrylic Acid Compositions

A corrosion inhibition system consisting of a polyphosphate, a phosphonic acid or one of its salts, and a polymer of acrylic or methacrylic acid has been shown to be capable of operating at a wide variety of conditions including high temperature and high pH. A typical 25 ppm composition, consisting of 20 percent sodium hexametaphosphate, 8 percent of sodium salt of amino-tri(methylene phosphonic acid), and 2 percent polyacrylic acid, inhibits corrosion of SAE 1010 steel by 98 percent (18).

A similar composition of a phosphate and phosphonate along with a homopolymer of maleic acid or maleic anhydride is effective at high pH ranges. A 20 ppm composition of 15 percent sodium hexametaphosphate, 4 percent amino(trimethylene phosphonic acid), and 1 percent hydrolyzed polymaleic anhydride inhibits the corrosion of 1010 steel by 90 percent at room temperature and pH 8.5 - 9.0 (19).

3. Phosphonomethylamino Carboxylates

The use of phosphonomethylamino carboxylates (PMAC) with enhanced corrosion inhibition by the addition of heavy metal ions of zinc or chromates was found effective in cooling systems. However, a recent formulation utilized certain phosphonomethylamino carboxylates either alone or in combination to inhibit corrosion of metal surfaces (20). This system inhibits corrosion of ferrous metals including iron and steel, nonferrous metals including copper and its alloys, aluminum and its alloys, and brass.

The PMAC formulation corresponds to the following:

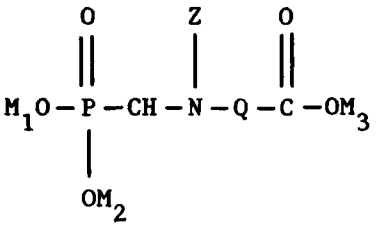

where M_1, M_2, M_3: selected from the group consisting of hydrogen, metal ions, ammonium ions or alkyl ammonium ions

Z: C_{1-4} alkanol;
$-CH_2PO_3M_1M_2$;
C_{1-4} alkyl carboxylic acid;
C_{1-10} alkaminomethylene phosphonic acid;

Q: C_{3-15} alkylene;
C_{3-15} alkenylene;
alkaryl radical.

The PMAC corrosion inhibitors were effective in both acidic and basic corrosive media. The minimum concentration for effective inhibition for ferrous metals is 1-3 ppm and concentrations of 10-150 ppm were preferable for all ferrous and nonferrous metals. The corrosion rate of 1010 AISI steel was reduced from 45 mpy to less than 1 mpy in water at pH 7.0 and 35°C by the use of 150 ppm of PMAC where M_1, M_2, M_3 are hydrogen ions, and Q and Z are $(CH_2)_3$ and $(CH_2PO_3H_2)$, respectively.

4. Gluconate - Polyphosphate Mixtures

The use of a combination of water-soluble gluconate and water-soluble polyphosphate inhibitors results in a synergistic improvement of corrosion inhibition (21). Gluconate prevents the conversion of polyphosphates into orthophosphates. The use of 100 ppm of a mixture of sodium hexametaphosphate and sodium gluconate in the ratio 70:30 reduces the corrosion rate of 1020 steel specimens in water at 120°F to 2 percent of the value without inhibitors present.

5. Phenolic Resin - Polyphosphate Compositions

Linear, water-soluble phenol-aldehyde resinous condensation products have been shown to be good candidates for nonchromate, nontoxic corrosion inhibitors for steel and other ferrous metals. However, at the concentration required for effective corrosion inhibition, water-soluble phenolic resins are relatively expensive. The addition of inorganic metal salts permits inhibition at lower resin concentrations. Another class of inhibitors is the polyphosphates, which include inorganic polyphosphates and polyfunctional acid phosphate esters of polyols or phosphorylated polyols (22).

6. Silicate - Nitrate Compositions

The inhibitor formulation containing a mixture of water-soluble metasilicate and water-soluble nitrate with a total anionic concentration of greater than 1,000 ppm and a ratio of $(SiO_3^{2-})/[(SiO_3^{2-}) + (NO_3^-)]$ between 0.15 and 0.20 displays a pronounced synergistic effect and is a good formulation for inhibition against pitting and general corrosion of aluminum (5,6).

7. Carboxylated Benzotriazoles

The use of triazoles, especially benzotriazole, as an anticorrosive agent is common. The use of carboxylated benzotriazoles reduces the effective concentrations required. The use of 500 ppm of the substance yields a corrosion inhibition efficiency of 91 percent for steel and 80 percent for aluminum (6).

8. Orthophosphate - Polyphosphate Combinations

The synergistic effect of orthophosphate buffers like phosphoric acid or sodium dihydrogen orthophosphate greatly reduces the concentration of a polyphosphate such as hexametaphosphate required for use as a corrosion inhibitor (23).

9. Sulfonium Compounds

Sulfonium compounds have been shown to be useful corrosion inhibitors at low pH and at concentrations of 2-4 m mol/l for steel (24-26). Typical compounds belonging to this category are nitrobenzyldimethylsulfon-

ium chloride, nitrobenzyl-dodecylmethyl sulfonium chloride, and fluorobenzyldodecylmethyl sulfonium chloride. These compounds yield 70-99 percent protection against corrosion of steel.

10. Nitrite - Phosphoric/Boric Esters

Phosphoric or boric esters have a synergistic effect over the inhibition behavior of sodium nitrite (27). Several mono-, di-, and triesters of poly-oxyethylene nonylphenyl phosphate and polyoxethylene-bis-glycerol borate, when added to $NaNO_2$ as 10 percent additives, inhibit corrosion of steel at a concentration of 0.5 percent at high pH and high Cl^- concentrations. The use of $Ca(NO_2)_2$, $NaNO_2$, and $Ca(NO_3)_2$ in cement to inhibit corrosion of steel is well known.

11. Molybdate Compositions

Several grades of zinc molybdate compositions as sodium, potassium, and ammonium zinc molybdates are commercially available under various trade names. These nontoxic corrosion inhibitors are comparable in cost and effectiveness to conventional zinc yellow (potassium zinc chromate) (28-31).

12. Multicomponent Inhibitor Formulations

A composition based on polyvinylbutyral resin, organo functional silane, borate compounds, polyphosphate compounds, and phosphonic acid, when used as a wash primer, protected steel and aluminum from corrosion in outdoor exposure tests up to six months (32).

A corrosion inhibitor formulation for use in a primer utilizing zinc borate ($4ZnO \cdot 6B_2O_5 \cdot 7H_2O$) and barium metaborate is commercially available from PPG Industries (33).

13. Calcium-silico-zirconate Inhibitor

A new type of corrosion inhibitive primer utilizes calcium-silico-zirconate inhibitor in concentrations ranging from 0.1 to 65 percent by weight. A mixture of zircon and limestone is calcined at a temperature of 1500°C and the calcined mixture is pelletized, resulting in calcium-silico-zirconate inhibitor of formula $X_nCaO \cdot SiO_2 \cdot ZrO_2$. When this inhibitor was used in a marine primer coating, its inhibitive effect was far superior to the conventional zinc yellow pigment (potassium zinc chromate) (34).

14. Formulation Based on Nitrite, Benzoate, Amine, and Urea

Several types of water-soluble formulations based on alkali metal nitrites, ammonium benzoates, alkylalkanolamine, and nitrogenous base materials were tested for passivation of ferrous metals (35). The following compositions were found effective on these metals:

1. urea 25%, ammonium benzoate 25%, sodium nitrite 25%, and aminoethylethanolamine 25%.
2. urea 30%, sodium nitrite 30%, ammonium benzoate 15%, and aminoethylethanolamine 25%.
3. guanidine 25%, sodium nitrite 25%, ammonium benzoate 25%, and aminoethylethanolamine 25%.
4. urea 25%, sodium nitrite 25%, ammonium benzoate 25%, and dimethyl-aminopropanolamine 25%.
5. aminomethylethanolamine 25%, urea 30%, sodium nitrite 30%, and ammonium benzoate 15%.
6. aminoethylethanolamine 15%, sodium nitrite 35%, urea 35%, and ammonium benzoate 15%.

15. Nitrate, Phosphate, Benzotriazole, Borate, and Silicate Compositions

Several experimental multicomponent, water-soluble, nontoxic compositions were tested for passivating steel and aluminum for use in solar heating and cooling systems and the following compositions (concentrations in decigrams/liter; MBT - mercaptobenzothiazole, NaMBT - 50 percent solution of mercaptobenzothiazole) were found to be effective (36-39):

1. 1.0 $NaNO_3$, 2.0 $Na_3PO_4 \cdot 12H_2O$, 2.5 NaMBT, 3.0 $Na_2B_4O_7$, 1.0 Na_2 $SIO_3 \cdot 9H_2O$, 1.0 NaOH (General Motors formulation).
2. Same as #1, without NaOH.
3. 1.4 Na_2HPO_4, 2.4 MBT, 6.2 $Na_2B_4O_7$ (Federal Specification 0-1-490A for cooling system inhibitors).
4. 20.0 sodium benzoate based Mobay Product OC2002 (proprietary formulation).
5. 30.0 Nalco 2755 (proprietary formulation).
6. Nalco 39L (proprietary formulation).
7. 2 $NaNO_3$, 2 $NaNO_2$, 2 $Na_3PO_4 \cdot H_2O$, 4 $Na_2SiO_3 \cdot 9H_2O$.
8. 1 $NaNO_3$, 1 $Na_3PO_4 \cdot 12H_2O$, 1.5 $Na_2SiO_5 \cdot 9H_2O$, 1.5 NaMBT.
9. 2 $NaNO_3$, 2 $Na_3PO_4 \cdot 12H_2O$, 3 $Na_2SiO_3 \cdot 9H_2O$, 1 NaMBT.

10. 2 $NaNO_3$, 1 $NaNO_2$, 2 $Na_3PO_4 \cdot 12H_2O$, 3 $Na_2SiO_3 \cdot 9H_2O$, 2 NaMBT.
11. 2 $NaNO_3$, 1 $NaNO_2$, 0.5 H_3PO_4, 3 $Na_2SiO_3 \cdot 9H_2O$, 2 NaMBT.
12. 2 $NaNO_3$, 2 $Na_3PO_4 \cdot 12H_2O$, 2 $Na_2B_4O_7$, 2 $Na_2SiO_3 \cdot 9H_2O$, 2 NaMBT.
13. 2 $NaNO_3$, 1 $NaNO_2$, 2 $Na_3PO_4 \cdot 12H_2O$, 1 $Na_2B_4O_7$, 2 $Na_2SiO_3 \cdot 9H_2O$, 2 NaMBT.

16. Piperidine, Piperazine

In addition to the above categories, hydrazine hydrate, piperidine, and piperazine were also found to be effective in inhibiting corrosion of high strength alloys (36,37,39).

III. EVALUATION OF CORROSION INHIBITORS

A. General Comments

In this section, the results of the experimental evaluation of corrosion inhibitors for steel 4340 and aluminum 2024 alloys are presented. For each alloy-inhibitor combination, a potentiodynamic anodic polarization experiment was obtained, along with a pH measurement of the inhibitor solution. Equilibrium (open circuit) potential vs time plots were also recorded for selected inhibitors. Before the presentation and analysis of the experimental results in Part C, a description of the potentiodynamic anodic polarization method will be given in B, and the general interpretative scheme outlined.

B. Potentiodynamic Polarization Evaluation of Inhibitors (5,6)

When a metal or alloy is in contact with a corrosive environment, the sample functions as both anode and cathode, since oxidative and reductive processes will be occurring simultaneously on the surface . Under these conditions, where there is no net current flow through the cell (i.e., open circuit conditions), the metal assumes a mixed potential value which is intermediate between that of the anodic and cathodic reactions; this is known as the corrosion potential, E_{corr}. Since there is no net current flow at this potential, the rates of the anodic and cathodic processes must be equal. As mentioned previously, the anodic process usually involves metal oxidation followed by ionic dissolution, while the cathodic process involves reduction of H^+ or O_2 in the solvent to form H_2 or OH^-, respectively. Even though the sample is at the mixed potential value of E_{corr}, the anodic process represents the primary mechanism in the corrosion of metal. From considerations basic to electrochemical phenomena and Faraday's Law, the rate of the anodic process may be equated with the rate of the corrosion process;

$$\text{corrosion rate} \propto I_{corr} \text{ (at } E_{corr}),$$

where I is the current density.

Thus, the study of the corrosion process may be identified mainly with the study of the anodic process at the surface of the metal. However, to study the corrosion process of a metal under open circuit conditions is extremely difficult (if not impossible), due to simultaneous occurrence of the cathodic process, and the polarizing effects on the cell caused by attempts to make electrochemical measurements.

To study the corrosion process in such a complex situation, the potentiodynamic polarization method was developed. In this method, an external voltage source is employed to drive the potential of the metal away from E_{corr} in both anodic and cathodic directions. The extent of the departure of the metal's potential from E_{corr} is defined as the polarization. Depending upon the direction (+/-) and extent of this polarization, either the anodic or cathodic process may be enhanced in magnitude, with simultaneous suppression of the other. This allows the study of either the anodic or cathodic process as a separate phenomenon. Due to the different natures of the anodic and cathodic reactions, not all of the variables which affect one process will necessarily affect the other. The potentiodynamic polarization method facilitates study of such factors which affect only one of the cell reactions.

At potentials more positive than E_{corr}, the anodic current is increased and the cathodic current is suppressed (anodic polarization). At potentials more negative than E_{corr}, the cathodic current is increased and the anodic current is suppressed (cathodic polarization).

The effects of environmental changes such as temperature, pH, and corrosion inhibitor type and concentration may be studied on a comparative basis, and inferences drawn concerning the corrosion behavior of the metal in that environment. Not only may a given metal be studied in different environments, but a series of metals may be examined in a specific environment of interest.

An idealized potentiodynamic anodic polarization diagram is given in Figure 1. Region A represents the active region of the metal response. Oxidation of the metal gives rise to metal ions in the solvent medium ($M \rightarrow M^{+} + e^{-}$). The oxidation of the metal increases greatly in this potential range, as indicated by the increase in the current density. The proportionality relationship between measured current and the concentration of conducting metal ions in solution accounts for this observed behavior.

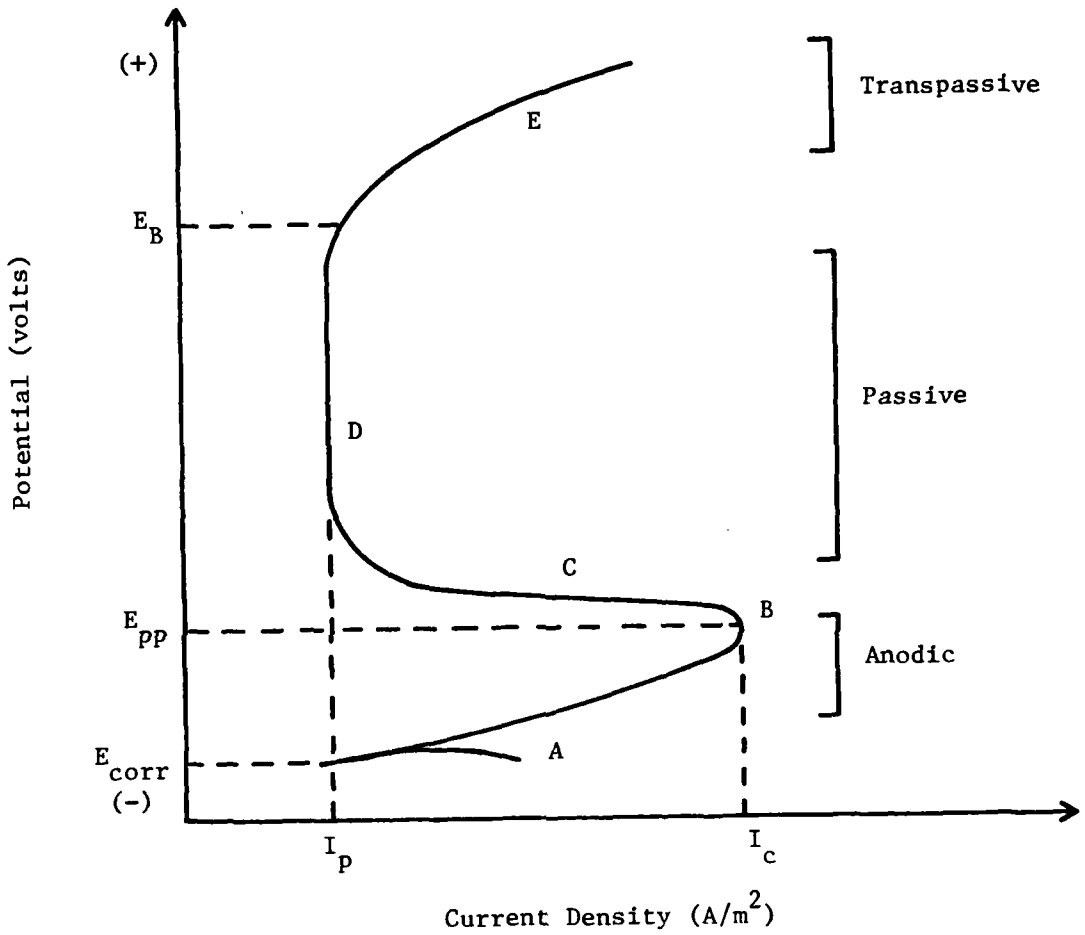

Figure 1. An idealized potentiodynamic anodic polarization plot.

Point B corresponds to initial formation of the passive oxide layer over the metal surface. The potential at this point is the primary passive potential E_{pp}, and I_c is the critical anodic current density. The passive film builds up rapidly as the potential scan enters into region C; passivation is well underway here, with significant changes in the response curve.

Region D corresponds to passivation of the metal surface, characterized by the passive current density I_p over a specified potential range. The rate of metal oxidation is at its lowest value here; the metal oxidation and dissolution phenomena occur less readily here than in any other region, due to formation of the protective oxide.

Region E is the transpassive zone, where the passive layer breaks down; E_B is called the breakdown potential. Higher valence oxidation states of the metal ($M \rightarrow M^{+2} + 2e^-$) tend to occur in this region.

In Figure 1, the corrosion potential E_{corr} is shown. By definition, the rates of the anodic and cathodic processes are equal at this point. This implies that E_{corr} is a point of intersection between the anodic and cathodic polarization curves, even though the cathodic process is suppressed during potentiodynamic anodic polarization, and otherwise not observed.

Figure 2 shows some possible types of cathodic response for these systems. Here A represents the anodic polarization curve, and C_1, C_2, C_3, C_4, C_5 are the corresponding cathodic polarization curves for either (1) increasing inhibitor concentration in solution for a given inhibitor compound, or (2) the cathodic responses for a series of different inhibitor compounds. The points of intersection with the anodic polarization curve show how E_{corr} may vary over the potential range of the experiment. Such shifts in the E_{corr} value are an important feature when evaluating corrosion inhibitor performance.

The analysis of anodic and cathodic polarization curves, along with other related types of experiments, is complex. Thus, to make predictions of long term corrosion behavior based on such short term, accelerated testing procedures as these may not be reliable. However, comparative studies may be made on adding corrosion inhibitors into the metal/solution environment, and qualitative and quantitative changes in the anodic polarization response may be observed. First the anodic polarization curve of the blank

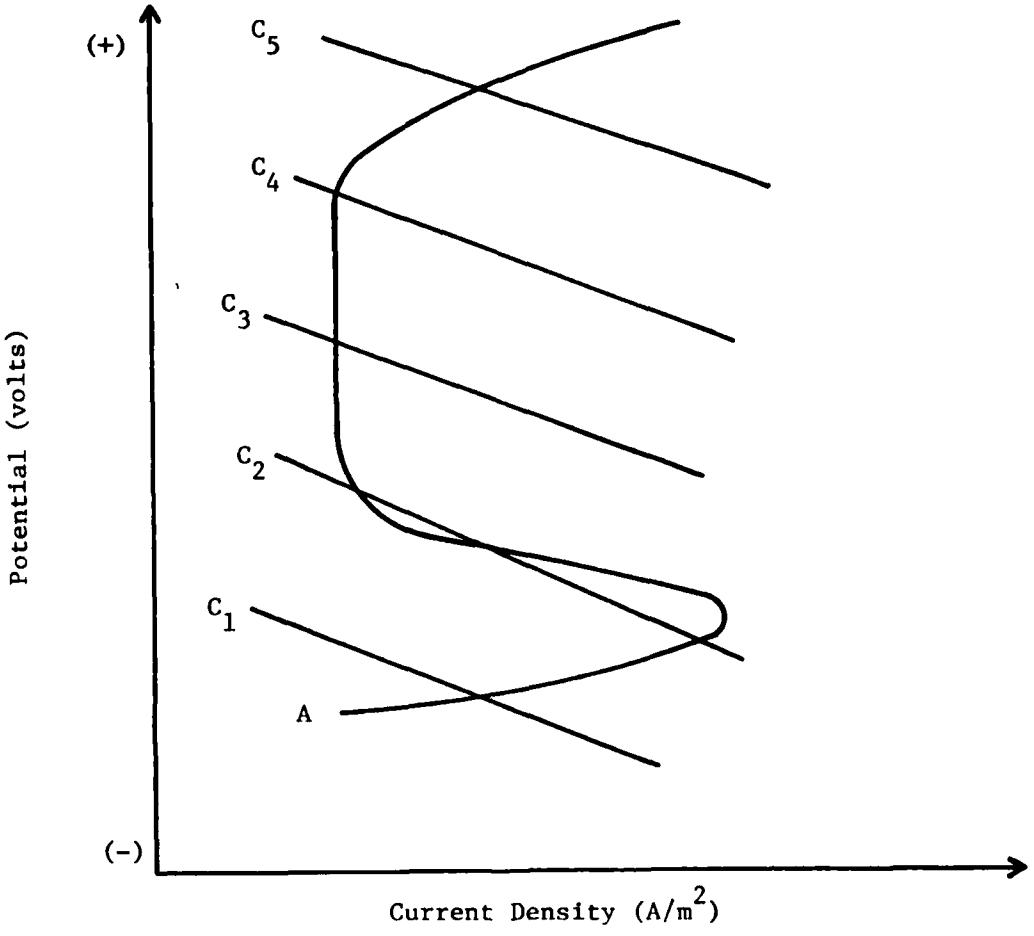

Figure 2. Relationship of anodic polarization response (A) and cathodic curves (C_1, C_2, C_3, C_4, C_5) for inhibitor type (or concentration).

is obtained. Then, with the corrosion inhibitor added, the anodic polarization curve for the new environment is run, preferably displayed on the same scale and graph as the control run. A number of features from such experiments are of interest: (1) presence or absence of passivation region I_p, and its potential range, (2) shifts of E_{pp}, (3) values of I_c, (4) shifts of E_{corr}, and (5) regions of increased or decreased metal oxidation as a function of potential. The availability of open circuit potential values for these metal-environment systems helps determine the actual in-service response of these systems with respect to corrosion and inhibition phenomena.

Thus, the potentiodynamic anodic polarization experiment provides a quick and relatively easy method for the initial screening of a series of corrosion inhibitors, insofar as such a relative assessment of corrosion inhibitive effects is valid for long term use in complex corrosive environments.

C. Analysis of Corrosion Inhibitors

Aluminum alloy 2024-T3 and hot-rolled 4340 steel were obtained as rods of 1.27 cm diameter from Reynolds Aluminum Company and Earl M. Jorgensen Company, respectively. A cylindrical section of diameter 1.27 cm and height 9.5 cm was mounted in cold-cure epoxy with one circular face of the sample exposed. The mounted sample was drilled and tapped on the opposite end to fit a standard sample holder for electrochemical measurements. The sample preparation included a 600-grit final grinding followed by rinsing in distilled water immediately before electrochemical evaluation.

A Princeton 350A Corrosion Measurement System, made by Princeton Applied Research, was used to obtain the potentiodynamic anodic polarization data. The general settings and conditions for the anodic polarization runs were:

Start potential:	-1000 mV (SCE) for 4340 steel
	-1500 mV (SCE) for 2024 aluminum
Final potential:	-250 mV (SCE) for 4340 steel
	-500 mV (SCE) for 2024 aluminum
Scan rate:	1 mV/sec
Auxillary electrode:	bright platinum
Reference electrode:	saturated calomel
Sample area:	1.267 cm^2
Cell temperature:	ambient (~25°C)
Electrolyte solution:	5% NaCl in deionized water

1. 4340 Steel

The results of the potentiodynamic anodic polarization experiments for 4340 steel are summarized in Table 1. Results for each inhibitor candidate are detailed in the following sections.

a. AFIF and Its Components. The potentiodynamic anodic polarization (PAP) curves for 4340 steel with and without the AFIF mixture are shown in Figure 3.

The control curve displays significant metal oxidation over the entire potential scan region. This type of response is characteristic of an unprotected system, and metallic corrosion would be expected. Recall that the extent of metal oxidation and dissolution at a given potential is proportional to the current density (I, A/m^2), or to the current (i, A).

The addition of AFIF to this system greatly reduces the metal activity in the potential region -480 mV to -550 mV. The essentially flat portions of the curve ($\frac{dI}{dV} \sim 0$) correspond to passive film formation upon the metal surface. This barrier protects the metal from the oxidative dissolution process, and represents the desired feature when using this type of corrosion inhibitor. The passivation current density (I_{pass}, A/m^2) is a measure of the relative effectiveness of this film in reducing metal activity, as is the width, $\Delta\phi$ (mV), of the passivation region. The 30 min exposure increases $\Delta\phi$ and decreases I_{pass}, which is consistent with an increased integrity of the passive film layer at longer exposure times. Shifts are also observed in the E_{corr} values of the AFIF systems in the positive direction relative to E_{corr} for the control. Such shifts to more positive potentials take E_{corr} away from the region of increased metal reducing activity, and reflect a state of greater corrosion protection.

The open circuit potential value (Figure 4) of the control (-540 ± 20)falls positive to the general value of E_{corr} (-630). A similar response would be expected for the AFIF formulation. Thus, the AFIF is a promising choice for a corrosion inhibitor, and should be tested further in long term experiments.

The PAP curve for $(NaPO_3)_6$ is given in Figure 5. There is no passivation region observed for this inhibitor. The E_{corr} values are shifted positive relative to the control value, which is favorable. For the potential region between -600 mV and -425 mV, there is reduced metal activity, with the 30 min exposure providing somewhat lower activity than the others.

TABLE 1. RESULTS OF POTENTIODYNAMIC ANODIC POLARIZATION EXPERIMENTS ON CORROSION INHIBITORS FOR 4340 STEEL

Inhibitor	Concentration	pH	E_{corr} mV(SCE)	I_{pass} A/m^2	Width of Passive Region mV(SCE)	Open Circuit Potential mV(SCE)	Comments
AFIF	0.0%	6.2	-642±10	0.0	0.0	-545±20	control: no corrosion inhibitor
AFIF		9.8	-590±20	0.042	120.0		no exposure period
AFIF		9.8	-590±60	0.025	155.0		30 min exposure in solution before experiment
$(NaPO_3)_6$	20 ppm	7.4	-522±10	0.0	0.0		no exposure period
$(NaPO_3)_6$	20 ppm	7.4	-540±10	0.0	0.0		30 min exposure period
$NaNO_3$	0.1%	6.2	-740±20	0.0	0.0		no exposure period
$NaNO_3$	0.1%	6.2	-750±50	0.0	0.0	-578±30	30 min exposure period
2-mercaptobenzo-thiazole	10 ppm	6.2	-673±10	0.0	0.0		no exposure period
2-mercaptobenzo-thiazole	10 ppm	6.2	-642±10	0.0	0.0		30 min exposure period
$Na_2B_4O_7 \cdot 10H_2O$	0.0	6.2	-790±10	0.0	0.0		control
$Na_2B_4O_7 \cdot 10H_2O$	0.35%	8.5	-749±10	0.0924	291.0	-556±20	no exposure period
$Na_2SiO_3 \cdot 9H_2O$	0.01%	10.2	-530±10	0.0	0.0		no exposure period
$Na_2SiO_3 \cdot 9H_2O$	0.01%	10.2	-530±10	0.288	50.0		30 min exposure period
$NaNO_2$	0.05%	6.3	-625:)	0.0	0.0		no exposure period

(continued)

TABLE 1. (continued).

Inhibitor	Concentration	pH	E_{corr} mV(SCE)	I_{pass} A/m^2	Width of Passive Region mV(SCE)	Open Circuit Potential mV(SCE)	Comments
NaNO2	0.05%	6.3	-630±10	0.450	90.0		30 min exposure period
Hydroxyquinoline	0.0%	6.2	-670±20	0.0	0.0		control
Hydroxyquinoline	0.1%	6.2	-582±10	0.0	0.0		no exposure period
2-propyn-1-ol	0.0%	6.2	-795±10	0.0	0.0		control
2-propyn-1-ol	1.0%	5.35	-724±10	0.0	73.0		no exposure period
$(NH_4)_2MoO_4$	0.1%	4.6	-626±10	0.0	0.0		no exposure period
$(NH_4)_2MoO_4$	0.1%	8.1	-456±10	0.215	144.0		no exposure period
$MgSiF_6 \cdot 6H_2O$	1.0%	3.1	-650±10	0.0	0.0		no exposure period
$NH_4HB_4O_2 \cdot 3H_2O$	0.35%	8.7	-671±10	0.100	222.0		no exposure period
1-ethynyl-1-cyclohexanol	0.1%	6.2	-500±10	0.0	0.0		no exposure period
3,5-dimethyl-1-hexyne-3-ol	1.0%	4.4	-515±10	0.072	133.0		no exposure period
sarcosine	1.0%	5.9	-790±10	0.0	0.0		no exposure period
alizarin red S	0.0		-674±10	0.0	0.0		no exposure period
alizarin red S	1.0%		-590±10	0.0	0.0		no exposure period
sodium sarcosine	1.0%	10.6	-867±10	0.034	88.0		no exposure period

(continued)

TABLE 1. (continued).

Inhibitor	Concentration	pH	E_{corr} mV(SCE)	I_{pass} A/m^2	Width of Passive Region mV(SCE)	Open Circuit Potential mV(SCE)	Comments	
sodium cinnamate	1.0%	8.7	-439±10	0.041	300.0		no exposure period	21
potassium cinnamate	1.0%	7.1	-750±10	0.049	100.0		no exposure period	22
mercaptoacetic acid	0.1%	4.3	-765±10	0.242	180.0		no exposure period	23
$Na_2MoO_4 \cdot 2H_2O$	1.0%	8.8	-740±10	0.039	278.0		no exposure period	24
471-1	0.0	6.2	-978±10	0.0	0.0		control	25
471-1		8.3	-677±10	0.136	296.0		no exposure period	25
471-2		7.7	-488±10	0.251	305.0		no exposure period	26
471-5		6.2	-782±10	0.242	224.0		no exposure period	27
471-6		8.5	-705±10	0.174	229.0		no exposure period	28
471-8		7.1	-500±10	0.0713	262.0	-520±10	no exposure period	29
471-9		7.0	-650±10	0.0413	254.0	-520±10	no exposure period	30

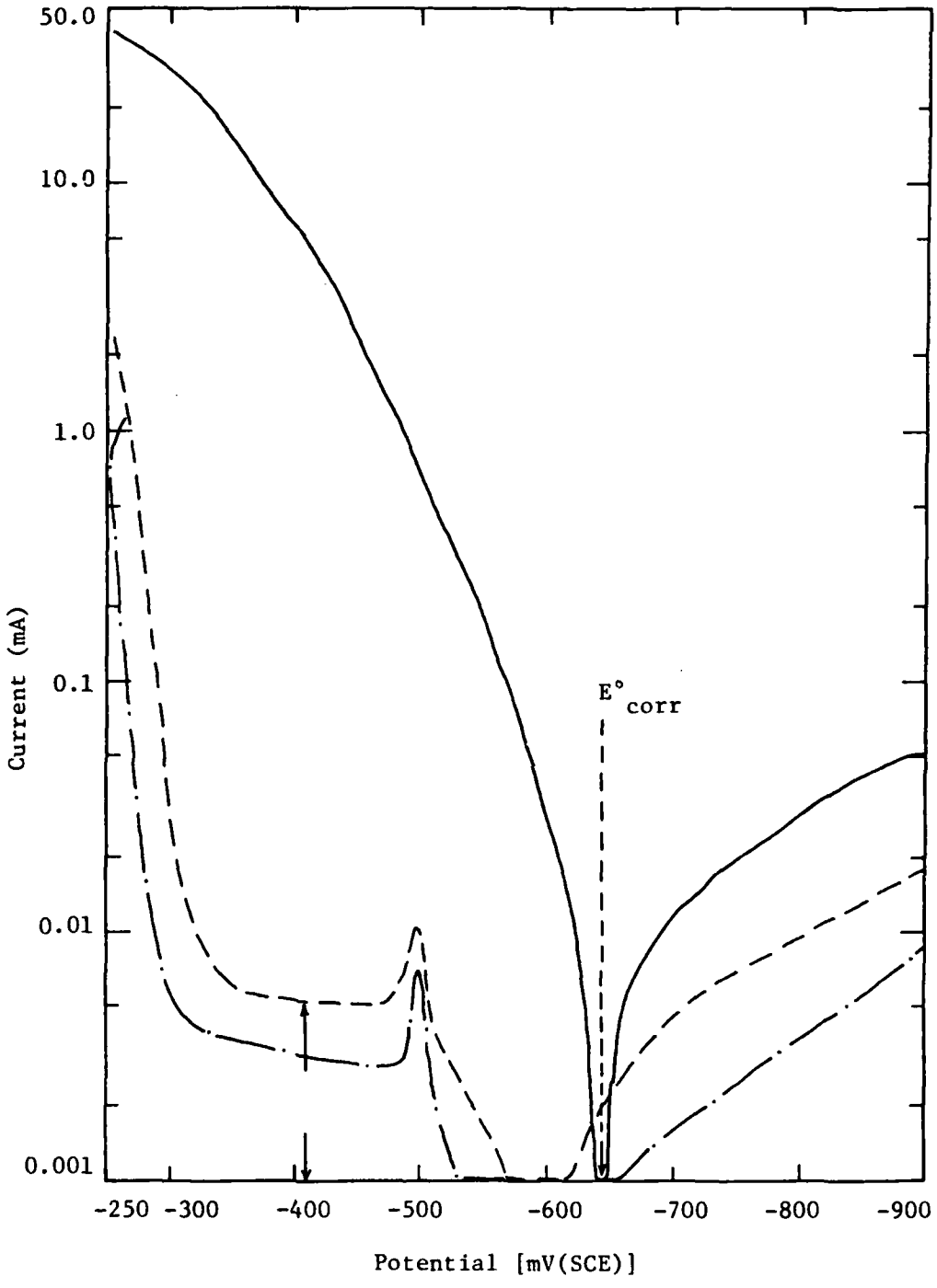

Figure 3. Current vs. potential for potentiodynamic polarization experiment with 4340 steel sample of 1.267 cm^2 surface area in 5% NaCl electrolyte solution: ———— control; - - - with AFIF; —— · —— after 30 min exposure to inhibitor formulation.

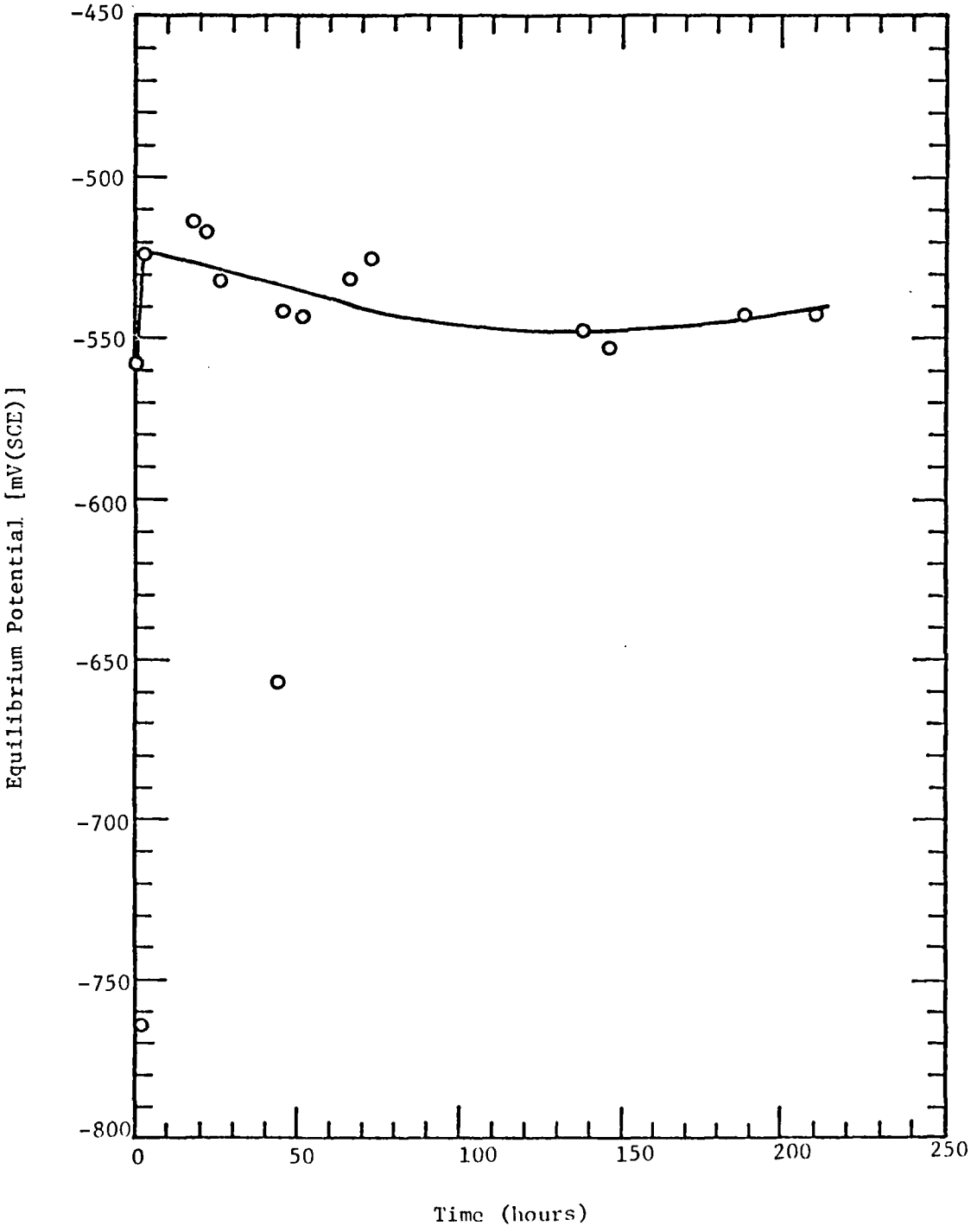

Figure 4. Equilibrium potential vs. time for chronopotentiometric experiment with 4340 steel in a 5% NaCl solution.

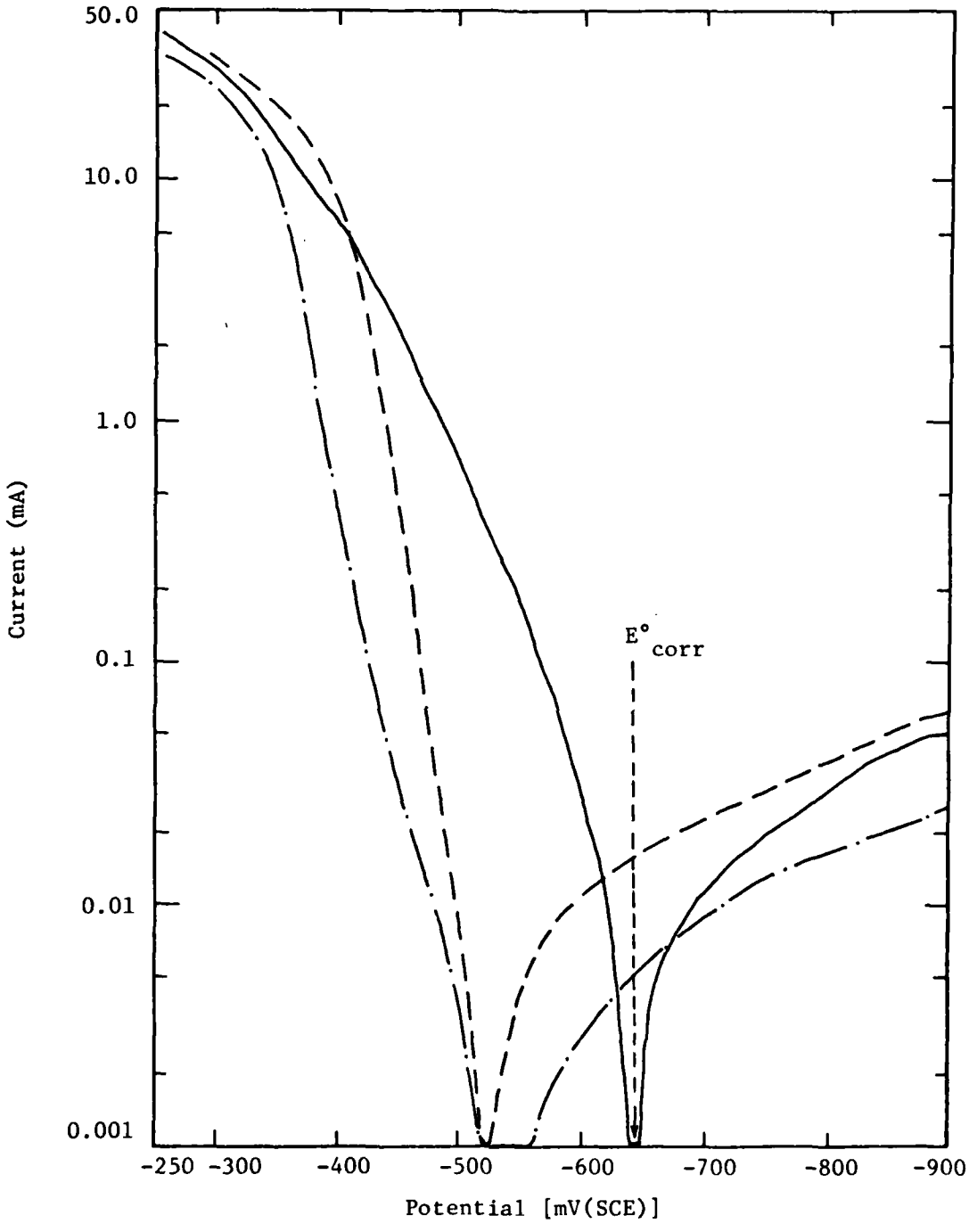

Figure 5. Current vs. potential for potentiodynamic polarization experiment with 4340 steel sample of 1.267 cm^2 surface area in 5% NaCl electrolyte solution: ____ control; - - - with 20 ppm $(NaPO_3)_6$ inhibitor; ___ . ___ after 30 min exposure to inhibitor.

This compound may be useful as a corrosion inhibitor, probably more so when used in a mixture of other inhibitors.

The PAP plot for $NaNO_3$ is shown in Figure 6. A passivation region is not observed for this inhibitor. Reduced metal activity is apparent over the potential range from -620 mV to -400 mV, with the 30 min exposure providing the best response. The shift of the E_{corr} values of the AFIF systems in the negative (cathodic) direction relative to the control is somewhat disturbing, since the shift is into a region of increased metal dissolution. The open circuit potential for the nitrate system is shown in Figure 7. The nitrate is probably effective as a corrosion inhibitor.

The PAP curve for 2-mercaptobenzothiazole is displayed in Figure 8. This compound alone does not work as a corrosion inhibitor for 4340 steel, since the control shows more reduced metal activity than that with the 2-mercaptobenzothiazole.

The PAP curve for $Na_2B_4O_7 \cdot 10H_2O$ is shown in Figure 9, and the open circuit potential curve in Figure 10. The E_{corr} of the inhibitor system is shifted positive to that of the control, which is good. The passivation region extends from approximately -675 mV to -380 mV. I_{pass} for the inhibitor system is significantly lower than I values along the control curve. This compound is effective as a passivating corrosion inhibitor for 4340 steel. $Na_2B_4O_7 \cdot 10H_2O$ is the major component (wt %) of the AFIF mixture.

The PAP curve for $Na_2SiO_3 \cdot 9H_2O$ is given in Figure 11. Only the system with 30 min exposure to the inhibitor showed a passive zone, and it is very narrow (~50 mV). Although the E_{corr} values are shifted favorably toward the positive direction, it is questionable if this compound may be considered a good corrosion inhibitor for steel. The open circuit potential curve is shown in Figure 12.

The PAP plot for $NaNO_2$ is given in Figure 13. The system with 30 min inhibitor exposure has a passive zone between -480 mV and -350 mV; I_{pass} is lower than any I value on the other two curves in this region. The $NaNO_2$ system (without time exposure) shows reduced metal activity in the same region, but did not quite form a passive zone. This compound is probably an effective corrosion inhibitor for steel.

b. Hydroxyquinoline. The PAP curve for hydroxyquinoline is shown in Figure 14. An apparent passivation zone is observed in the cathodic region

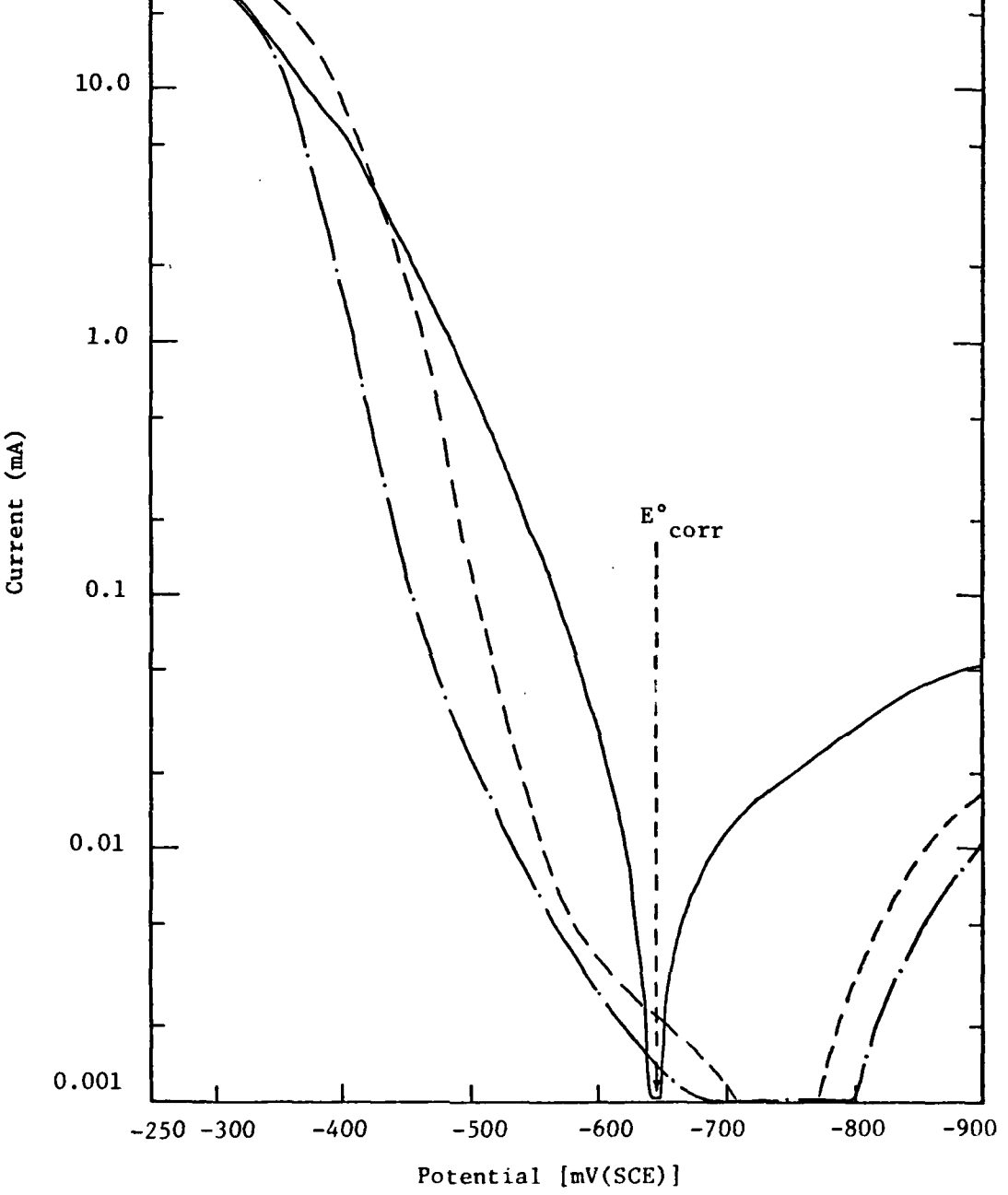

Figure 6. Current vs. potential for potentiodynamic polarization experiment with 4340 steel sample of 1.267 cm^2 surface area in 5% NaCl electrolyte solution: ——— control; - - - with 0.1% $NaNO_3$ inhibitor; ——— · ——— after 30 min exposure to inhibitor.

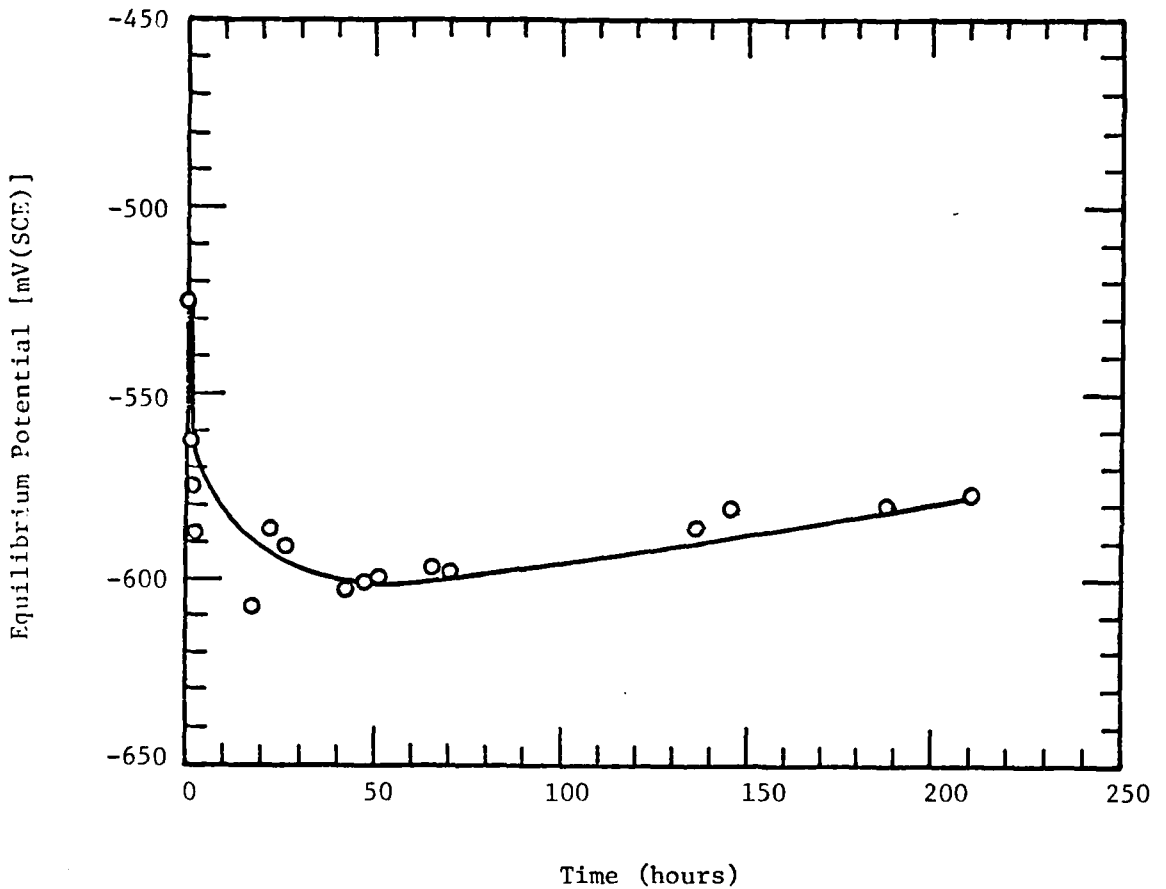

Figure 7. Equilibrium potential vs. time for chronopotentiometric experiment with 4340 steel in a 5% NaCl solution containing 0.1% $NaNO_3$.

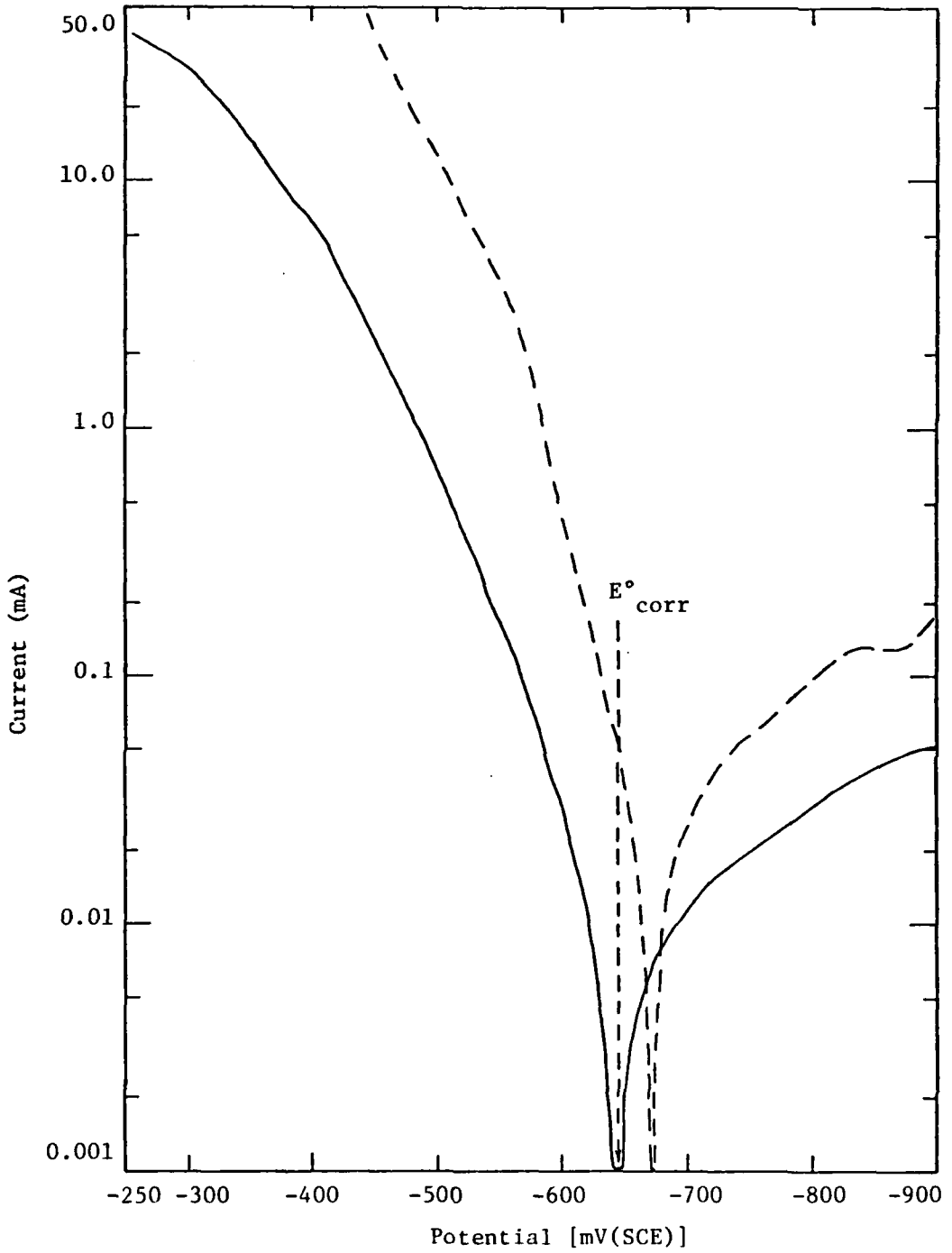

Figure 8. Current vs. potential for potentiodynamic polarization experiment with 4340 steel sample of 1.267 cm^2 surface area in 5% NaCl electrolyte solution: ——— control; - - - with 10 ppm 2-mercaptobenzothiazole inhibitor.

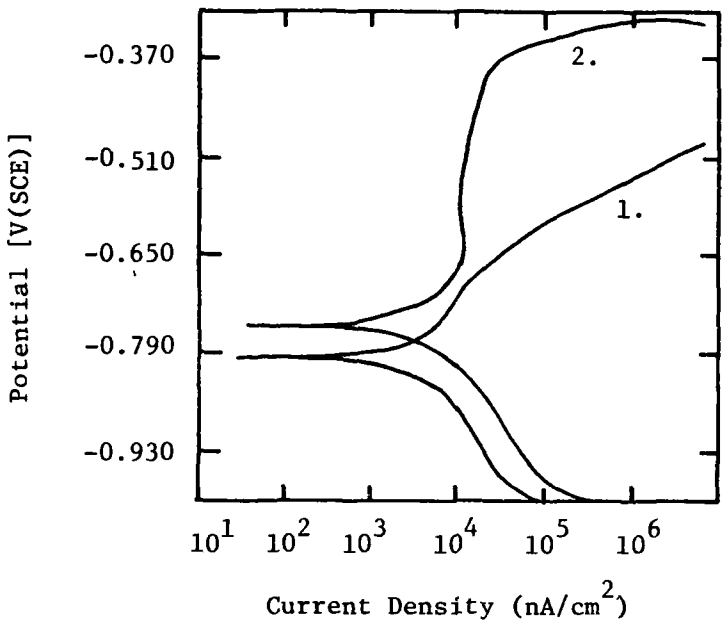

Figure 9. Potential vs. current density for potentiodynamic polarization experiment with 4340 steel in 5% NaCl electrolyte solution: (1) control; (2) with 0.35% $Na_2B_4O_7 \cdot 10H_2O$ inhibitor.

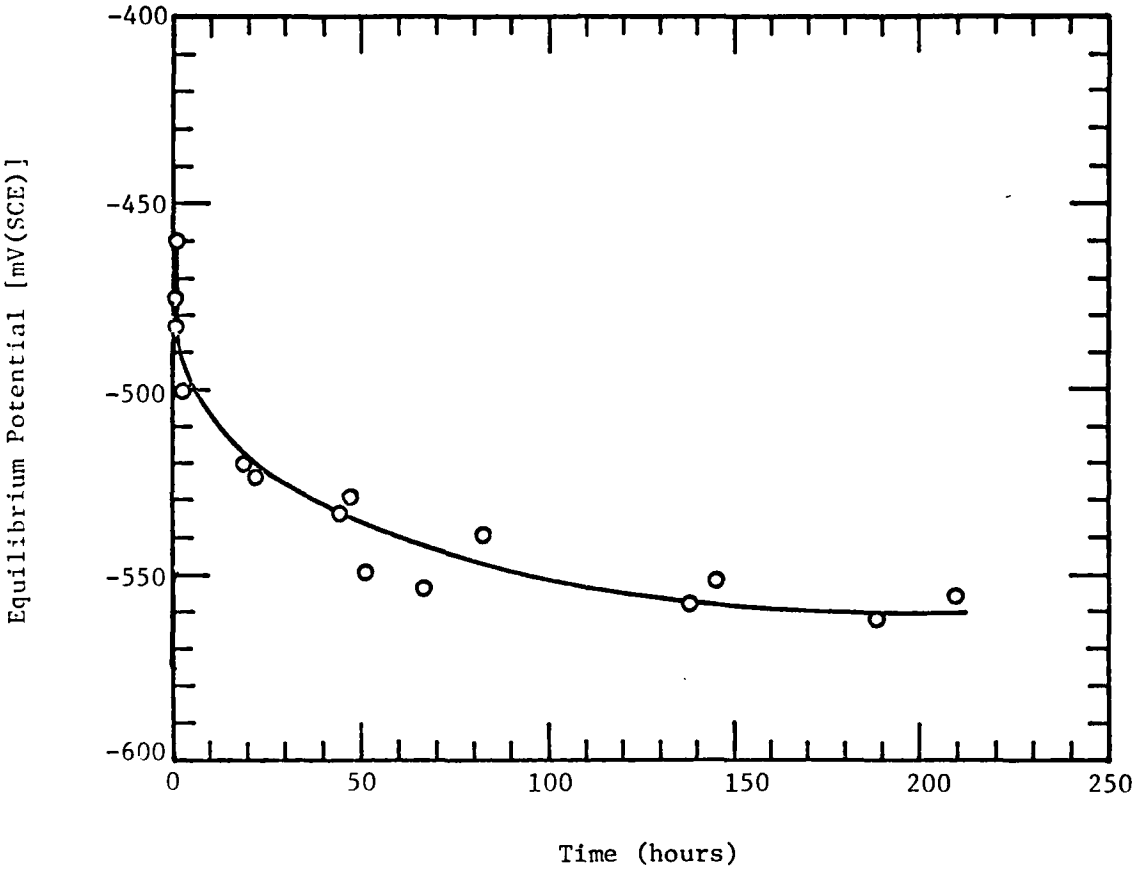

Figure 10. Equilibrium potential vs. time for chronopotentiometric experiment with 4340 steel in a 5% NaCl solution containing 0.35% $Na_2B_4O_7 \cdot 10\ H_2O$.

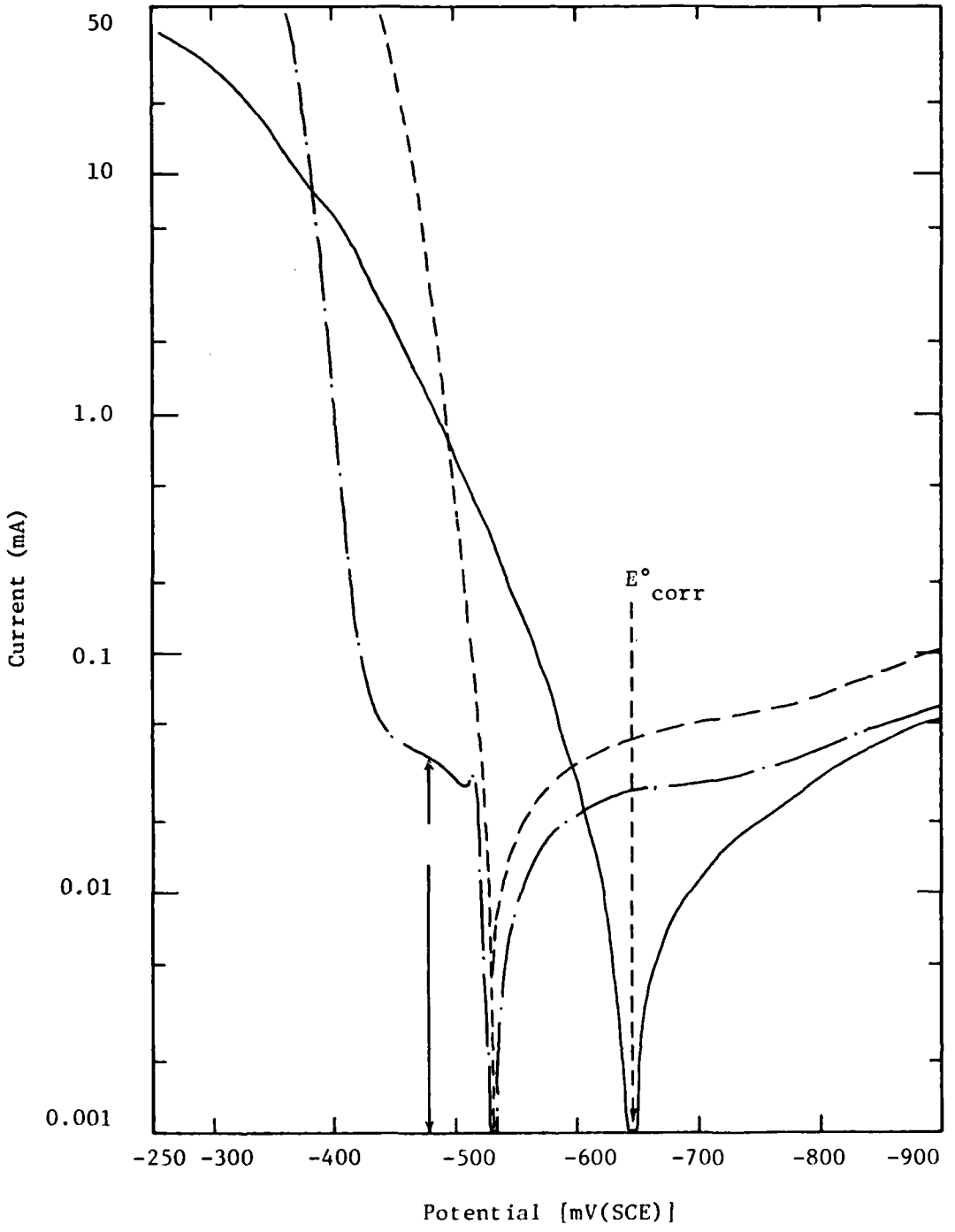

Figure 11. Current vs. potential for potentiodynamic polarization experiment with 4340 steel sample of 1.267 cm^2 surface area in 5% NaCl electrolyte solution: ——— control; - - - with 0.01% $Na_2SiO_3 \cdot 9H_2O$ inhibitor; ——— · ——— after 30 min exposure to inhibitor.

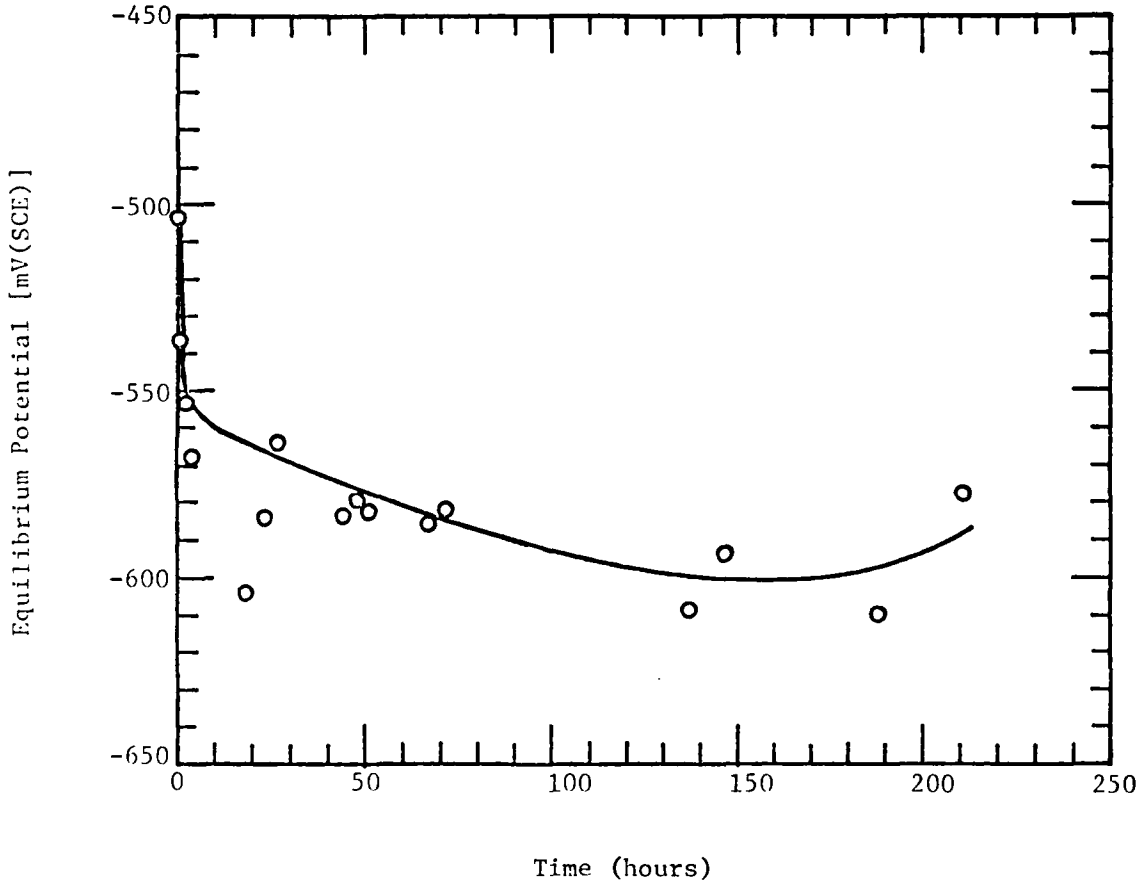

Figure 12. Equilibrium potential vs. time for chronopotentiometric experiment with 4340 steel in a 5% NaCl solution containing 0.01% $Na_2SiO_3 \cdot 9H_2O$.

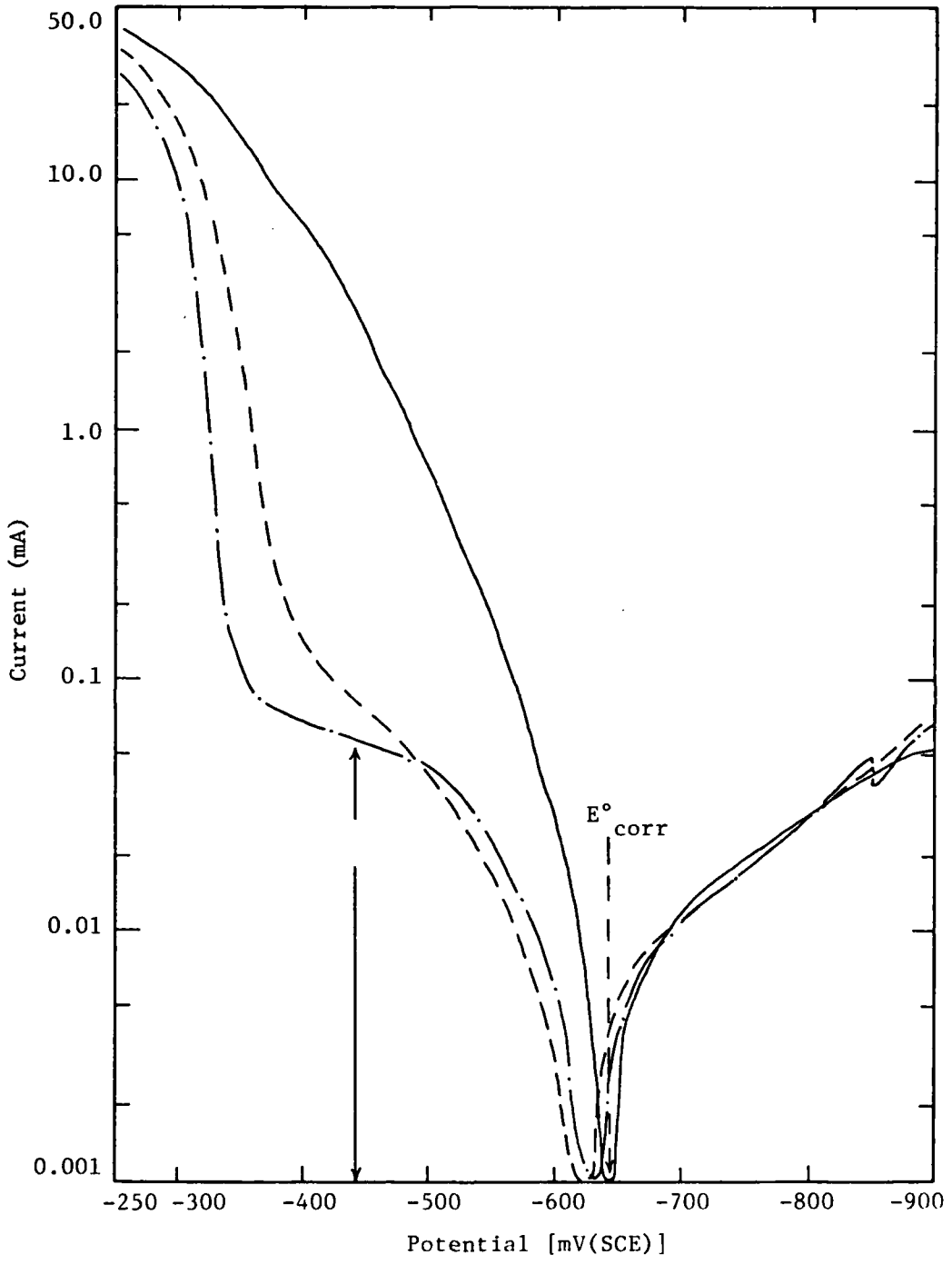

Figure 13. Current vs. potential for potentiodynamic polarization experiment with 4340 steel of 1.267 cm^2 surface area in 5% NaCl electrolyte solution: ____ control; - - - with 0.05% $NaNO_2$ inhibitor; ____.____ after 30 min exposure to inhibitor.

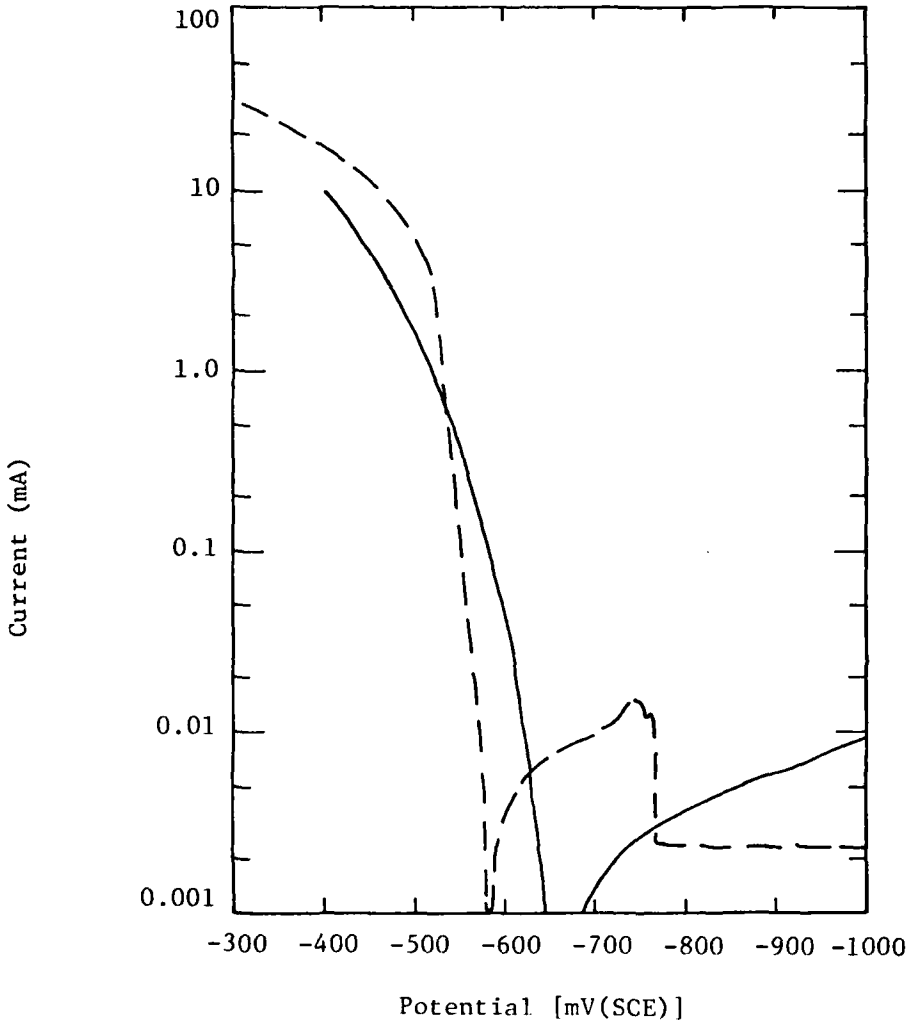

Figure 14. Current vs. potential for potentiodynamic polarization experiment with 4340 steel of 1.267 cm^2 surface area in 5% NaCl electrolyte solution: —— control; - - - with 0.1% hydroxyquinoline.

from -1000 mV to -760 mV, with a very low I_{pass}. The region between -760 mV to -690 mV represents some oxidation process which is occurring (unknown nature). This compound could be a very effective corrosion inhibitor for steel. The potential region from -600 mV to -400 mV shows no real improvement in corrosion protection over that of the control.

c. 2-Propyn-1-ol. The PAP curve for 2-propyn-1-ol is given in Figure 15. This compound is an effective passivating inhibitor, with a passive zone from -680 mV to -570 mV. Even in the transpassive zone (beyond -570 mV) the metal reducing activity is still greatly decreased in comparison with the control. The E_{corr} value is also shifted favorably toward more positive values.

d. $(NH_4)_2MoO_4$. The PAP curve for $(NH_4)_2MoO_4$ is shown in Figure 16. The E_{corr} value is shifted significantly toward positive values, although no passivation zone is observed. Reduced metal activity is observed with the inhibitor in the region from -660 mV to -500 mV. This compound would probably work as a corrosion inhibitor (it depends upon the open circuit potential, of course).

e. NH_4NO_2. The PAP curve for NH_4NO_2 is displayed in Figure 17. This is a passivating inhibitor, and is effective over a very wide potential region, -550 mV to -150 mV. This is an excellent corrosion inhibitor.

f. $MgSiF_6 \cdot 6H_2O$. The PAP curve for $MgSiF_6 \cdot 6H_2O$ is shown in Figure 18. This compound is not an inhibitor at all; the control is much better.

g. $NH_4HB_4O_7 \cdot 3H_2O$. The PAP plot for $NH_4HB_4O_7 \cdot 3H_2O$ is shown in Figure 19. This compound displays an apparent passive zone from approximately -750 mV to -390 mV, although the I_{pass} value seems fairly large. The E_{corr} is shifted positively over the control. This compound would be effective as a corrosion inhibitor.

h. 1-Ethynyl-1-cyclohexanol. The PAP curve for 1-ethynyl-1-cyclohexanol is shown in Figure 20. Reduced metal activity is observed over the range corresponding to -760 mV to -525 mV. However, this is not technically a passive zone, since it occurs on the cathodic side of E_{corr}. This E_{corr} value is shifted significantly into the anodic region. This compound might work as a corrosion inhibitor, though not a passivator.

i. 3,5-Dimethyl-1-hexyne-3-ol. The PAP curve for 3,5-dimethyl-1-hexyne-3-ol is given in Figure 21. There appears to be a passive zone in the region between -720 mV and -575 mV, and reduced metal activity is ob-

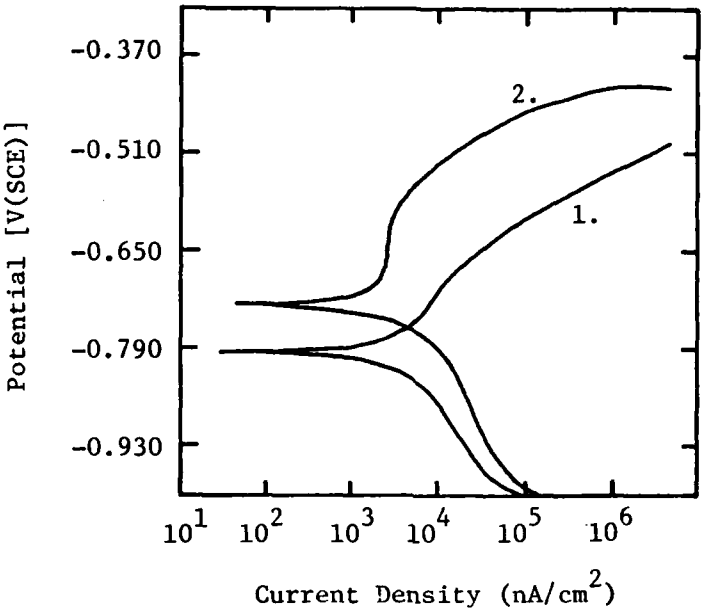

Figure 15. Potential vs. current density for potentiodynamic polarization experiment with 4340 steel in 5% NaCl electrolyte solution: (1) control; (2) with 1% 2-propyn-1-ol inhibitor.

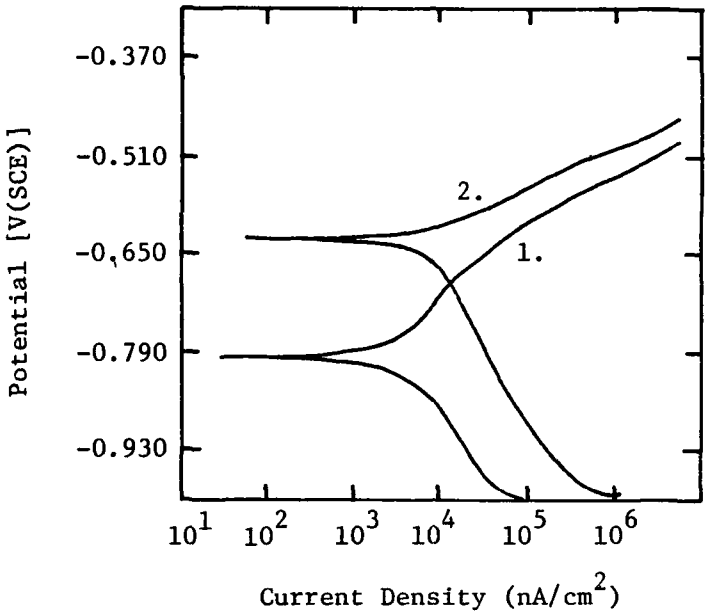

Figure 16. Potential vs. current density for potentiodynamic polarization experiment with 4340 steel in 5% NaCl electrolyte solution: (1) control; (2) with 0.1% $(NH_4)_2MoO_4$.

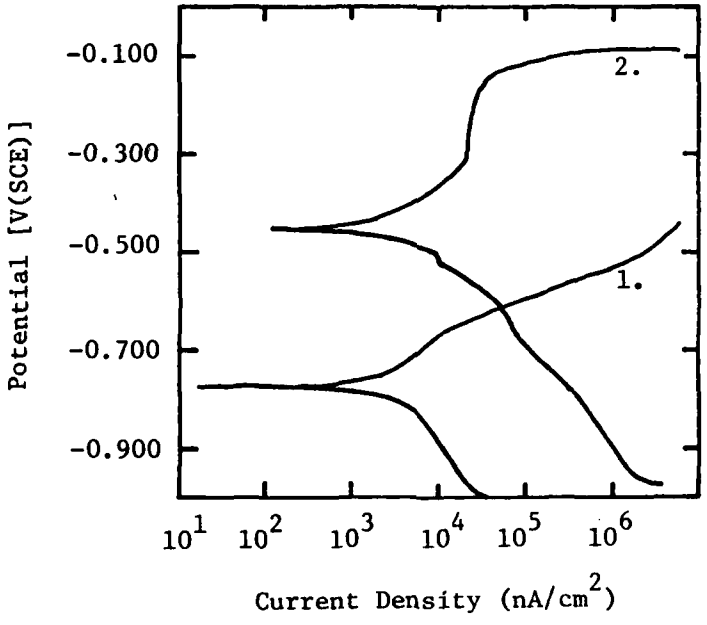

Figure 17. Potential vs. current density for potentiodynamic polarization experiment with 4340 steel in 5% NaCl electrolyte solution: (1) control; (2) with 0.1% NH_4NO_2 inhibitor.

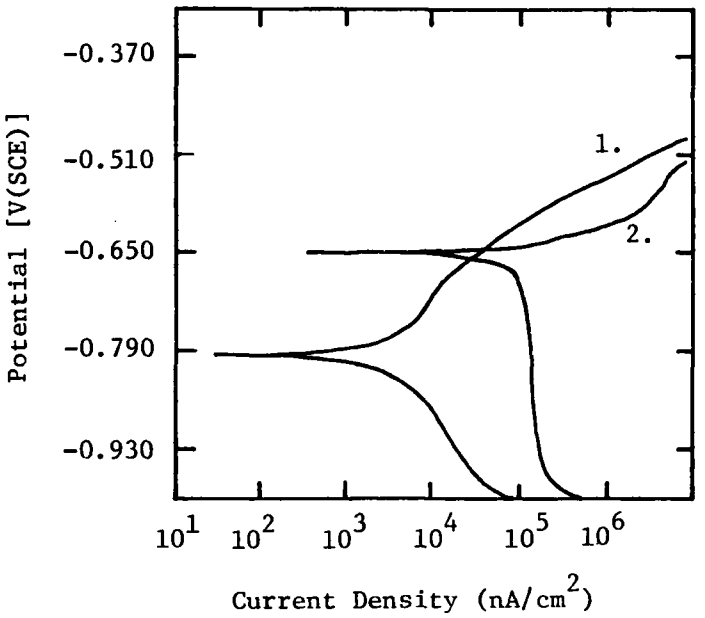

Figure 18. Potential vs. current density for potentiodynamic polarization experiment with 4340 steel in 5% NaCl electrolyte solution: (1) control; (2) with 1% $MgSiF_6 \cdot 6H_2O$.

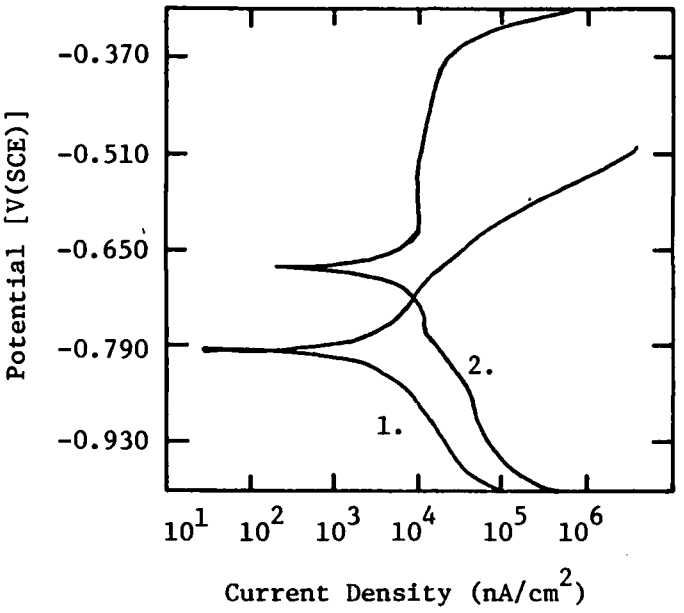

Figure 19. Potential vs. current density for potentiodynamic polarization experiment with 4340 steel in 5% NaCl electrolyte solution: (1) control; (2) with 0.35% $NH_4HB_4O_7 \cdot 3H_2O$.

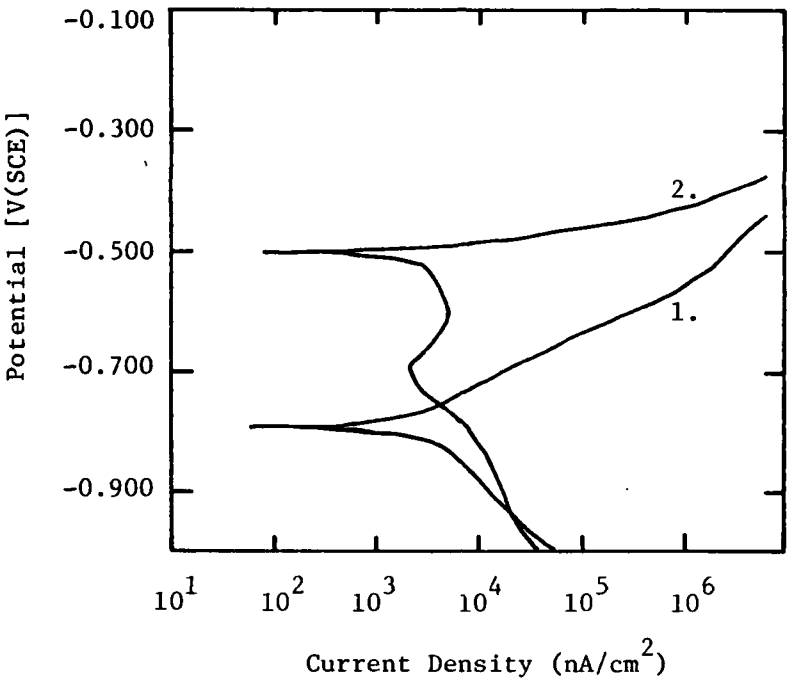

Figure 20. Potential vs. current density for potentiodynamic polarization experiment with 4340 steel in 5% NaCl electrolyte solution: (1) control; (2) with 0.1% 1-ethynyl-1-cyclohexanol.

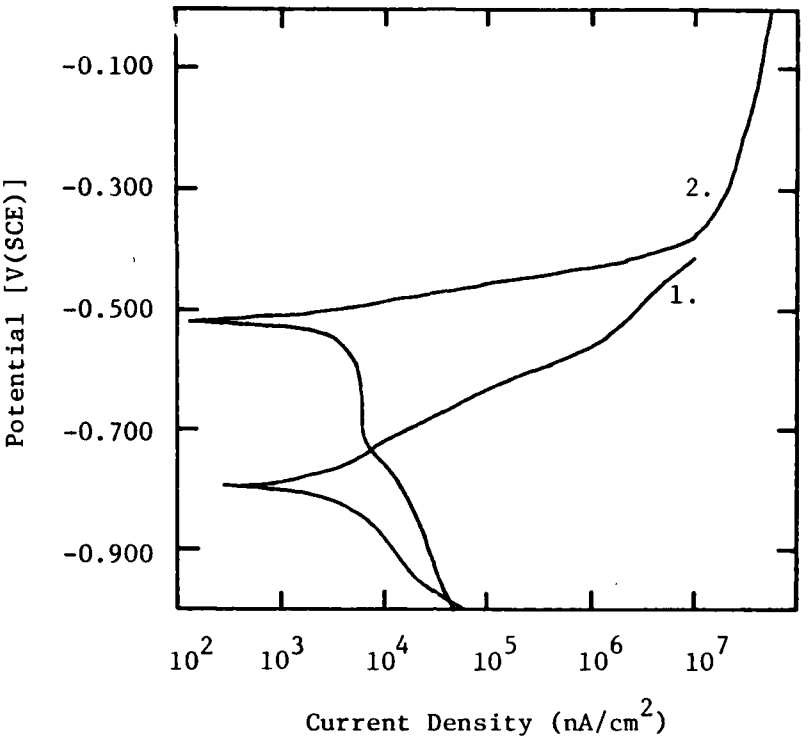

Figure 21. Potential vs. current density for potentiodynamic polarization experiment with 4340 steel in 5% NaCl electrolyte solution: (1) control; (2) with 1.0% 3,5-dimethyl-1-hexyne-3-ol.

served between -720 mV and -450 mV. The E_{corr} of the inhibitor system is shifted positively. This compound could possibly serve as a corrosion inhibitor.

j. Sarcosine. The PAP curve for sarcosine is shown in Figure 22. Curves for the inhibitor and control systems are practically superimposed. Sarcosine is apparently not a corrosion inhibitor.

k. Alizarin-Red-S. The PAP curve for alizarin-red-S is given in Figure 23. E_{corr} for the inhibited system is shifted anodically. No passivation zone is observed. However, reduced metal activity is seen from -700 mV to -100 mV. This compound may be a reasonable corrosion inhibitor, although not a passivator.

l. Sodium Sarcosine. The PAP curve for sodium sarcosine is given in Figure 24. This is not really a passivating inhibitor, although there is a small region, about 90 mV wide, which does have some of the characteristics of a passive zone. There is reduced metal activity from -700 mV to -400 mV. The E_{corr} of the inhibitor system is shifted cathodically, which is not favorable. This compound does have some usefulness as a corrosion inhibitor.

m. Sodium Cinnamate. The PAP curve for sodium cinnamate appears in Figure 25. This is an excellent corrosion inhibitor, which has E_{corr} anodically shifted, a passive region from -700 mV to -500 mV, and reduced metal dissolution activity over much of the remainder of the curve.

n. Potassium Cinnamate. The PAP curve for potassium cinnamate is shown in Figure 26. E_{corr} is shifted slightly in the anodic direction, and an oxidation process (mechanism unknown) is occurring between -700 mV and -550 mV. What could be termed a passive zone lies between -525 mV and -425 mV, although it is somewhat narrow. Reduced metal activity may be observed over much of the potential region from -650 mV to -300 mV. This compound is a good corrosion inhibitor.

o. Mercaptoacetic Acid. The PAP curve for mercaptoacetic acid is given in Figure 27. E_{corr} is cathodically shifted, with a passivation zone between -700 mV to -525 mV. This compound probably would serve as an adequate corrosion inhibitor, depending upon the open circuit potential of the system. The low pH of this inhibitor system is an unusual feature, which must be taken into account in the service application of this material.

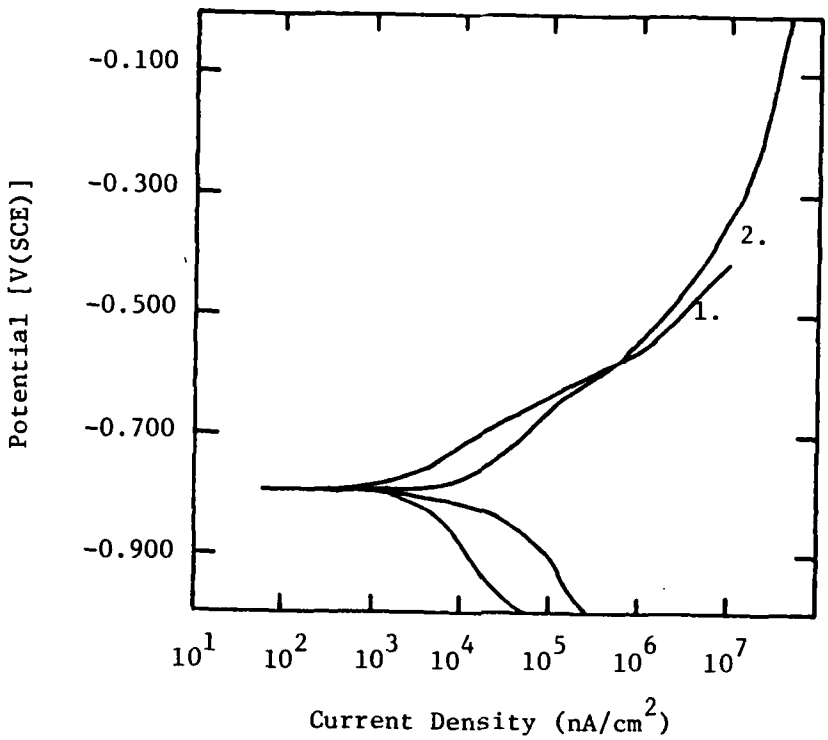

Figure 22. Potential vs. current density for potentiodynamic polarization experiment with 4340 steel in 5% NaCl electrolyte solution: (1) control; (2) with 1% sarcosine.

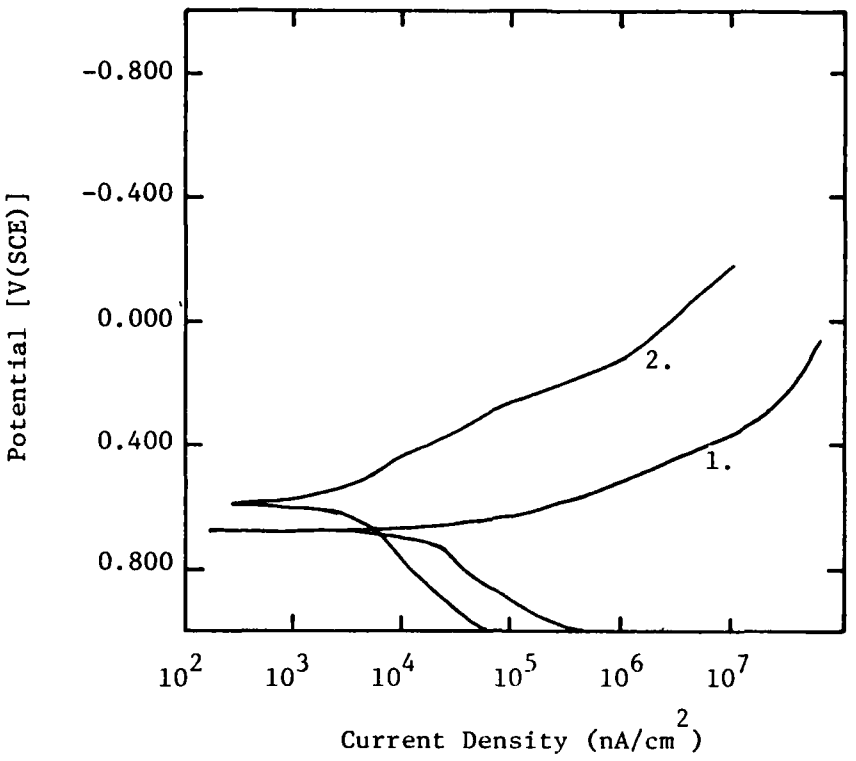

Figure 23. Potential vs. current density potentiodynamic polarization experiment with 4340 steel in 5% NaCl electrolyte solution: (1) control; (2) with 1% alizarin-red-S.

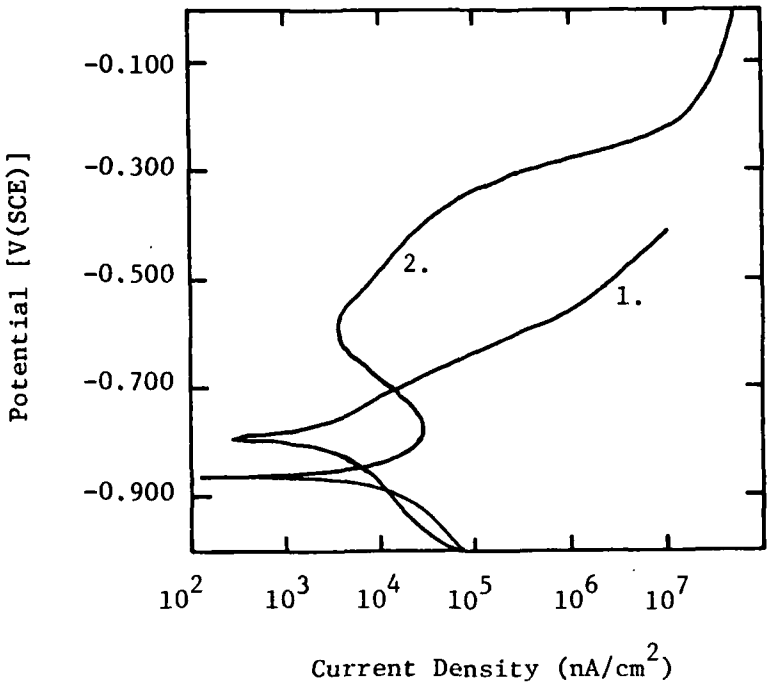

Figure 24. Potential vs. current density for potentiodynamic polarization experiment with 4340 steel in 5% NaCl electrolyte solution: (1) control; (2) with 1% sodium sarcosine.

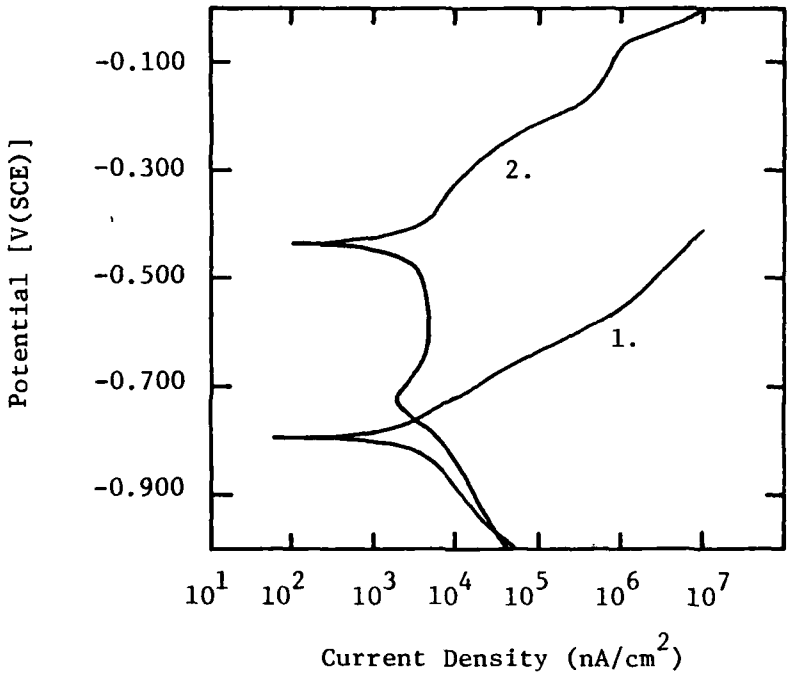

Figure 25. Potential vs. current density for potentiodynamic polarization experiment with 4340 steel in 5% NaCl electrolyte solution: (1) control; (2) with 1% sodium cinnamate.

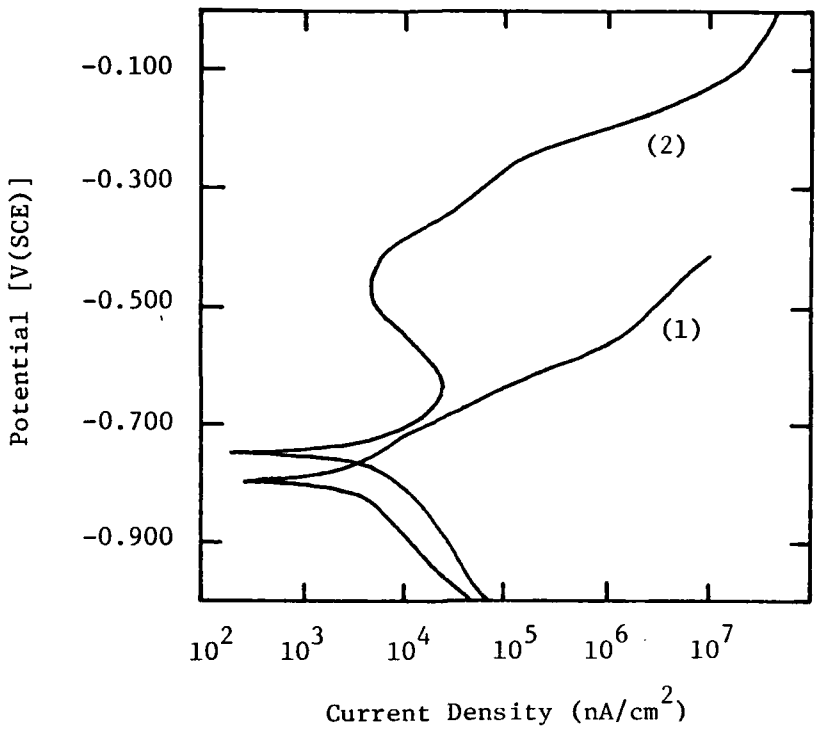

Figure 26. Potential vs. current density for potentiodynamic polarization experiment with 4340 steel in 5% NaCl electrolyte solution: (1) control; (2) with 1% potassium cinnamate.

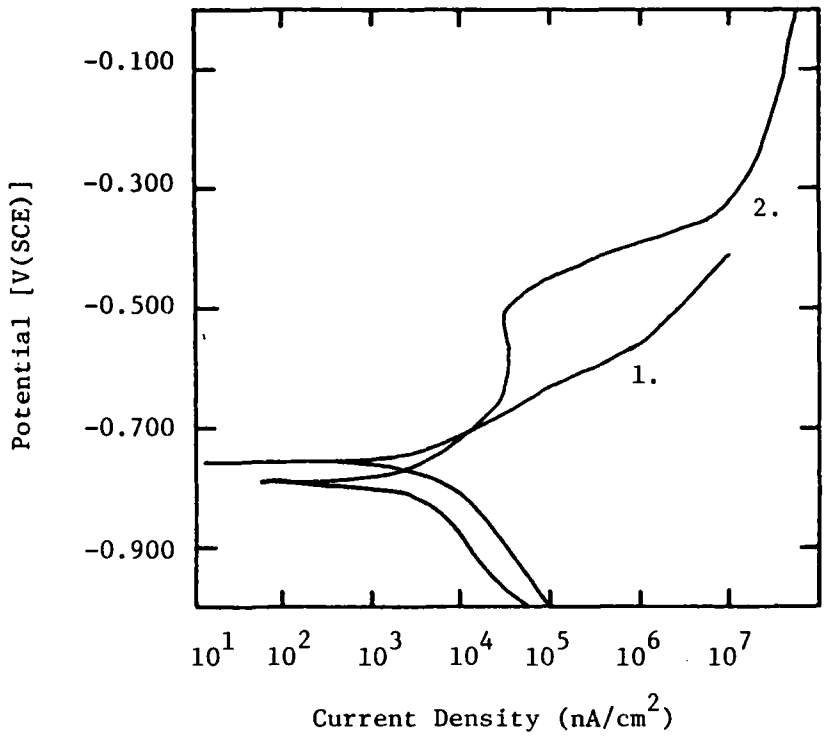

Figure 27. Potential vs. current density for potentiodynamic polarization experiment with 4340 steel in 5% NaCl electrolyte solution: (1) control; (2) with 0.1% mercaptoacetic acid.

p. $Na_2MoO_4 \cdot 2H_2O$. The PAP plot of $Na_2MoO_4 \cdot 2H_2O$ is shown in Figure 28. This compound is an effective passivating corrosion inhibitor. E_{corr} is anodically shifted, and the passivation zone extends from approximately -725 mV to -375 mV. Metal dissolution activity is significantly reduced over this region.

q. 471-1 (0.35% $NH_4HB_4O_7 \cdot 3H_2O$, 0.10% $NaNO_3$, 0.05% $NaNO_2$, 0.01% $Na_2SiO_3 \cdot 9H_2O$, and 20 ppm $(NaPO_3)_6$). The PAP curve for 471-1 is displayed in Figure 29. E_{corr} is anodically shifted, and a wide passivation zone lies between -650 mV and -350 mV. This material appears to be a good corrosion inhibitor, comparable in many ways with AFIF.

r. 471-2 (1% 2-propyn-1-ol, 0.5% NH_3NO_2, and 0.5% $NaNO_2$). The PAP curve for 471-2 is given in Figure 30. E_{corr} is shifted significantly in the anodic direction relative to the control, and a passivation zone extends from -475 mV to -100 mV. This material would function as an effective corrosion inhibitor, similar to AFIF.

s. 471-5 (0.01% $Na_2B_4O_7 \cdot 10H_2O$, 0.1% mercaptoacetic acid). The PAP curve for 471-5 is shown in Figure 31. There is essentially no change in the E_{corr} value relative to the control. A passivation zone extends from -720 mV to -500 mV. This inhibitor could function well under the right circumstances, although its behavior appears more restricted than the other mixtures studied.

t. 471-6 (0.35% $Na_2B_4O_7 \cdot 10H_2O$, 0.1% $NaNO_3$, 0.05% $NaNO_2$, 0.01% $Na_2SiO_3 \cdot 9H_2O$, and 20 ppm $(NaPO_3)_6$). The PAP curve of this inhibitor is shown in Figure 32. The control outperforms the inhibitor in the region from -1000 mV to -800 mV. An apparent oxidation process may be occurring in the region from -675 mV to -575 mV. A narrow passivation zone extends from -575 mV to -375 mV. The E_{corr} is anodically shifted relative to the control. This mixture would most likely perform as an effective corrosion inhibitor.

u. 471-8 (0.5% potassium cinnamate, 0.1% $NaNO_2$, and 0.02% $(NaPO_3)_6$). The PAP curve for 471-8 is shown in Figure 33. The region from -1000 mV to -825 mV shows the control outperforming the inhibitor. However, a passivation zone lies between -650 mV and -350 mV, where reduced metal dissolution is observed. E_{corr} is shifted anodically relative to the control. This material would probably function effectively as a corrosion inhibitor for steel. The open circuit potential behavior is shown in Figure 34.

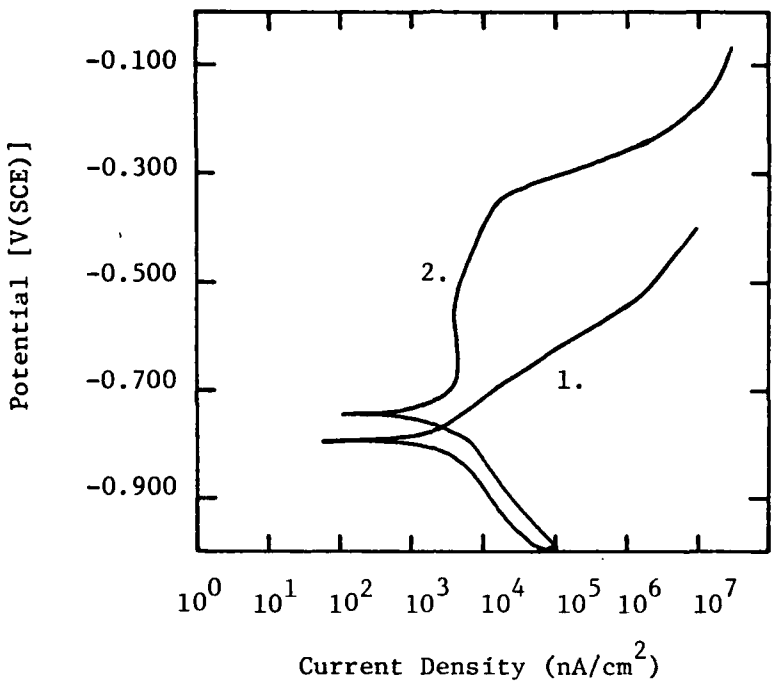

Figure 28. Potential vs. current density for potentiodynamic polarization experiment with 4340 steel in 5% NaCl electrolyte solution: (1) control; (2) with 1% $Na_2MoO_4 \cdot 2H_2O$.

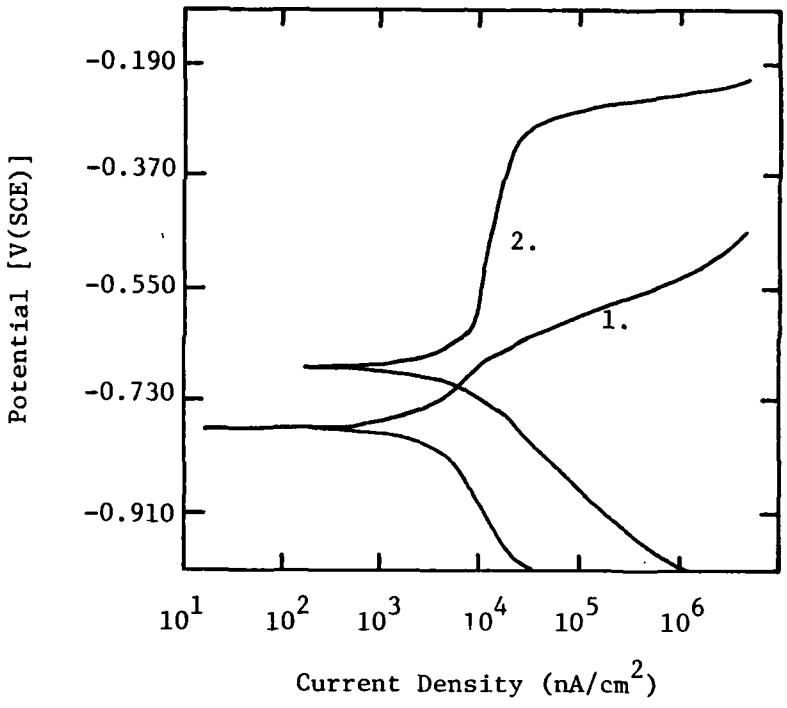

Figure 29. Potential vs. current density for potentiodynamic polarization experiment with 4340 steel in 5% NaCl solution: (1) control; (2) with Formulation 471-1.

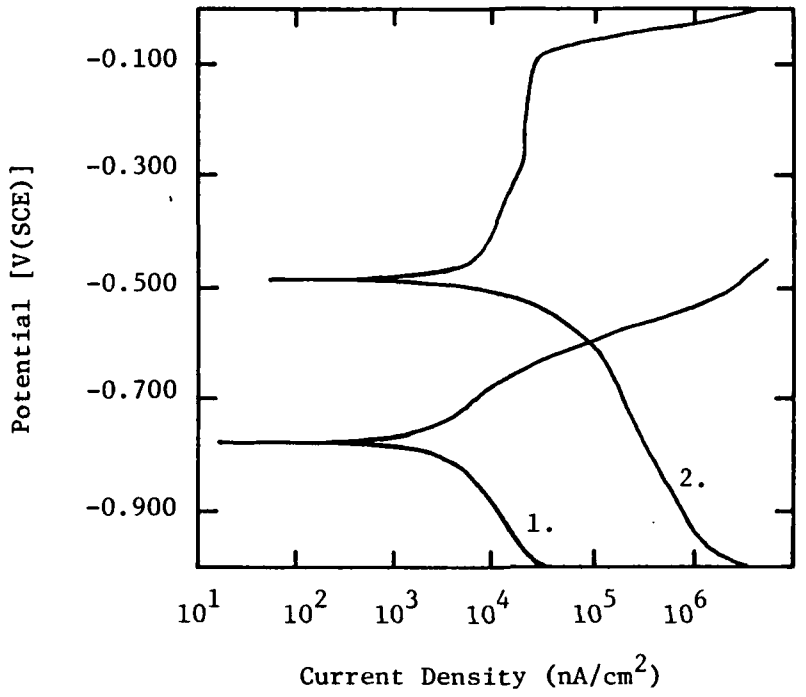

Figure 30. Potential vs. current density for potentiodynamic polarization experiment with 4340 steel in 5% NaCl electrolyte solution: (1) control; (2) with Formulation 471-2.

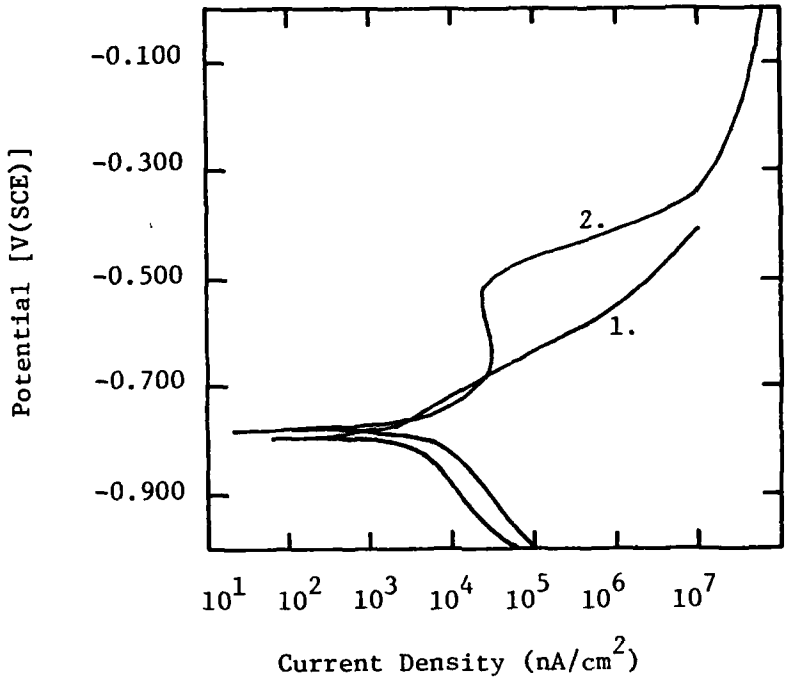

Figure 31. Potential vs. current density for potentiodynamic polarization experiment with 4340 steel in 5% NaCl electrolyte solution: (1) control; (2) with Formulation 471-5.

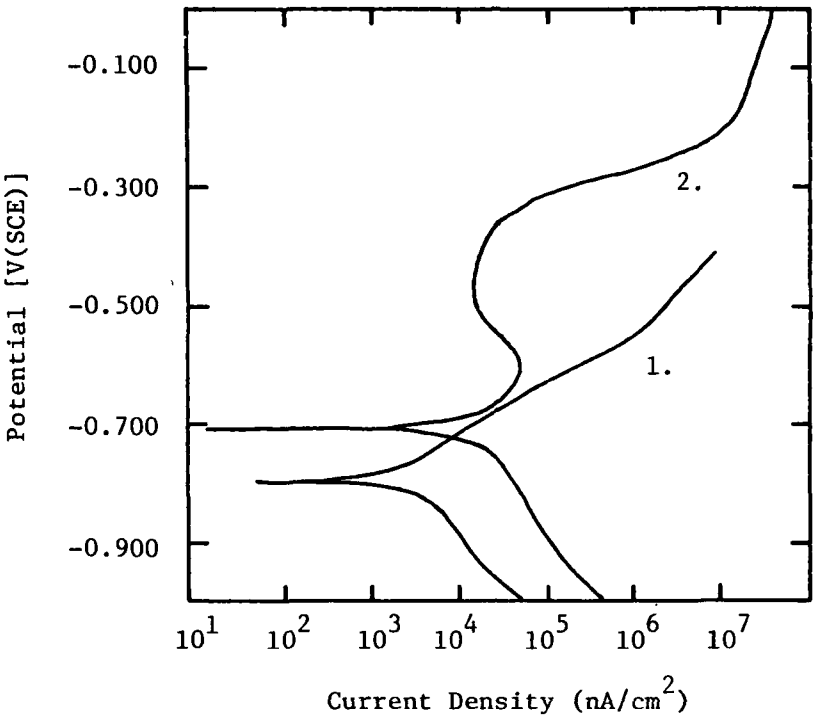

Figure 32. Potential vs. current density for potentiodynamic polarization experiment with 4340 steel in 5% NaCl electrolyte solution: (1) control; (2) with Formulation 471-6.

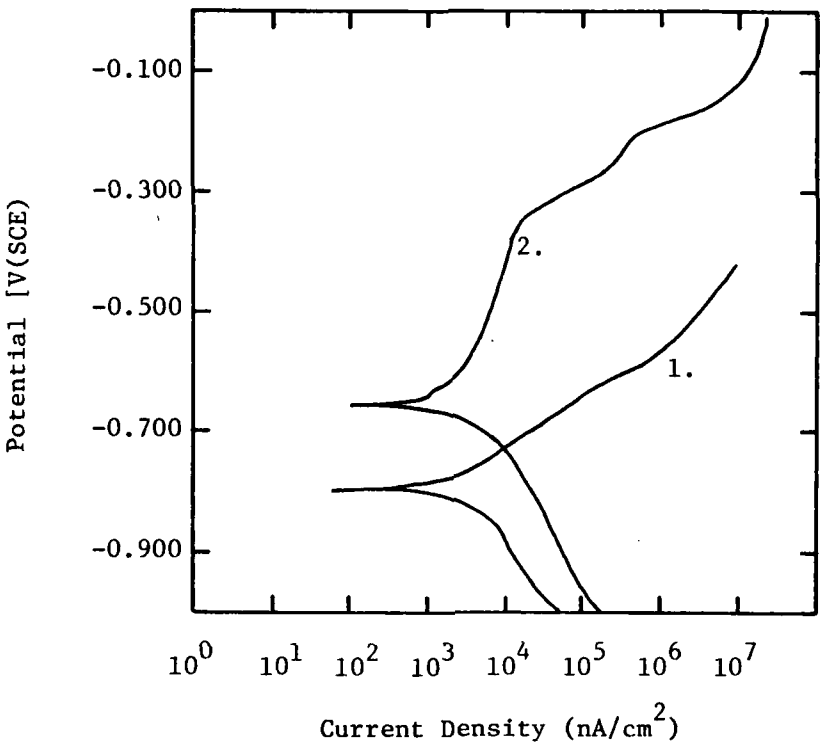

Figure 33. Potential vs. current density for potentiodynamic polarization experiment with 4340 steel in 5% NaCl electrolyte solution: (1) control; (2) with Formulation 471-8.

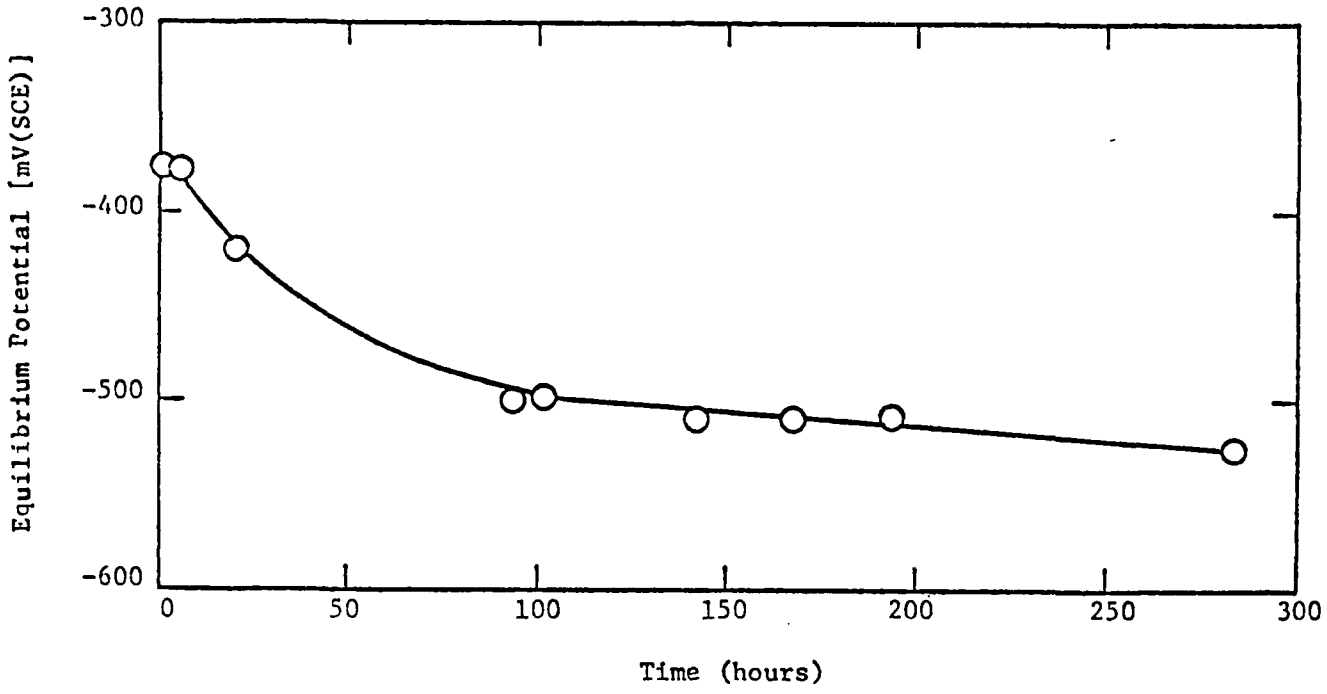

Figure 34. Equilibrium potential vs. time for chronopotentiometric experiment with 4340 steel in a 5% NaCl solution containing Formulation 471-8.

v. 471-9 ((0.5% potassium cinnamate, 0.15% $NaNO_2$, 0.05% $Na_2MoO_4 \cdot 2H_2O$, 0.1% 3,5-dimethyl-1-hexynol, and 0.02% $(NaPO_3)_6$). The PAP curve for 471-9 is shown in Figure 35. The behavior of this inhibitor is very similar to that observed for 471-8. This material would also serve as a good corrosion inhibitor. The open circuit potential curve is given in Figure 36.

2. 2024 Aluminum

The results of the potentiodynamic anodic polarization experiments for 2024 aluminum are summarized in Table 2. Results for each inhibitor candidate are detailed in the following sections.

a. AFIF and its components. The potentiodynamic anodic polarization curve for AFIF and 2024 aluminum is shown in Figure 37. Passive oxide layers are obviously present in all three runs, as may be observed in the potential region from -1050 mV to -600 mV. However, the presence of AFIF significantly increases the passive current density relative to the control, although the passive film still appears to exist. An increased exposure period has little effect on the system. The corrosion potential, E_{corr}, is shifted cathodically upon AFIF addition. The open circuit potential curves are shown in Figures 38 and 39. Several basic facts pertaining to the corrosion of aluminum are useful in interpreting these results. An aluminum metal surface forms a protective aluminum oxide passive film layer upon exposure to water, with or without the presence of dissolved O_2. Also, aluminum corrodes at both acidic and basic pH values, with a relatively reduced response from pH 4-8. The presence of chloride anions causes pitting corrosion, with other added anions sometimes performing as pitting corrosion inhibitors.

Thus, even though passive film formation may be apparent in a PAP experiment with a given corrosion inhibitor candidate, it must still be checked against the control in water with 0% inhibitor. In this case, the criterion for effective corrosion protection depends upon the relative magnitude of the passive current density values (the lower the better).

The results for AFIF and 2024 aluminum may be interpreted within this general scheme. The control run shows passive film formation of aluminum oxide in the presence of water, at a relatively low passive current density. The addition of AFIF also shows passive film formation, although at a much higher passive current density value. The control sample performs better as

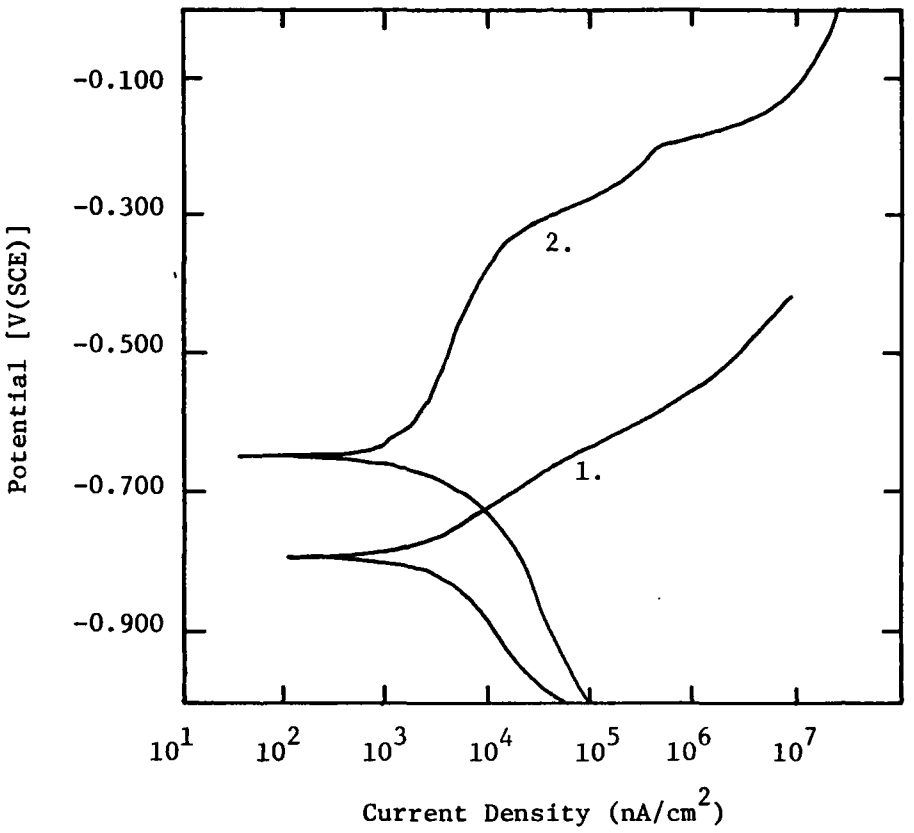

Figure 35. Potential vs. current density for potentiodynamic polarization experiment with 4340 steel in 5% NaCl electrolyte solution: (1) control; (2) with Formulation 471-9.

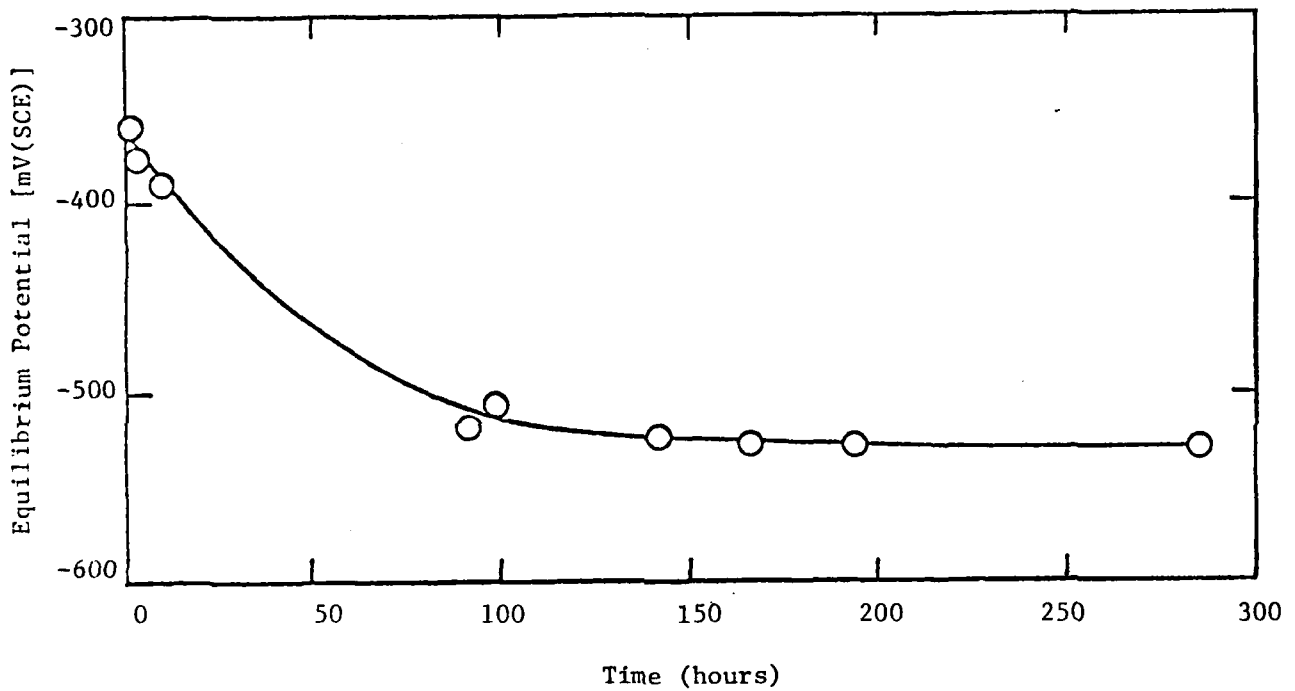

Figure 36. Equilibrium potential vs. time for chronopotentiometric experiment with 4340 steel in a 5% NaCl solution containing Formulation 471-9.

TABLE 2. POTENTIODYNAMIC ANODIC POLARIZATION EXPERIMENTS ON CORROSION INHIBITORS FOR 2024 ALUMINUM

Inhibitor	Concentration	pH	E_{corr} mV(SCE)	I_{pass} A/m^2	Width of Passive Region mV(SCE)	Open Circuit Potential mV(SCE)	Comments
AFIF	0.0%	6.2	-1090±10	-	-	-	control curve
AFIF	-	9.8	-1250±10	-	-	-	-
AFIF	-	9.8	-1140±10	-	-	?	30 min exposure
$Na_2B_4O_7$	0.35%	8.5	-1070±20	-	-	?	difficult to interpret
$Na_2Si_3 \cdot 9H_2O$	0.01%	10.2	? current loops	-	-	-	no exposure effect observed
$NaNO_2$	0.05%	6.3	-1020±10	0.0145	276	?	-
$NaNO_3$	0.10%	6.2	- 880±10	-	-	-620	-
$(NaPO_3)_6$	20 ppm	7.4	-1090±10	-	-	-	no exposure effect observed
β-mercaptobenzothiazole	10 ppm	6.2	-1130±10	-	-	-	-
hydroxyquinoline	0.10%	6.2	-1110±10	-	-	-	-
2-propyn-1-ol	1.0%	5.4	- 800±20	-	-	-	-
$(NH_4)_2MoO_4$	0.10%	8.1	- 770±20	-	-	-	-
NH_4NO_2	0.10%	8.1	- 700±20	-	-	-	offers some corrosion protection

(continued)

TABLE 2. (continued).

Inhibitor	Concentration	pH	E_{corr} mV(SCE)	I_{pass} A/m^2	Width of Passive Region mV(SCE)	Open Circuit Potential mV(SCE)	Comments
$MgSiF_6 \cdot 6H_2O$	1.00%	3.1	-1300±20	-	-	-	-
$NH_4HB_4O_2 \cdot 3H_2O$	0.33%	8.7	-720±20	-	-	-	-
1-ethynyl-1-cyclohexanol	1.00%	6.2	-700±20	-	-	-	offers some corrosion protection
3,5-dimethyl-1-hexyne-3-ol	1.00%	4.4	-760±20	-	-	-	offers some corrosion protection
sarcosine	1.00%	5.9	-710±20	-	-	-	offers some corrosion protection
sodium sarcosine	1.0%	10.6	-990±20	-	-	-	-
sodium cinnamate	0.10%	8.7	-800±20	-	-	-	offers some corrosion protection
potassium cinnamate	1.00%	7.1	-820±20	0.0081	188	-	-
mercaptoacetic acid	1.0%	4.3	-990±20	-	-	-	-
sodium molybdate	1.0%	8.8	-1150±20	0.0465	350	-	-

(continued)

AD-A144 311 ENCAPSULATED MULTIFUNCTION CORROSION INHIBITIVE PRIMER 2/4
(U) GULF SOUTH RESEARCH INST NEW ORLEANS LA
D V GUPTA ET AL. NOV 83 AFWAL-TR-83-4123
UNCLASSIFIED F33615-79-C-5061 F/G 11/3 NL

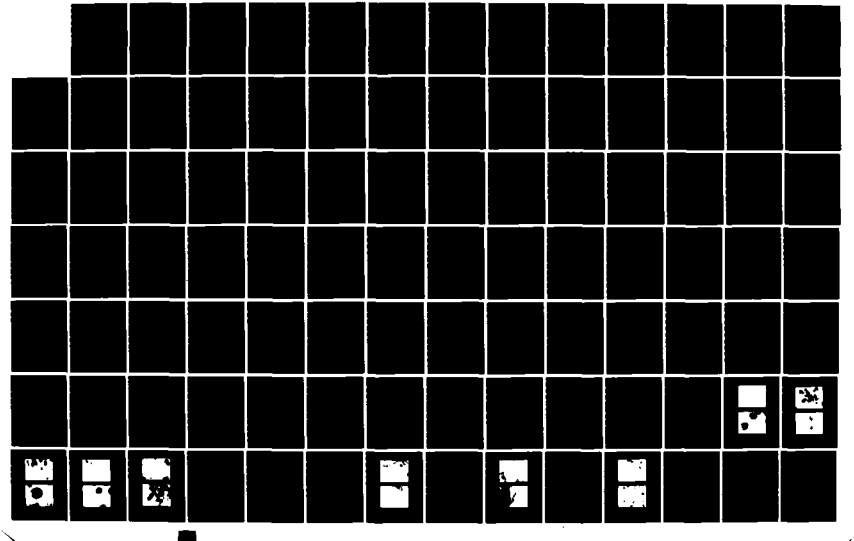

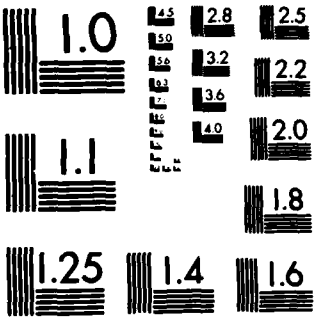

TABLE 2. (continued).

Inhibitor	Concentration	pH	E_{corr} mV(SCE)	I_{pass} A/m^2	Width of Passive Region mV(SCE)	Open Circuit Potential mV(SCE)	Comments
471-1	-	8.3	-580±20	-	-	-	-
471-3	-	7.7	-610±20	-	-	-	-
471-4	-	8.5	-790±20	-	-	-	-
471-5	-	6.2	-800±20	-	-	-	-
471-6	-	8.5	-850±20	-	-	-620	-
471-7	-	7.0	-640±20	-	-	-	-
471-8	-	7.1	-950±20	-	-	-620	-
471-9	-	7.0	-900±20	-	-	-	-

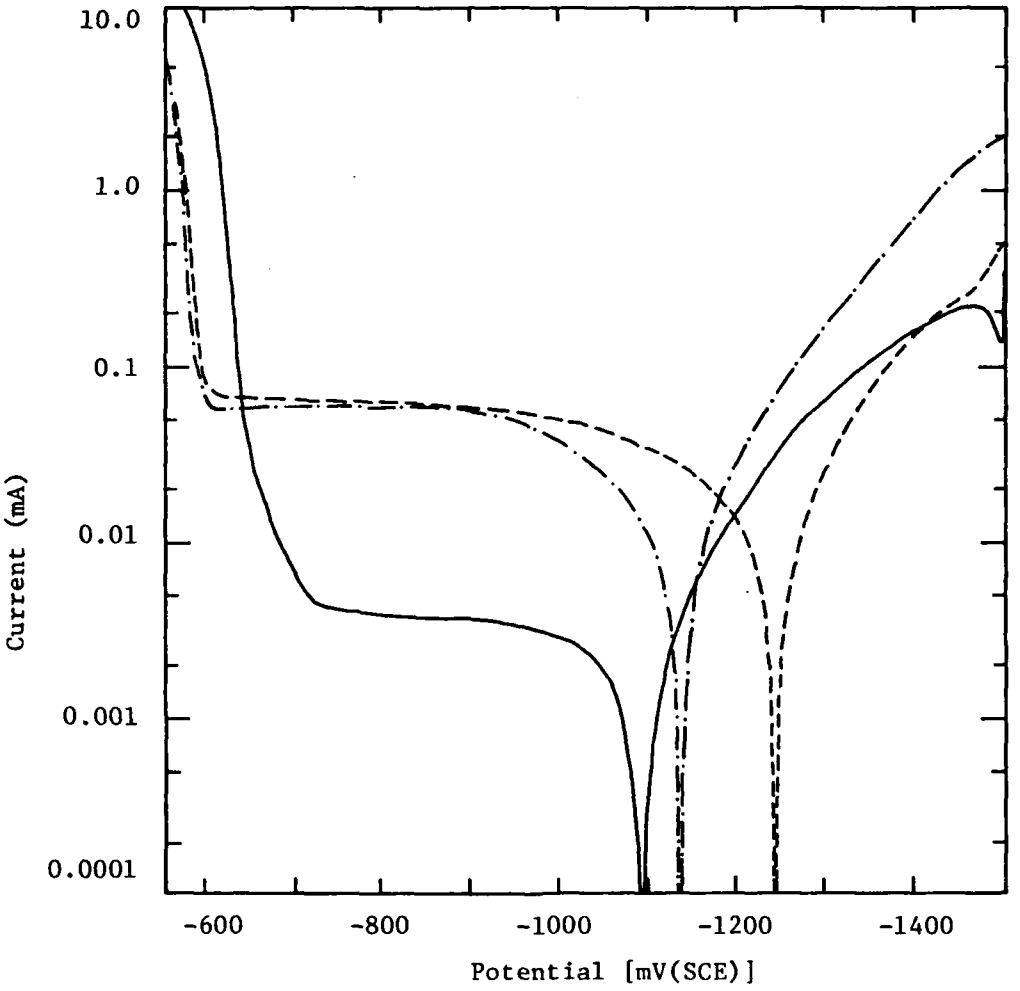

Figure 37. Current vs. potential for potentiodynamic polarization experiment with alloy 2024 of 1.267 cm^2 surface area in 5% NaCl electrolyte solution: ____ control; - - - with Air Force inhibitor formulation; ____ · ____ after 30 min exposure to Air Force inhibitor formulation.

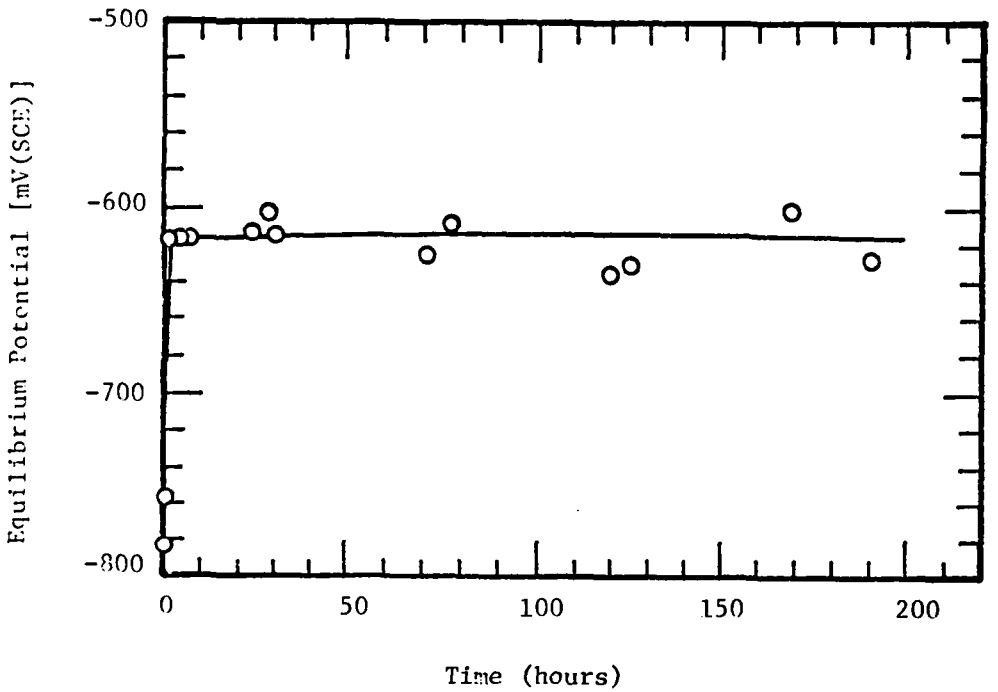

Figure 38. Equilibrium potential vs. time for chronopotentiometric experiment with aluminum alloy 2024 in a 5% NaCl solution.

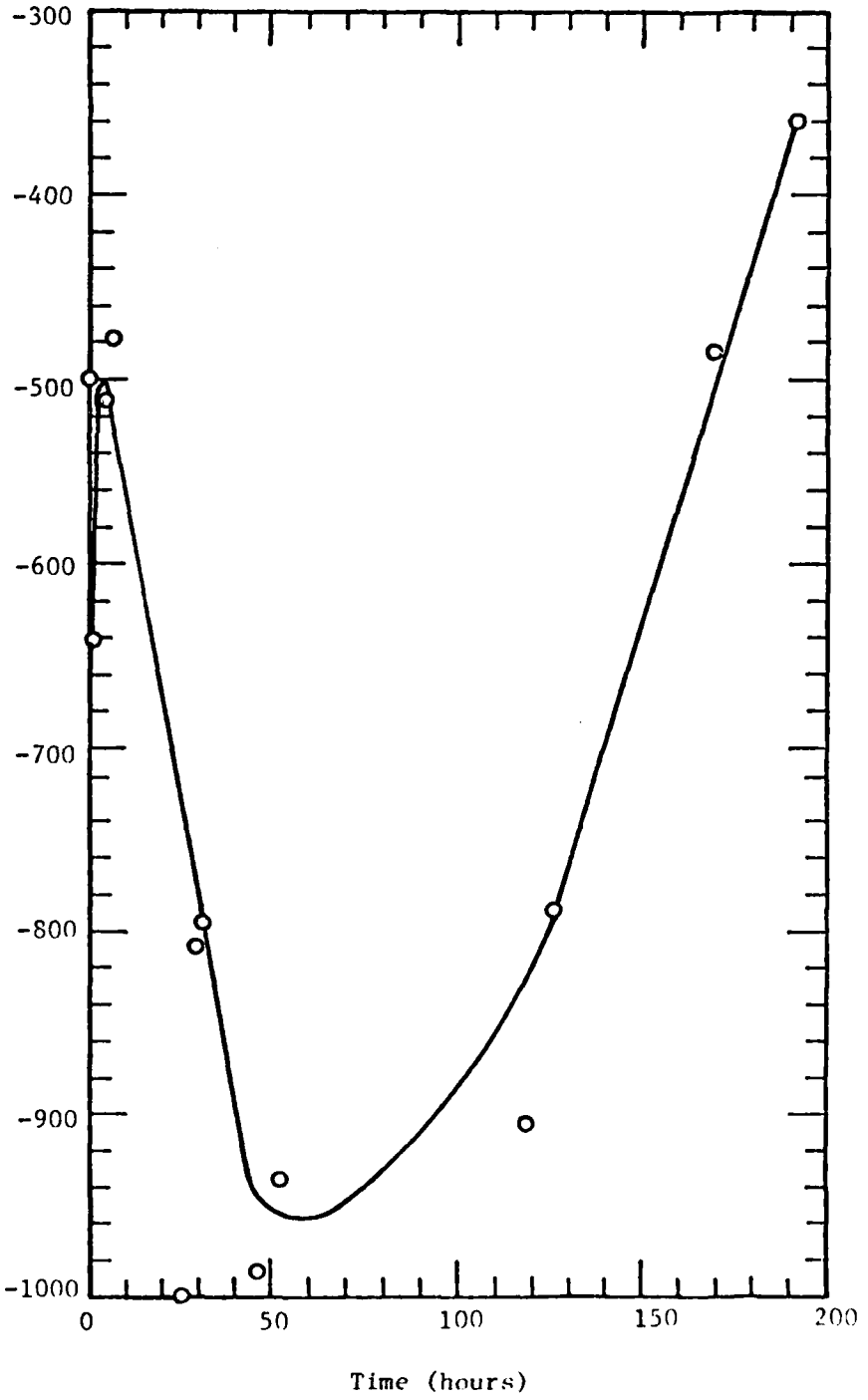

Figure 39. Equilibrium potential vs. time for chronopotentiometric experiment with aluminum alloy 2024 in a 5% NaCl solution containing AFIF.

a corrosion inhibitor than does the AFIF. Most likely, the increase in pH upon AFIF addition disrupts (or dissolves) a portion of the aluminum oxide film, thus allowing metal contact with the environment and promoting the anodic process of metal oxidation and dissolution. There would be no advantage in using AFIF in this type of environment. AFIF cannot be considered a corrosion inhibitor for aluminum 2024 in aqueous contact.

The PAP curve for $Na_2B_4O_7 \cdot 10H_2O$ is shown in Figure 40 (open circuit potential curve in Figure 41). The results are similar to those for AFIF, with the passive current density for the control being less than for the $Na_2B_4O_7 \cdot 10H_2O$ addition. This material is not a corrosion inhibitor for aluminum 2024.

The PAP curve for $Na_2SiO_3 \cdot 9H_2O$ is given in Figure 42. The current loops observed render this system highly questionable for corrosion protection relative to the control. No real passive layer is observed with this material.

The PAP curve for $NaNO_2$ is shown in Figure 43 (open circuit potential curve in Figure 44). This compound appears to be an effective corrosion inhibitor, with a reduced value of the passive current density I_p observed.

The PAP curve for $NaNO_3$ is given in Figure 45. No improvement over the control is observed with this material (the open circuit potential curve is shown in Figure 46).

The PAP curve for $(NaPO_3)_6$ is given in Figure 47, and the response curve is essentially superimposed over the control curve; no effect.

The PAP curve for 2-mercaptobenzothiazole is shown in Figure 48, and it is basically equivalent to the control curve. No improvement is observed with this material.

b. Hydroxyquinoline. The PAP curve for hydroxyquinoline is shown in Figure 49. No effect may be observed with this compound, when compared to the control.

c. 2-Propyn-1-ol. The PAP curve for 2-propyn-1-ol is given in Figure 50. This compound does not perform as well as the control, and may not be considered as a corroson inhibitor for 2024 aluminum.

d. $(NH_4)_2MoO_4$). The PAP curve for $(NH_4)_2MoO_4$ is shown in Figure 51. This compound does not passivate the metal, and the metal oxidation process is enhanced over the control over much of the potential region. This com-

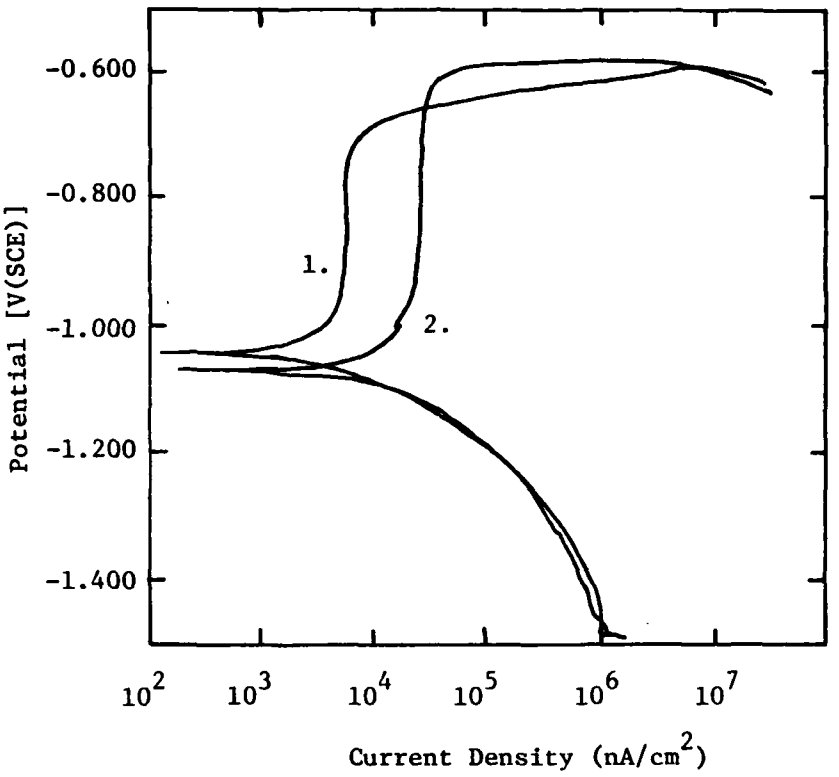

Figure 40. Potential vs. current density for potentiodynamic polarization experiment with aluminum alloy 2024-T3 in 5% NaCl electrolyte solution: (1) control; (2) with 0.35% $Na_2B_4O_7 \cdot 10H_2O$.

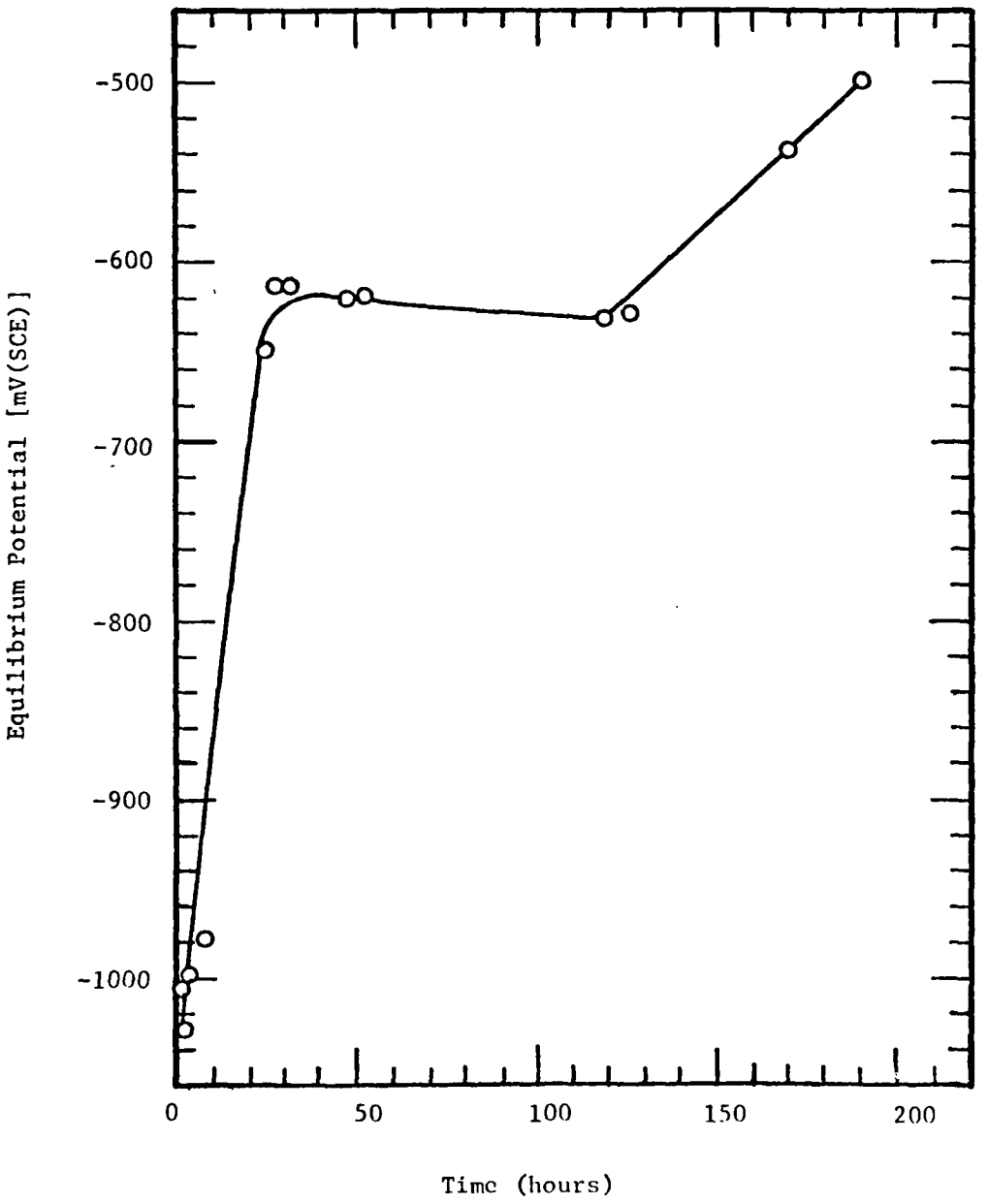

Figure 41. Equilibrium potential vs. time for chronopotentiometric experiment with aluminum alloy 2024 in a 5% NaCl solution containing 0.35% $Na_2B_4O_7 \cdot 10\ H_2O$.

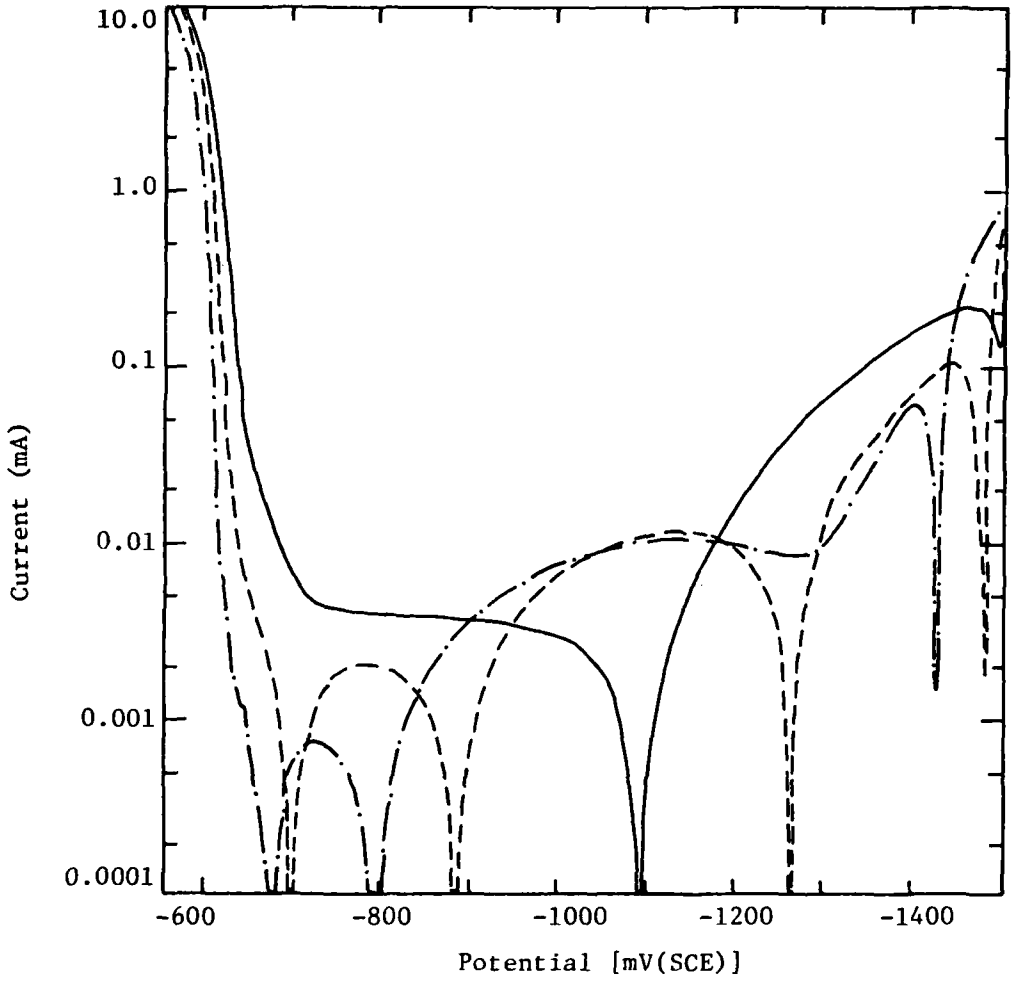

Figure 42. Potential vs. current for potentiodynamic polarization experiment with alloy 2024 sample of 1.267 cm^2 surface area in 5% NaCl electrolyte solution: ____ control; - - - with 0.01% $Na_2SiO_3 \cdot 9H_2O$ inhibitor; ___ . ___ after 30 min exposure to inhibitor.

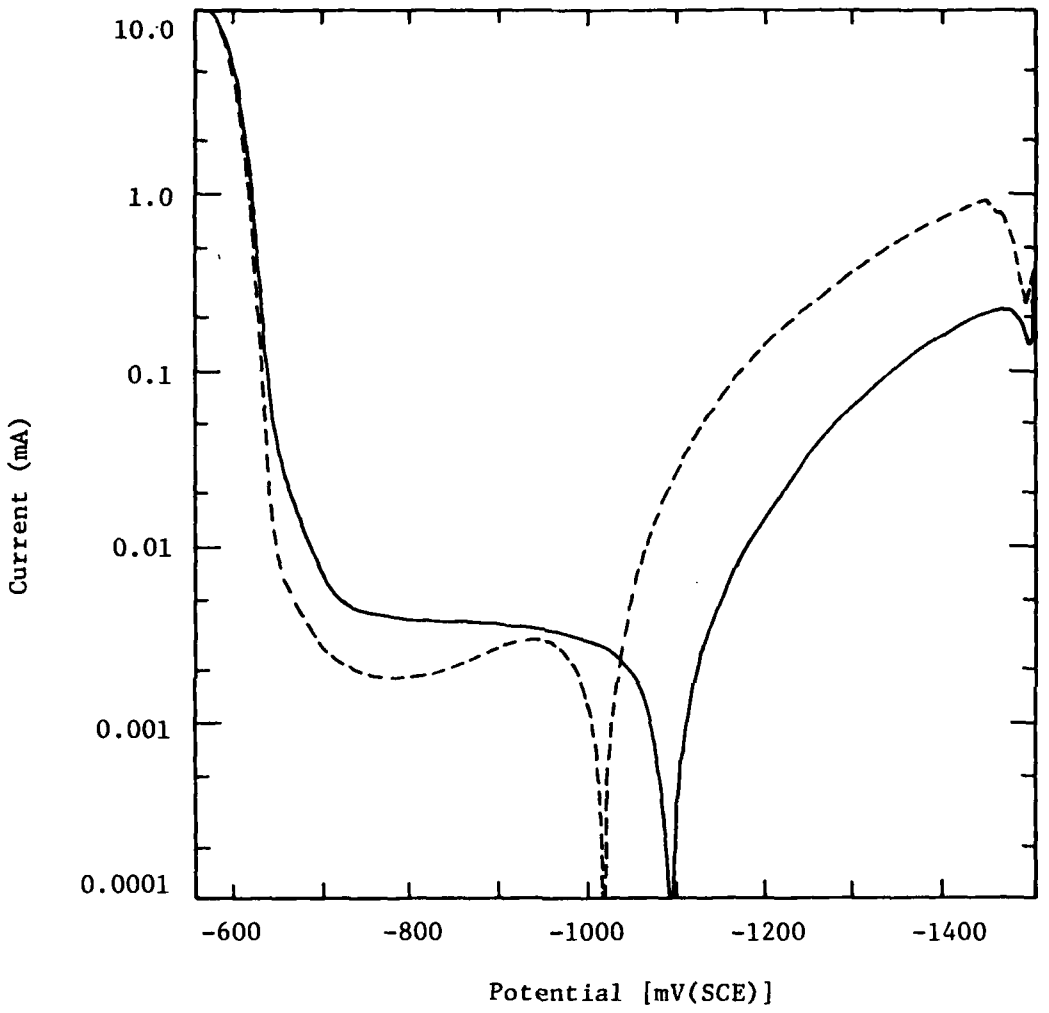

Figure 43. Potential vs. current for potentiodynamic polarization experiment with alloy 2024 of 1.267 cm^2 surface area in 5% NaCl electrolyte solution: ____ control; - - - with 0.05% $NaNO_2$ inhibitor.

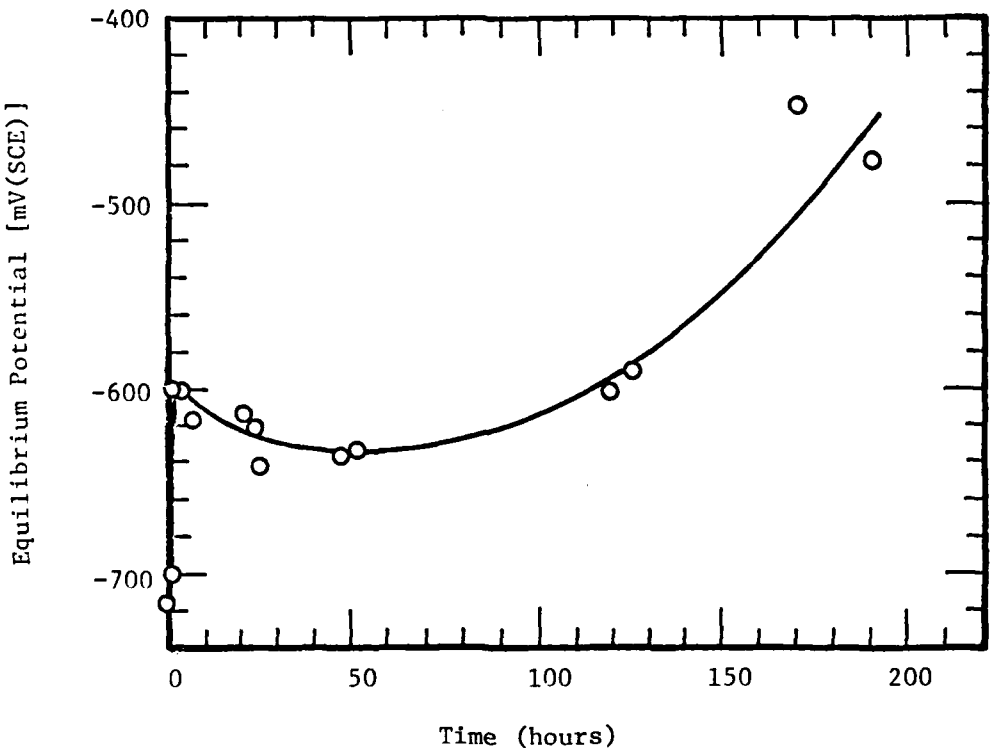

Figure 44. Equilibrium potential vs. time for chronopotentiometric experiment with aluminum alloy 2024 in a 5% NaCl solution containing 0.1% $NaNO_2$.

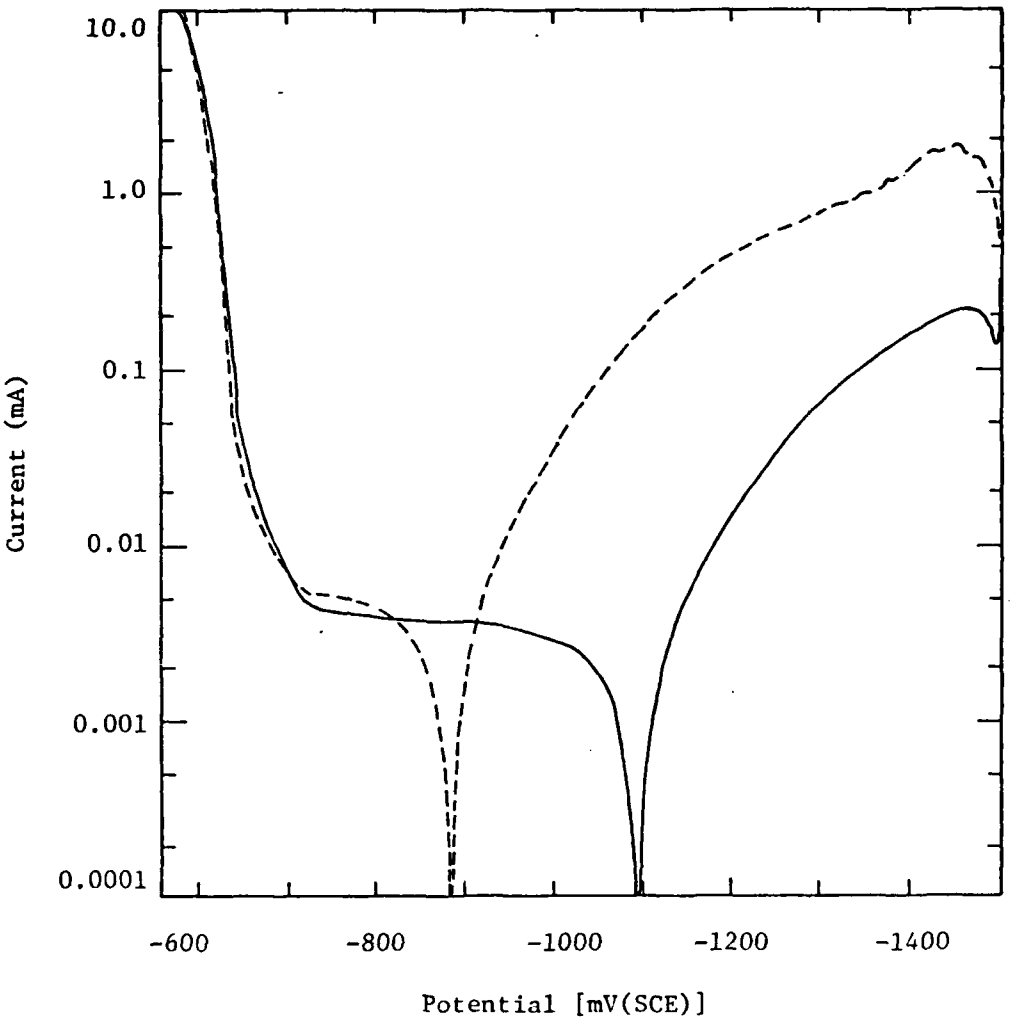

Figure 45. Potential vs. current for potentiodynamic polarization experiment with alloy 2024 sample of 1.267 cm^2 surface area in 5% NaCl electrolyte solution: —— control; - - - with 0.1% $NaHO_3$ inhibitor.

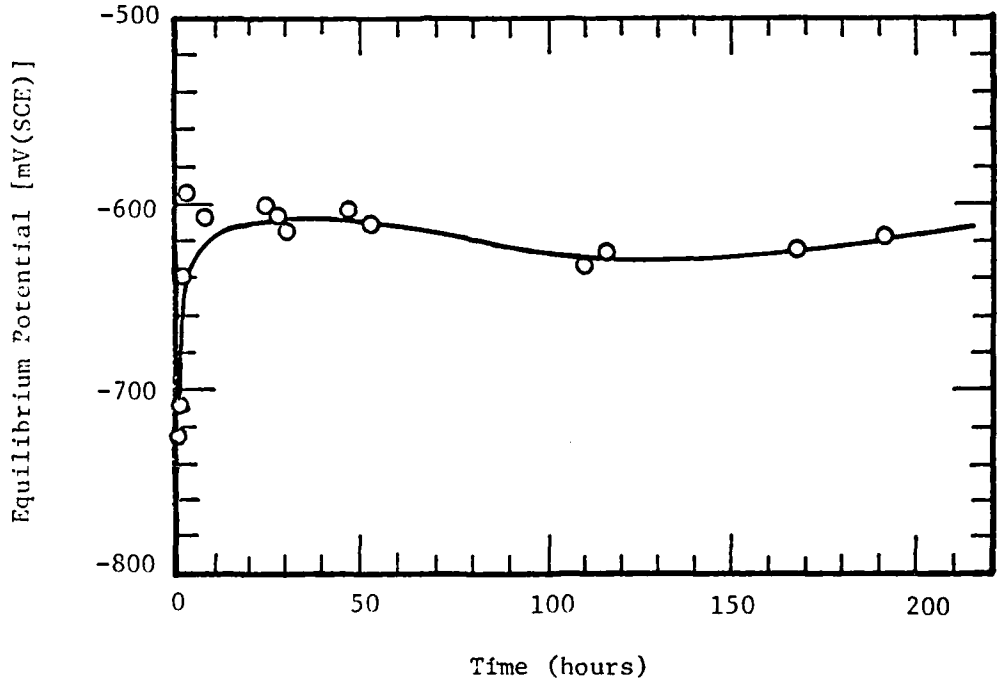

Figure 46. Equilibrium potential vs. time for chronopotentiometric experiment with aluminum alloy 2024 in a 5% NaCl solution containing 0.1% $NaNO_3$.

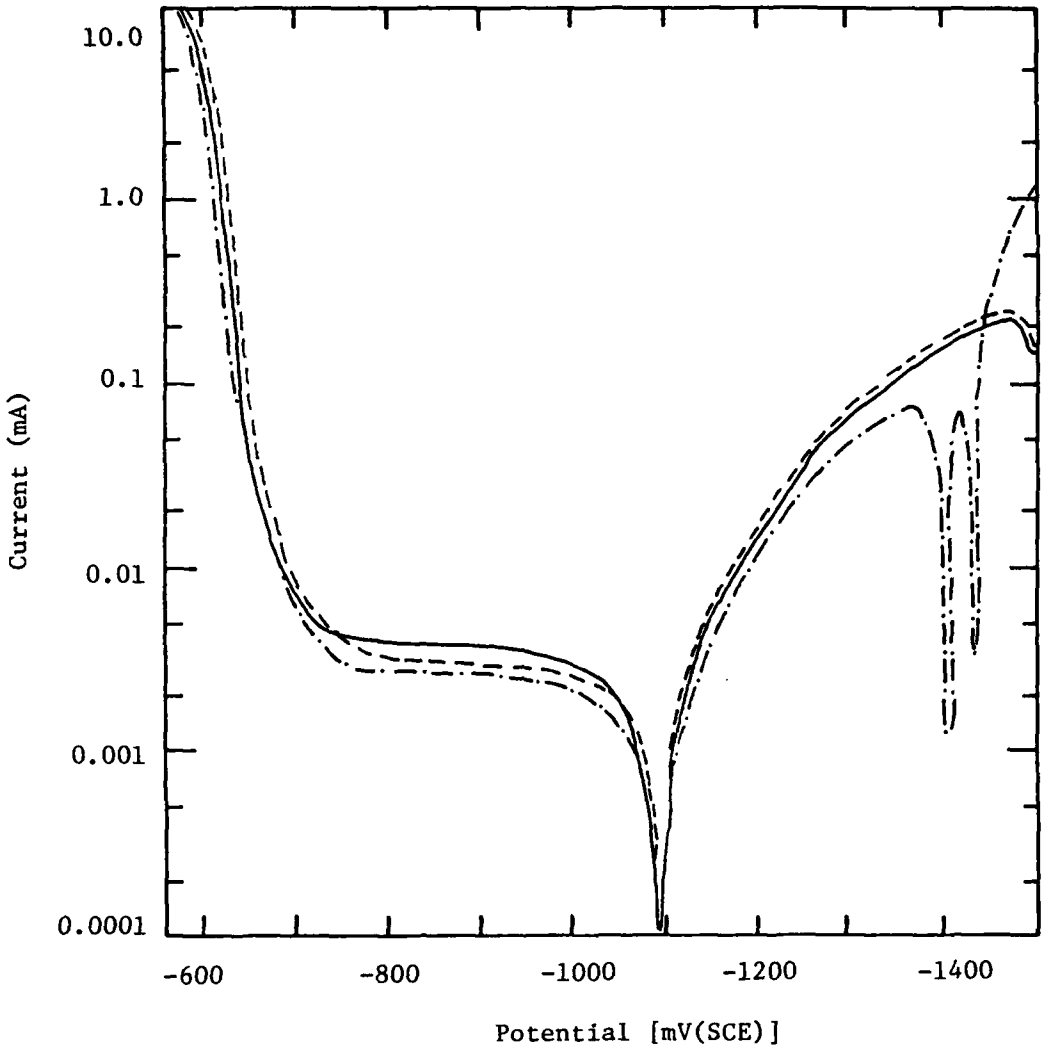

Figure 47. Potential vs. current for potentiodynamic polarization experiment with alloy 2024 sample of 1.267 cm^2 surface area in 5% NaCl electrolyte solution: —— control; - - - with 20 ppm $(NaPO_3)_6$ inhibitor; —— · —— after 30 min exposure to inhibitor.

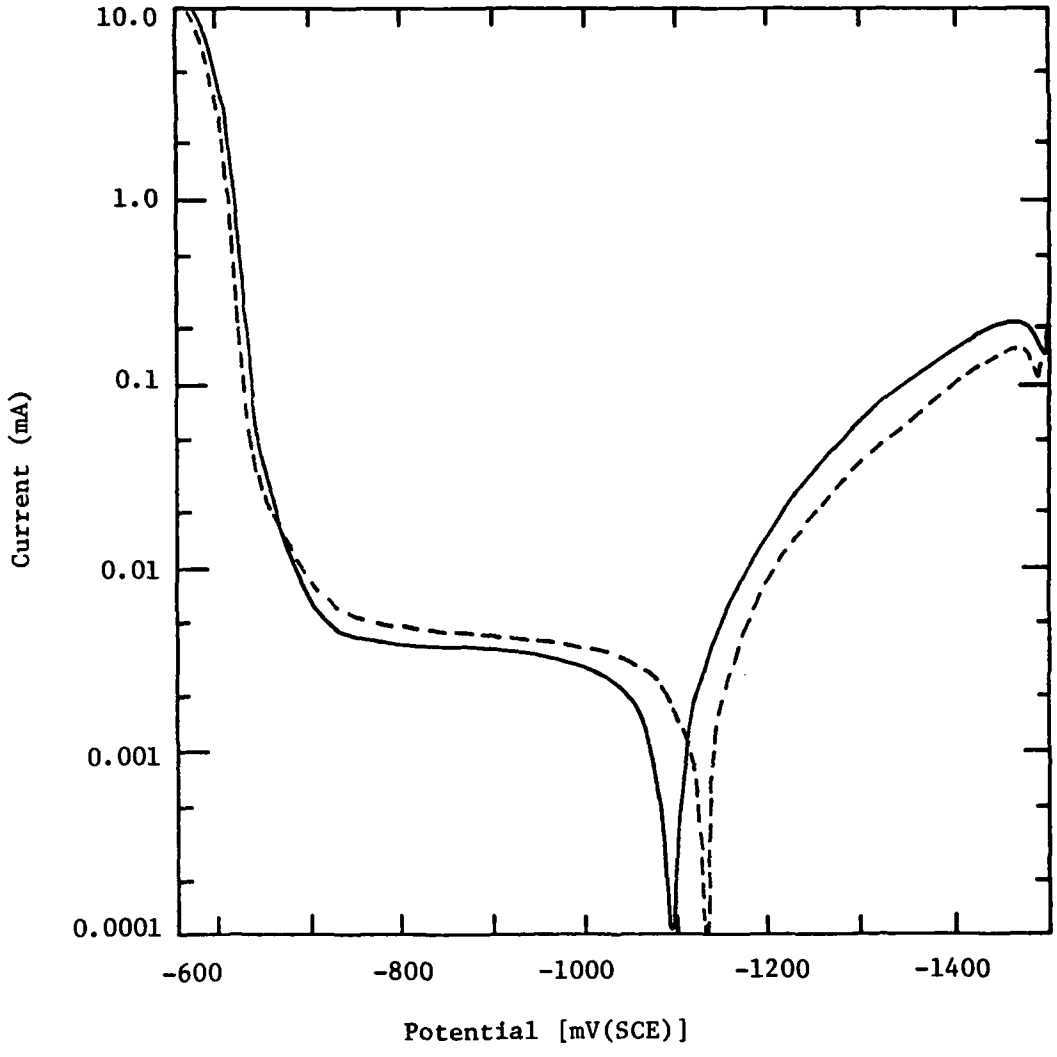

Figure 48. Potential vs. current for potentiodynamic polarization experiment with alloy 2024 sample of 1.267 cm^2 surface area in 5% NaCl electrolyte solution: —— control; - - - with 10 ppm 2-mercaptobenzothiazole.

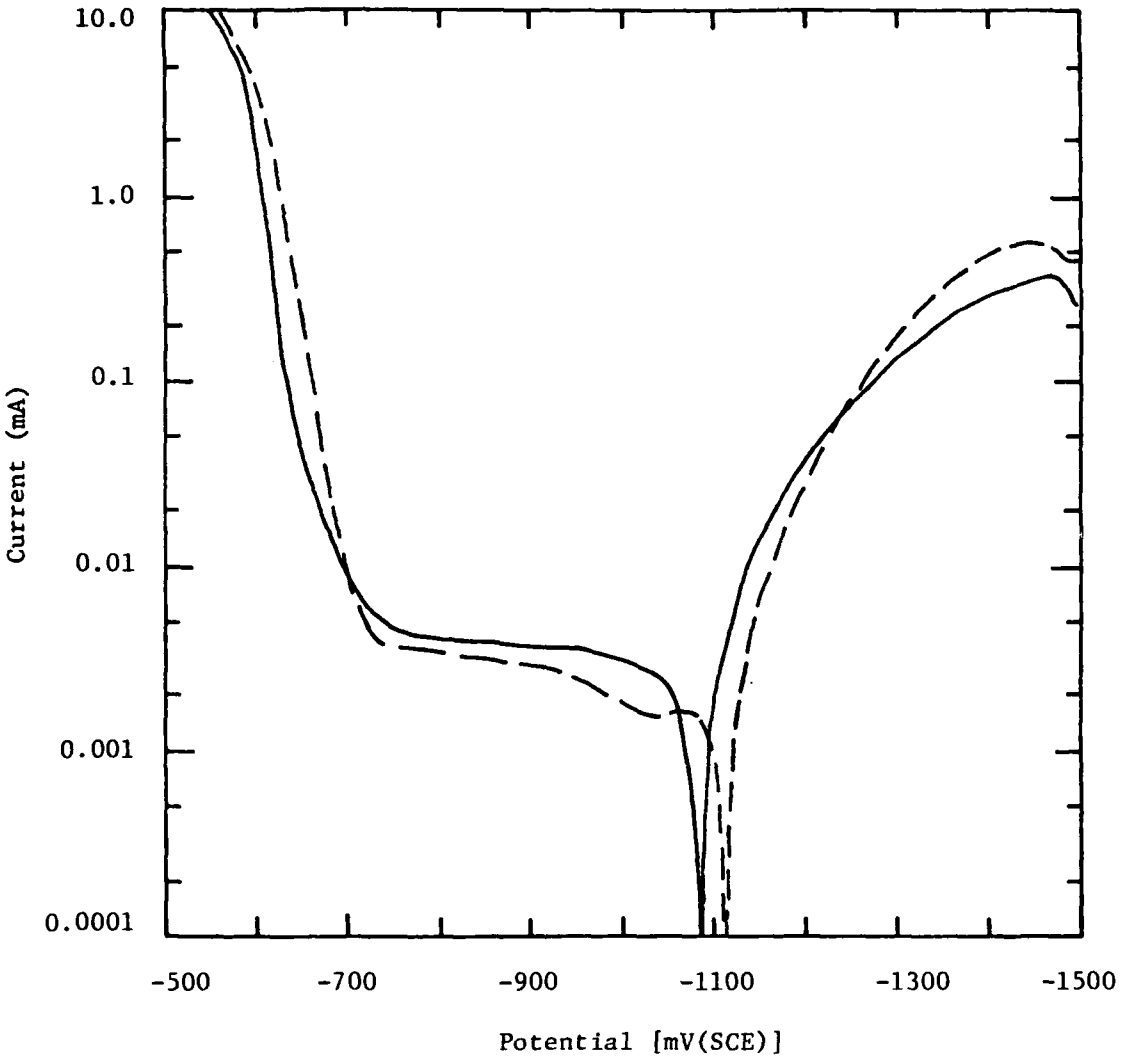

Figure 49. Current vs. potential for potentiodynamic polarization experiment with alloy 2024 of 1.267 cm^2 surface area in 5% NaCl electrolyte solution: ——— control; - - - with 0.1% hydroxyquinoline.

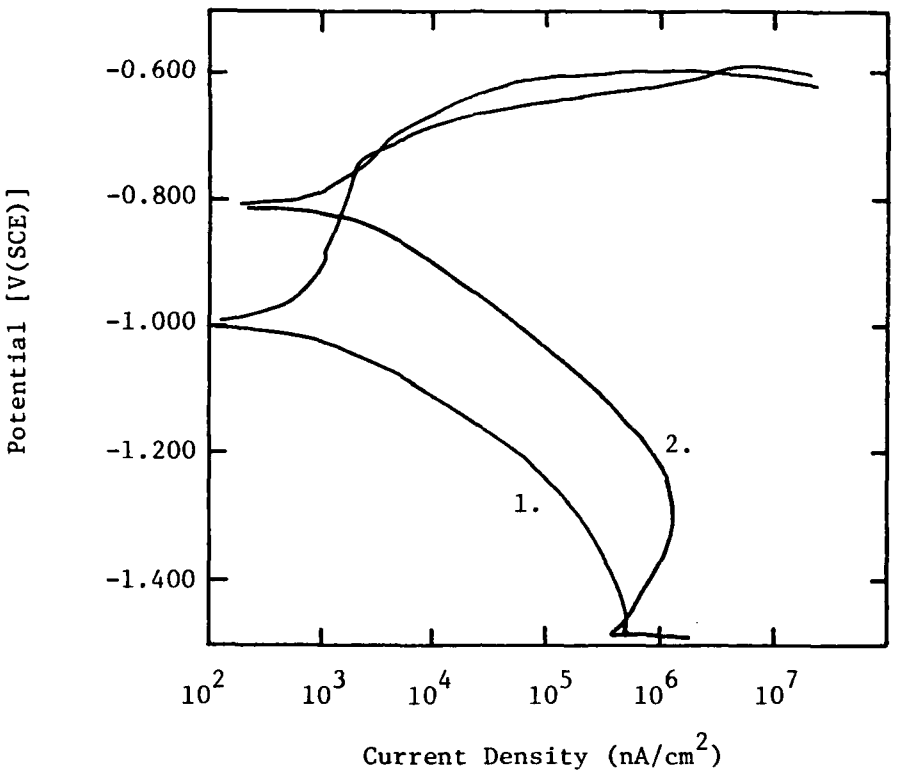

Figure 50. Potential vs. current density for potentiodynamic polarization experiment with aluminum alloy 2024-T3 in 5% NaCl electrolyte solution: (1) control; (2) with 1% 2-propyn-1-ol.

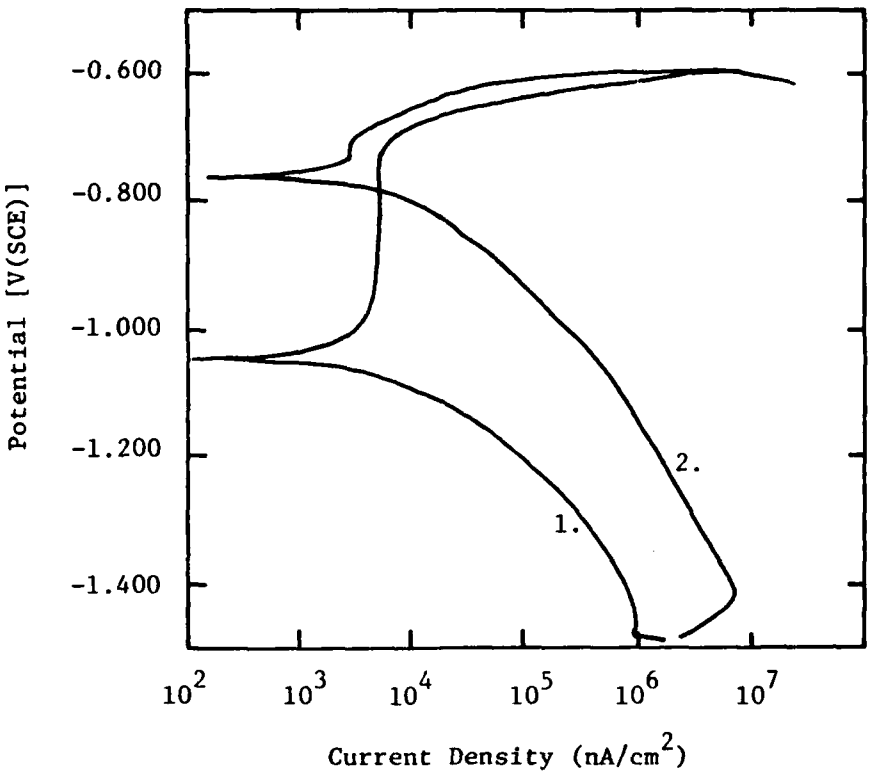

Figure 51. Potential vs. current density for potentiodynamic polarization experiment with aluminum alloy 2024-T3 in 5% NaCl electrolyte solution: (1) control; (2) with 0.1% $(NH_4)_2MoO_4$.

pound is not a corrosion inhibitor for this system.

e. NH_4NO_2. The PAP curve for NH_4NO_2 is given in Figure 52. For much of the potential region observed, -1400 mV to -700 mV, the control displays better corrosion inhibition than the NH_4NO_2. From -690 mV to -590 mV, a reduction in the anodic process is observed with NH_4NO_2, although this potential range is fairly narrow. It is possible that this material could function as a corrosion inhibitor for 2024 aluminum, depending on the open circuit potential of the system.

f. $MgSiF_6 \cdot 6H_2O$. The PAP curve for $MgSiF_6 \cdot 6H_2O$ is given in Figure 53. This compound drastically increases the anodic dissolution process over much of the potential range, and cannot be considered a corrosion inhibitor in any sense.

g. $NH_4HB_4O_7 \cdot 3H_2O$. The PAP curve for $NH_4HB_4O_7 \cdot 3H_2O$ is given in Figure 54. No improvement over the control may be observed. This compound is not a corrosion inhibitor for aluminum 2024.

h. 1-Ethynyl-1-cyclohexanol. The PAP curve for 1-ethynyl-1-cyclohexanol is shown in Figure 55. Although this compound is not a passivator for aluminum, the anodic process is reduced over the potential region from -850 mV to -600 mV, and E_{corr} is shifted in the anodic direction. This material could probably function as a corrosion inhibitor for aluminum, depending upon the open circuit potential.

i. 3,5-Dimethyl-1-hexyne-3-ol. The PAP curve for 3,5-dimethyl-1-hexyne-3-ol is given in Figure 56. This compound does not passivate the metal, though a reduction in the response curve is observed in the potential region from -950 mV to -800 mV. An oxidative process (mechanism unknown) occurs at -825 mV. This material might function as a corrosion inhibitor, depending upon the value of the open circuit potential.

j. Sarcosine. The PAP curve for sarcosine is shown in Figure 57. Sarcosine is not a passivator, but there is a reduction in the anodic dissolution process from -800 mV to -600 mV. E_{corr} is shifted anodically, also. This compound might be effective as a corrosion inhibitor for aluminum.

k. Sodium Sarcosine. The PAP curve for sodium sarcosine is shown in Figure 58. The control out-performs this compound by a wide margin. This material cannot be considered a corrosion inhibitor for aluminum.

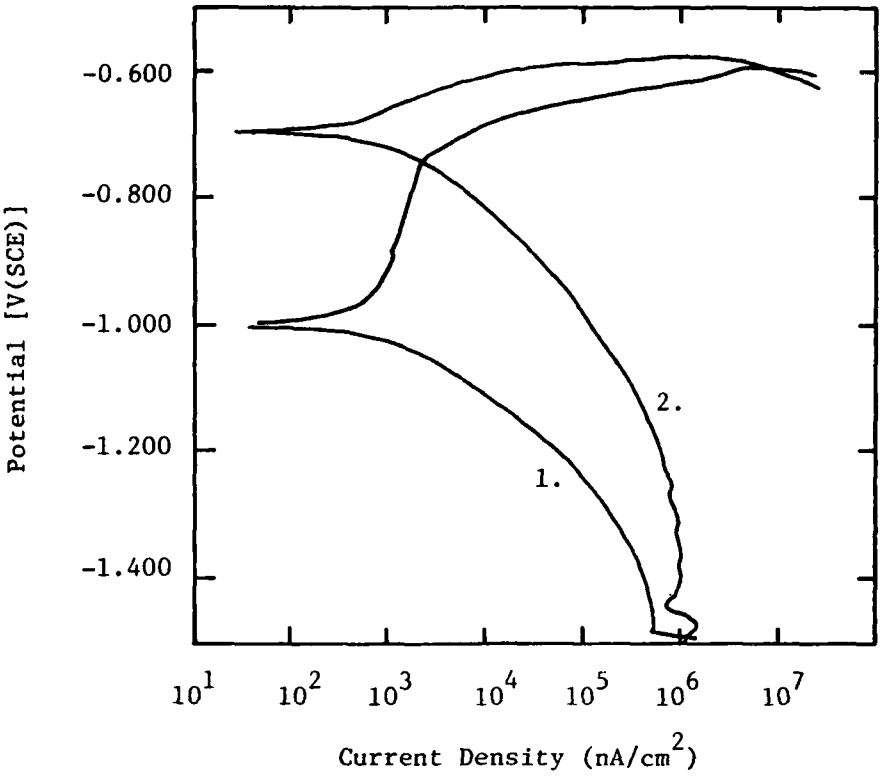

Figure 52. Potential vs. current density for potentiodynamic polarization experiment with aluminum alloy 2024-T3 in 5% NaCl electrolyte solution: (1) control; (2) with 0.1% NH_4NO_2.

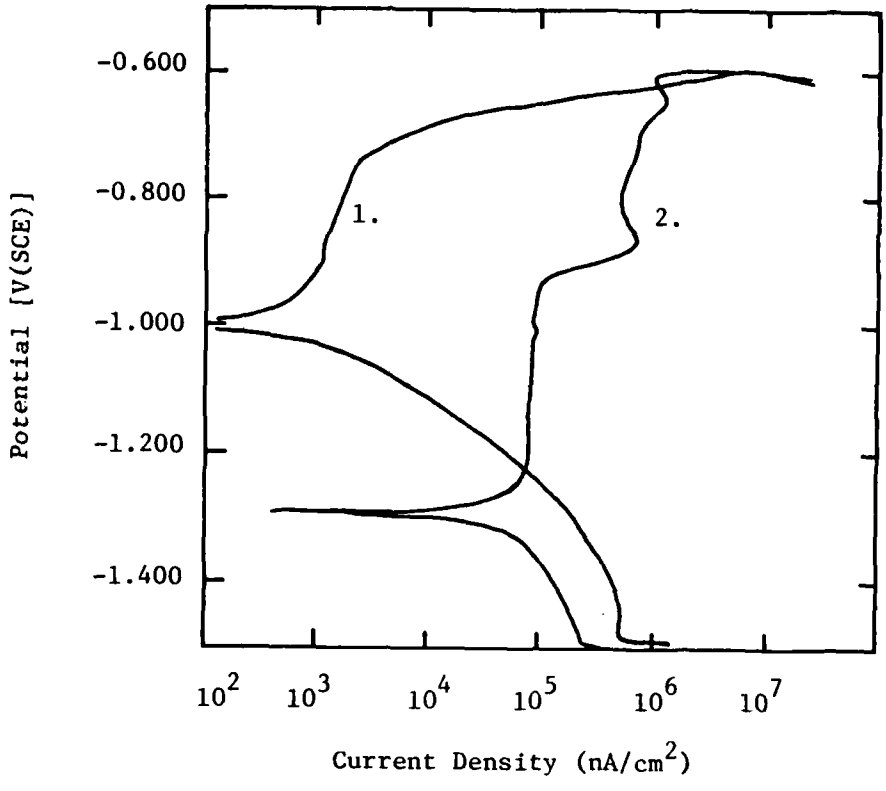

Figure 53. Potential vs. current density for potentiodynamic polarization experiment with aluminum alloy 2024-T3 in 5% NaCl electrolyte solution: (1) control; (2) with 1% $MgSiF_6 \cdot 6H_2O$.

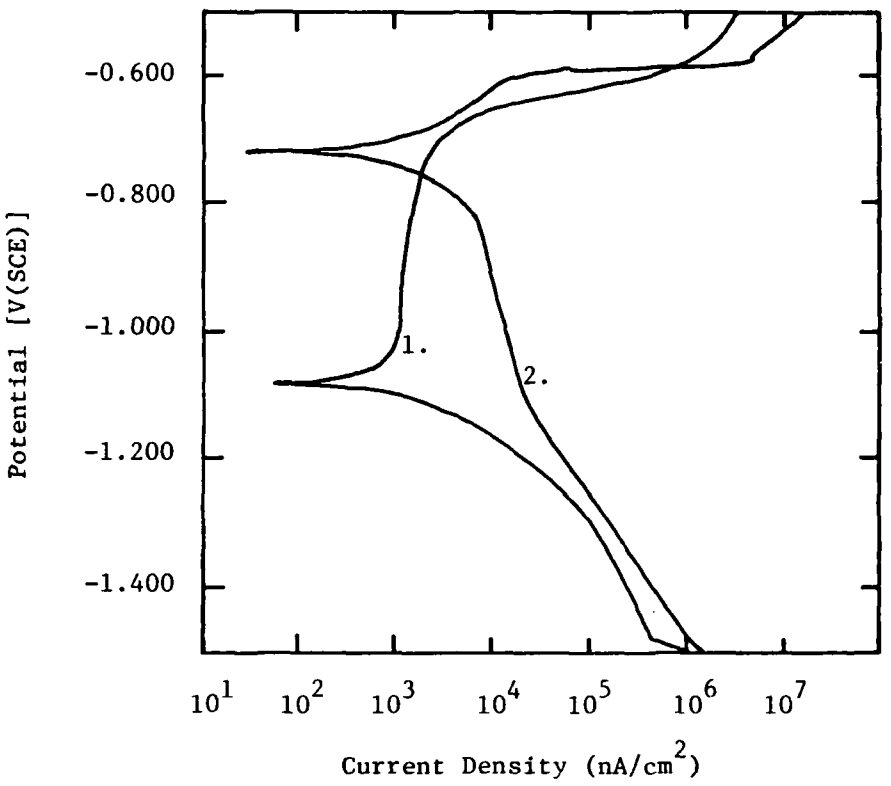

Figure 54. Potential vs. current density for potentiodynamic polarization experiment with aluminum alloy 2024-T3 in 5% NaCl electrolyte solution: (1) control; (2) 0.35% $NH_4HB_4O_7 \cdot 3H_2O$.

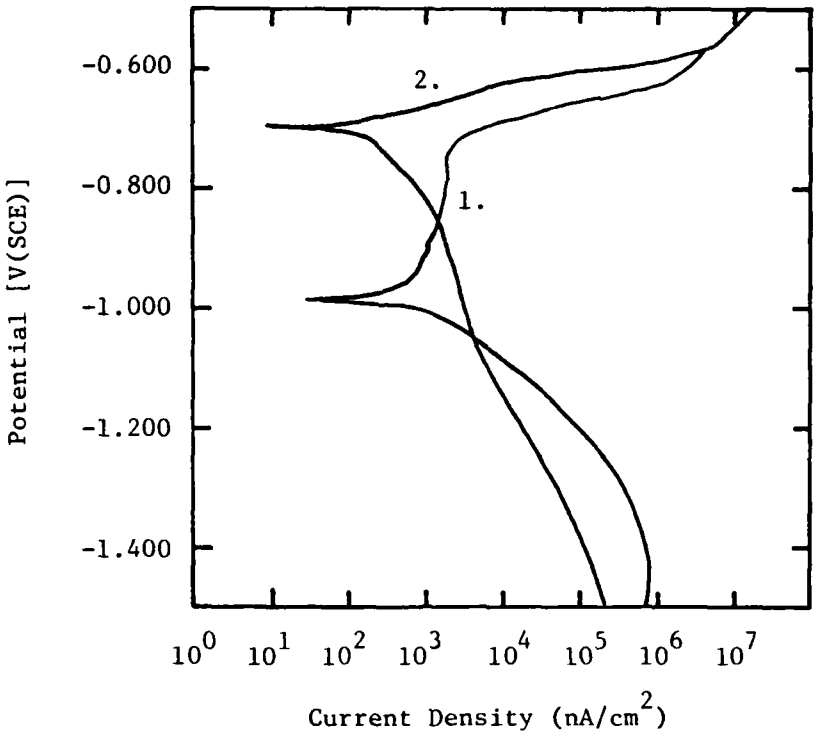

Figure 55. Potential vs. current density for potentiodynamic polarization experiment with aluminum alloy 2024 in 5% NaCl electrolyte solution: (1) control; (2) with 1% 1-ethynyl-1-cyclohexanol.

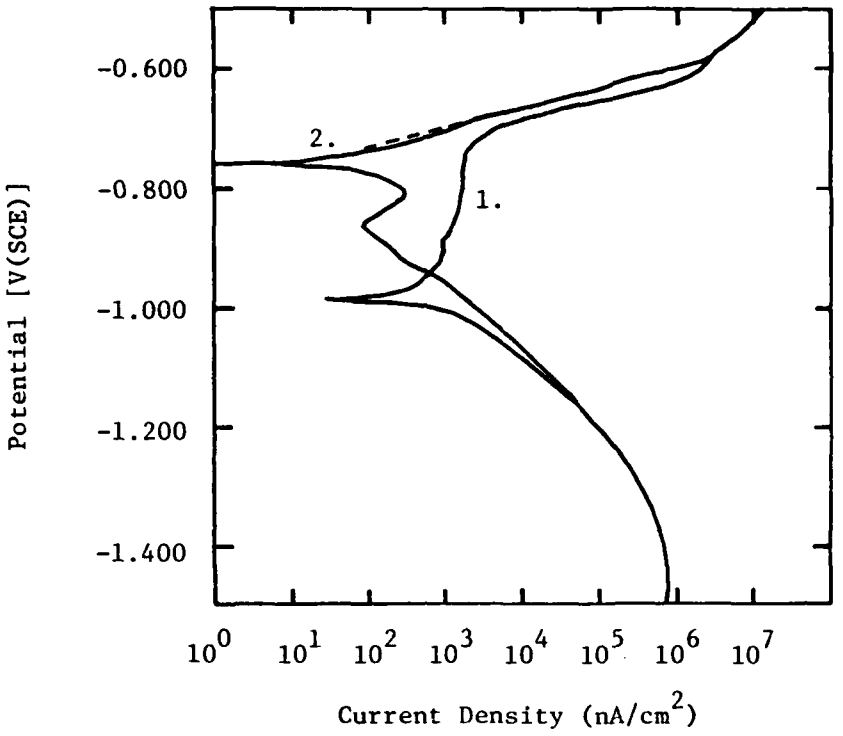

Figure 56. Potential vs. current density for potentiodynamic polarization experiment with aluminum alloy 2024 in 5% NaCl electrolyte solution: (1) control; (2) with 1% 3,5-dimethyl-1-hexyne-3-ol.

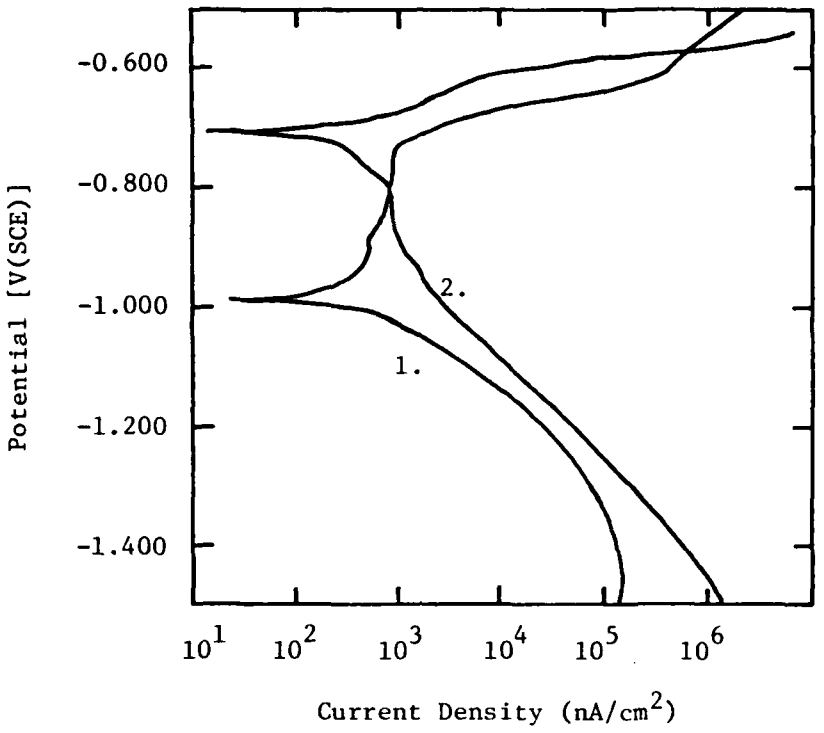

Figure 57. Potential vs. current density for potentiodynamic polarization experiment with aluminum alloy 2024 in 5% NaCl electrolyte solution: (1) control; (2) with 1% sarcosine.

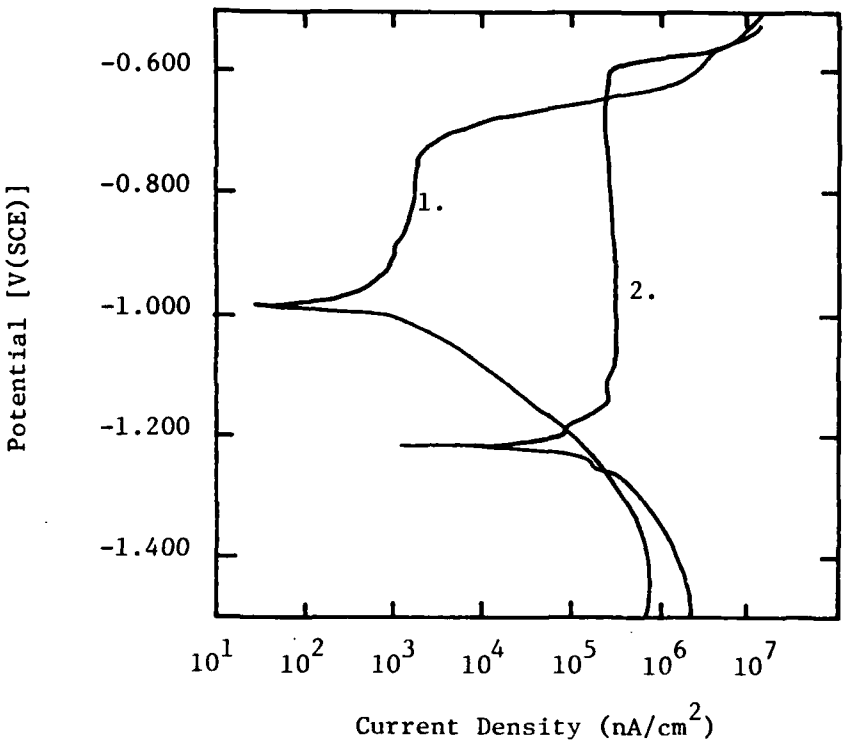

Figure 58. Potential vs. current density for potentiodynamic polarization experiment with aluminum alloy 2024 in 5% NaCl electrolyte solution: (1) control; (2) with 1% sodium sarcosine.

l. Sodium Cinnamate. The PAP curve for sodium cinnamate is given in Figure 59. Though not a passive film former, sodium cinnamate does provide a reduction of the anodic dissolution process in the potential range from -875 mV to -625 mV. However, the magnitude of this effect is not large, and may not be significant relative to experimental error.

m. Potassium Cinnamate. The PAP curve for potassium cinnamate is shown in Figure 60. The passive layer observed in the control is also observed with the inhibitor, and a reduction in the passive current density occurs. The metal oxidation and dissolution process is suppressed by use of this compound; it is an effective inhibitor for this system. E_{corr} is shifted in the anodic direction, into the passive zone.

n. Mercaptoacetic Acid. The PAP curve for mercaptoacetic acid is shown in Figure 61. Very little effect is observed from this inhibitor, although in the potential range from -700 mV to -600 mV there appears to be a slight reduction in the anodic process. No passivation is present, in any case. This compound would probably not work very well as a corrosion inhibitor.

o. Sodium Molybdate. The PAP curve for sodium molybdate is given in Figure 62. A reduction in the passive current density is observed, although E_{corr} is shifted cathodically relative to the control. In the transpassive region, the control performs better than the inhibitor. This compound could function as an effective corrosion inhibitor.

p. Formulations 471-1, 471-3 through 471-9. The PAP curves for these inhibitors are given in Figures 63-70 (open circuit potential curves are shown in Figures 71, 72, and 73). The analysis of these plots is essentially the same, since there is little variation in the response of the metal to these inhibitor candidates. E_{corr} for these mixtures is always shifted anodically, sometimes to a significant degree. For 471-1, 471-3 (1% 2-propyn-1-ol, 0.3% NH_3NO_2, and 0.7% $NaNO_2$), and 471-7 (0.5% potassium cinnamate, 0.1% $NaNO_2$, 0.02% $(NaPO_3)_6$, 0.05% $(NH_4)_2MoO_5$) there is no passivation barrier at all, even though one exists in the control, and the anodic oxidation and dissolution process is seriously increased over much of the potential region. For 475-4 (0.05% $NH_3HB_2O_7 \cdot 3H_2O$, 1% $NaNO_3$, 0.05% $NaNO_2$, 0.01% $NaSiO_3 \cdot 9H_2O$, 20 ppm $(NaPO_3)_6$, and 10 ppm mercaptobenzothiazole), 471-5, and 471-6 a passive layer is observed, although I_{pass} is larger than in the controls, and the width of the passive zone is narrowed. For 471-8

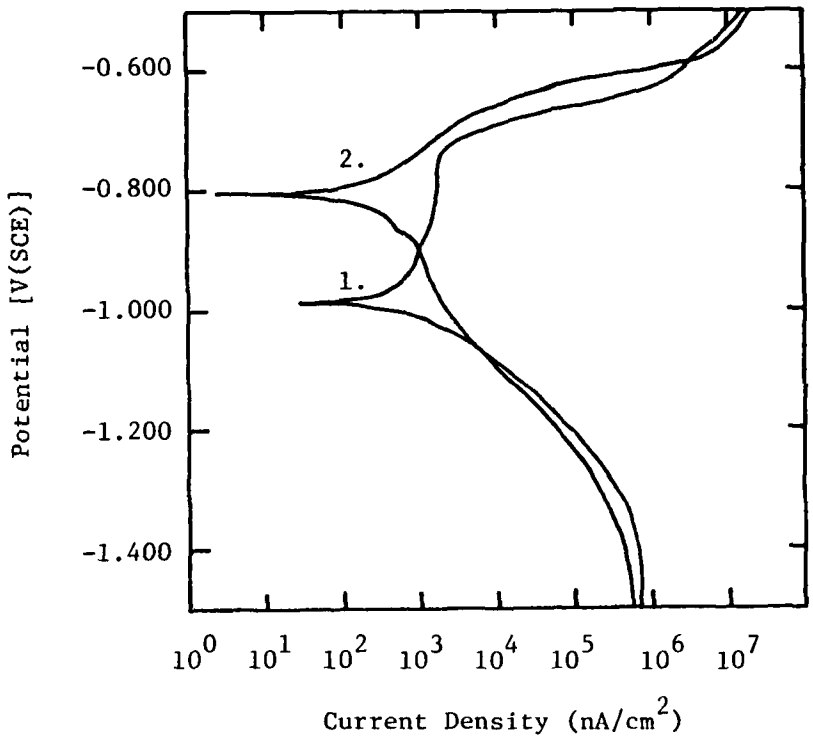

Figure 59. Potential vs. current density for potentiodynamic polarization experiment with aluminum alloy 2024 in 5% NaCl electrolyte solution: (1) control; (2) with 0.1% sodium cinnamate.

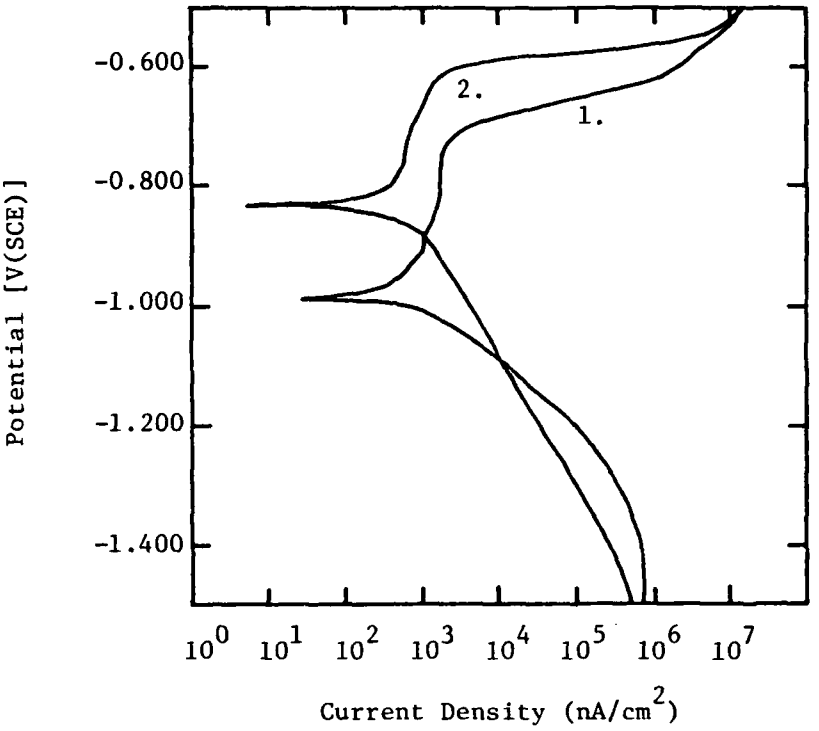

Figure 60. Potential vs. current density for potentiodynamic polarization experiment with aluminum alloy 2024 in 5% NaCl electrolyte solultion: (1) control; (2) with 1% potassium cinnamate.

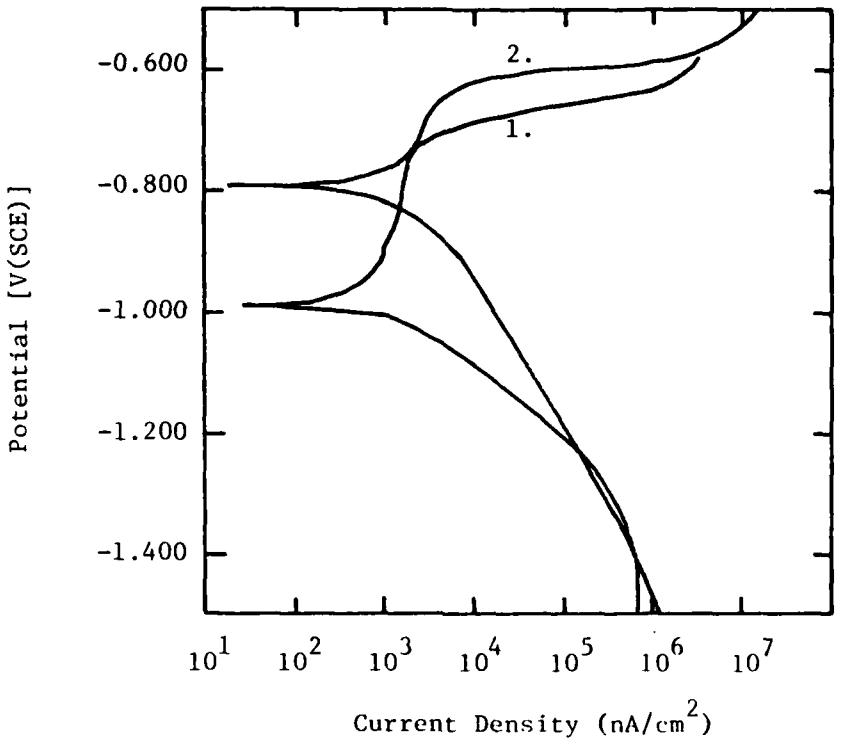

Figure 61. Potential vs. current density for potentiodynamic polarization experiment with aluminum alloy 2024 in 5% NaCl electrolyte solution: (1) control; (2) with 1% mercaptoacetic acid.

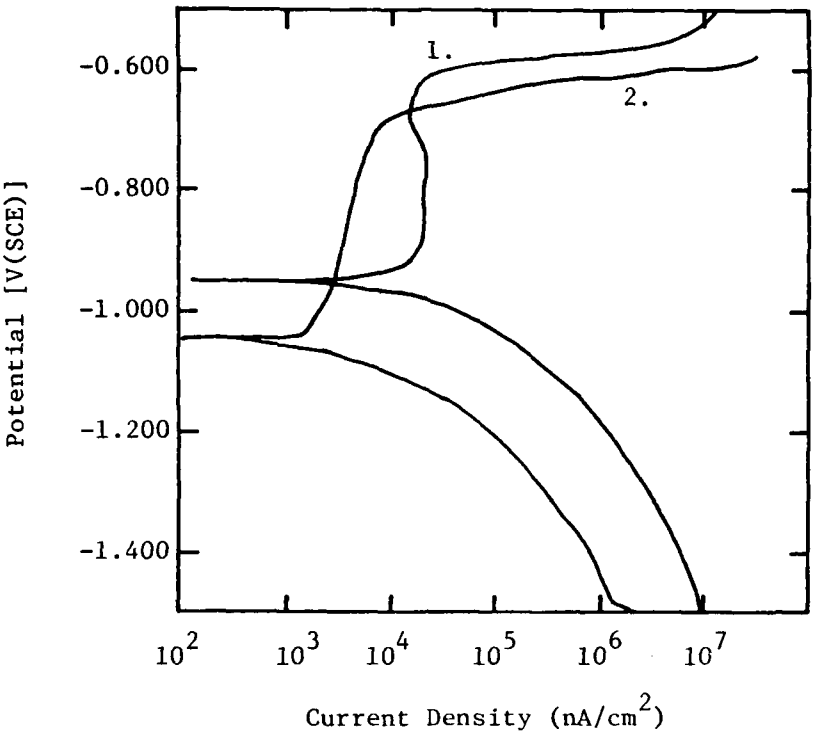

Figure 62. Potential vs. current density for potentiodynamic polarization experiment with aluminum alloy 2024 in 5% NaCl electrolyte solution: (1) control; (2) with 1% sodium molybdate.

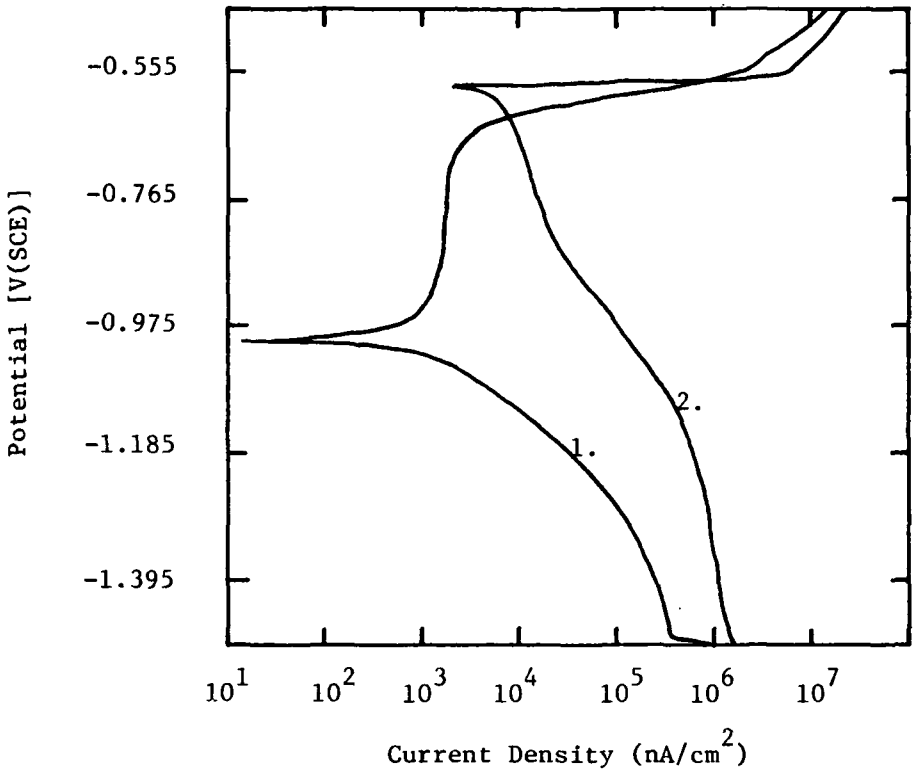

Figure 63. Potential vs. current density for potentiodynamic polarization experiment with aluminum alloy 2024-T3 in 5% NaCl electrolyte solution: (1) control; (2) with Formulation 471-1.

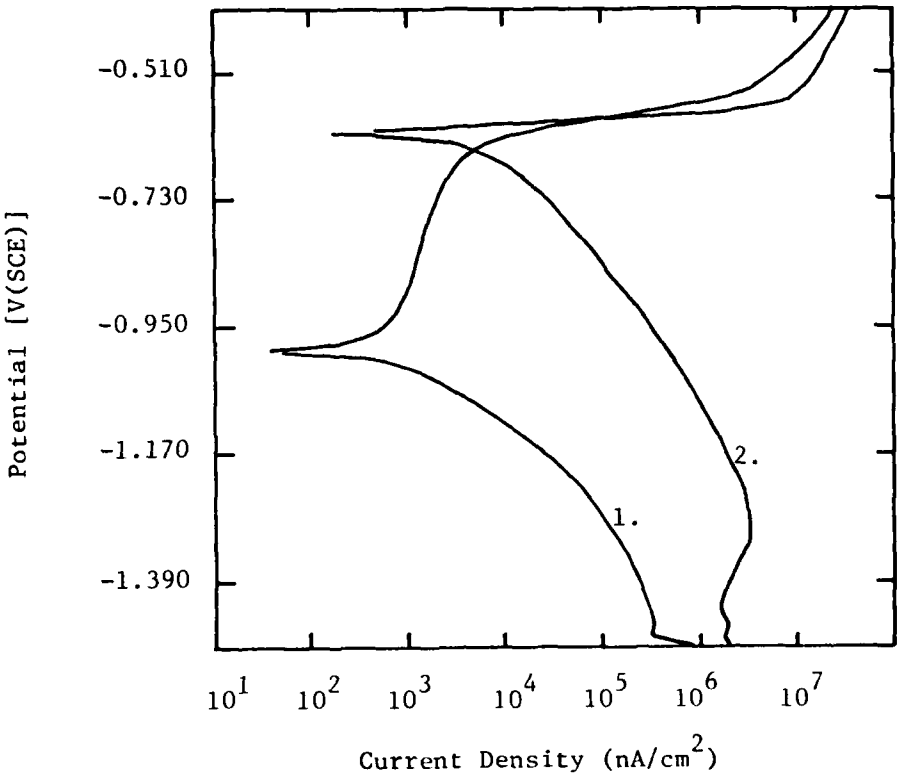

Figure 64. Potential vs. current density for potentiodynamic polarization experiment with aluminum alloy 2024-T3 in 5% NaCl electrolyte solution: (1) control; (2) with Formulation 471-3.

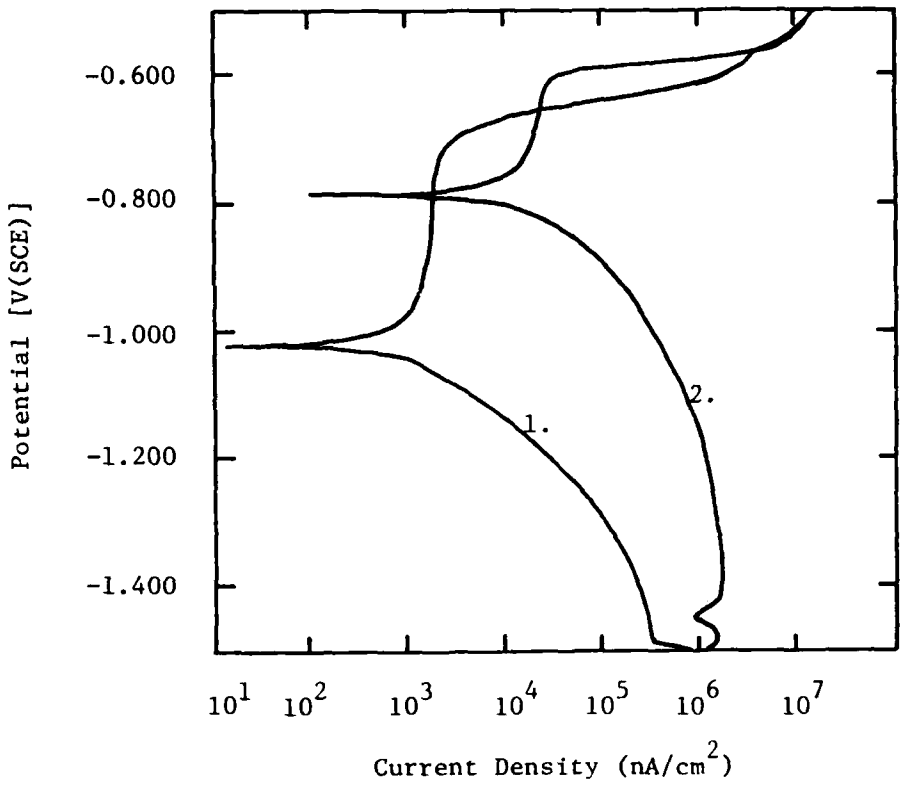

Figure 65. Potential vs. current density for potentiodynamic polarization experiment with aluminum alloy 2024-T3 in 5% NaCl electrolyte solution: (1) control; (2) with Formulation 471-4.

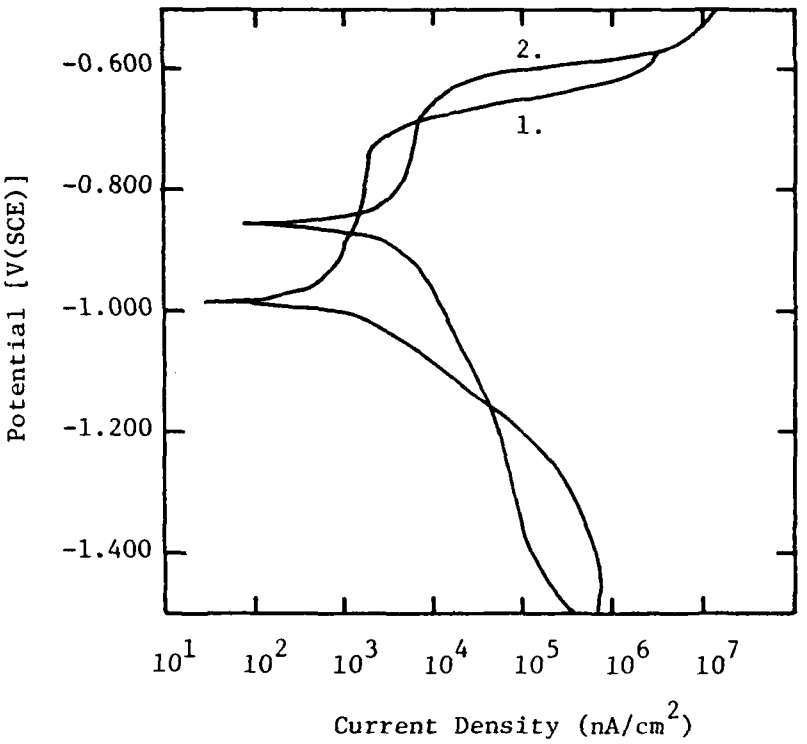

Figure 66. Potential vs. current density for potentiodynamic polarization experiment with aluminum alloy 2024 in 5% NaCl electrolyte solution: (1) control; (2) with Formulation 471-5.

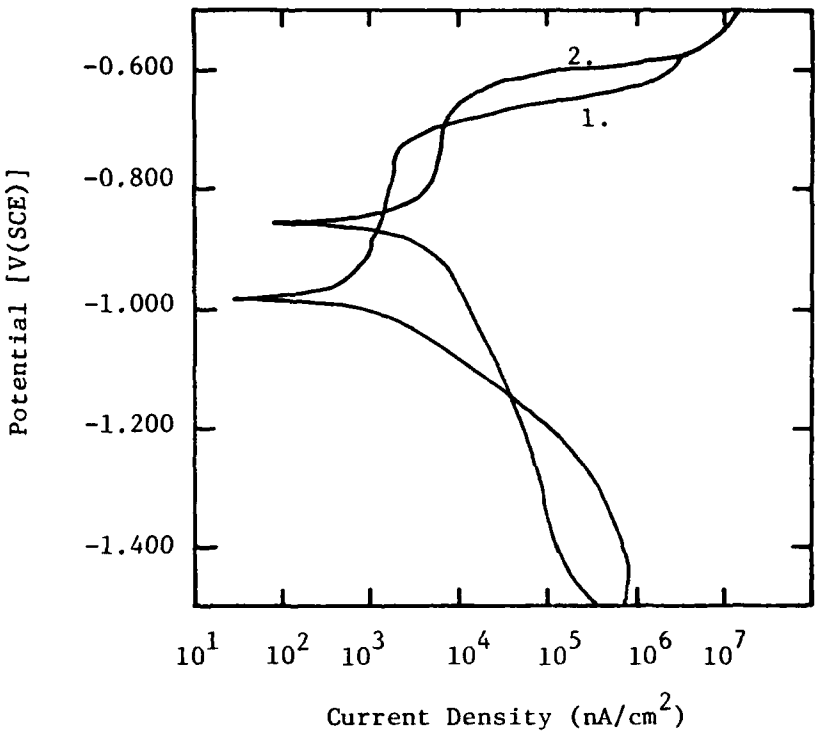

Figure 67. Potential vs. current density for potentiodynamic polarization experiment with aluminum alloy 2024 in 5% NaCl electrolyte solution: (1) control; (2) with Formulation 471-6.

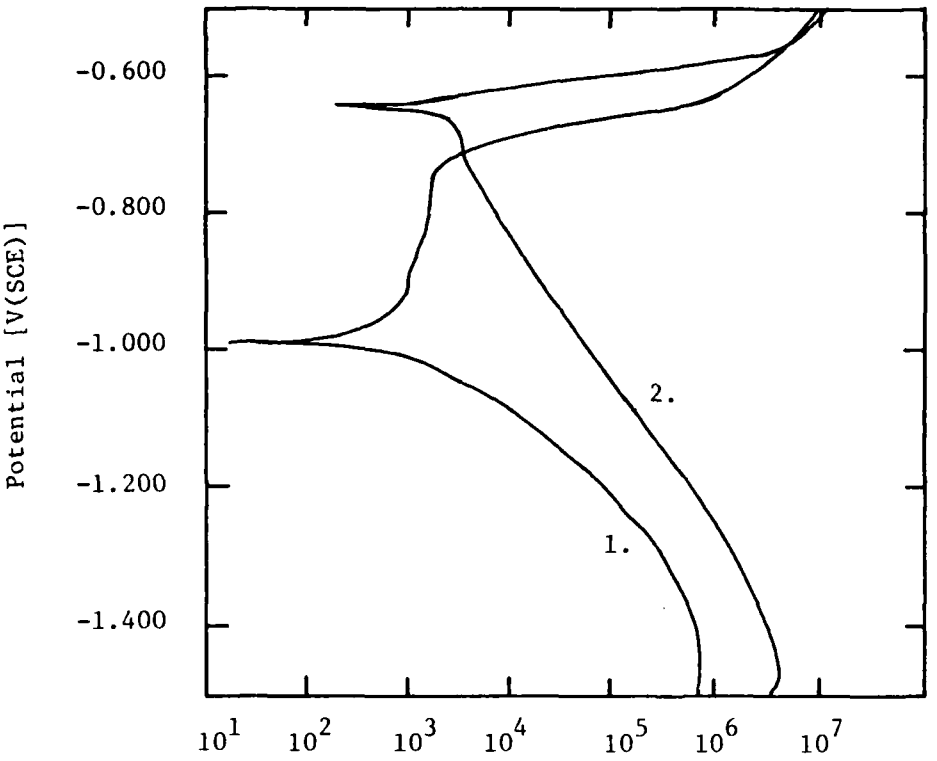

Figure 68. Potential vs. current density for potentiodynamic polarization experiment with aluminum alloy 2024-T3 in 5% NaCl electrolyte solution: (1) control; (2) with Formulation 471-7.

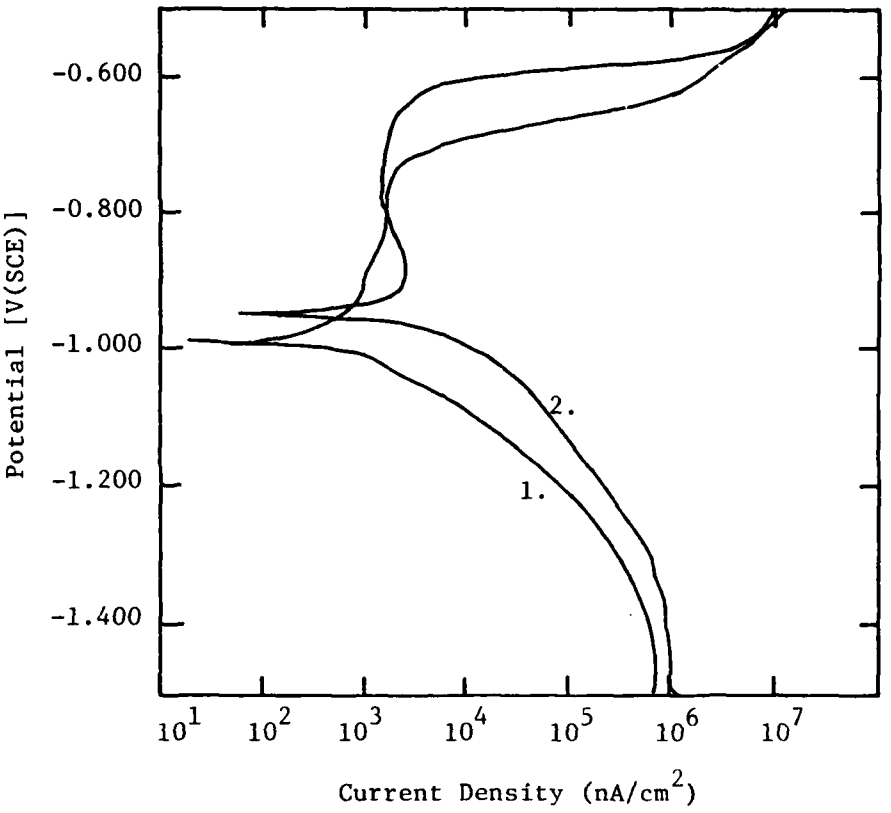

Figure 69. Potential vs. current density for potentiodynamic polarization experiment with aluminum alloy 2024-T3 in 5% NaCl electrolyte solution: (1) control; (2) with Formulation 471-8.

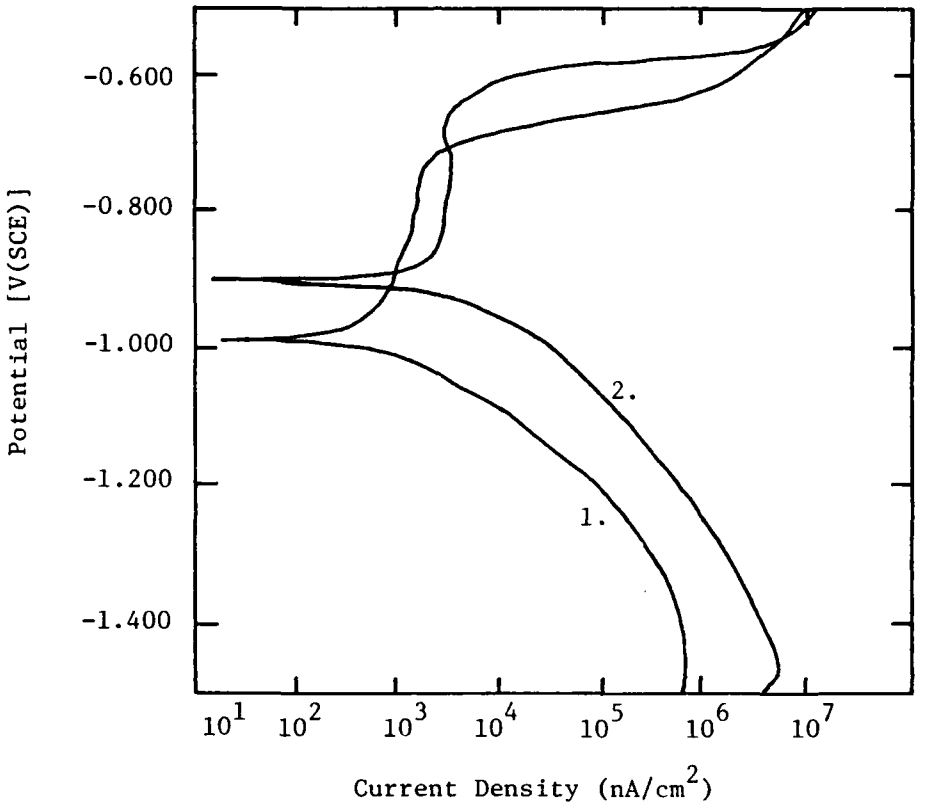

Figure 70. Potential vs. current density for potentiodynamic polarization experiment with aluminum alloy 2024-T3 in 5% NaCl electrolyte solution: (1) control; (2) with Formulation 471-9.

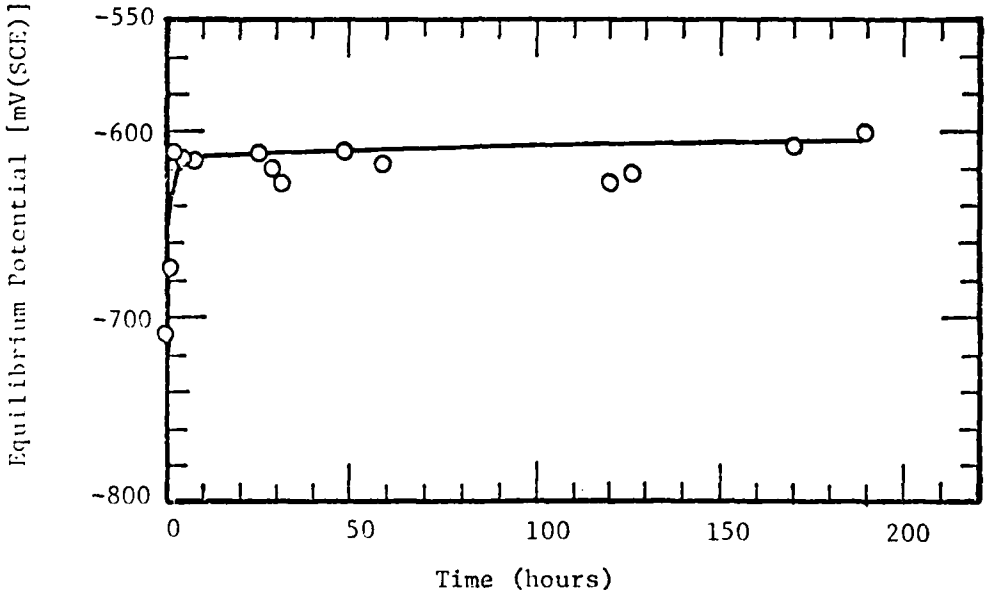

Figure 71. Equilibrium potential vs. time for chronopotentiometric experiment with aluminum alloy 2024 in a 5% NaCl solution containing Formulation 471-6.

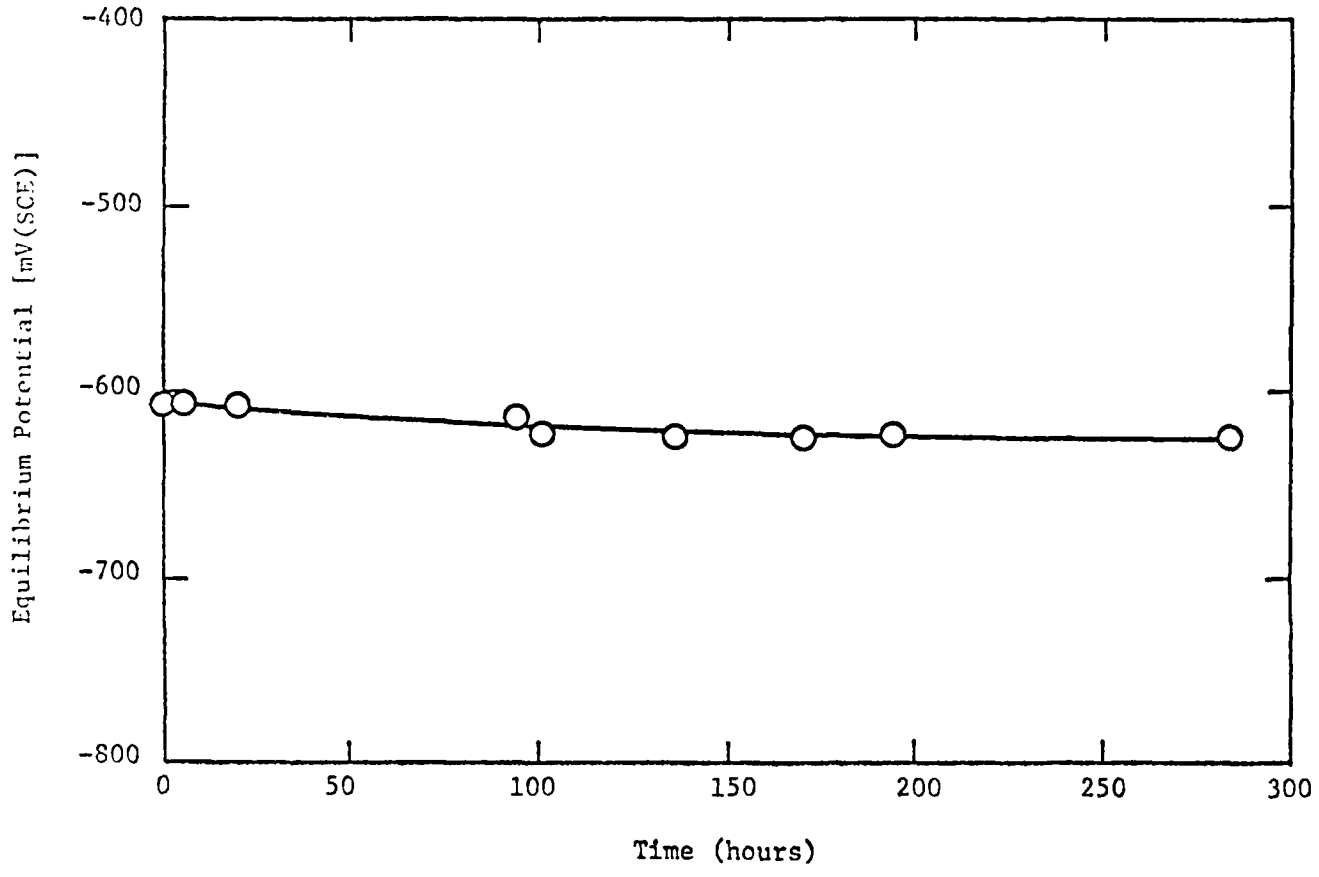

Figure 72. Equilibrium potential vs. time for chronopotentiometric experiment with aluminum alloy 2024-T3 in a 5% NaCl solution containing Formulation 471-8.

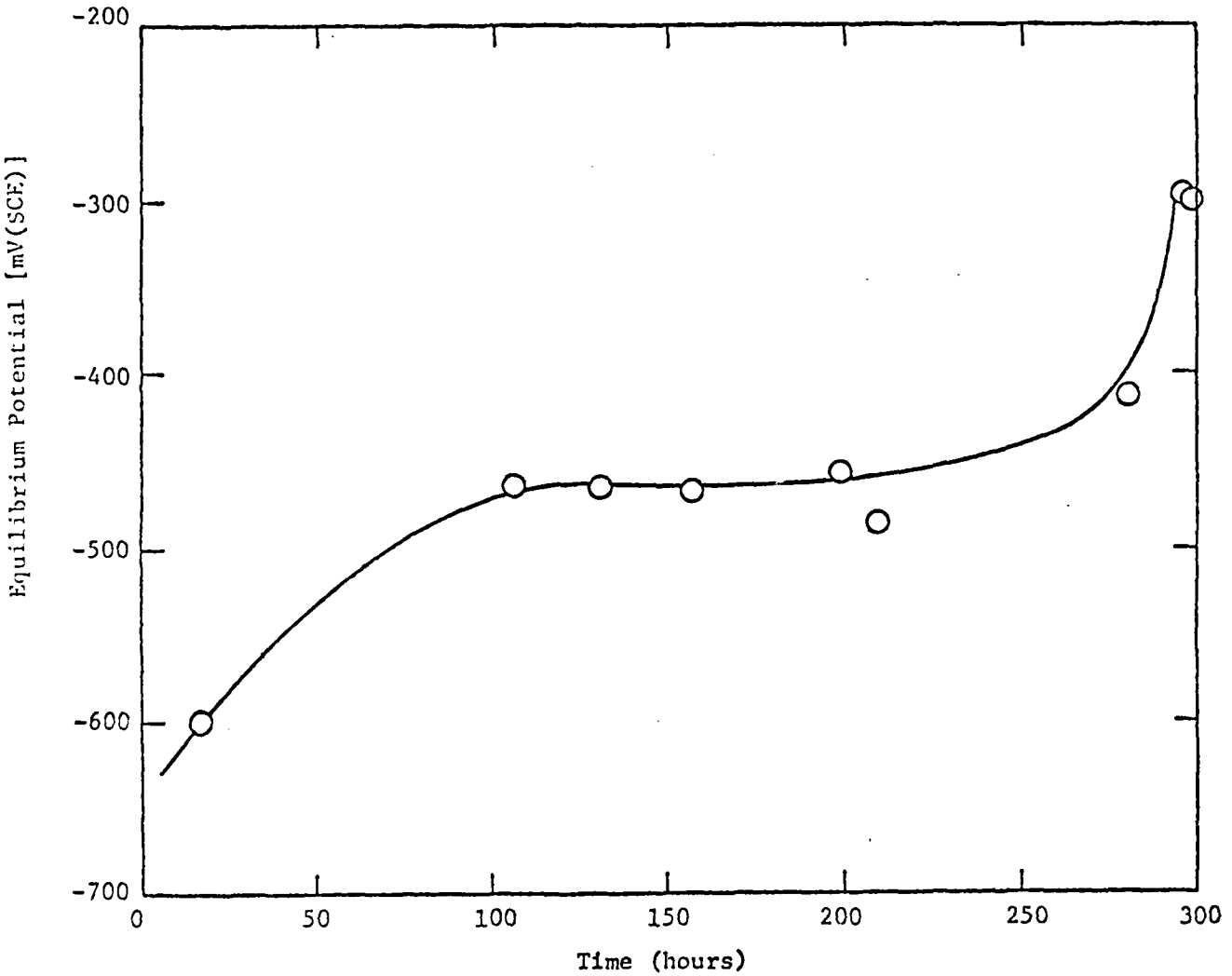

Figure 73. Equilibrium potential vs. time for chronopotentiometric experiment with aluminum alloy 2024-T3 in a 5% NaCl solution containing Formulation 471-9.

and 471-9, there exist passive layers also, and the I_{pass} values for these systems are not too different from the control values. Some small inhibitive effect might be discernable in the transpassive zone relative to the control for these two systems, but it could be due to experimental error. None of these mixtures would serve as an effective corrosion inhibitor.

IV. MICROENCAPSULATION OF CORROSION INHIBITORS

A. Objective

The AFIF mixture is comprised of several constituents that possess a relatively high degree of water solubility as compared to those pigments and additives commonly employed in coatings formulations. Ostensibly, primer formulations containing water-soluble salts may display such undesirable performance characteristics as a high blister tendency, poor inter-coat and wet adhesion, and inadequate corrosion protection because of premature loss of the inhibitor.

Thus, the objective of the microencapsulation approach was to investigate the feasibility of developing a time-release controlled formulation which could be added to an epoxy-polyamide primer for prolonged corrosion protection without sacrificing those performance characteristics required by the system. Ideally, microencapsulation of the AFIF mixture would provide an additional safeguard to protect the water-soluble corrosion inhibitor from catastrophic loss through leaching upon contact with moisture, and a means of diffusion controlled release from the inhibitor reservoir into the coating. Release could occur by diffusion or through mechanical damage, such as abrasion or impact.

B. Selection of the Microencapsulation Technique

Microencapsulation may be accomplished through several types of methodologies, and each has distinct advantages and limitations, as indicated in Table 3. Upon evaluation of the advantages and disadvantages of each method, interfacial polymerization was selected as the most promising technique for the initial stage of the investigation. The advantages offered by interfacial polymerization include:

1. applicability to a wide variety of condensation polymers,
2. particle size distribution control through organic/aqueous phase ratio, surfactant concentration and type, and agitation rate,
3. control over microcapsule wall thickness,

TABLE 3. COMMON METHODS FOR MICROENCAPSULATION

Method	Advantages	Disadvantages
Interfacial polymerization	1. adaptable to water-soluble core material 2. amenable to many polymer types 3. good control over particle size 4. easily adaptable to production	1. many variables 2. reaction by-products
In-situ polymerization	1. requires simple equipment 2. amenable to many polymer types 3. good control over particle size	1. both monomers must be dissolved in an organic and/or aqueous phase
Solidifying from liquid	1. both water-soluble and solvent-soluble materials may be used	1. orifice determines diameter; usually several millimeters
Phase separation from aqueous solution (pH coacervation)	1. availability of established technology; small particle size is possible	1. core material is limited to water-insoluble materials
phase separation from organic solution (simple coacervation)	1. amenable to a variety of polymer types; core material may be water-soluble	1. each shell-core combination requires optimization of a a 3-phase system; large particle sizes result
Drying in liquid	1. amenable to any solvent-soluble polymer; suitable for water-soluble core materials	1. particle size distribution may be broad; many variables
Cooling melted dispersion	1. suitable for water-soluble materials	1. shell material is limited to wax and hydrogenated oils
Fluidized bed	1. simple process	1. limited to particle size of 200μ and larger
Spray drying	1. may be applied to water-soluble material	1. requires tensio-active reactive monomers

4. amenable to water-soluble and insoluble core materials,
5. high efficiency of microcapsule production, and
6. ease of synthesis in laboratory and production quantities.

The major disadvantage associated with interfacial polymerization (as well as simple and complex coacervation) involves achieving the required balance in those dependent variables which control performance. Since microencapsulation through interfacial polymerization may involve manipulation of several controlling variables, the formulations and procedures may be somewhat complex from a material balance and function viewpoint. The following illustrates a typical formulation and procedure for the microencapsulation of the AFIF mix using interfacial polymerization. The materials in parentheses indicate those used in the latter stages of the development work.

The initial stage of the microencapsulation process involves the formation of a water-in-oil emulsion. The aqueous phase would contain one of the reactant monomers (1,6-hexanediamine), a surfactant (Brij 58), and the material to be encapsulated (AFIF). The organic phase would consist of two organic solvents (2.2:1 cyclohexane:chloroform) which possessed a volume-weighted ratio with a density of 1.0 g/ml, and a surfactant (Brij 72). The volume ratio of the aqueous and organic phases in the initial stage is usually on the order of 50:125 (aqueous:organic). The water-in-oil emulsion is formed by mixing the organic-phase solution with the aqueous-phase solution in a water-jacketed Waring blender under high shear conditions at a temperature of 35-40°C. After formation of the emulsion, a volume of the organic phase (50 ml of 2.2:1 cyclohexane:chloroform) containing the other reactant monomer (toluene 2,4-diisocyanate) is added dropwise. The polymerization reaction occurs at the phase boundary between the aqueous and organic solutions by diffusive transport of the reactants to the interface. The typical reaction time necessary for microcapsule formation is 5-10 min after addition of the organic phase containing the second reactant. After the reaction is complete, the microcapsules are extracted repeatedly with pure cyclohexane to remove any unreacted monomers from the material. The microcapsules are then stored as a slurry in cyclohexane until use.

C. Selection of the Membrane Polymer

The degree of success achieved in preparing a high yield of AFIF-containing microcapsules with the proper release characteristics is largely dependent upon the polymer candidate selected for the membrane wall. The choice of polymer candidates is principally governed by the kinetics required for interfacial polymerization, the tractability of the microencapsulated system with the coatings formulation, and the degree of permeability required to provide the needed corrosion resistance. Of these criteria, perhaps the most challenging demands imposed upon the polymer membrane arise from those constraints associated with the environment of the primer formulation.

Thus, prior to spray application, the microcapsules would be combined with the epoxy-polyamide primer formulation by means of conventional mixing. Obviously, if the microcapsule wall is to withstand the shear stress associated with stirring the viscous medium, the polymer candidate must possess a relatively high degree of cohesive energy density. Furthermore, even greater shear stress may be encountered during spray application, where the shear rates may reach 40,000/sec.

The epoxy-polyamide formulation may contain polar solvents such as ketones, esters, and alcohols, along with polar resins capable of strong hydrogen bonding. Under these circumstances, the membrane wall must display a low solvent-polymer interaction parameter if swelling and the properties associated with polymer-polymer intermolecular forces (permeability) are to remain constant.

Upon solvent evaporation within the coating, the microcapsules are subjected to the internal stress which arises as the system undergoes a phase change to the solid state. The microcapsules may encounter a significant degree of close-packing and compression resulting from orientation of the pigment particles. The polymer candidate should possess a high degree of tear resistance if the microcapsule wall is to withstand intimate contact with the pigment surface.

Finally, in the latter stages of film formation, the microcapsules are subjected to changes in polarity of the matrix as the oxirane rings react with the amine groups. The curing reaction is exothermic, and a temperature increase up to 50°C may occur in the bulk of the paint film.

In the cured coating, the microcapsules function theoretically as a reservoir for sustained release of the corrosion inhibitor mixture. The half-life, $\tau_{\frac{1}{2}}$, for release of an encapsulated material is given by:

$$\tau_{\frac{1}{2}} = \frac{(2a)^2(\ln 2)}{RD}$$

where a = the diameter of the microcapsule;

R = ratio of volume or mass of encapsulated material to that of the membrane;

D = the diffusion coefficient of the membrane (40).

The permeability, P, of a substance through a polymer matrix is related to the diffusion coefficient by the expression $P = D \cdot S$, where S is the solubility constant of the permeant in the polymer. The permeability is dependent upon such polymer properties as density, molecular weight, crystallinity, chain orientation, degree of crosslinking, humidity, method of film formation, and the presence of fillers (41). Table 4 illustrates the variability of the permeability coefficient with polymer structure (42).

TABLE 4. THE VARIATION OF PERMEABILITY COEFFICIENT OF WATER WITH POLYMER TYPE

Polymer Type	Permeability Coefficient $P_{10} \times 10^9$ ($\frac{\text{cc STP cm}}{\text{sec cm}^2 \text{ cmHg}}$)
polyethyleneterephthalate	17.5
cellulose triacetate	1270
ethyl cellulose	2100
polyvinylchloride	15
vinylidenechloride (81%) acrylonitrile (19%) copolymer	1.6
polymethylmethacrylate	250
polystyrene	97
polydimethyl siloxane	4300
polybutadiene	507
nylon 6	40

The above data illustrates that permeability is significantly dependent upon polymer structure, and achieving the required degree of sustained release will be dependent upon the proper selection of membrane material.

The final criterion used in determining the best polymer candidate involved evaluation of those limitations imposed by the interfacial polymerization reaction. In general, in-situ encapsulation involves polymerization of vinyl-type monomers while microencapsulation through interfacial polymerization involves the use of monomers which form condensation-type polymers. Interfacial polymerization was founded upon the principles involved in the Schotten-Baumann reaction and is, thus, limited to those monomers which possess the required polymerization kinetics. The classes of polymers which are amenable to interfacial polymerization include polyamides, polyesters, polyurethanes, polycarbonates, polysulfonates, epoxy resins and silicone resins. Thus, after considering the physical and chemical properties required for incorporation of the microcapsules into the primer formulation, the low degree of permeability required for sustained release, and the limitations imposed by interfacial polymerization, the polyamides were judged as providing a suitable match with the requirements established as the controlling criterion.

While numerous structurally different polyamides have been synthesized over the last four decades, the most common polyamides include nylon 6,6; nylon 6,10; nylon 6,12; nylon 6, nylon 7, nylon 11, and nylon 12. Interfacial polymerization cannot be used to prepare polymers of the latter four types.

To achieve high molecular weight polymer, a suitable partitioning of the diamine into the organic phase is required as illustrated by the data presented in Table 5 (43).

These data indicate that under interfacial polymerization conditions nylon 6,10 is capable of providing the highest yield and greatest molecular weight ranges as a result of the hydrophobicity of the diamine. Moreover, Table 6 indicates the physical properties of nylon 6,10 are comparable to those of nylon 6,6 and nylon 6.

D. Optimization of the Parameters Controlling Microcapsule Formation

The nylon 6,10 system was used in a pilot study designed to optimize the numerous parameters which control microcapsule formation by means of interfacial polymerization. The principal variables investigated include surfactant type and concentration, organic phase compositions, phase volume

TABLE 5. EFFECT OF DIAMINE PARTITION COEFFICIENT ON THE MOLECULAR WEIGHT OF POLYAMIDES[a]

Polyamide	Yield (%)	Viscosity in m-cresol (ηiuh, dl/g)[b]
6,10	85	1.87
6,6	80	1.51
6,5	73	0.64
6,2	56	0.54

[a]Diamine conc. = 0.067M tetrachloroethylene/water phase
Volumes: 210:300

[b]Inherent viscosity

TABLE 6. COMPARISON OF THE PHYSICAL PROPERTIES[a] OF NYLON 6,6; 6,10 and 6[b]

Physical Property	Nylon 6,6	Nylon 6,10	Nylon 6
tensile strength,[c] psi x 10^3	11.2	8.6	8.7
elongation at break,[c] %	300	300	285
yield stress,[c] psi x 10^3	8.5	7.1	5.9
elongation at yield,[c] %	25	30	30
shear strength, psi x 10^3 (0.2% H_2O)	9.6	8.4	
flexural modulus,[c] psi x 10^3	175	160	108
Rockwell hardness (0.2% H_2O)	R118, M79	R111	R107
brittleness temperature, °F	-85	-139	
Izod impact strengh,[c] ft-lb/in.	2.0	1.2	2.5
coefficient of linear expansion, in./in./°F x 10^{-5}	4.5	5.0	4.0
specific heat	0.3-0.5	0.3-0.5	0.3-0.5

[a]Equilibrated at 50% rh unless noted.
[b]E. I. du Pont de Nemours & Co., Inc., Zytel Nylon Resins Bulletin.
[c]At 73°F.

ratio, monomer concentration and ratio, reaction temperature, stirring rate, and addition rate. The study involved over 400 experimental runs of the interfacial polymerization procedure over a 12 month period. The data in the following sections present the trends uncovered in the study.

1. Determination of a Suitable Aqueous Phase Surfactant

Under the conditions employed in interfacial polymerization, the final microcapsule particle size distribution is determined by the manner in which the dispersed aqueous emulsion droplets reach stability in the emulsion system through the minimization of the interfacial tension, and by other complex and interrelated processes. For example, the interfacial tension for a paraffin oil/water emulsion is 40.6 dynes/cm, which is lowered to 31.05 dynes/cm when the aqueous phase contains 0.001M oleic acid. Neutralization of the acid by an equivalent amount of sodium hydroxide (which forms the corresponding soap) reduces the interfacial tension to 7.2 dynes/cm. The relationship between the surface tension of the system and the nature and concentration of surfactant is given by:

$$\gamma = \gamma^{o} - KC_{s}$$

where C_s = concentration of the surfactant,
and K = parameter associated with the physical nature of the surfactant.

Thus, emulsion stability is dependent upon the surface active agent. Considerable effort was initially placed in utilizing methylcellulose as the aqueous phase surfactant. Since methyl cellulose functions more as a viscosity modifier (protective colloid) than as a true surfactant, microcapsules prepared with the methyl cellulose would cause less of an adverse effect to the film properties of the primer than would microcapsules prepared with surface active agents. Unfortunately, the approach was not successful. Therefore, a study was designed to evaluate the ability of several structurally different surfactants to facilitate emulsion stability. Hexane (100 ml) containing 1% Brij 52 surfactant was added to various 50 ml aliquots of water, containing 1% of the surfactants methylcellulose, PEG 600, Span 60, or Brij 58. The mixture was emulsified in a blender at high speed for 1 min, and the phase separation (creaming) time of the emulsion was

measured. Based upon the stability results obtained, Brij 58 was selected as the most suitable aqueous phase surfactant.

2. Determination of a Suitable Organic Phase Surfactant and Optimization of the Surfactant Concentration

The hydrophilic-lipophilic balance (HLB) system is generally used for the selection of the surface active agent. Those emulsifiers with HLB values in the range of 4 to 6 are suitable as emulsifiers for water/oil emulsions while those with HLB values ranging 8 to 18 are suitable for the preparation of oil-water emulsions. The HLB may be related to the coalescence rates of droplets at the oil-water interface, as shown by the expression (44):

$$\ln (Rate_2/Rate_1) = 2.2\ \Theta\ (HLB-7)$$

where $Rate_1$ = coalescence of an oil droplet at the phase interface;

$Rate_2$ = coalescence of an oil droplet at the phase interface;

Θ = the fraction of the droplet surface covered by the surface-active emulsifiers.

Since emulsion stability is related to both the HLB value of the surfactant and the concentration of surfactant used for emulsification (Θ), a study was designed which evaluated the effectiveness of microcapsule formation as a function of both controlling parameters. The surfactants were chosen to represent the appropriate range of HLB values, and the concentrations included the usual minimum and maximum levels. Additionally, intermediate levels of surfactant were evaluated, since this parameter controls the microcapsule size distribution, as illustrated in Figure 74 (45).

Since in many cases a given experimental surfactant failed to yield a stable emulsion, only data concerning those surfactants which were successful in generating microencapsulated product will be presented. Table 7 indicates the general procedure and ingredients used in the surfactant

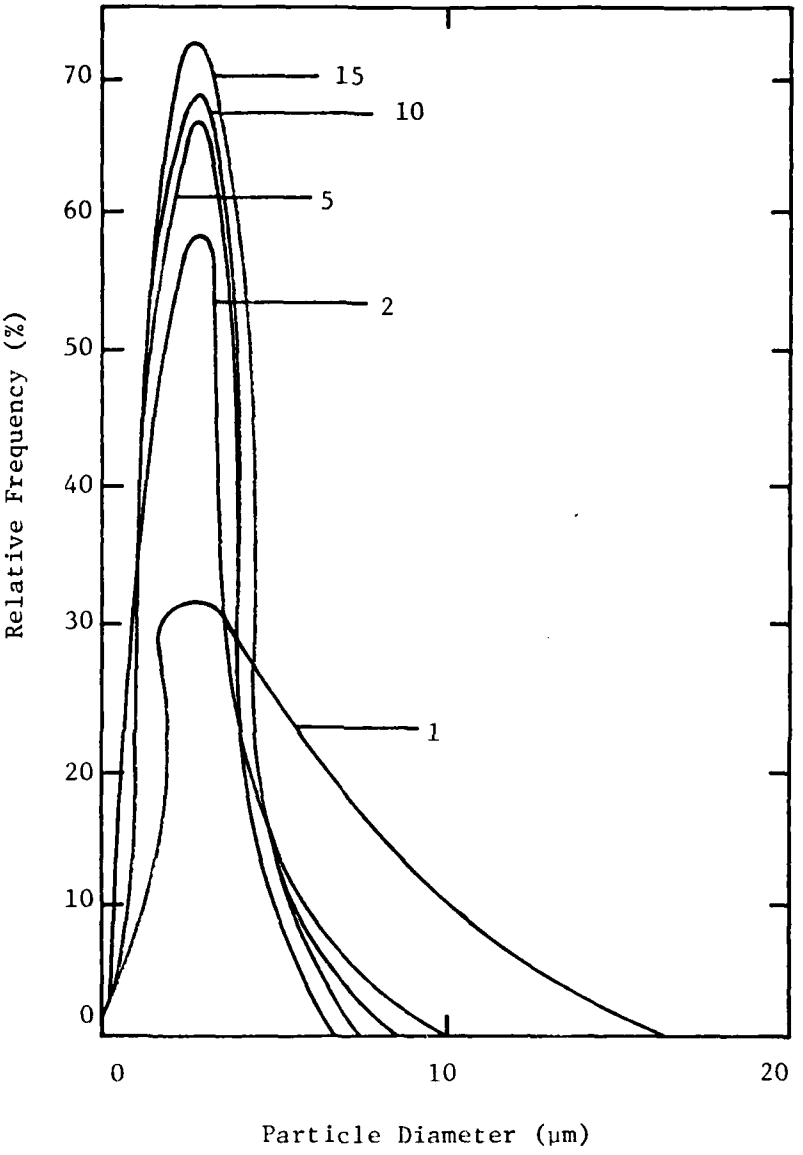

Figure 74. Effect of the concentration of Span 85 on the size distribution of microcapsules prepared from 1,6-hexamethylenediamine and p-phthaloyl dichloride in chloroform:cyclohexane (1:4) at a speed setting of 620 rpm.

TABLE 7. SPECIFIC EXAMPLE OF MICROCAPSULE FORMATION

A. Solution Preparation

1. 10.0 g hexane 1,6 diamine + 5.0 g AFIF + 0.05 g Brij 58 + 50.0 ml D.I. H_2O
2. 0.1 g Igepal RC-520 + 100 ml 2.2:1 (v:v) cyclohexane:chloroform
3. 10.0 g sebacyl chloride + 25 ml 2.2:1 (v:v) cyclohexane:chloroform

B. Reaction Procedure

Temperature = 30°C

1. Add solution (1) to the blender at speed = 7 (16500 rpm)
2. Add solution (2) dropwise, rapidly, still at speed = 7
3. Add solution (3) dropwise, over 3-5 min, still at speed = 7
4. Allow blender to run at speed = 7 for ~30 sec after the last addition
5. Remove product from reaction vessel

C. Purification, Isolation, Drying

1. Gravity filter the reaction product with Whatman No. 1 filter paper
2. Wash with 300-400 ml of the organic phase solvent
3. Allow product to air dry under the hood for 24 hr

D. Release Testing

1. Add 0.5 g of microcapsule sample to 50.0 ml of deionized water
2. Measure conductivity vs time until a constant value is obtained

E. SEM Analysis

1. A Jeol JSM-35C SEM with gold-palladium sputter coating was used.
2. Wet mount method was used: a drop of microcapsules from the reaction vessel, still in slurry form, is placed on the SEM pedestal for characterization.

evaluation, and experimental variations are indicated in Tables 8-11. Release times corresponding to surfactant concentrations are shown in Figures 75-78.

In spite of certain material variations which are apparent in the previous data, the release times for microcapsules prepared from Brij 52, Igepal RC-520, Igepal CO-430 and Brij 72 show little variation as a function of surfactant type.

3. Evaluation of the Ratio of (Organic Phase/Aqueous Phase) Surfactants

When using a combination of surfactants, the composite HLB of the system is a weighted average of the assigned values corresponding to the percentage composition of the mixture used. For example, emulsification of an oil with an HLB of 12.3 would require a mixture of 60 wt% of a surfactant with HLB at 16.9 and 40 wt% of a surfactant with HLB at 5.3.

$$\text{HLB combination} = (16.9 \times 0.60) + (5.3 \times 0.40) = 12.3$$

Thus, to determine if HLB optimization would result in production of microcapsules with greater release times, a study was conducted in which the ratio of (aqueous phase/organic phase) surfactants was varied. The procedure was essentially that presented in Table 7, and the design of the study and results are presented in Tables 12 and 13 and Figures 79 and 80. Interestingly, in each case the release times were a maximum for microcapsules prepared at an (aqueous phase/organic phase) surfactant ratio of 0.33. While each combination of surfactants produced microcapsules with less than the desired release time, the microcapsules prepared from the Brij 58/ Brij 72 and Brij 58/Igepal CO-430 displayed significantly better properties than those prepared from other surfactant combinations.

4. Evaluation of the Ratio of Diacid Chloride to Diamine

If the polymerization kinetics were altered by the presence of the AFIF mixture or through interference by the emulsifier, the membrane accretion process might not be homogeneous, resulting in the generation of open

TABLE 8. VARIATION OF BRIJ 52 SURFACTANT AMOUNT

Sample	Hexane 1,6 diamine (grams)	Sebacyl chloride (grams)	Aqueous Surf. Type and Amount (grams)	Organic Surf. Type and Amount (grams)	Inhibitor (grams)	Organic Solvent Comp. and Ratio**	Organic Solvent (ml)	Aqueous Solvent (ml)	Temp. (°C)	Burst* Effect Ratio	Release Time (min)
555-53	5.0	2.0	0.25 Brij 58	1.0 Brij 52	5.0 471-6	3:1 Cyc: $CHCl_3$	125	50	25	1300/2500	18
555-56	5.0	2.2	0.25 Brij 58	1.0 Brij 52	5.0 471-6	3:1 Cyc: $CHCl_3$	125	50	25	2700/4700	20
555-60	5.0	2.2	0.25 Brij 58	0.5 Brij 52	5.0 471-6	3:1 Cyc: $CHCl_3$	125	50	25	1700/4300	24
555-61	5.0	2.0	0.25 Brij 58	0.5 Brij 52	5.0 471-6	3:1 Cyc: $CHCl_3$	125	50	25	1400/3900	22
555-67	10.0	5.0	0.50 Brij 58	2.0 Brij 52	5.0 471-6	3:1 Cyc: $CHCl_3$	125	50	25	2050/2200	9
555-69	10.0	5.0	0.50 Brij 58	2.0 Brij 52	5.0 471-6	3:1 Cyc: $CHCl_3$	125	50	25	1470/2100	9

* Burst effect ratio = $\frac{\text{conductivity at 1.0 min}}{\text{conductivity at max. release time}}$

**Cyc = Cyclohexane

TABLE 9. VARIATION OF IGEPAL RC-520 SURFACTANT AMOUNT

Sample	Hexane 1,6 diamine (grams)	Sebacyl chloride (grams)	Aqueous Surf. Type and Amount (grams)	Organic Surf. Type and Amount (grams)	Inhibitor (grams)	Organic Solvent Comp. and Ratio**	Organic Solvent (ml)	Aqueous Solvent (ml)	Temp. (°C)	Burst* Effect Ratio	Release Time (min)
602-4	10.0	10.0	0.005 Brij 58	0.01 Igepal RC-520	5.0 471-6	2.2:1 Cyc: $CHCl_3$	125	50	30	900/3600	22
602-5	10.0	10.0	0.005 Brij 58	0.01 Igepal RC-520	5.0 471-6	2.2:1 Cyc: $CHCl_3$	125	50	30	2700/3800	14
602-2	10.0	10.0	0.05 Brij 58	0.1 Igepal RC-520	5.0 471-6	2.2:1 Cyc: $CHCl_3$	125	50	30	1100/4700	9
602-3	10.0	10.0	0.05 Brij 58	0.1 Igepal RC-520	5.0 471-6	2.2:1 Cyc: $CHCl_3$	125	50	30	3800/4100	4
584-10	10.0	6.0	0.5 Brij 58	2.0 Igepal RC-520	5.0 471-6	2.2:1 Cyc: $CHCl_3$	125	50	30	3500/9400	18
584-11	10.0	6.0	0.5 Brij 58	2.0 Igepal RC-520	5.0 471-6	2.2:1 Cyc: $CHCl_3$	125	50	30	3600/9700	18
584-25	10.0	4.0	0.5 Brij 58	1.0 Igepal RC-520	5.0 471-6	2.2:1 Cyc: $CHCl_3$	125	50	30	2100/9700	26
584-26	10.0	4.0	0.5 Brij 58	1.0 Igepal RC-520	5.0 471-6	2.2:1 Cyc: $CHCl_3$	125	50	30	2400/4800	12

* Burst effect ratio = $\frac{\text{conductivity at 1.0 min}}{\text{conductivity at max. release time}}$

**Cyc = Cyclohexane

TABLE 10. VARIATION OF IGEPAL CO-430 SURFACTANT AMOUNT

Sample	Hexane 1,6 diamine (grams)	Sebacyl chloride (grams)	Aqueous Surf. Type and Amount (grams)	Organic Surf. Type and Amount (grams)	Inhibitor (grams)	Organic Solvent Comp. and Ratio**	Organic Solvent (ml)	Aqueous Solvent (ml)	Temp. (°C)	Burst* Effect Ratio	Release Time (min)
602-38	10.0	6.0	1.0 Brij 58	1.0 Igepal CO-430	5.0 471-6	2.2:1 Cyc: $CHCl_3$	125	50	30	400/2900	26
602-39	10.0	6.0	1.0 Brij 58	1.0 Igepal CO-430	5.0 471-6	2.2:1 Cyc: $CHCl_3$	125	50	30	300/3300	58
602-34	10.0	7.0	1.0 Brij 58	1.5 Igepal CO-430	5.0 471-6	2.2:1 Cyc: $CHCl_3$	125	50	30	500/3300	40
602-35	10.0	8.0	1.0 Brij 58	1.5 Igepal CO-430	5.0 471-6	2.2:1 Cyc: $CHCl_3$	125	50	30	600/3200	34
602-26	10.0	6.0	1.0 Brij 58	2.0 Igepal CO-430	5.0 471-6	2.2:1 Cyc: $CHCl_3$	125	50	30	700/2900	26
602-27	10.0	6.0	1.0 Brij 58	2.0 Igepal CO-430	5.0 471-6	2.2:1 Cyc: $CHCl_3$	125	50	30	700/2800	22

* Burst effect ratio = $\frac{\text{conductivity at 1.0 min}}{\text{conductivity at max. release time}}$

**Cyc = Cyclohexane

TABLE 11. VARIATION OF BRIJ 72 SURFACTANT AMOUNT

Sample	Hexane 1,6 diamine (grams)	Sebacyl chloride (grams)	Aqueous Surf. Type and Amount (grams)	Organic Surf. Type and Amount (grams)	Inhibitor (grams)	Organic Solvent Comp. and Ratio**	Organic Solvent (ml)	Aqueous Solvent (ml)	Temp. (°C)	Burst* Effect Ratio	Release Time (min)
602-6	10.0	10.0	0.5 Brij 58	0.1 Brij 72	5.0 471-6	2.2:1 Cyc: $CHCl_3$	125	50	40	1400/3200	22
584-17	10.0	4.0	0.5 Brij 58	1.0 Brij 72	5.0 471-6	2.2:1 Cyc: $CHCl_3$	125	50	40	3000/6600	16
584-24	10.0	4.0	0.5 Brij 58	1.0 Brij 72	5.0 471-6	2.2:1 Cyc: $CHCl_3$	125	50	40	2000/4400	30
602-42	2.0	6.0	0.5 Brij 58	2.0 Brij 72	5.0 471-6	2.2:1 Cyc: $CHCl_3$	125	50	40	300/2100	32
602-44	2.0	6.0	0.5 Brij 58	2.0 Brij 72	5.0 471-6	2.2:1 Cyc: $CHCl_3$	125	50	40	800/2200	22
602-55	2.0	7.0	1.0 Brij 58	3.0 Brij 52	5.0 471-6	2.2:1 Cyc: $CHCl_3$	125	50	25	1470/2100	9

* Burst effect ratio = $\frac{\text{conductivity at 1.0 min}}{\text{conductivity at max. release time}}$

**Cyc = Cyclohexane

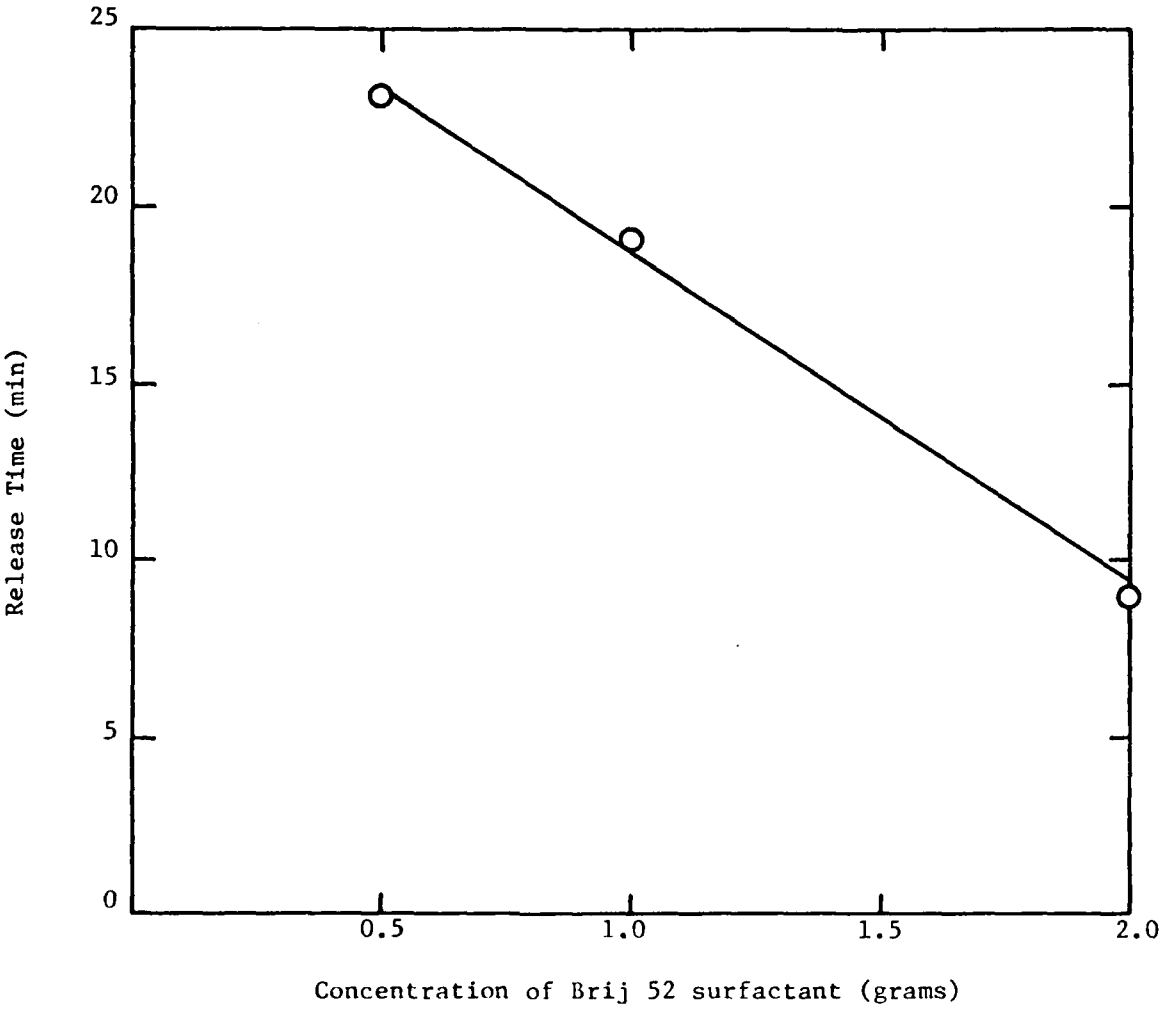

Figure 75. Variation of Amount of Brij 52 Surfactant.

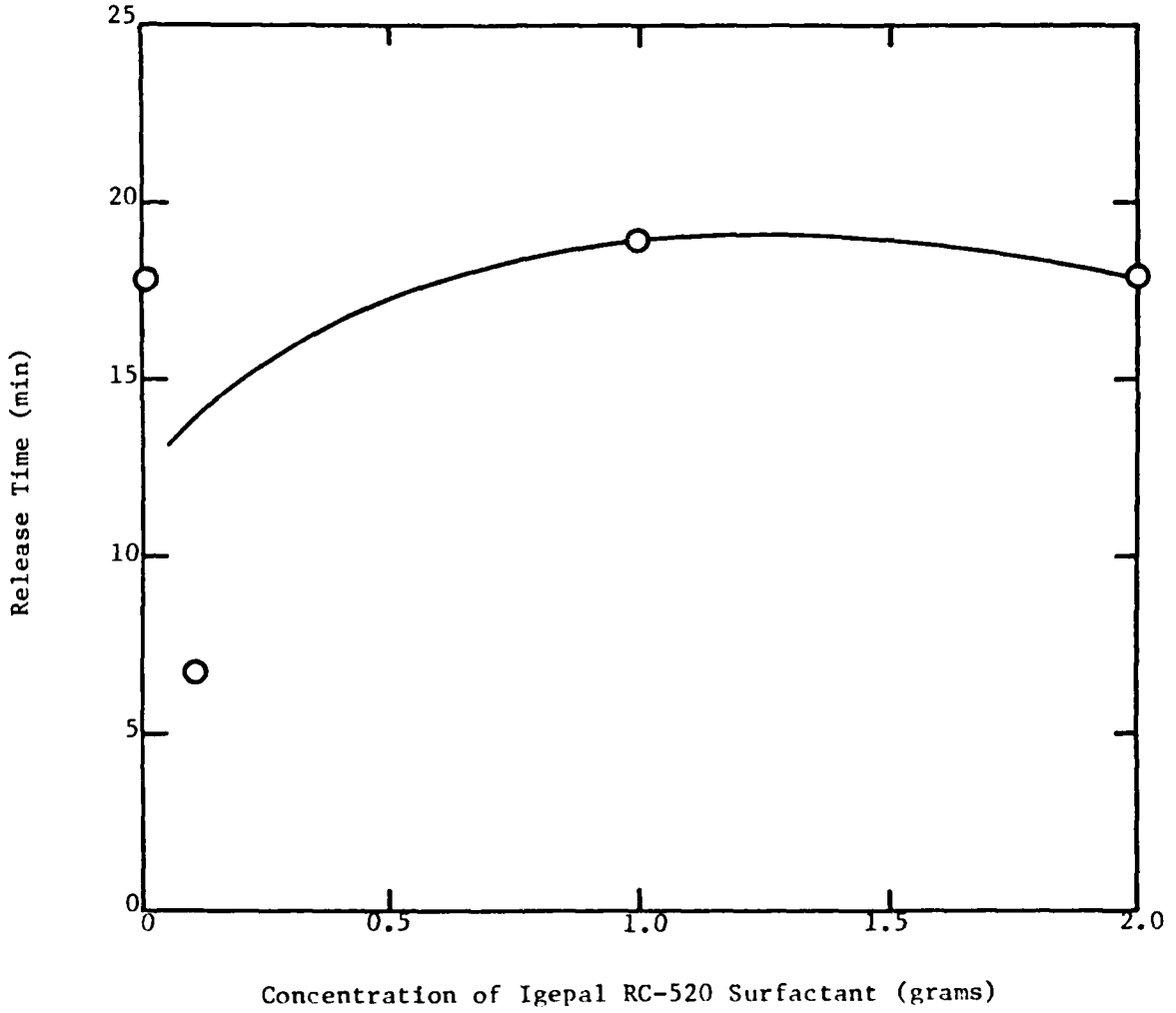

Figure 76. Variation of Igepal RC-520 Surfactant Concentration.

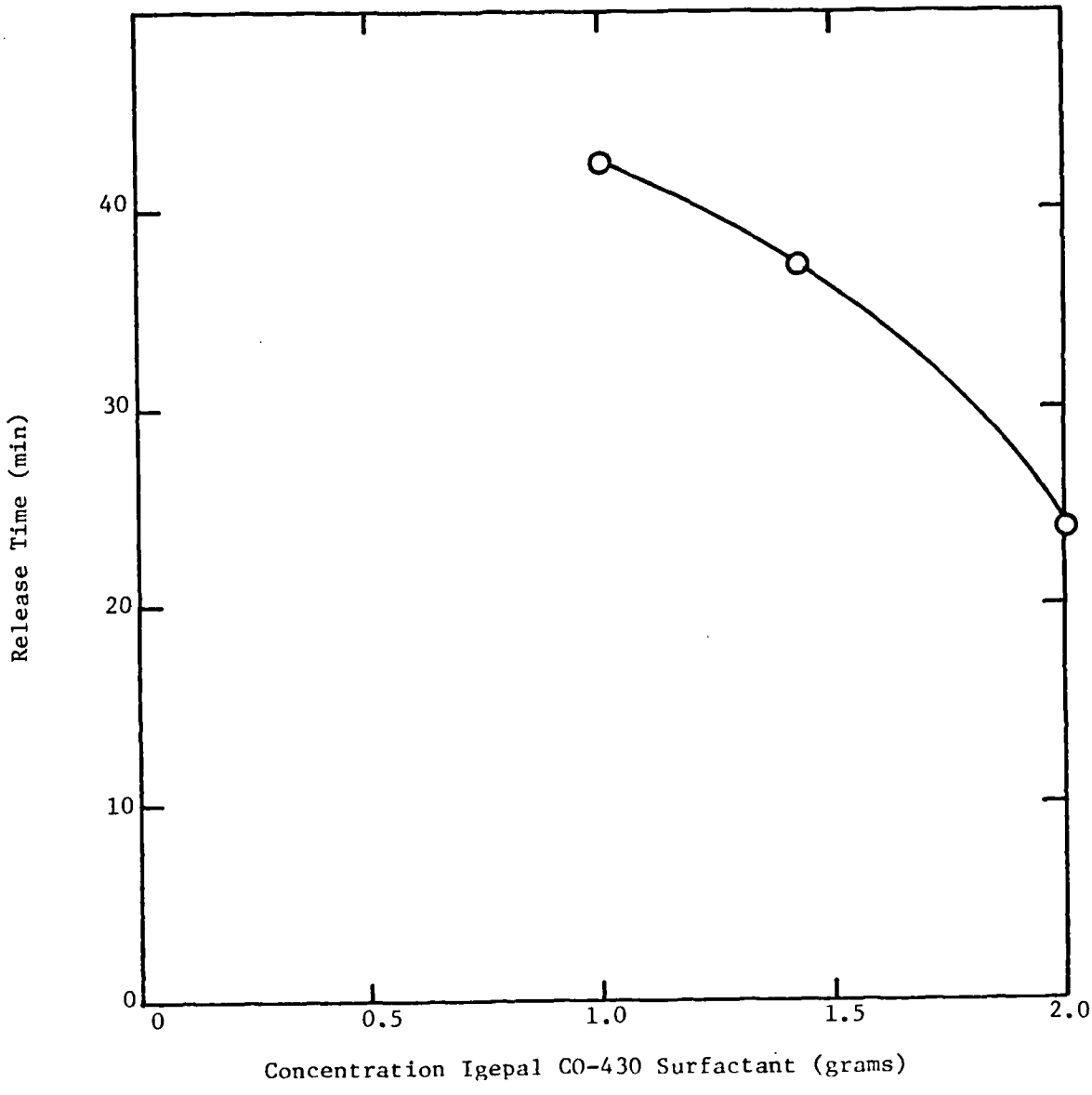

Figure 77. Variation of Igepal CO-430 Surfactant Concentration.

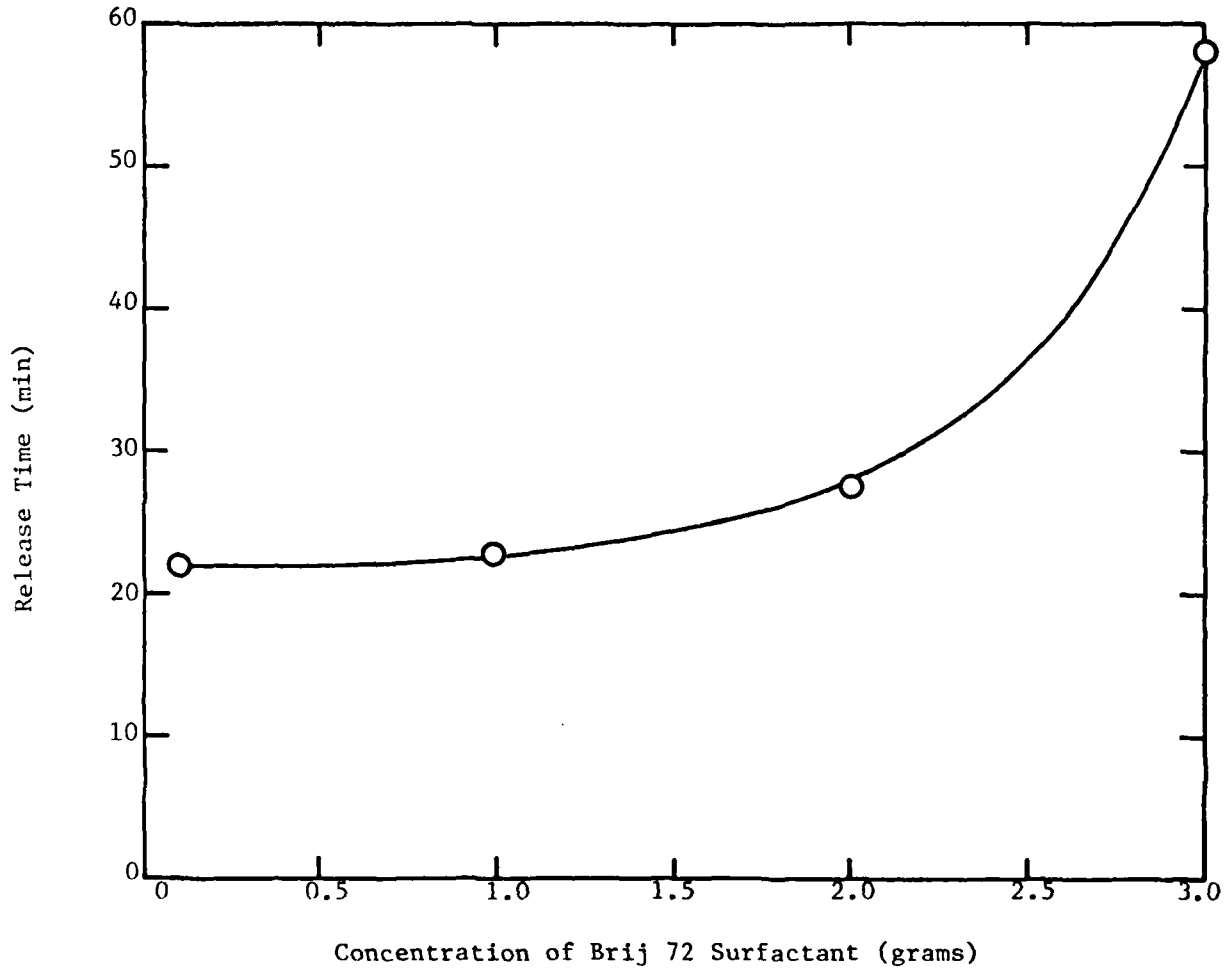

Figure 78. Variation of Brij 72 Surfactant Concentration.

TABLE 12. RELEASE TIME VERSUS SURFACTANT RATIO FOR BRIJ 72

Sample	Hexane 1,6 diamine (grams)	Sebacyl chloride (grams)	Aqueous/Organic Surfactant Type and Ratio	Inhibitor (grams)	Organic Solvent Comp. and Ratio**	Organic Solvent (ml)	Aqueous Solvent (ml)	Temp. (°C)	Burst* Effect Ratio	Release Time (min)
602-51	2.0	8.0	Brij 58/Brij 72, 0.25	5.0 471-6	2.2:1 Cyc: $CHCl_3$	125	50	40	600/5000	58
602-52	2.0	8.0	Brij 58/Brij 72, 0.25	5.0 471-6	2.2:1 Cyc: $CHCl_3$	125	50	40	400/4500	48
602-55	2.0	7.0	Brij 58/Brij 72, 0.33	5.0 471-6	2.2:1 Cyc: $CHCl_3$	125	50	40	900/4700	58
602-53	2.0	8.0	Brij 58/Brij 72, 0.25	5.0 471-6	2.2:1 Cyc: $CHCl_3$	125	50	40	300/2600	36
602-54	2.0	8.0	Brij 58/Brij 72, 0.50	5.0 471-6	2.2:1 Cyc: $CHCl_3$	125	50	40	700/4200	32

* Burst effect ratio = $\frac{\text{conductivity at 1.0 min}}{\text{conductivity at max. release time}}$

**Cyc = Cyclohexane

TABLE 13. RELEASE TIME VERSUS SURFACTANT RATIO FOR IGEPAL CO-430

Sample	Hexane 1,6 diamine (grams)	Sebacyl chloride (grams)	Aqueous/Organic Surfactant Type and Ratio	Inhibitor (grams)	Organic Solvent Comp. and Ratio**	Organic Solvent (ml)	Aqueous Solvent (ml)	Temp. (°C)	Burst* Effect Ratio	Release Time (min)
602-68	10.0	4.0	Brij 58/Igepal CO-430, 0.25	5.0 471-6	p=1.0 Cyc: $CHCl_3$	125	50	40	700/3900	28
602-56	10.0	4.0	Brij 58/Igepal CO-430, 0.33	5.0 471-6	p=1.0 Cyc: $CHCl_3$	125	50	40	500/3800	54
602-36	10.0	6.0	Brij 58/Igepal CO-430, 0.36	5.0 471-6	p=1.0 Cyc: $CHCl_3$	125	50	40	500/3200	44
602-37	10.0	6.0	Brij 58/Igepal CO-430, 0.33	5.0 471-6	p=1.0 Cyc: $CHCl_3$	125	50	40	500	36
602-34	10.0	7.0	Brij 58/Igepal CO-430, 0.66	5.0 471-6	p=1.0 Cyc: $CHCl_3$	125	50	40	500/3300	40
602-35	10.0	8.0	Brij 58/Igepal CO-430, 0.66	5.0 471-6	p=1.0 Cyc: $CHCl_3$	125	50	40	600/3200	34

(continued)

* Burst effect ratio = $\frac{\text{conductivity at 1.0 min}}{\text{conductivity at max. release time}}$

**Cyc = Cyclohexane

TABLE 13. (continued)

Sample	Hexane 1,6 diamine (grams)	Sebacyl chloride (grams)	Aqueous/Organic Surfactant Type and Ratio	Inhibitor (grams)	Organic Solvent Comp. and Ratio**	Organic Solvent (ml)	Aqueous Solvent (ml)	Temp. (°C)	Burst* Effect Ratio	Release Time (min)
602-38	10.0	6.0	Brij 58/Igepal CO-430 1.0	5.0 471-6	p=1.0 Cyc: $CHCl_3$	125	50	40	400/2900	26
602-39	10.0	6.0	Brij 58/Igepal CO-430 1.0	5.0 471-6	p=1.0 Cyc: $CHCl_3$	125	50	40	300/3300	58

* Burst effect ratio = $\frac{\text{conductivity at 1.0 min}}{\text{conductivity at max. release time}}$

**Cyc = Cyclohexane

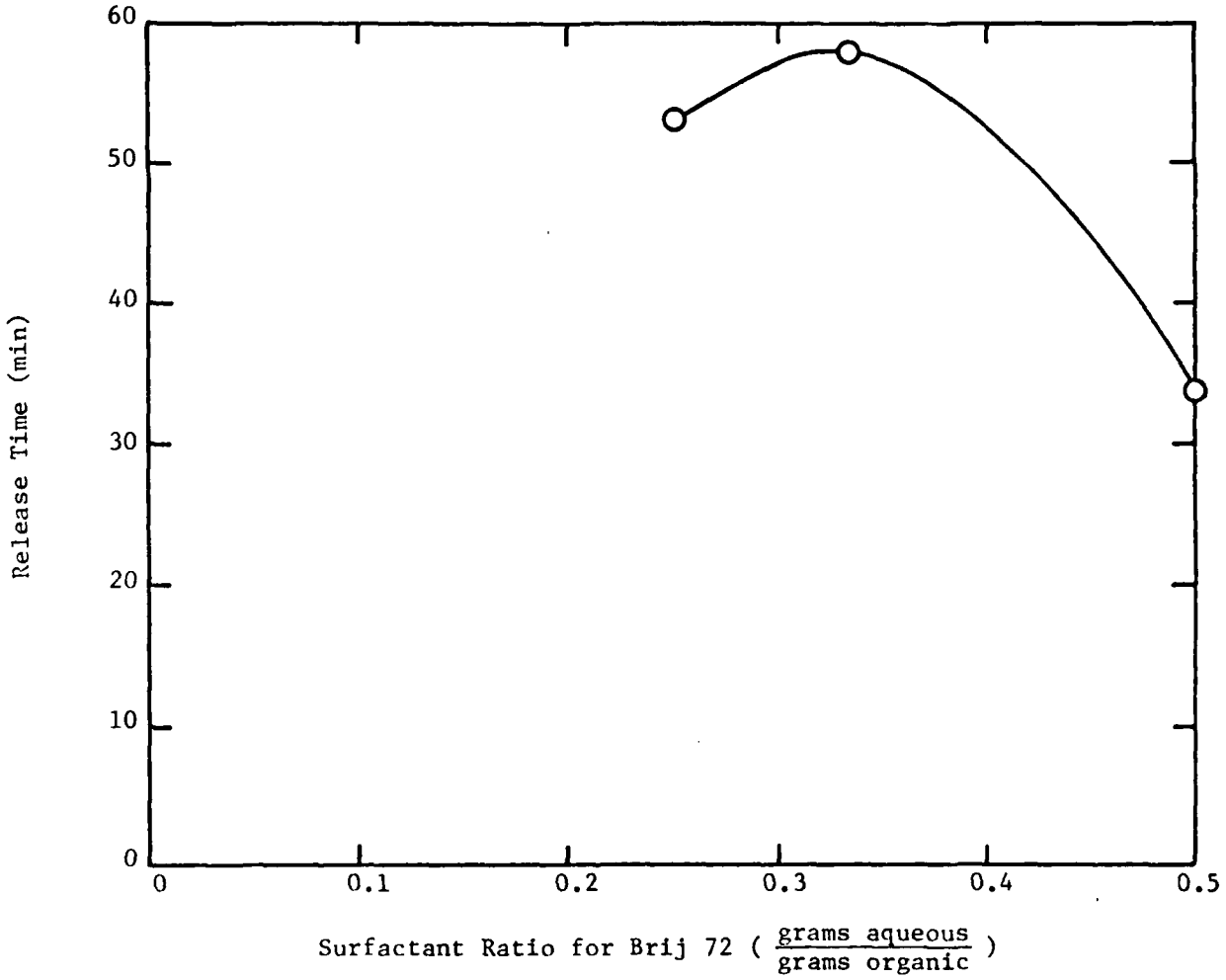

Figure 79. Surfactant Ratio for Brij 72 Versus Release Time.

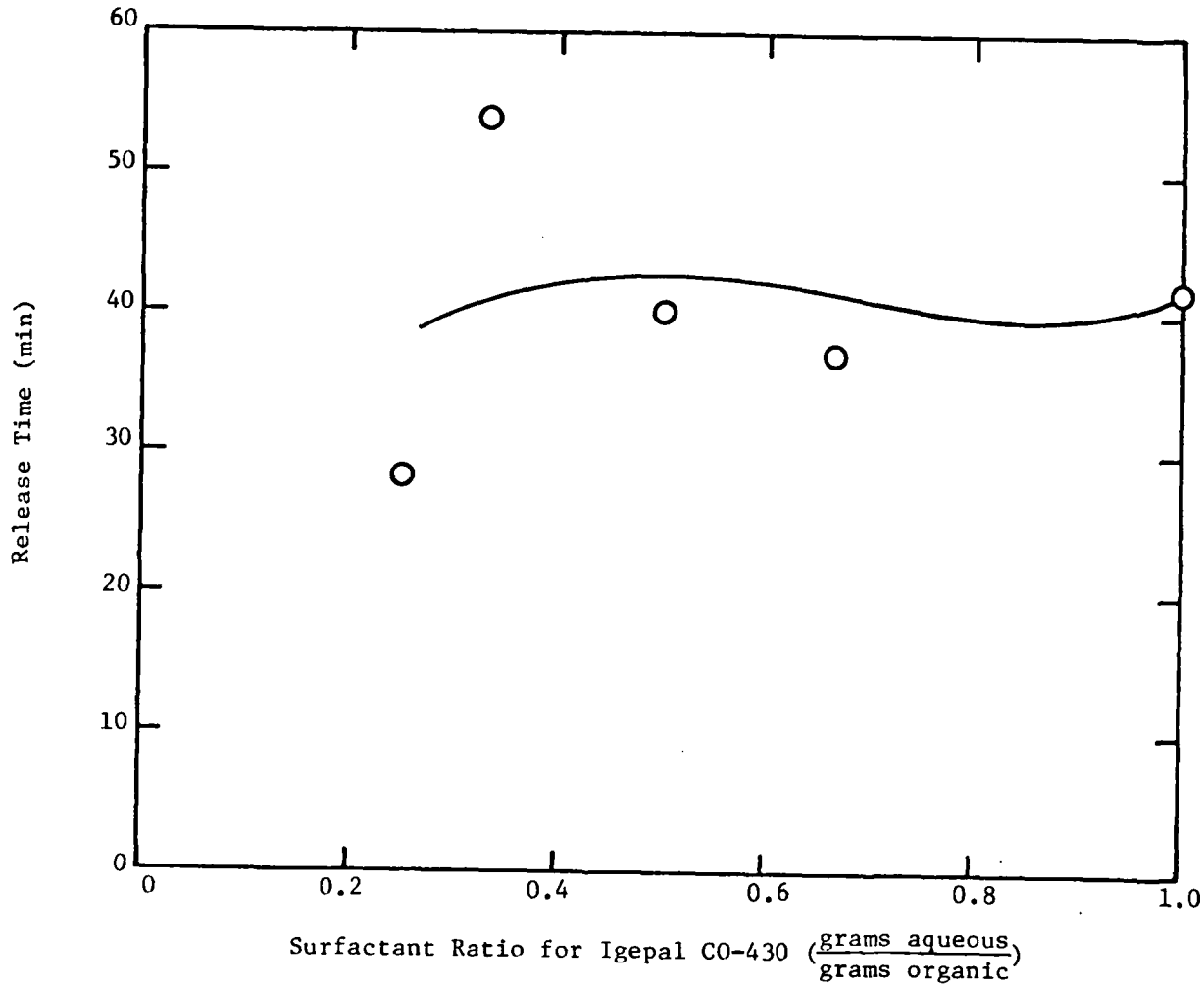

Figure 80. Surfactant Ratio for Igepal CO-430 Versus Release Time.

cell microcapsules. Since permeation of the encapsulated material is directly related to cell wall thickness, the presence of surface areas with reduced membrane thickness would markedly alter the release time of the core material. To investigate this possibility, a study was conducted in which the material balance of the monomers was greatly altered in an effort to further disrupt the normal accretion process and generate open cell microcapsules.

The data presented in Table 14 and Figure 81 uses the emulsifying agents Brij 58 and Igepal RC-430 and illustrates the effects of varying the ratio of sebacyl chloride/hexane-1,6-diamine from 0.3 to 0.8 in increments of 0.1. Interestingly, the release times of the AFIF mixture from the microcapsules appears to be fairly independent of the monomer material balance. However, as expected, the higher ratios of monomer did provide somewhat better results.

The study presented in Table 15 and Figure 82 involved using Brij 58 and Igepal RC-520 as the combination of emulsifying agents and varying the monomer material balance from 0.2 to 0.7 in increments of 0.1. These data illustrate the typical variability found in many of the studies attempted using the nylon 6,10 encapsulation procedure.

The study presented in Table 16 and Figure 83 utilized Brij 58 and Brij 72 as the combination of emulsifying agents and reverses the monomer material balance of sebacyl chloride/hexane-1,6-diamine to inordinately high values (ratios of 3.0 to 4.0). These data further substantiate the independence of monomer material balance and AFIF release time.

5. Evaluation of the Organic Solvent Phase Composition

Interfacial polymerization involves diffusion of the diamine across the aqueous/organic phase interface and subsequent condensation with the diacid chloride in the organic phase (46) (Figure 84).

Under these conditions the homogeneity of the wall accretion process is greatly dependent upon the thermodynamic nature of the organic phase. In line with this consideration, a study was conducted which evaluated the effects of microcapsule formation as a function of organic phase character. The solvents and mixtures evaluated included cyclohexane, toluene, 3/1 cyclohexane/chloroform, and 2.2/1 cyclohexane/chloroform.

TABLE 14. RELEASE TIME VERSUS SEBACYL CHLORIDE/HEXANE-1,6-DIAMINE USING BRIJ 58 AND IGEPAL CO-430

Sample	Sebacyl Chloride/ Hexane-1,6-diamine Ratio	Aqueous Surf. Type and Amount (grams)	Organic Surf. Type and Amount (grams)	Inhibitor (grams)	Organic Solvent Comp. and Ratio**	Organic Solvent (ml)	Aqueous Solvent (ml)	Temp. (°C)	Burst* Effect Ratio	Release Time (min)
602-28	.30	1.0 Brij 58	2.0 Igepal CO-430	5.0 471-6	2.2:1 Cyc: $CHCl_3$	125	50	30	500/2800	28
602-29	.40	1.0 Brij 58	2.0 Igepal CO-430	5.0 471-6	2.2:1 Cyc: $CHCl_3$	125	50	30	800/3700	38
602-25	.50	1.0 Brij 58	2.0 Igepal CO-430	5.0 471-6	2.2:1 Cyc: $CHCl_3$	125	50	30	600/2600	30
602-26	.60	1.0 Brij 58	2.0 Igepal CO-430	5.0 471-6	2.2:1 Cyc: $CHCl_3$	125	50	30	700/2900	26
602-30	.70	1.0 Brij 58	2.0 Igepal CO-430	5.0 471-6	2.2:1 Cyc: $CHCl_3$	125	50	30	600/3800	56
602-31	.80	1.0 Brij 58	2.0 Igepal CO-430	5.0 471-6	2.2:1 Cyc: $CHCl_3$	125	50	30	300/2800	48

* Burst effect ratio = $\frac{\text{conductivity at 1.0 min}}{\text{conductivity at max. release time}}$

**Cyc = Cyclohexane

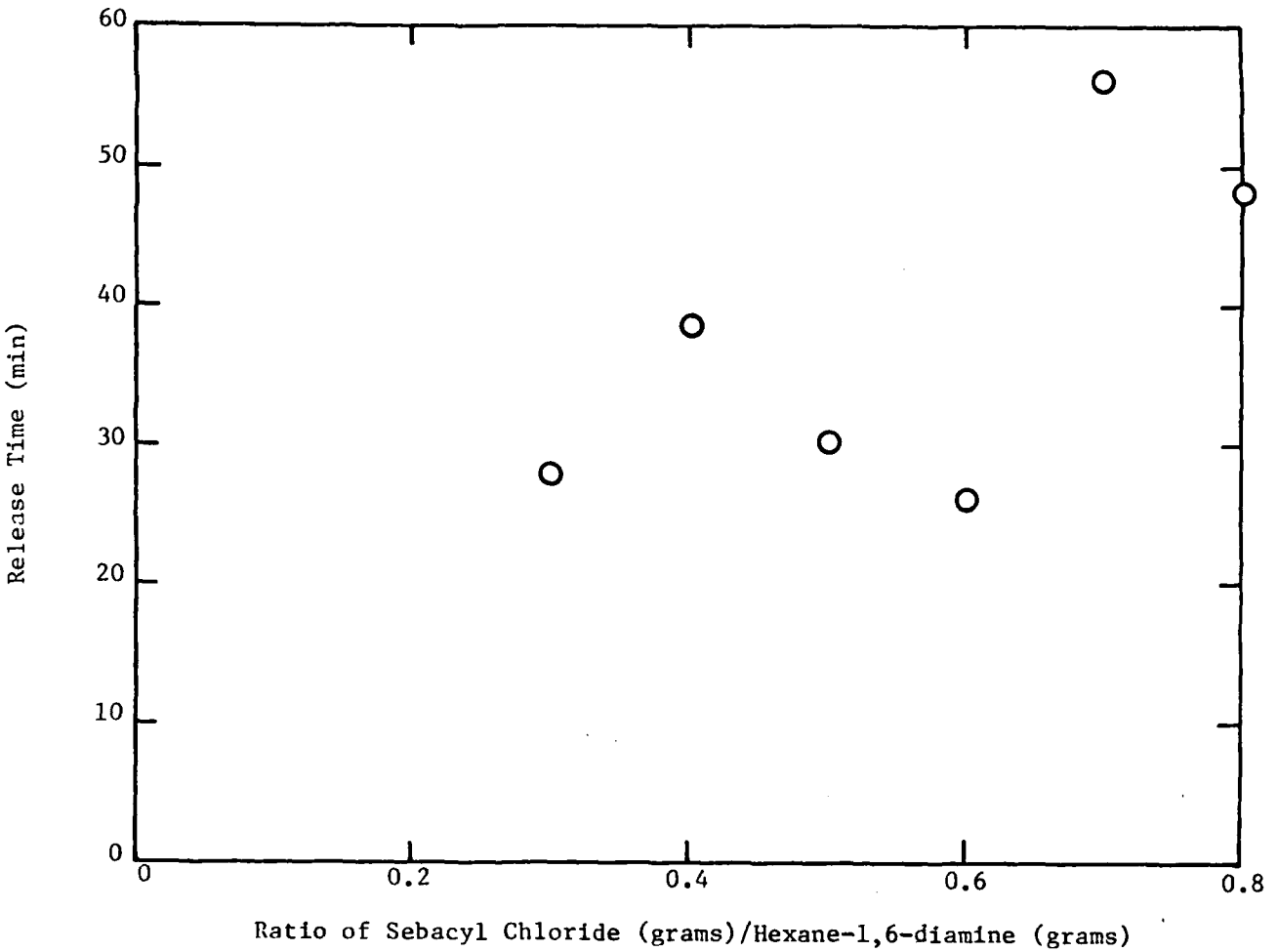

Figure 81. Ratio of Sebacyl Chloride/Hexane-1,6-diamine Versus Release Time Using Brij 58 and Igepal CO-430 as Emulsifying Agents.

TABLE 15. RELEASE TIME VERSUS SEBACYL CHLORIDE/HEXANE-1,6-DIAMINE USING BRIJ 58 AND IGEPAL RC-520

Sample	Sebacyl Chloride/ Hexane-1,6-diamine Ratio	Aqueous Surf. Type and Amount (grams)	Organic Surf. Type and Amount (grams)	Inhibitor (grams)	Organic Solvent Comp. and Ratio**	Organic Solvent (ml)	Aqueous Solvent (ml)	Temp. (°C)	Burst* Effect Ratio	Release Time (min)
584-29	.20	0.5 Brij 58	2.0 Igepal RC-520	5.0 471-6	3:1 Cyc: $CHCl_3$	125	50	40	900/3300	42
584-30	.20	0.5 Brij 58	2.0 Igepal RC-520	5.0 471-6	3:1 Cyc: $CHCl_3$	125	50	40	800/3300	28
584-31	.40	0.5 Brij 58	1.0 Igepal RC-520	5.0 471-6	3:1 Cyc: $CHCl_3$	125	50	30	1500/6000	22
584-32	.40	0.5 Brij 58	2.0 Igepal RC-520	5.0 471-6	3:1 Cyc: $CHCl_3$	125	50	40	1900/6000	14
584-50	.50	0.5 Brij 58	2.0 Igepal RC-520	5.0 471-6	3:1 Cyc: $CHCl_3$	125	50	40	1200/6300	80
584-60	.50	0.5 Brij 58	1.0 Igepal RC-520	5.0 471-6	3:1 Cyc: $CHCl_3$	125	50	40	2000/6300	44

(continued)

* Burst effect ratio = $\frac{\text{conductivity at 1.0 min}}{\text{conductivity at max. release time}}$

**Cyc = Cyclohexane

TABLE 15. (continued)

Sample	Sebacyl Chloride/ Hexane-1,6-diamine Ratio	Aqueous Surf. Type and Amount (grams)	Organic Surf. Type and Amount (grams)	Inhibitor (grams)	Organic Solvent Comp. and Ratio**	Organic Solvent (ml)	Aqueous Solvent (ml)	Temp. (°C)	Burst* Effect Ratio	Release Time (min)
584-37	.60	0.5 Brij 58	2.0 Igepal RC-520	5.0 471-6	3:1 Cyc: $CHCl_3$	125	50	40	1000/5000	28
584-38	.60	0.5 Brij 58	2.0 Igepal RC-520	5.0 471-6	3:1 Cyc: $CHCl_3$	125	50	40	1200/5700	34
584-57	.70	0.5 Brij 58	1.0 Igepal RC-520	5.0 471-6	2.2:1 Cyc: $CHCl_3$	125	50	30	2000/7000	34
584-58	.70	0.5 Brij 58	2.0 Igepal RC-520	5.0 471-6	3:1 Cyc: $CHCl_3$	125	50	40	2000/6100	30

* Burst effect ratio = $\frac{\text{conductivity at 1.0 min}}{\text{conductivity at max. release time}}$

**Cyc = Cyclohexane

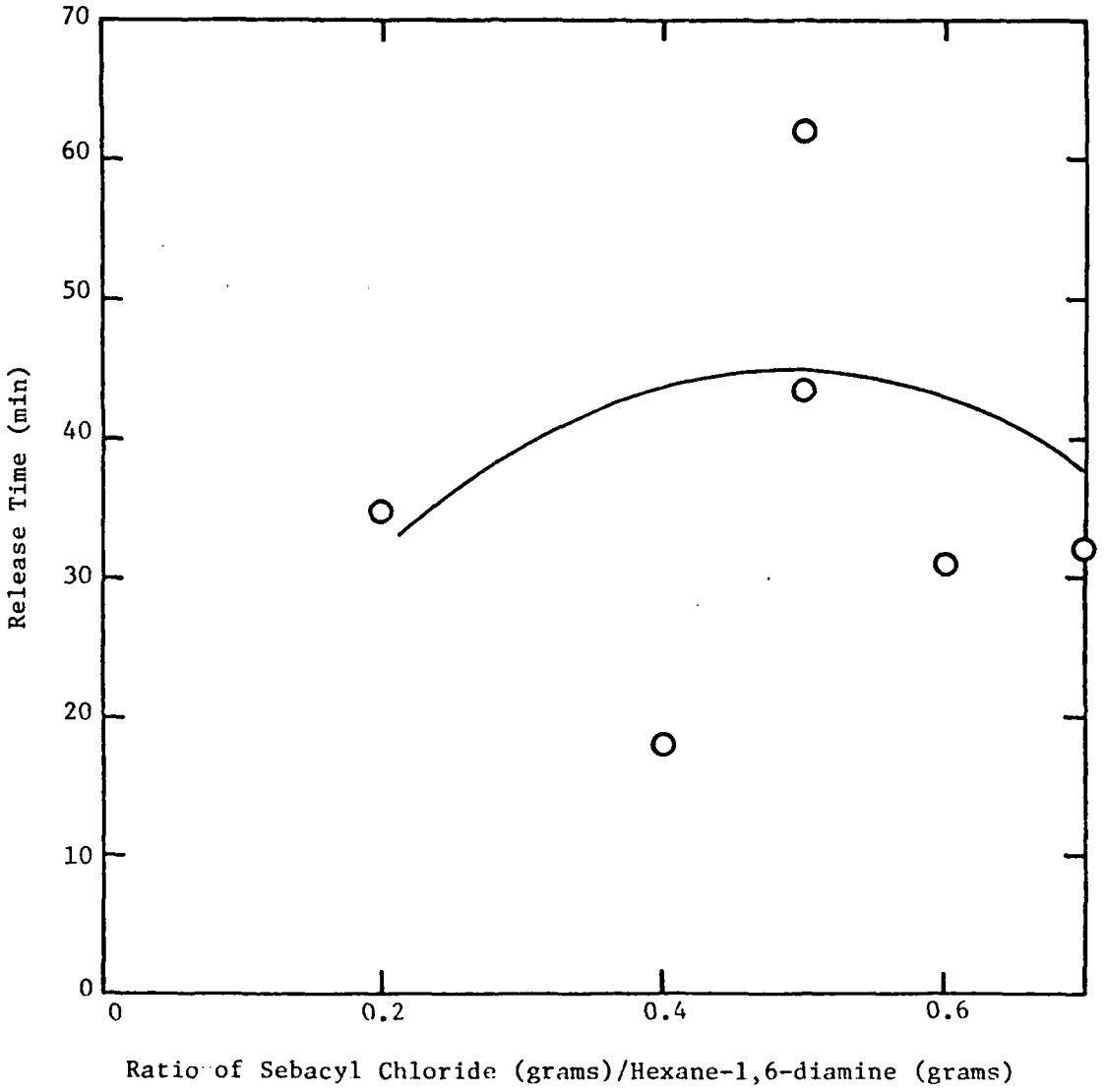

Figure 82. Ratio of Sebacyl Chloride/Hexane-1,6-diamine Versus Release Time Using Brij 58 and Igepal RC-520 as Emulsifying Agents.

TABLE 16. RELEASE TIME VERSUS SEBACYL CHLORIDE/HEXANE-1,6-DIAMINE USING BRIJ 58 AND BRIJ 72

Sample	Sebacyl Chloride/ Hexane-1,6-diamine Ratio	Aqueous Surf. Type and Amount (grams)	Organic Surf. Type and Amount (grams)	Inhibitor (grams)	Organic Solvent Comp. and Ratio**	Organic Solvent (ml)	Aqueous Solvent (ml)	Temp. (°C)	Burst* Effect Ratio	Release Time (min)
602-43	3.0	0.5 Brij 58	2.0 Brij 72	5.0 471-6	2.2:1 Cyc: $CHCl_3$	125	50	40	500/5400	62
602-44	3.0	0.5 Brij 58	2.0 Brij 72	5.0 471-6	2.2:1 Cyc: $CHCl_3$	125	50	40	800/5500	48
602-47	3.5	0.5 Brij 58	2.0 Brij 72	5.0 471-6	2.2:1 Cyc: $CHCl_3$	125	50	40	400/3000	8
602-48	3.5	0.5 Brij 58	2.0 Brij 72	5.0 471-6	2.2:1 Cyc: $CHCl_3$	125	50	40	600/5200	52
602-51	4.0	0.5 Brij 58	2.0 Brij 72	5.0 471-6	2.2:1 Cyc: $CHCl_3$	125	50	40	600/5000	58
602-52	4.0	0.5 Brij 58	2.0 Brij 72	5.0 471-6	2.2:1 Cyc: $CHCl_3$	125	50	40	400/4500	48

* Burst effect ratio = $\frac{\text{conductivity at 1.0 min}}{\text{conductivity at max. release time}}$

**Cyc = Cyclohexane

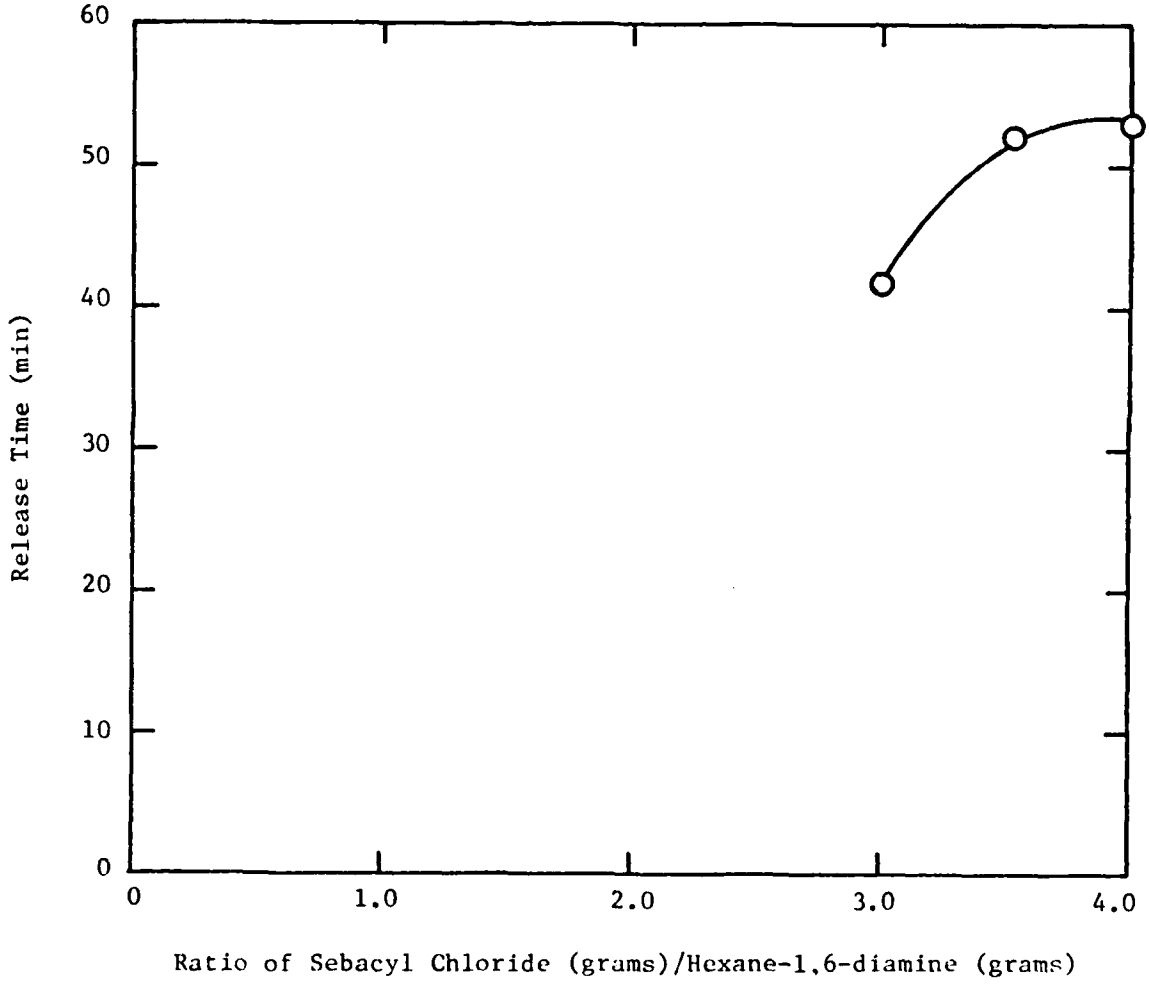

Figure 83. Ratio of Sebacyl Chloride/Hexane-1,6-diamine Versus Release Time Using Brij 58 and Brij 72 as Emulsifying Agents.

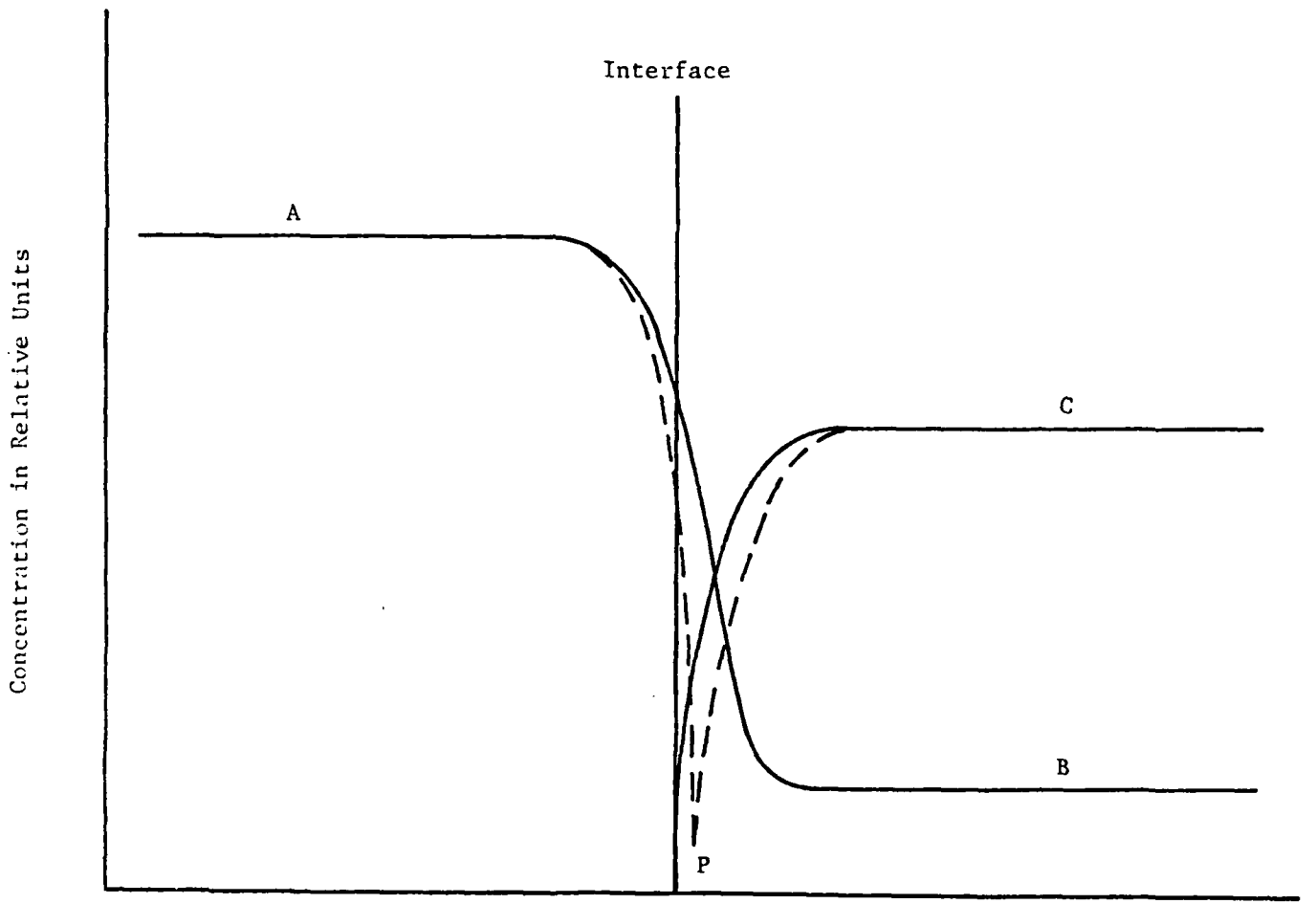

Figure 84. Schematic diagram of concentrations in an interfacial polyamidation. Amine groups (A) are in the water phase. Acid chloride (C) and amine groups at partition equilibrium (B) are in the organic phase. P and the dotted lines show the relation of the reactive groups when the first incremental layer of polymer forms.

The data presented in Table 17 again illustrates that the release time of the AFIF mixture from the microcapsules was somewhat independent of the investigated parameter. However, since the 2.2/1 cyclohexane/chloroform ratio possessed a density which equaled that of the aqueous phase and also provided relatively better release times, this solvent combination was used in subsequent studies to evaluate other variables.

6. Evaluation of the Reaction Temperature

Since increases in reaction temperature have a profound effect on reaction rate, a study was conducted which investigated the release time of microcapsules formed at varying temperatures. The study utilized Brij 58 and Brij 72 as the surfactant combination, and the 2.2/1 ratio of cyclohexane to chloroform as the organic phase. Evaluation of the data presented in Table 18 and Figure 85 indicates that no significant advantage was gained in release time as the reaction temperature was varied over normal ranges.

7. Overview of the Nylon 6,10 Pilot Study

Although the objective of identifying the parameters which could be used to control the release characteristics of the microcapsules was not fully realized, the nylon 6,10 pilot study provided several positive results.

a) A procedure was developed which yielded AFIF-containing microcapsules with diameters ranging from 1-10 μm. Photomicrographs of representative samples are presented in Figures 86-90.

b) It is possible to microencapsulate the AFIF mixture, and obtain some degree of sustained release. In most cases the average release time was approximately 15-30 minutes, with the longest time at 56 minutes.

c) The amount of corrosion inhibitor (% loading) contained in a given sample of microcapsules was determined through atomic absorption analysis of boron: 2.0 g of microcapsule sample was triturated with 25.0 ml deionized water, and the solution was allowed to stand overnight; the sample was then filtered to remove the solid material, and the filtrate was analyzed for boron. The loading (g inhibitor/g sample) was calculated using the data for the inhibitor formulation composition. The values fell in the 18-24 percent range as illustrated in Table 19. Comparison of these values with the the-

TABLE 17. ORGANIC SOLVENT PHASE COMPOSITION

Sample	Hexane 1,6 diamine (grams)	Sebacyl chloride (grams)	Aqueous Surf. Type and Amount (grams)	Organic Surf. Type and Amount (grams)	Inhibitor (grams)	Organic Solvent Comp. and Ratio**	Organic Solvent (ml)	Aqueous Solvent (ml)	Temp. (°C)	Burst* Effect Ratio	Release Time (min)
555-95	10.0	4.0	0.5 Brij 58	1.0 Brij 72	5.0 471-6	Cyc	125	50	25	3000/5400	8
584-3	10.0	4.0	0.5 Brij 58	1.0 Brij 72	5.0 471-6	Toluene	125	50	25	2900/5400	20
555-92	10.0	4.0	0.5 Brij 58	1.0 Brij 72	5.0 471-6	3:1 Cyc: $CHCl_3$	125	50	25	1900/5000	30
584-24	10.0	4.0	0.5 Brij 58	1.0 Brij 72	5.0 471-6	2.2:1 Cyc: $CHCl_3$	125	50	25	2000/4400	30

* Burst effect ratio = $\frac{\text{conductivity at 1.0 min}}{\text{conductivity at max. release time}}$

**Cyc = Cyclohexane

TABLE 18. RELEASE TIME VERSUS TEMPERATURE

Sample	Hexane 1,6 diamine (grams)	Sebacyl chloride (grams)	Aqueous Surf. Type and Amount (grams)	Organic Surf. Type and Amount (grams)	Inhibitor (grams)	Organic Solvent Comp. and Ratio**	Organic Solvent (ml)	Aqueous Solvent (ml)	Temp. (°C)	Burst* Effect Ratio	Release Time (min)
555-92	10.0	4.0	0.5 Brij 58	1.0 Brij 72	5.0 471-6	2.2:1 Cyc: $CHCl_3$	125	50	25	1900/5000	30
584-16	10.0	4.0	0.5 Brij 58	1.0 Brij 72	5.0 471-6	2.2:1 Cyc: $CHCl_3$	125	50	30	3200/6600	16
602-67	10.0	6.0	0.5 Brij 58	1.0 Brij 72	5.0 471-6	2.2:1 Cyc: $CHCl_3$	125	50	40	700/3500	10

* Burst effect ratio = $\frac{\text{conductivity at 1.0 min}}{\text{conductivity at max. release time}}$

**Cyc = Cyclohexane

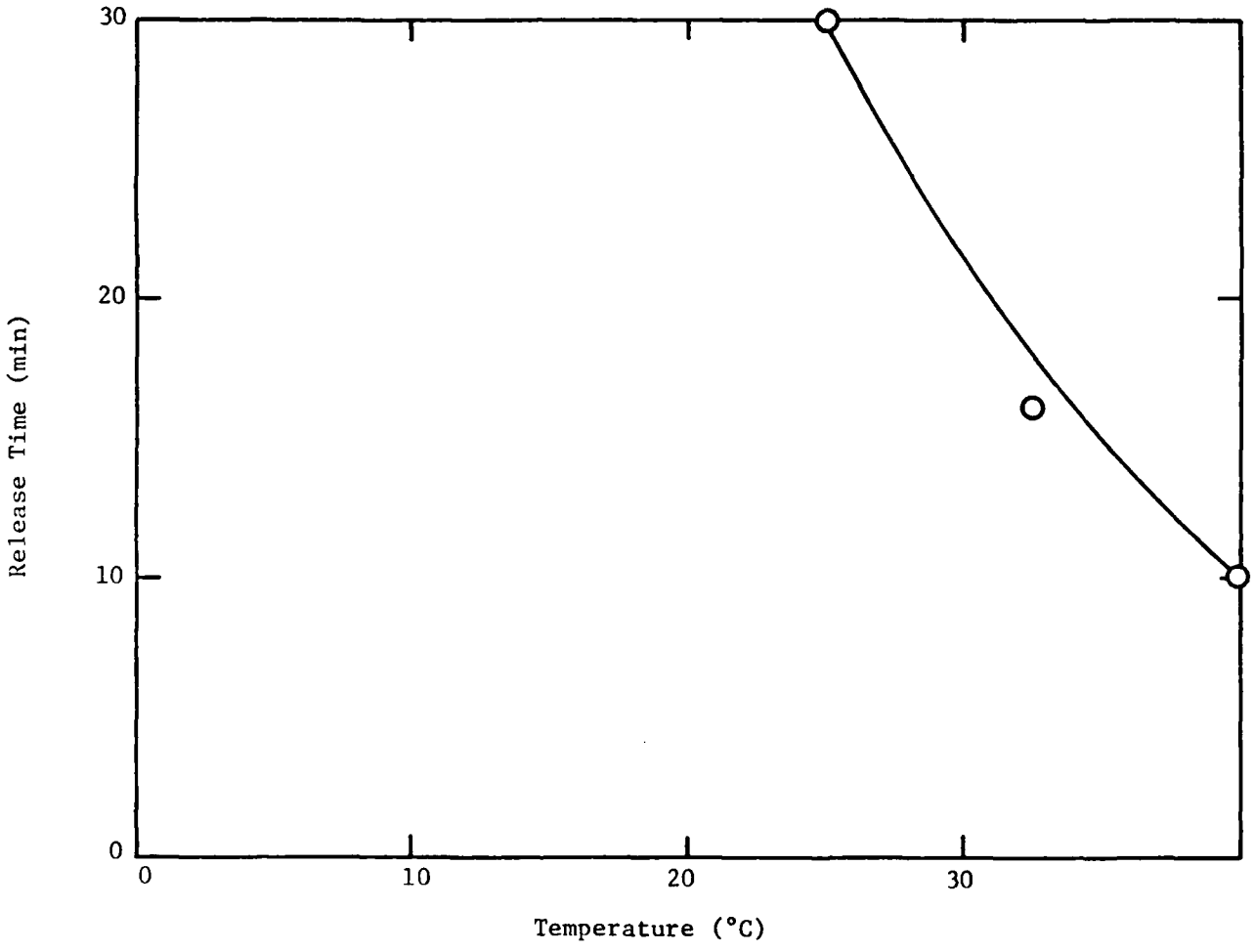

Figure 85. Temperature Versus Release Time.

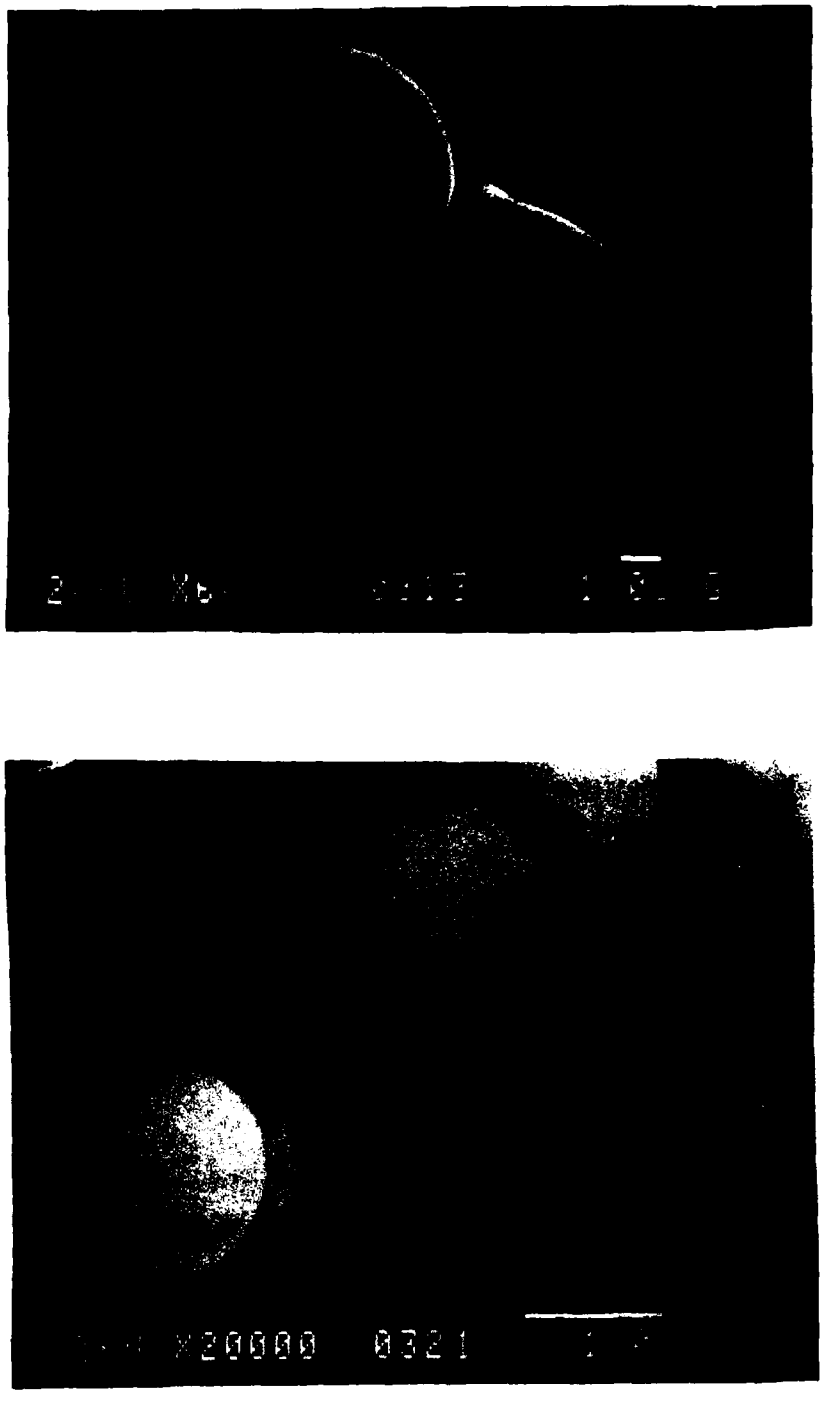

Figure 86. Scanning electron photomicrographs of samples 602-2 and 602-3, taken at 6,000X and 20,000X, respectively.

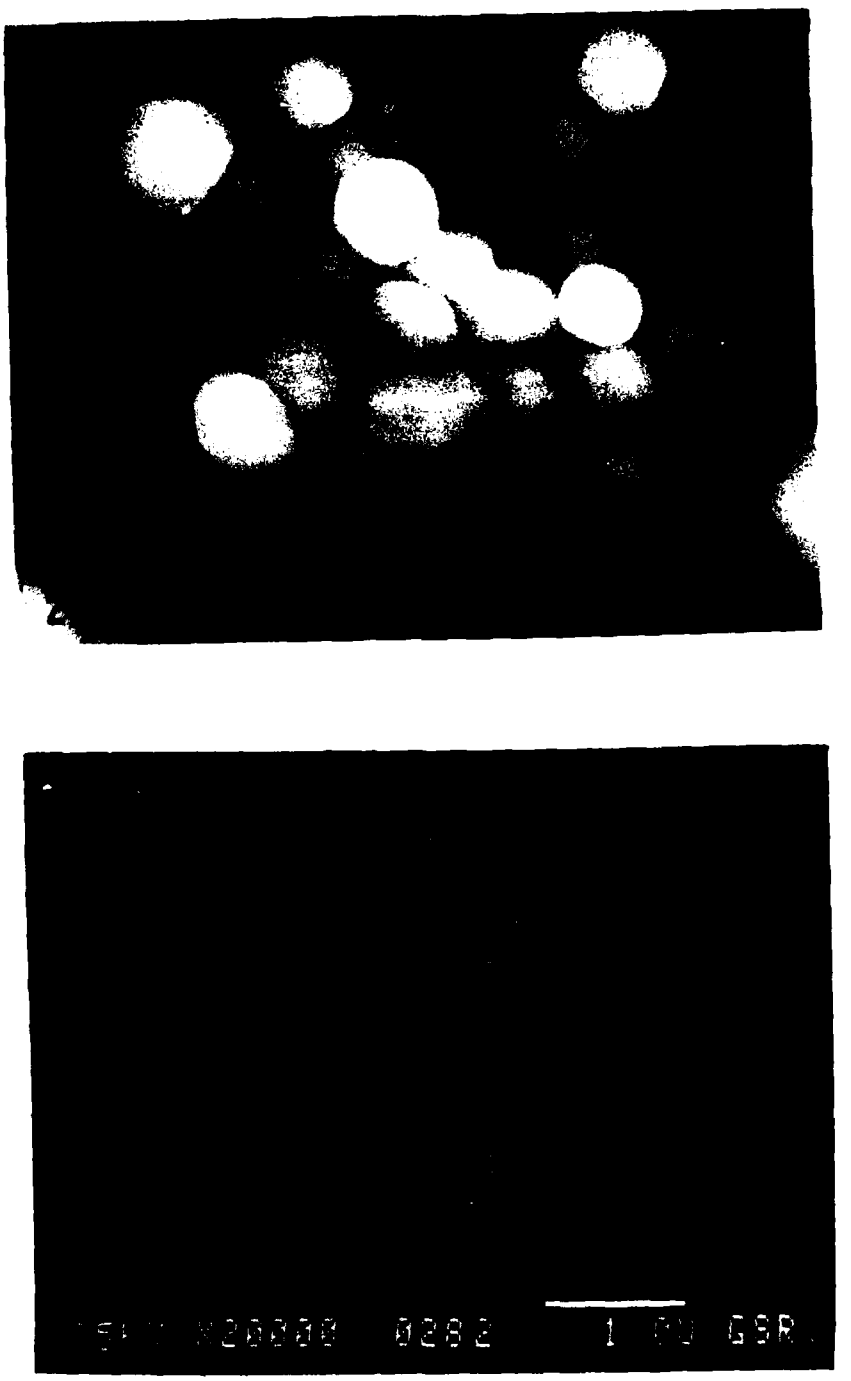

Figure 87. Scanning electron photomicrographs of samples 602-4 and 584-92, taken at 6,000X and 20,000X, respectively.

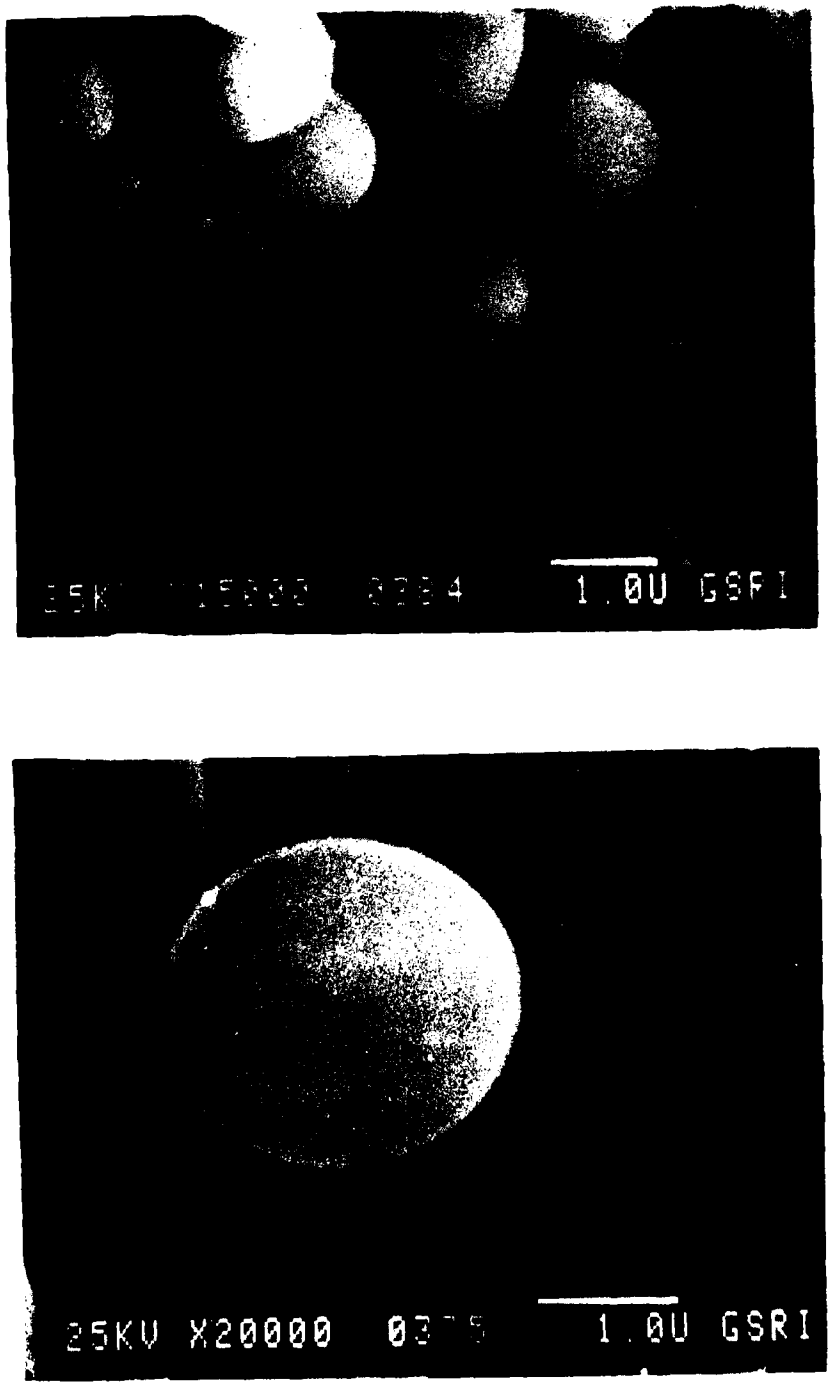

Figure 88. Scanning electron photomicrographs of samples 602-9 and 602-7, taken at 15,000X and 20,000X, respectively.

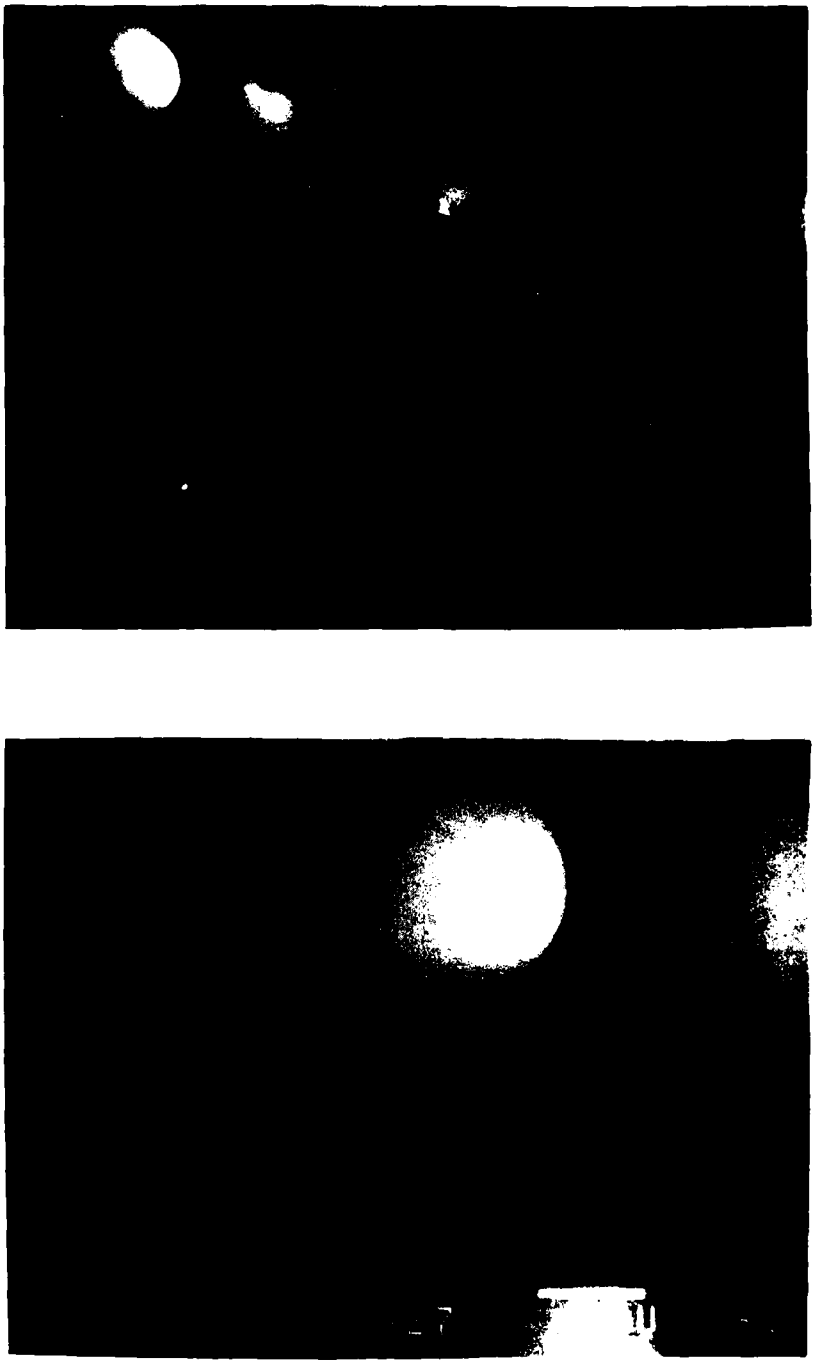

Figure 89. Scanning electron photomicrographs of samples 602-11 and 602-10 taken at 3,000X and 15,000X, respectively.

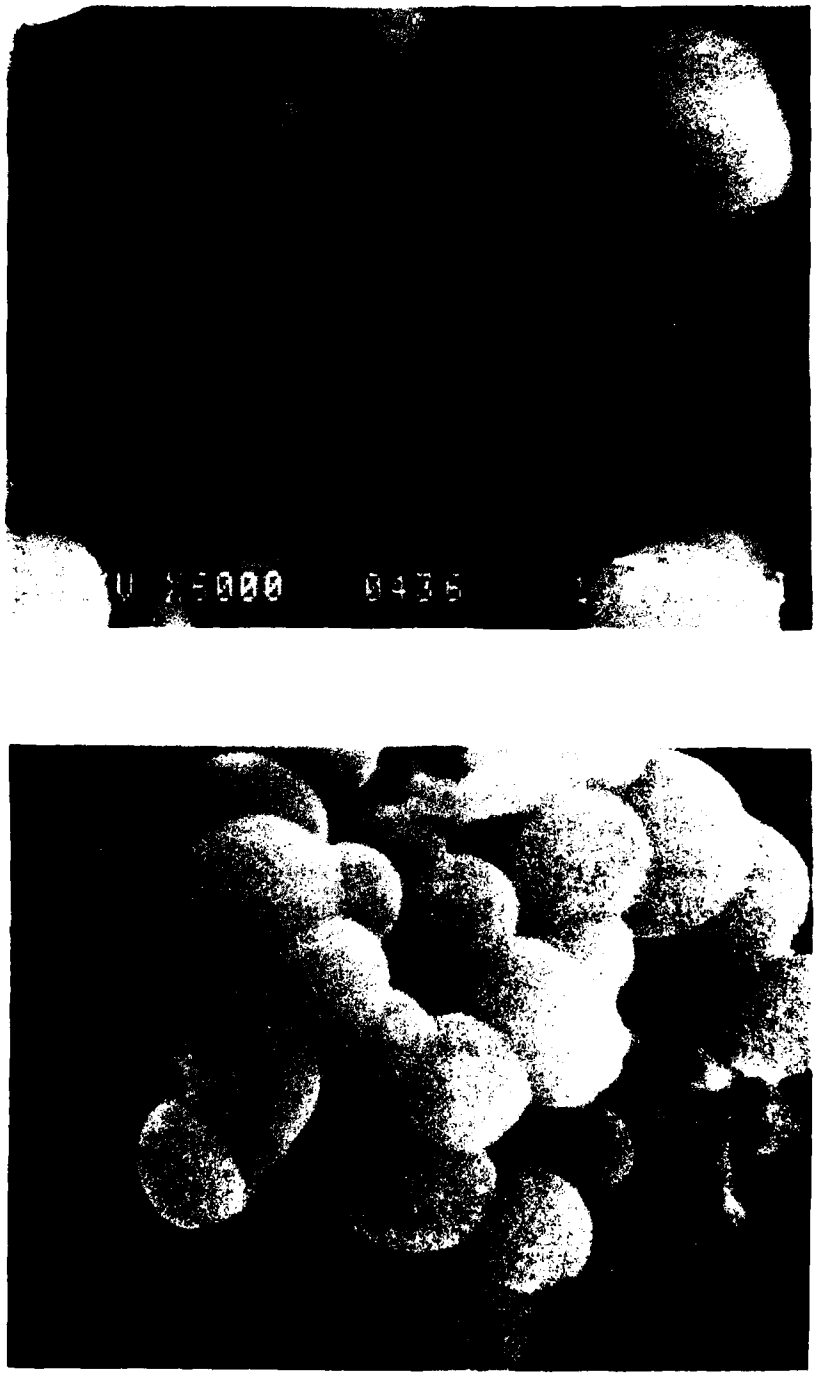

Figure 90. Scanning electron photomicrographs of samples 602-12 and 584-56, taken at 6,000X and 20,000X, respectively.

TABLE 19. BORON ANALYSIS BY ATOMIC ABSORPTION SPECTROSCOPY

Sample	Percent Loading
602-56	18.0
602-43	21.4
602-48	14.4
602-51	23.7

oretical percent loading values indicated that the microcapsules contained from 76 to 96 percent of their theoretical capacity, indicating the interfacial polymerization technique for microencapsulation was quite efficient for the AFIF mixture.

d) pH measurements of the net change in pH value over the time course of corrosion inhibitor release indicated a net release of an acidic core material from the microcapsule into the aqueous medium (Table 20). Since HCl is a by-product of the condensation reaction, the microcapsules were also tested for release of chloride anions. The weight percentage of chloride ion contained in the microcapsule core was found to range from 5.6 to 11.0 percent (Table 21). While the condensation reaction is known to occur primarily in the organic phase, apparently there is a sufficient thermodynamic and/or kinetic driving force for migration and partitioning of the HCl into the aqueous core phase. Obviously, since the entrapment of chloride ions in the microcapsules is unacceptable for an anticorrosive system, alternatives to the nylon 6,10 reaction were sought which would not yield an undesirable by-product.

E. Polyurea Microcapsules

1. Initial Formulation Work

Of the polymer candidates which are useful in forming microcapsule membrane walls through interfacial polymerization, the polyureas offer the best chance of success for providing the improvement needed over the nylon 6,10 system. Polyureas are similar in physical and mechanical properties to

TABLE 20. pH PROFILE OF MICROCAPSULE RELEASE

Sample	pH (water blank)	ΔpH
602-70	8.4	+0.6
602-72	8.0	+0.9
602-73	8.0	+1.0
602-74	7.2	-4.8
602-75	7.3	-5.0
602-76	7.6	-5.6
602-77	7.3	-5.3
602-78	7.1	-4.3
602-79	7.1	-4.2
602-80	7.3	-4.5
602-81	7.4	-4.5
602-82	7.3	-4.4
602-89	7.1	-4.1

TABLE 21. WEIGHT PERCENT CHLORIDE IN SELECTED MICROCAPSULE SAMPLES

Sample	Percent Chloride
602-41	5.6
602-67-L	6.8
602-75	11.0
602-77	6.4
602-79	7.8
602-81	8.2
602-83	10.2

the nylon systems, and are therefore capable of providing the high degree of integrity needed in the end application. The high level of cohesive energy density associated with the urea linkages ensures good solvent resistance and tractability of the microcapsules with the solvent mixture used in the epoxy-polyamide primer formulation. Polyureas are formed through the reaction of a diamine and a diisocyanate without the release of a by-product, thereby avoiding the chloride problem associated with the nylon system. The major disadvantage of substituting a polyurea for nylon arises from differences in reaction kinetics and surfactant-polymer interaction energies, which may mitigate direct transference of the technologies established with the nylon 6,10 system.

The initial attempts to form polyurea microcapsules involved only one change in the established nylon 6,10 procedure. Sebacyl chloride was replaced by toluene-2,4-diisocyanate (TDI), leaving all other ingredients and parameters unaltered. The modified encapsulation process took place without any significant observable change, but scanning electron microscopic (SEM) analysis indicated the formation of a spongy, reticulated structure possessing only the remnant characteristics of microcapsules (Figure 91).

In subsequent attempts, the kinetics of the polyurea reaction were modified by use of a catalyst, dibutyltin dilaurate (DBTDL). Tin catalysts increase the rate of the addition reaction needed to form the membrane wall over that of side reactions, such as hydrolysis by water. The procedure used for the preparation is presented in Table 22. SEM analysis of the product revealed the formation of polyurea microcapsules, with a large population possessing particle sizes below 1.0 μm (Figure 92).

Further evidence that the use of TDI resulted in the generation of a finer particle size product was inferred from the changes which occurred in the rheological characteristics of the emulsion during the polymerization reaction. In fine particle size emulsions the nearest neighbor distance between particles is greatly diminished, and as a result the viscosity of the suspension greatly increases. While increased viscosity was not a problem with the nylon 6,10 system, the polyurea system displayed such a marked viscosity increase during the final stages of the TDI addition that mixing was impaired. Subsequent preparation variations demonstrated that complete cessation of mixing could be avoided by programming the addition rate of the TDI-containing phase over an approximate 3-minute period. SEM analysis of a sample prepared in this manner (619-5) indicated the formation

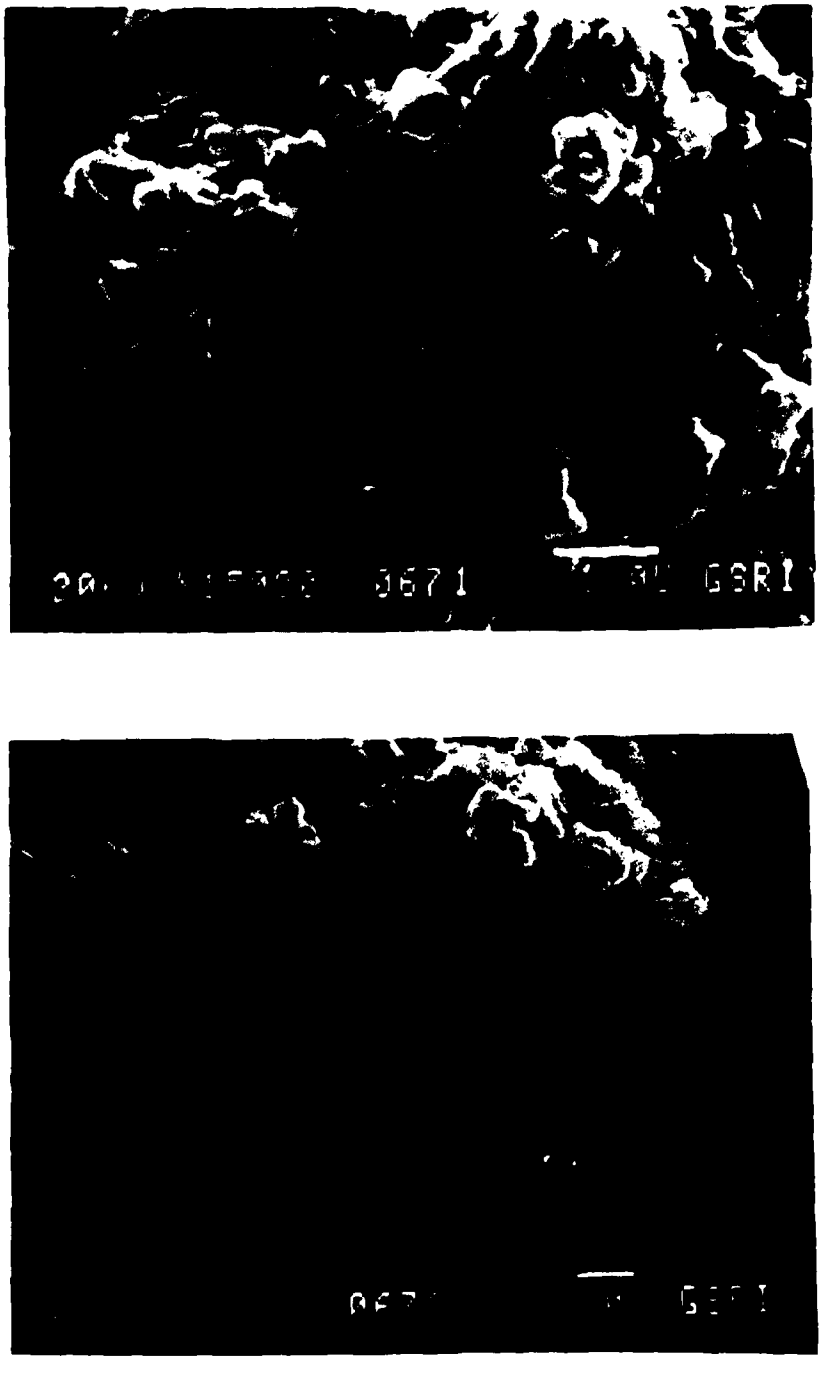

Figure 91. Microcapsule structure for the reaction product of TDI and hexane-1,6-diamine.

TABLE 22. INITIAL PROCEDURE FOR POLYUREA MICROENCAPSULATION OF THE AFIF MIXTURE

A. Solution Preparation

1. 4.0 g hexane-1,6-diamine + 5.0 g AFIF + 0.5 g Brij 58 + 50.0 ml of deionized water.
2. 2.0 g Brij 72 + 0.5 drop dibutyltin dilaurate in 100.0 ml of cyclohexane/chloroform, 2.2/1 (v/v).
3. 6.1 g toluene-2,4-diisocyanate (2% molar excess over the amine) in 25.0 ml of cyclohexane/chloroform, 2.2/1 (v/v).

B. Reaction Procedure

1. Set blender temperature at 40°C.
2. Add solution (1) to blender at 16500 rpm.
4. Add solution (3) to blender, dropwise, at 16500 rpm.
5. Add solution (3), dropwise; allow blender to run 30 sec after solution (3) is added.
6. Remove product from reaction vessel.

C. Purification and Isolation

1. Transfer reaction product into Erlenmeyer flask.
2. Extract the suspended product repeatedly with pure cyclohexane (300-400 ml, 3X).
3. Store the product in pure cyclohexane, suspended within the Erlenmeyer flask.

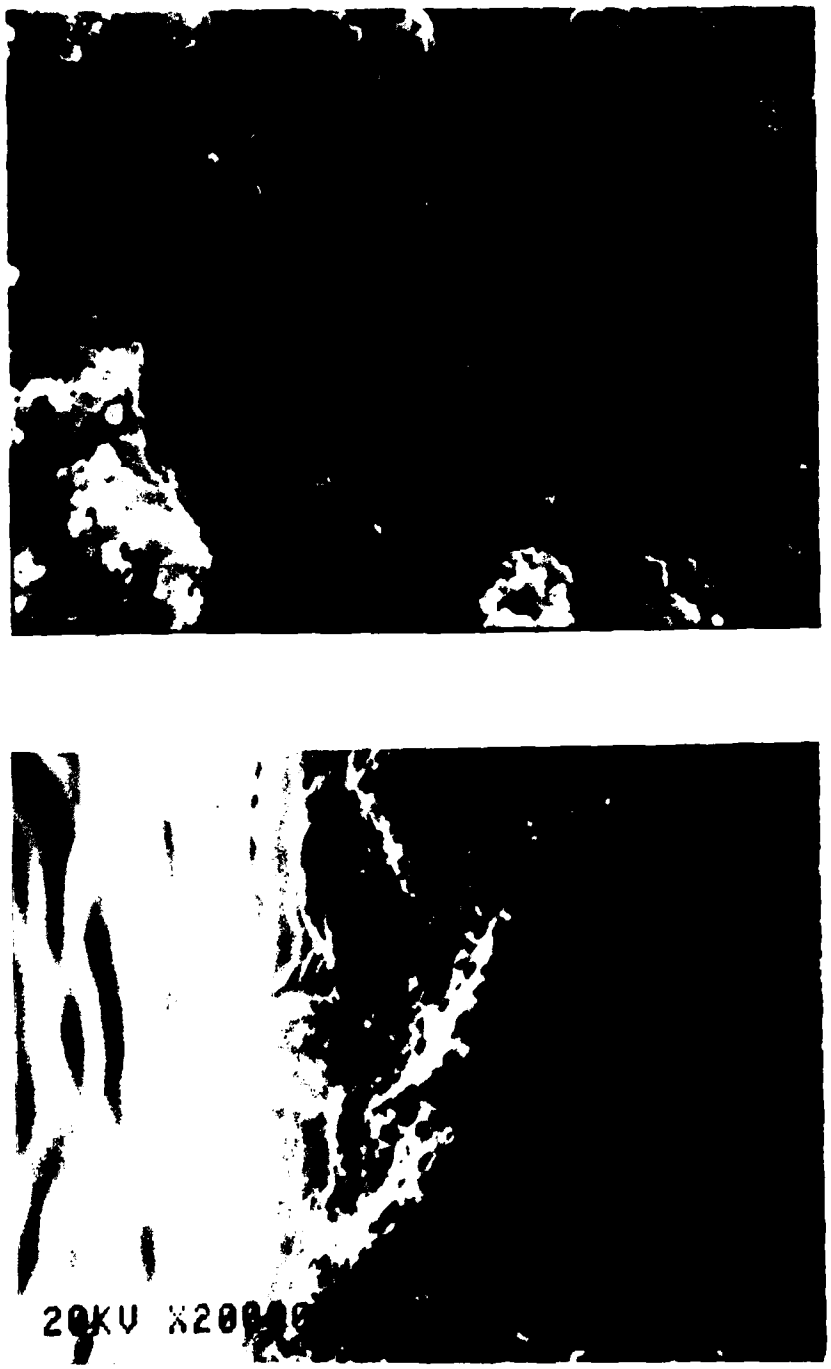

Figure 92. Microcapsule structure for the reaction product of TDI and hexane-1,6-diamine using DBTDL catalyst.

of intact microcapsules, many of which were in the 1.0-5.0 μm particle size range (Figure 93). Analysis of the particle size distribution by means of Coulter Counter indicated that only 1.8 volume percent of microcapsules possessed particle sizes in excess of 16 μm. The mean particle size (volume percent) was 6.17 μm with a 1.39 μm standard deviation (Figures 94 and 95).

In many of the experimental runs where mixing was impaired, the resulting product was found to possess aggregated material ranging from 0.1 to 1 mm in diameter. To eliminate the formation of the aggregated material, a partial optimization study was conducted which involved examining the effects of phase ratio, rate of TDI addition, and particle surface composition. Table 23 indicates the various parameters investigated in the study. The following qualitative conclusions were drawn:

a) An increase in phase volume decreased the aggregate formation but produced microcapsules which rapidly flocculated when dispersed in a 7% NH_4SCN/isopropanol (IPA) solution (619-18 versus 619-20). Dispersal in the NH_4SCN/IPA solution was a requirement for Coulter Counter particle size determinations.

b) An increase in the TDI addition time decreased the formation of the aggregates but produced capsules which flocculated in the NH_4SCN/IPA solution (619-18 versus 619-19).

c) Microcapsules prepared in the presence of an excess of TDI (perhaps producing a urethane surface) demonstrated greater tendency to remain dispersed in the NH_4SCN/IPA medium than those prepared using a limiting amount of TDI (producing an amine-rich surface).

The procedural modification which utilized a phase ratio of 50/150 (ml aqueous/ml organic), a TDI addition rate of approximately three minutes, and a slight excess (2 % based on stoichiometry) of TDI yielded a suspension with improved mixing characteristics (free of aggregates) and microcapsules with good flocculation resistance. Analysis of microcapsules prepared by means of these procedural changes indicated the presence of spherical, intact microcapsules (Figure 96) with a narrow particle size distribution (Figures 97 and 98).

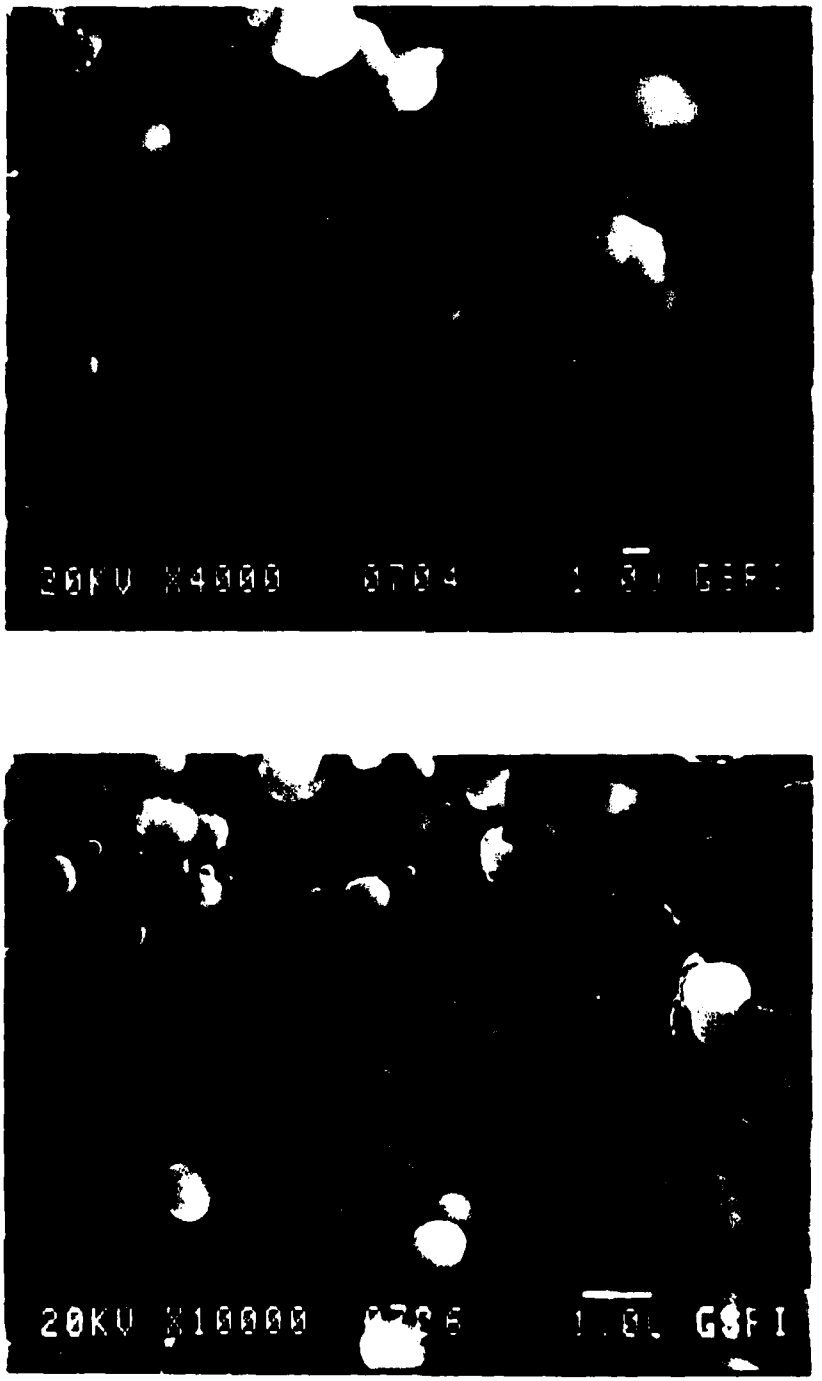

Figure 93. SEM analysis of 619-6 microcapsules.

SAMPLE: CE4275 GSRI MICROCAPSULES
ELECTROLYTE: 7% NH_4SCN/IPA
DISPERSANT: NONE

EQUIPMENT: TAII ACCUCOMP
APERTURES: 70

CH.#	SIZE	DIFF VOL%	CUM VOL%
1	1	.1	100
2	1.26	.1	99.9
3	1.59	.3	99.8
4	2	.7	99.5
5	2.52	1.8	98.8
6	3.17	5.4	97
7	4	14.2	91.6
8	5.04	27.5	77.4
9	6.35	31.5	49.9
10	8	14.6	18.4
11	10.08	2.5	3.8
12	12.7	.5	1.3
13	16	.3	.8
14	20.16	.2	.5
15	25.4	.1	.3
16	32	0	.2

VOLUME % STATISTICS

MEAN:	6.17 µm	STANDARD DEVIATION:	1.39 µm
MEDIAN:	6.34 µm	SKEWNESS:	.99 NEGATIVE
MODE:	6.63 µm	KURTOSIS:	1.07 PLATYKURTIC

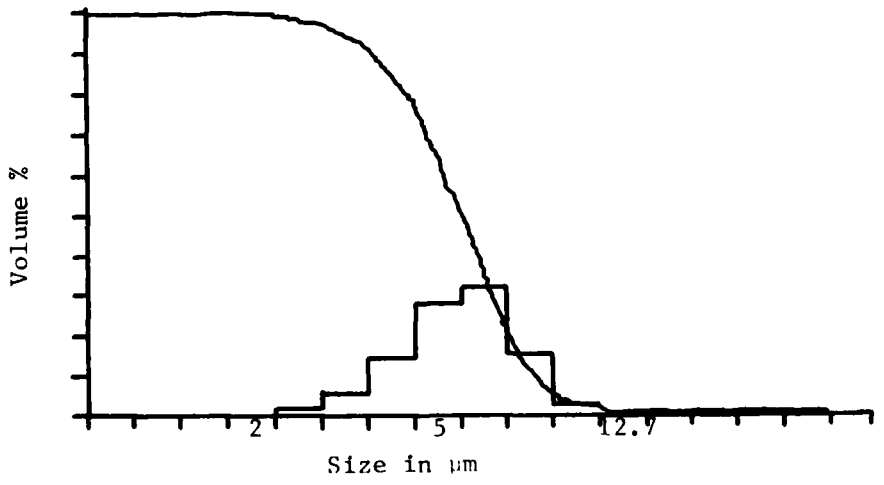

Figure 94. Coulter counter particle size analysis of 619-5 (volume percent).

SAMPLE: CE4275 GSRI MICROCAPSULES
ELECTROLYTE: 7% NH_4SCN/IPA
DISPERSANT: NONE

EQUIPMENT: TAII ACCUCOMP
APERTURES: 70

CH.#	SIZE	DIFF VOL%	CUM VOL%
1	1	24.7	100
2	1.26	8.3	75.3
3	1.59	7.1	67
4	2	6.7	59.9
5	2.52	7.3	53.2
6	3.17	10	45.9
7	4	13	35.9
8	5.04	13	22.9
9	6.35	8	9.9
10	8	1.8	1.9
11	10.08	.2	.1
12	12.7	0	0
13	16	0	0
14	20.16	0	0
15	25.4	0	0
16	32	0	0

POPULATION STATISTICS

MEAN:	2.65 µm	STANDARD DEVIATION:	1.97 µm
MEDIAN:	2.79 µm	SKEWNESS:	1.01 POSITIVE
MODE:	1.12 µm	KURTOSIS:	1.39 PLATYKURTIC

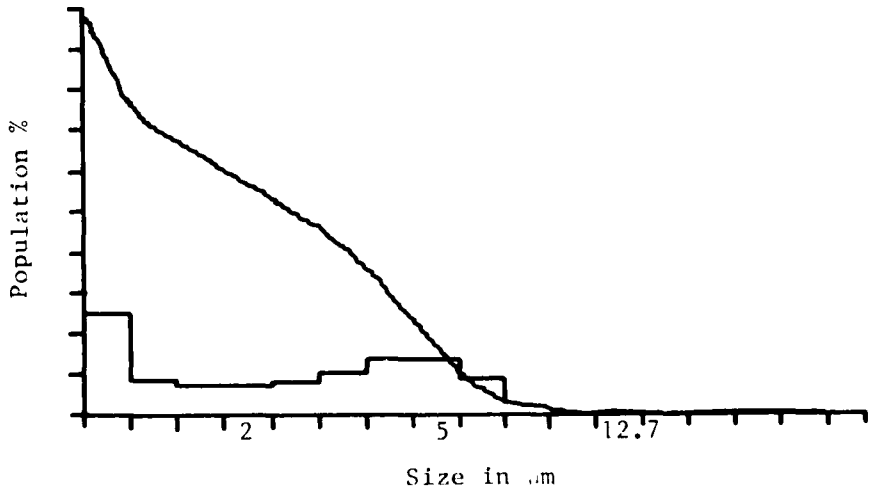

Figure 95. Coulter counter particle size analysis of 619-5 (population percent).

TABLE 23 . PARTIAL OPTIMIZATION OF MICROCAPSULE PREPARATION

Sample Number	Catalyst Level ($\frac{\text{moles DBTDL*}}{\text{moles TDI}}$)	Rate of Addition of TDI	Phase Volume Ratio ($\frac{\text{ml aqueous}}{\text{ml organic}}$)	Presence of Aggregates	Flocculation Resistance	Surface Characteristics
619-17	2.41×10^{-3}	<2 min	50/125	moderate	good	urethane
619-18	0.97×10^{-3}	<2 min	50/125	few-moderate	good	urethane
619-19	0.97×10^{-3}	7 min	50/125	none	poor	urethane
619-20	0.97×10^{-3}	4 min	50/200	none	poor	urethane
619-21	0.97×10^{-3}	3 min	50/150	none	good	urethane
619-22	0.97×10^{-3}	2 min	50/150	none	poor	amine

*DBTDL = dibutyltin dilaurate

AD-A144 311 ENCAPSULATED MULTIFUNCTION CORROSION INHIBITIVE PRIMER 3/4
(U) GULF SOUTH RESEARCH INST NEW ORLEANS LA
D V GUPTA ET AL. NOV 83 AFWAL-TR-83-4123
UNCLASSIFIED F33615-79-C-5061 F/G 11/3 NL

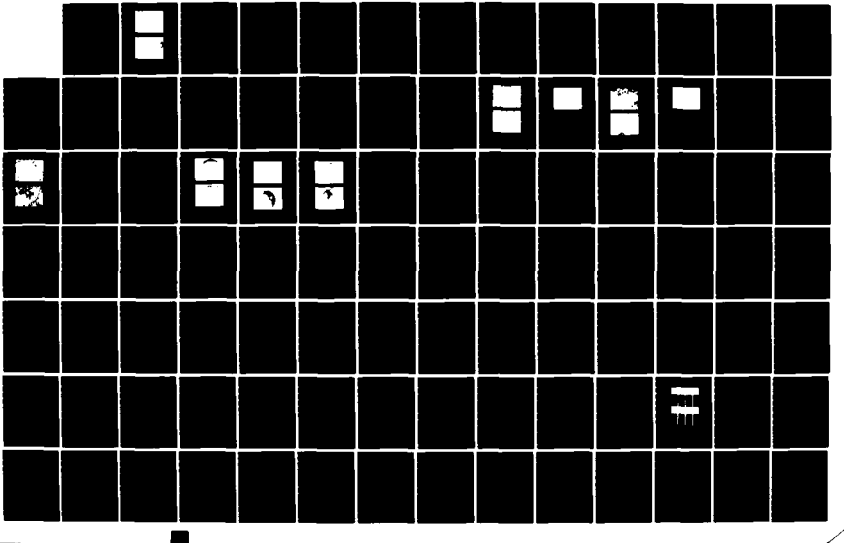

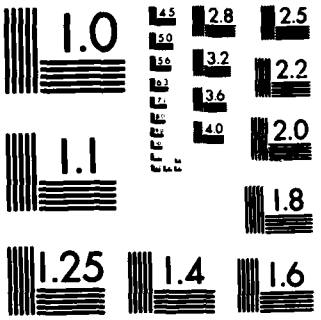

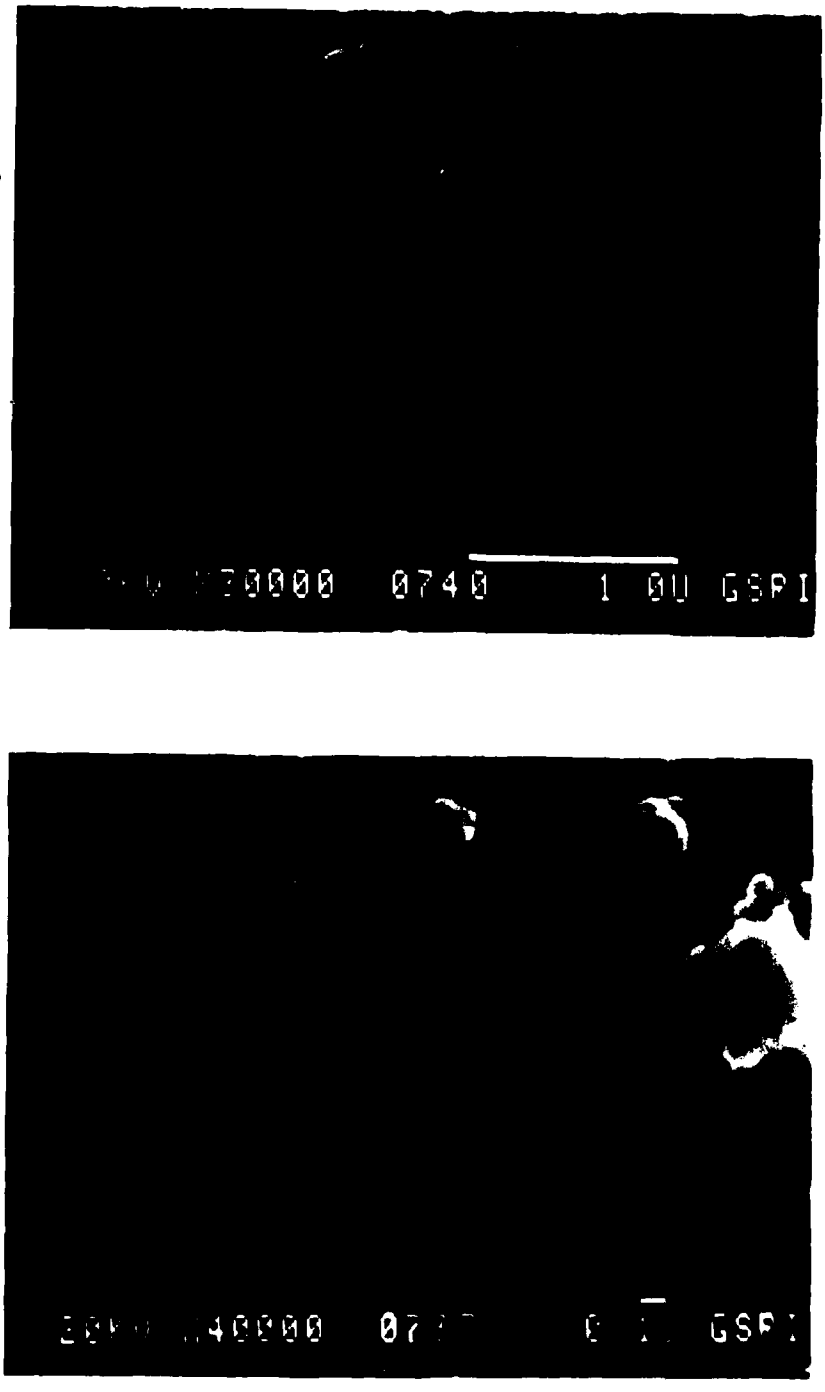

Figure 96. SEM analysis of microcapsules produced through a partially optimized procedure (619-21).

SAMPLE CE4323 GSRI MICROCAPSULES
ELECTROLYTE: 7% NH_4SCN/IPA
DISPERSANT: NONE

EQUIPMENT: TAII
APERTURES: 100

CH.#	SIZE	DIFF VOL%	CUM VOL%
1	1.26	0	100
2	1.59	0	100
3	2	.5	100
4	2.52	1.6	99.5
5	3.17	4.8	97.9
6	4	11.6	93.1
7	5.04	22.2	81.5
8	6.35	26.8	59.3
9	8	20.2	32.5
10	10.08	9	12.3
11	12.7	3	3.3
12	16	.3	.3
13	20.16	0	0
14	25.4	0	0
15	32	0	0
16	40.32	0	0

VOLUME % STATISTICS

MEAN:	6.8 µm	STANDARD DEVIATION:	1.42 µm
MEDIAN:	6.88 µm	SKEWNESS:	.99 NEGATIVE
MODE:	6.98 µm	KURTOSIS:	1.05 PLATYKURTIC

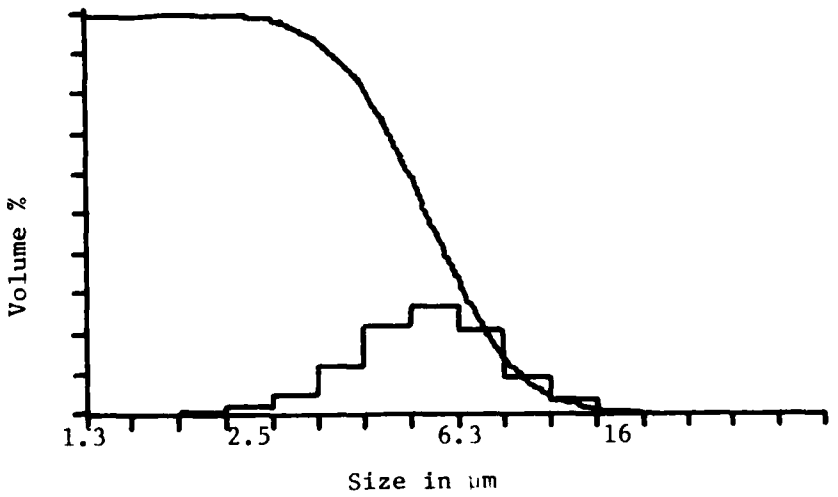

Figure 97. Coulter counter particle size analysis of 619-21 (volume percent).

SAMPLE: CE4323 GSRI MICROCAPSULES
ELECTROLYTE: 7% NH_4SCN/IPA
DISPERSANT: NONE

EQUIPMENT: TAII
APERTURES: 100

1	1.26	5.6	100
2	1.59	7	94.4
3	2	8.4	87.4
4	2.52	10.9	79
5	3.17	15.2	68.1
6	4	18.3	52.9
7	5.04	17.8	34.6
8	6.35	11.2	16.6
9	8	4.4	5.6
10	10.08	1	1.2
11	12.7	.2	.2
12	16	0	0
13	20.16	0	0
14	25.4	0	0
15	32	0	0
16	40.32	0	0

POPULATION STATISTICS

MEAN:	3.91 µm	STANDARD DEVIATION:	1.65 µm
MEDIAN:	4.15 µm	SKEWNESS:	.96 NEGATIVE
MODE:	4.89 µm	KURTOSIS:	1.17 PLATYKURTIC

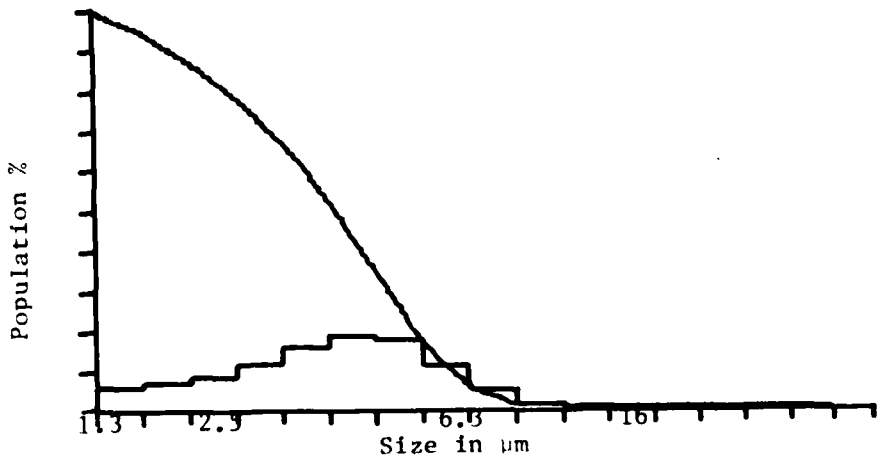

Figure 98. Coulter counter particle size analysis of 619-21 (population percent).

An in-depth optimization study of the polyurea system, or investigation of other modes of encapsulation, was beyond the scope of this program phase. The procedure modification outlined in Table 24 was judged suitable for the preparation of microcapsules which would serve as models for release studies.

TABLE 24. OPTIMIZED PROCEDURE FOR POLYUREA MICROENCAPSULATION

A. Solution Preparation

1. 4.0 g hexane-1,6-diamine + 5.0 g AFIF + 0.5 g Brij 58 + 50.0 ml deionized water.
2. 2.0 g Brij 72 + 0.5 g of 4.72% (w/w) dibutyltin dilaurate/cyclohexane + 125.0 ml of cyclohexane/chloroform, 2.2/1 (v/v).
3. 6.1 g toluene -2,4-diisocyanate + 25.0 ml of cyclohexane/chloroform, 2.2/1 (v/v).

B. Reaction Procedure

1. Set blender temperature = 40°C.
2. Add solution (1) and (2) to the blender, emulsify at 16500 rpm.
3. Add solution (3) dropwise over a 3 minute period.
4. Remove product from the reaction vessel.

C. Purification and Storage

1. Extract the polyurea microcapsules with 300-400 ml of pure cyclohexane, 3X.
2. Store, in suspended form, in pure cyclohexane.

2. AFIF Inhibitor Release Studies in Aqueous Solution from Polyurea Microcapsules

One of the problems associated with release testing of the nylon 6,10 system was aggregate formation when the microcapsules were introduced into the release medium. Since aggregation of the microcapsules in an aqueous medium may preclude obtaining quantitative release data, the methodology needed to obtain a finely divided dispersion was investigated. The preliminary approach involved sequential washings of the microcapsule/cyclohexane mixture with methanol to remove the water-immiscible hydrocarbon. Upon removal of the cyclohexane fraction, 0.5 g of microcapsules in methanol were added to 50 ml of deionized water containing 0.1 percent Brij 58 sur-

factant. The resulting mixture was stirred and conductivity readings were taken in the normal manner. Using polyurea microcapsules prepared at a phase ratio of 50/125 (ml aqueous/ml organic) (Sample 619-18 in Table 23), the procedural changes were found to produce good dispersions which showed approximately linear release of ionic species up to 1 hour (Figures 99 and 100).

Since rapid dehydration and rupture of the microcapsule wall could occur upon contact with the methanol phase, attempts were made to gradually remove the cyclohexane phase by vacuum stripping. Thus, 0.5 g of microcapsules dispersed in cyclohexane was stirred in 50 ml of a 0.1% Brij 58 surfactant solution while vacuum (approximately 20 mm of Hg) was applied to the head space. While this procedure effectively removed the cyclohexane phase, excessive aggregation of the microcapsules occurred during the later stages of vacuum stripping.

Fortunately, good dispersions of polyurea microcapsules could be obtained by emulsifying the microcapsule/cyclohexane mixture (0.5 g of microcapsules) in 50 ml of deionized water containing 0.1% Brij 58. The release profiles obtained through this procedure for Sample 619-21 are presented in Figures 101 and 102.

While some variation exists in these results, the release times obtained through this approach ranged from 60 to 90 minutes. Interestingly, Sample 619-48 continued to demonstrate slow release after 120 minutes. The burst effect did not occur with the polyurea microcapsules, which suggests that a nearly quantitative yield of microencapsulated inhibitor was achieved. The burst ratio is defined as the conductivity after 1 min of release divided by the conductivity at the maximum release time. The burst effect characteristic of the nylon 6,10 system was associated with rapid release of HCl into the release medium.

Since a primary objective for using the microencapsulation approach involved obtaining the proper release of the AFIF components, further investigations were undertaken to determine its suitability for providing quantitative release data. The release data obtained by means of conductivity measurements may be considered somewhat qualitative for several reasons:

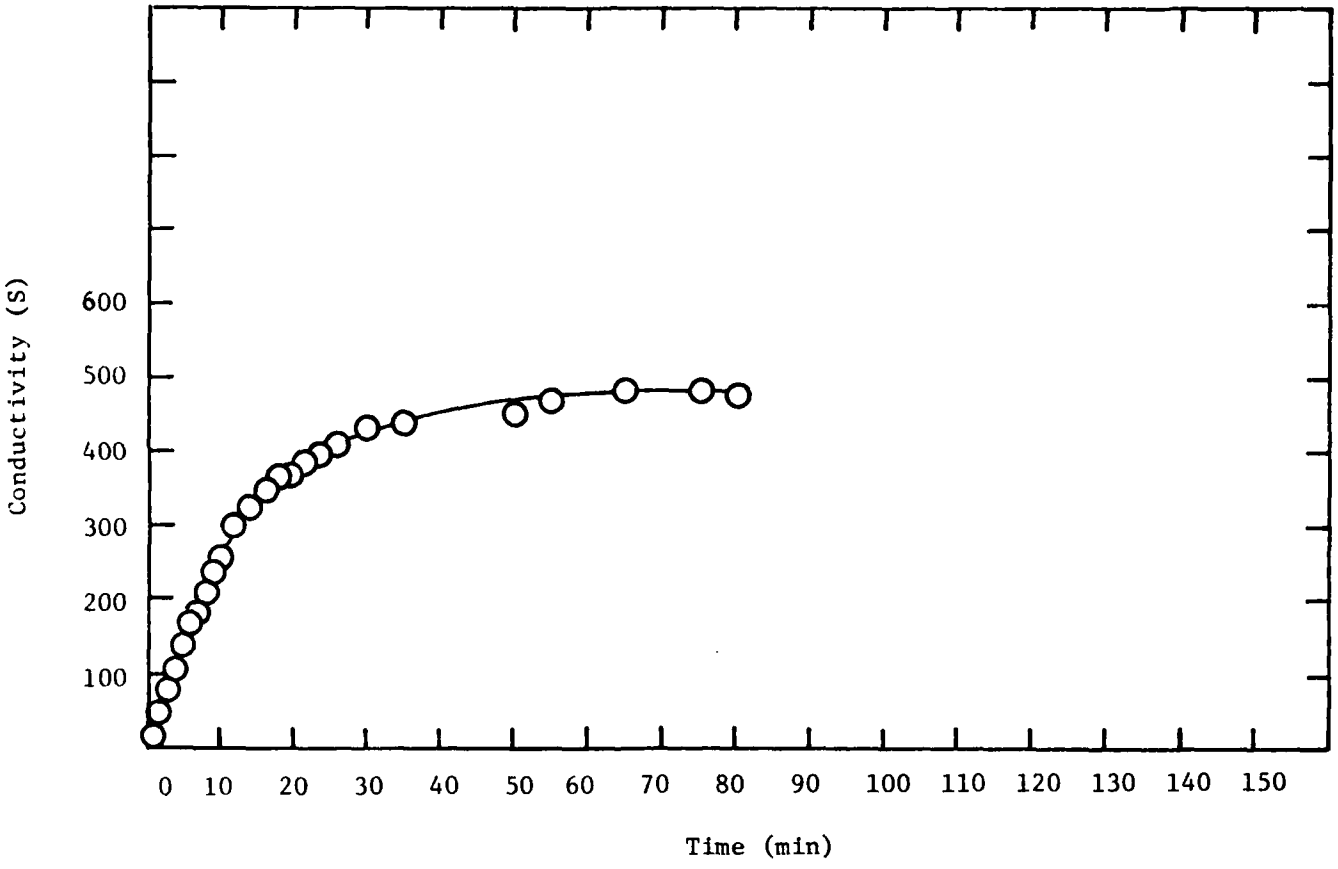

Figure 99. Release test of 619-18 (run number 619-27).

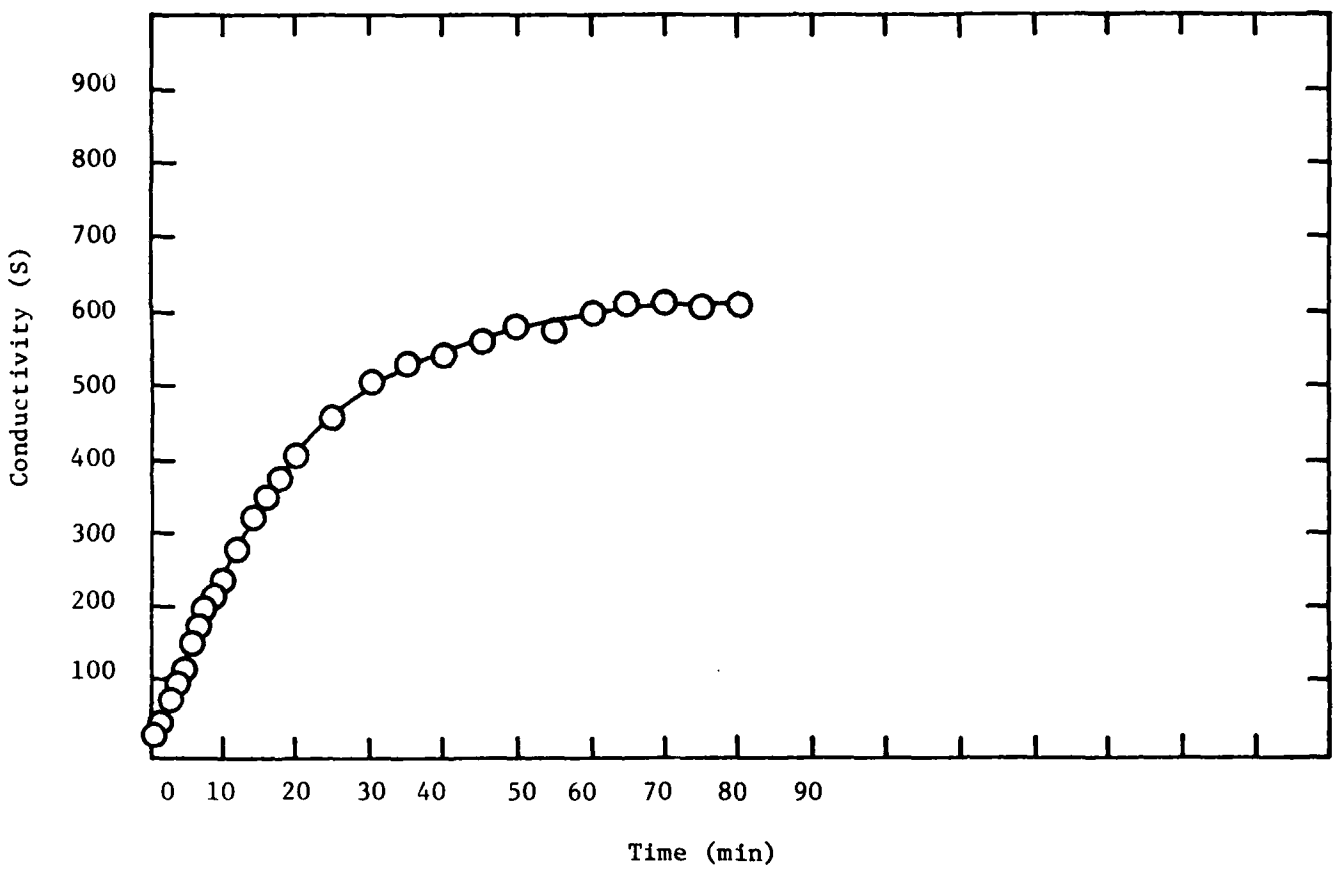

Figure 100. Release test of 619-18 (run number 619-28).

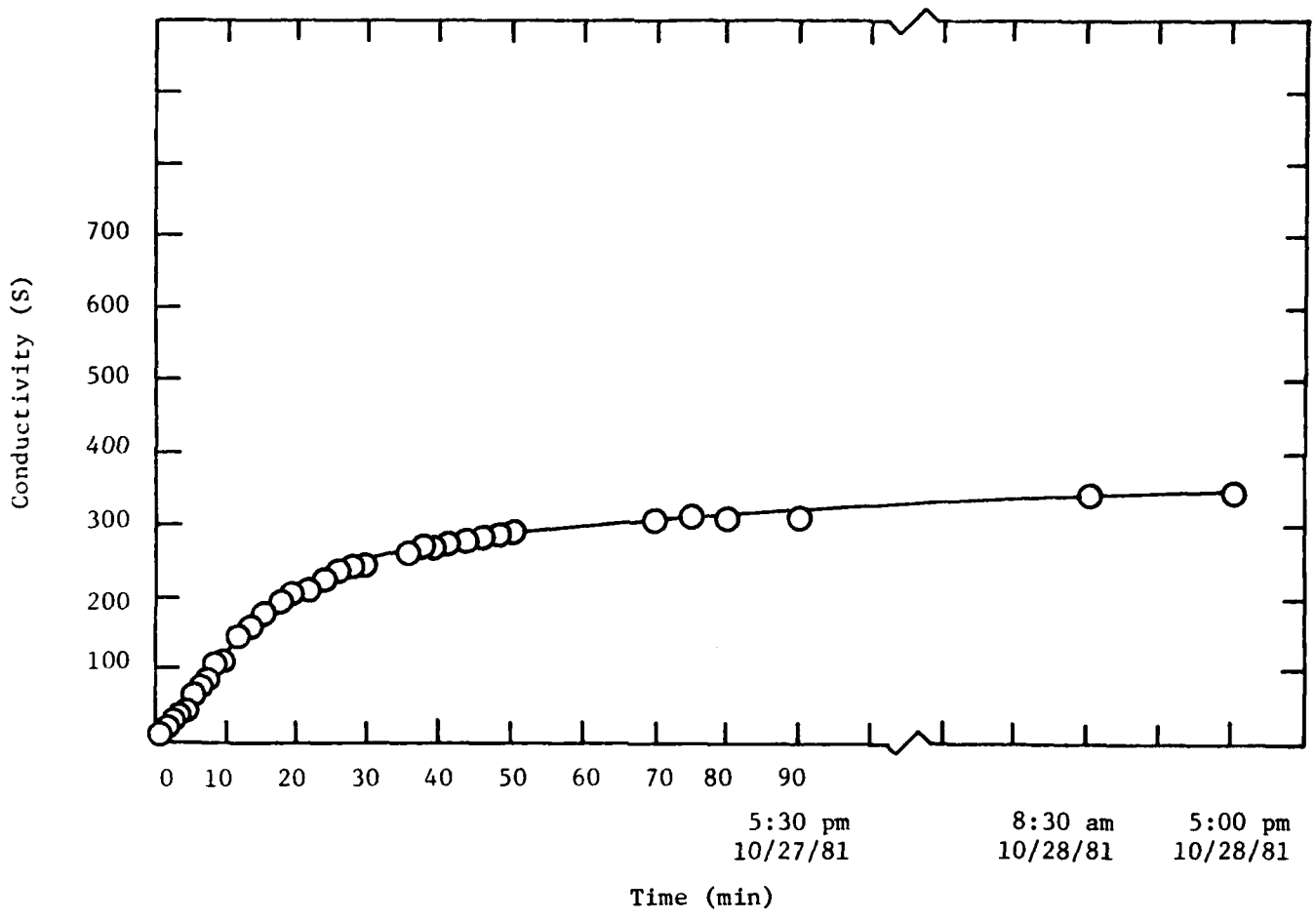

Figure 101. Release test of 619-21 (run number 619-30).

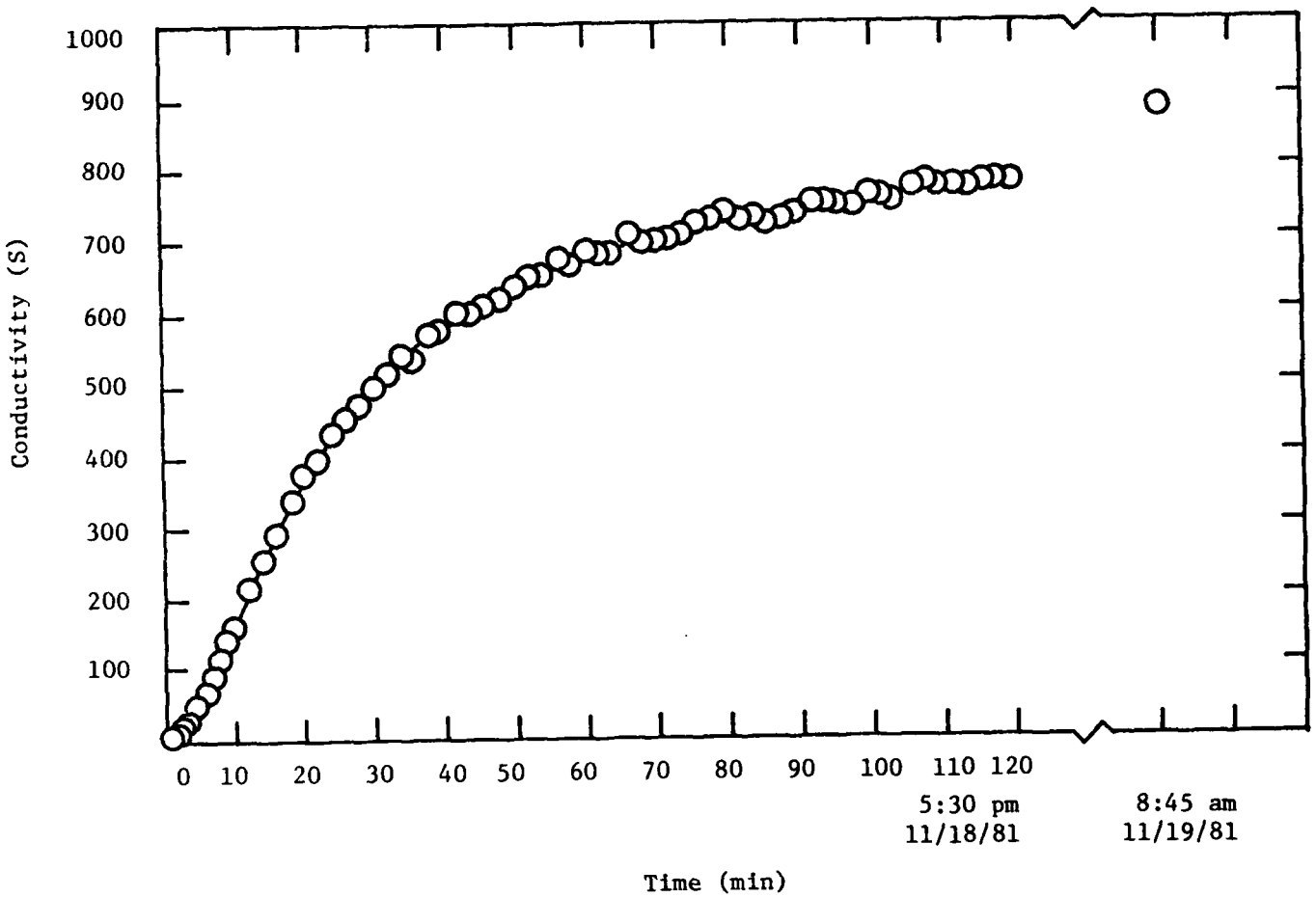

Figure 102. Release test of 619-21 (run number 619-48).

a) Five of the six inhibitor constituents utilize the sodium counter-ion. The sodium ion has the largest charge to mass ratio and also the smallest Van der Waals radius of the various species present. Thus, during the initial stage of diffusion, sodium ions may be the predominant species detected through conductivity measurements. Presumably, after contact of the aqueous phase with the microcapsule wall, the preferential diffusion of sodium ions will continue until the thermodynamic term for counter-ion attraction exceeds the kinetic and thermodynamic term associated with sodium ion hydration and solution activity. Thus, at some point, equilibrium between diffusion and re-entry may occur, and a Stern layer consisting of sodium ions may be associated with the microcapsule surface. The occurrence of this phenomenon may affect conductivity readings.

b) In spite of vigorous agitation, a boundary layer of water and/or cyclohexane may be associated with the microcapsule. This layer provides additional resistance to disruption of the Stern and diffuse layers, or in the case of cyclohexane, wetting of the microcapsule wall.

c) Since each inhibitor ionic component possesses a different charge-to-mass ratio, diffusion coefficient, and activity coefficient, the conductivity measurement does not provide information on the rate of diffusion of each inhibitor specie. Additionally, sodium hexametaphosphate assumes a cyclic configuration which may inhibit diffusion through the microcapsule wall. Mercaptobenzothiazole is not significantly water soluble, and may remain inside the microcapsule.

In light of these considerations, the need was obvious for establishing quantitative release data which would provide information regarding the diffusion rate of each inhibitor species. Additionally, if quantitative release data were obtained on microcapsules containing only a single inhibitor species, the following theoretical parameters could be determined:

a) For each of the separately encapsulated species, concentration versus time profiles could be determined, thereby providing the release time half-life, $\tau_{\frac{1}{2}}$, for the release process. From particle size distribution analysis and loading analysis, the diffusion coefficient, D, could be obtained using the following relationship (40):

$$\tau_{\frac{1}{2}} = \frac{(2a)^2 \ (\ln 2)}{36 \ RD} \ , \text{ where}$$

a = inner microcapsule radius;

R = mass ratio of encapsulated material to the wall membrane, where $R = \frac{L}{1-L}$, L = loading;

D = diffusion coefficient.

b) By curve fitting, the order of the diffusion process can be determined. Ideally, diffusion will be first order. Once the order is established, various thermodynamic parameters can be determined by establishing the temperature dependence of the diffusion process and fitting the kinetic data obtained at varying temperatures to the Arrhenius and Eyring Models. The Arrhenius and Eyring equations may be rewritten in the following forms to facilitate data reduction:

Arrhenius equation: $\ln k = \ln A - \left(\frac{Ea}{RT} \right)$

Eyring equation: $\ln \left(\frac{k}{T} \right) = \ln \left(\frac{k_B}{h} \right) - \frac{\Delta H^{\dagger}}{RT} + \frac{\Delta S^{\dagger}}{R}$

where R = gas constant,

k_B = Boltzman's constant,

h = Planck's constant, and

A = Arrhenius pre-exponential factor.

Thus, from an appropriate plot of ln k versus 1/T, or ln(k/T) versus 1/T, such thermodynamic quantities as activation energy (E_a), enthalpy of activation ($\Delta H^{\dagger}$), and entropy of activation ($\Delta S^{\dagger}$) may be obtained.

The above discussion illustrates that efforts to establish quantitative release data may be either semi-applied or theoretical. Obviously, the semi-applied approach is more likely to provide information aligned with the goals of the project. Since corrosion resistance is greatly dependent upon

the migration ability of specific AFIF components to potential sites of anodic and cathodic substrate reactions, emphasis was focused initially on establishing the release profiles for each constituent of the AFIF mixture. The AFIF mixture consists of 68% by weight sodium borate, and thus initial studies involved determining the release profile of the borate constituent. The following procedure was used to determine each separate sample data point.

Eight milliliters of a microcapsule/cyclohexane suspension (0.12 g microcapsules) was added to 30.0 ml of deionized water containing 0.1% Brij 58 surfactant. The sample was stirred vigorously for a specified interval of time (10 min, 20 min, 30 min, 60 min, 2 hrs, 4 hrs, 24 hrs, 48 hrs), then immediately poured into a pressure ultrafiltration unit fitted with a 0.45 μm pore size millipore filter. The solution was rapidly filtered, and the filtrate transferred to a separatory funnel for ∿ 1 hr. After the water and cyclohexane layers separated, the water layer was collected, conductivity measurements were made, and the sample was stored until atomic absorption analysis for boron was performed.

Figure 103 compares the release data obtained through conductivity and atomic absorption analysis. The release times in each case are greater than 3 hrs, and excellent agreement exists between the two methods of analysis. The surprisingly good correlation between the two methods suggests that the composite mixture of AFIF components diffuses through the polyurea membrane at the same rate as the borate anion. If such nonselective diffusion occurred, then the ionic permeability of the polyurea membrane might be larger than is desired.

3. Development of Microcapsules with Longer Release Times

The occurrence of a nonselective diffusion process indicates either the use of an inefficient encapsulating material (the reaction product of TDI and hexane-1,6-diamine) or the lack of microcapsule wall integrity (arising from wall defects or insufficient wall thickness).

If this anomalous effect is associated with the integrity of the microcapsule wall, the following theoretical considerations are relevant. Assume a spherical microcapsule of inner radius a and wall thickness h. The diameter of the microcapsule is therefore given by the expression $d = 2(a + h)$. The release rate of the active substance from a spherical microcapsule is

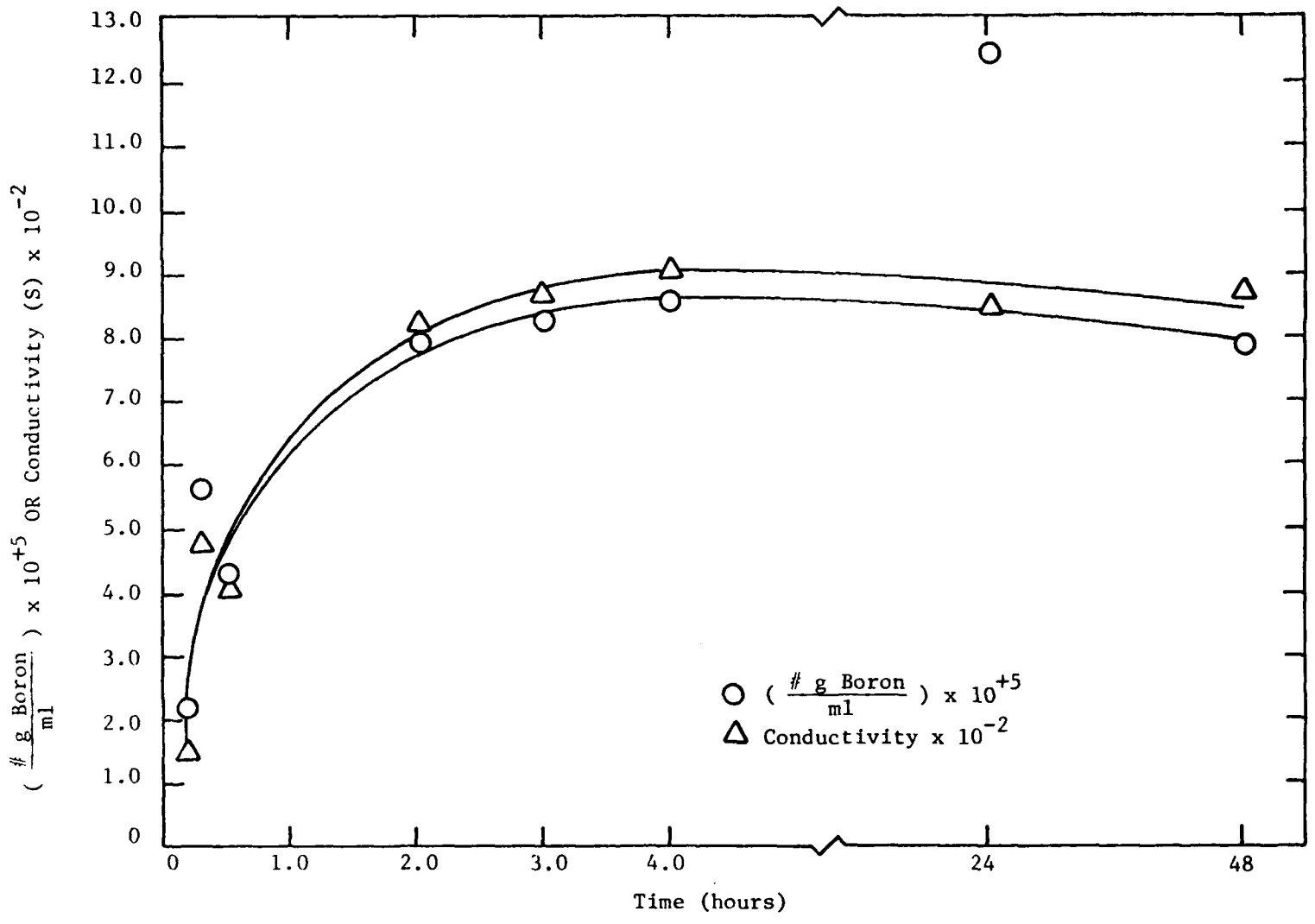

Figure 103. Time versus ($\frac{\#\ g\ Boron}{ml}$) x 10^{+5}, or time versus conductivity for sample 619-45.

intimately related to the parameters a and h, each of which is governed by several intrinsic factors associated with the properties of the emulsion.

Based on the mathematical model for diffusive release of an active material from a spherical microcapsule, the following relationship for the release half-life holds:

$$\tau_{\frac{1}{2}} = \frac{ah(\ln 2)}{D} ,$$

where D is the diffusion coefficient. D is sometimes called the diffusion constant, but experimental data has revealed that D often is a function of concentration, and is more appropriately termed a coefficient.

The parameter *a* is directly related to (and determined by) the emulsion particle size which exists immediately prior to the interfacial polymerization reaction. The release half-life, τ, may be increased by using surfactants and stirring rates which provide larger diameter particles; however, due to the end use of this particular product (e.g. very thin primer films), such an approach would be counterproductive for increasing τ.

The parameter h, the wall thickness, is directly related to the interfacial polymerization reaction rate and to the absolute amount of wall forming monomers available, or if stoichiometric amounts are not used, upon the limiting reagent. Assuming kinetics such that the reactions (via DBTDL catalysis) are rapid with respect to the experimental procedure, and that stoichiometric amounts of hexane-1,6-diamine and toluene-2,4-diisocyanate are used, the wall thickness h depends on the amount of monomer material present in the solutions initially made up for the synthetic process. Thus, increases in monomer concentration should increase τ in a proportional manner.

While internal parameter changes, such as surfactant ratio or stirring rate, could be made which affect the particle radius, *a*, theoretically it is preferable to initially consider approaches which will control the wall thickness, h. The most effective approach for increasing wall thickness lies in increasing the deposition of the polyurea on the outer surface of the growing particle (accretion of wall material) which may be effected readily through small changes in the monomer concentration.

In line with the above considerations, a study was conducted with the objective of gaining greater control over the ion diffusion process through increased microcapsule wall thickness. To obtain quantitative results (by

means of atomic absorption) on the rate of release, the microcapsules were prepared using sodium borate as the sole inhibitor species. The control system (619-70) employed the same preparation method that was utilized in a previous study (see Table 24). The experimental systems were prepared using quantities of TDI and hexane-1,6-diamine which represented a 30 and 70 percent increase in the polymer content (wall material) over the control, respectively (see Tables 25 and 26 for procedure). Since increases in wall thickness could be detected through diffusion rate measurements, conductivity release studies were performed to determine the success of the approach. The release characteristics for the control (619-70), the 30% modification (619-74) and 70% modification (619-81) are presented in Figures 104, 105, and 106, respectively.

While some variation exists among duplicate runs, in general these results indicated that both the 30% and 70% wall thickness modifications displayed slower rates of release than the control system. The approximate maximum release times for each system were: control $\sim$ 100 min, 30% wall increase $\sim$ 200 min, 70% wall increase $\sim$ 200 min.

Analysis of the microcapsule samples by scanning electron microscopy indicated that the procedure used to gain additional wall thickness may have created a somewhat anomalous growth pattern. Evaluation of the samples at 100 mm resolution suggested that the procedural change resulted in aggregation or clustering of the microcapsules (Figure 107). Higher resolution photomicrographs taken at 1 mm scale indicated the occurrence of a marked change in the surface morphology of the samples (Figure 108). These results suggest the possibility of three growth modalities: a) larger, irregularly shaped microcapsules, b) the generation of amorphous material embedding smaller microcapsules, or c) the generation of amorphous polymer which may or may not contain the aqueous AFIF mixture. However, the interpretation of these results is uncertain since amorphous polymer formation has been noted in SEM's of other microcapsule samples which has not been detected through other means of characterization.

Nevertheless, evaluation of these samples while dispersed in the cyclohexane phase by optical microscopy does indicate the presence of either aggregation or larger diameter microcapsules of irregular shape. Yet for the 30 percent and 70 percent increase in wall thickness samples, a preponderance of nonaggregated, spherical microcapsules was also noted. Under

TABLE 25. POLYUREA MICROCAPSULE (619-74) PROCEDURE FOR 30% WALL FORMATION INCREASE (OVER 619-45)

Solution Preparation

1. 5.2 g hexane-1,6-diamine + 0.5 g Brij 58 + 3.0 g $Na_2B_4O_7 \cdot 10H_2O$ + 50.0 ml deionized H_2O.

2. 2.0 g Brij 72 + 0.5 g of 4.73% (w/w) DBTDL/cyclohexane + 125 ml of 2.2/1 (v/v) cyclohexane/chloroform.

3. 7.93 g toluene-2,4-diisocyanate + 25.0 ml of 2.2/1 (v/v) cyclohexane/chloroform.

Reaction Procedure

1. Temperature = 40°C.

2. Add solution (1) to the blender at 16,500 rpm.

3. Add solution (2) to the blender at 16,500 rpm.

4. Add solution (3) to the blender, dropwise, at a rate of ~2.1 ml/15s [3.0 min total addition time].

5. Remove product.

Purification/Storage

1. Pour the reaction product into a 1.0 l Erlenmeyer flask.

2. Extract the microcapsules with 300-400 ml of pure cyclohexane x 3.

3. Store the product in the Erlenmeyer flask, under pure cyclohexane, in suspension form.

TABLE 26. POLYUREA MICROCAPSULE (619-81) PROCEDURE FOR 70% WALL FORMATION INCREASE (OVER 619-45)

Solution Preparation

1. 6.76 g hexane-1,6-diamine + 0.5 g Brij 58 + 3.0 g $Na_2B_4O_7 \cdot 10H_2O$ + 50.0 ml deionized H_2O.

2. 2.0 g Brij 72 + 0.5 g of 4.73% (w/w) DBTDL/cyclohexane + 125 ml of 2.2/1 (v/v) cyclohexane/chloroform.

3. 10.31 g toluene-2,4-diisocyanate + 25.0 ml of 2.2/1 (v/v) cyclohexane/chloroform.

Reaction Procedure

1. Temperature = 40°C.

2. Add solution (1) to the blender at 16,500 rpm.

3. Add solution (2) to the blender at 16,500 rpm.
4. Add solution (3) to the blender, dropwise, at a rate of ~2.1 ml/15s [3.0 min total addition time].

5. Remove product.

Purification/Storage

1. Pour the reaction product into a 1.0 l Erlenmeyer flask.

2. Extract the microcapsules with 300-400 ml of pure cyclohexane x 3.

3. Store the product in the Erlenmeyer flask, under pure cyclohexane, in suspension form.

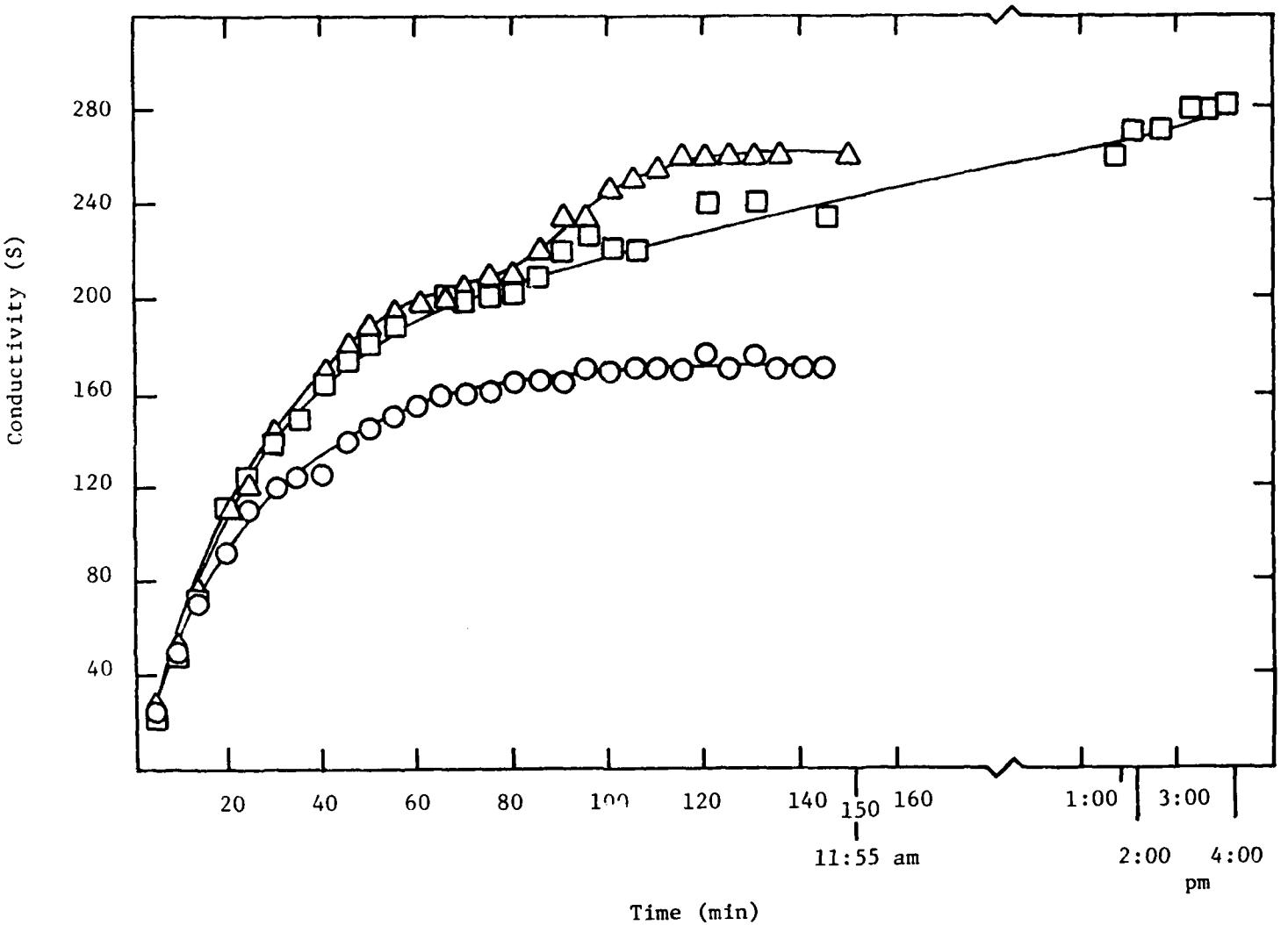

Figure 104. Release test of 619-70.

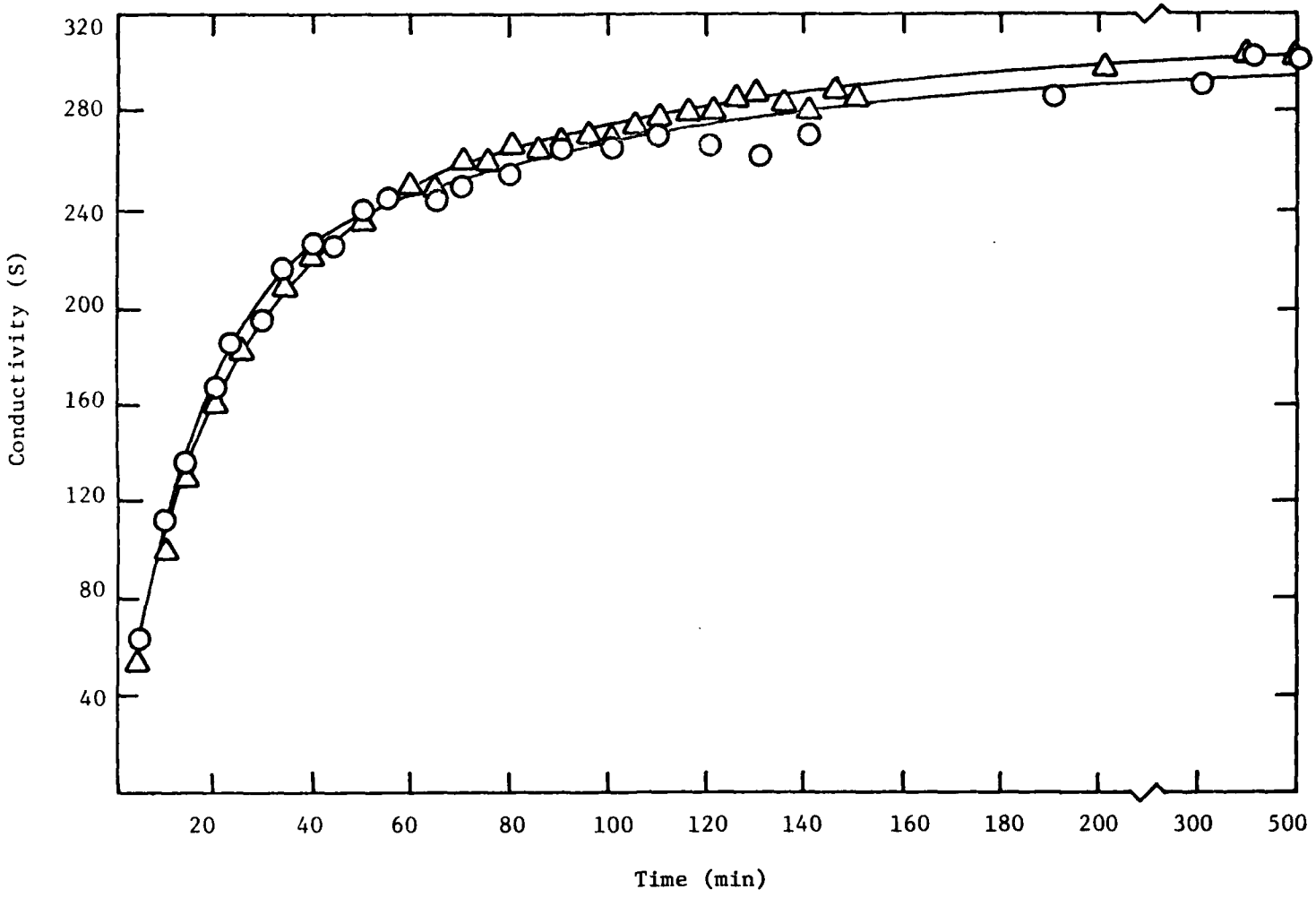

Figure 105. Release test of 619-74.

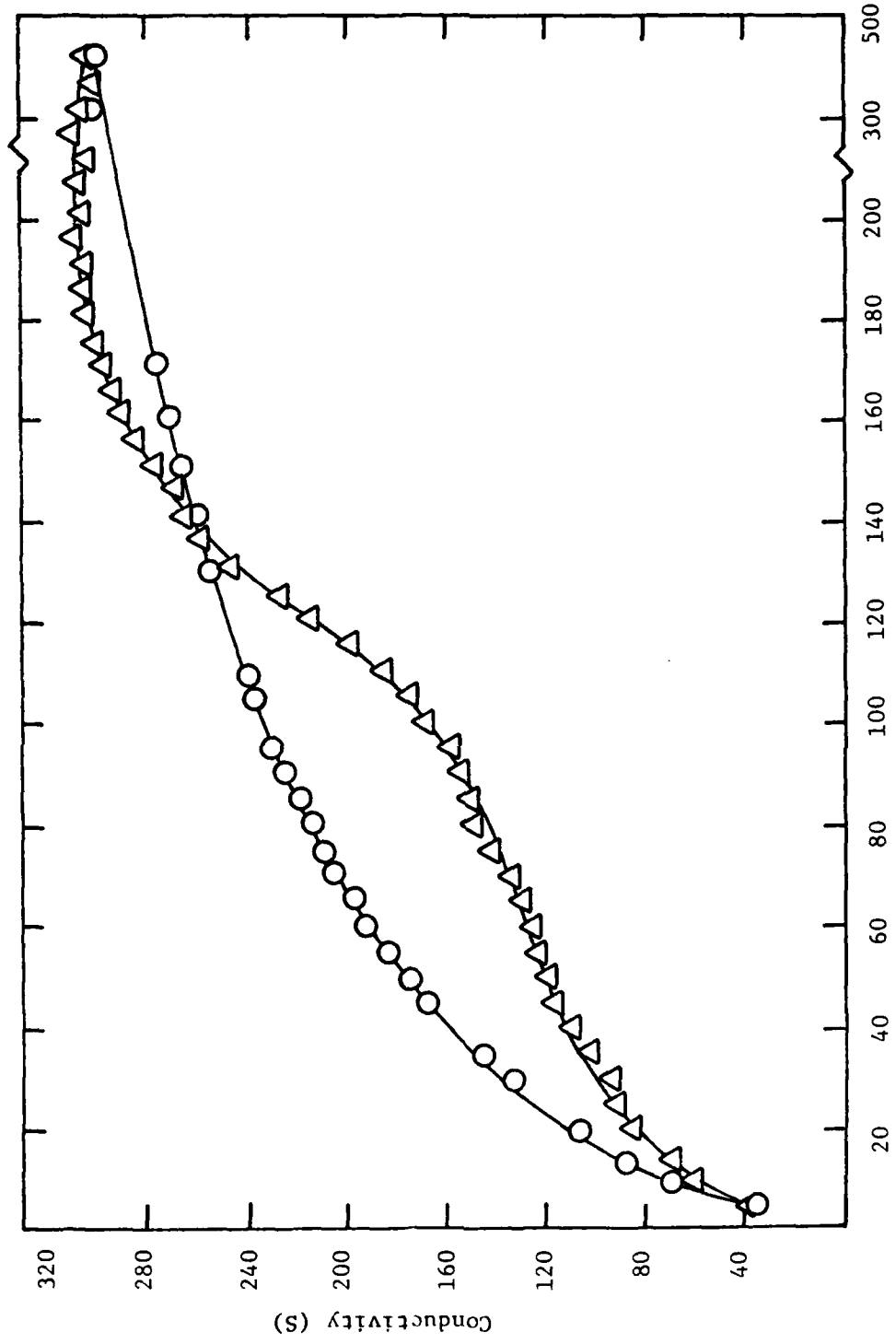

Figure 106. Release test of 619-8i.

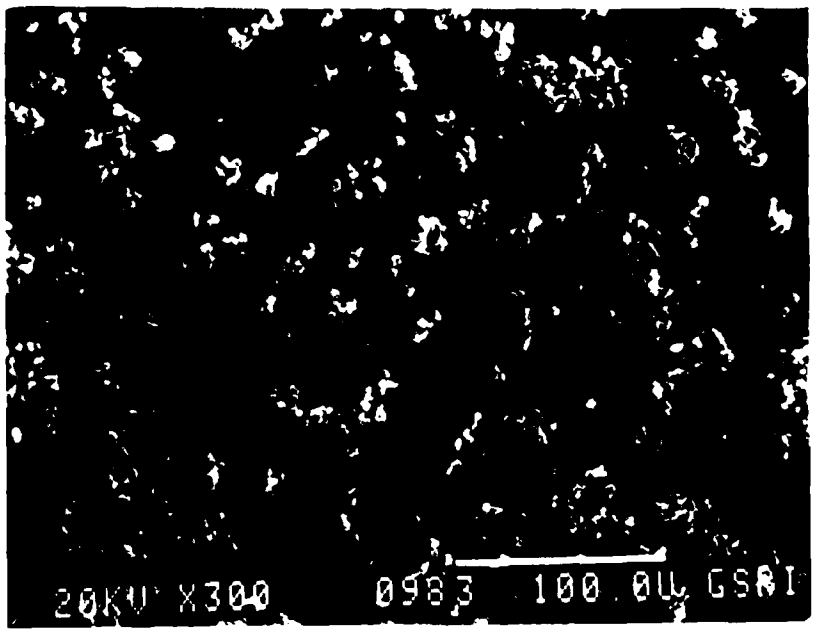

(A)

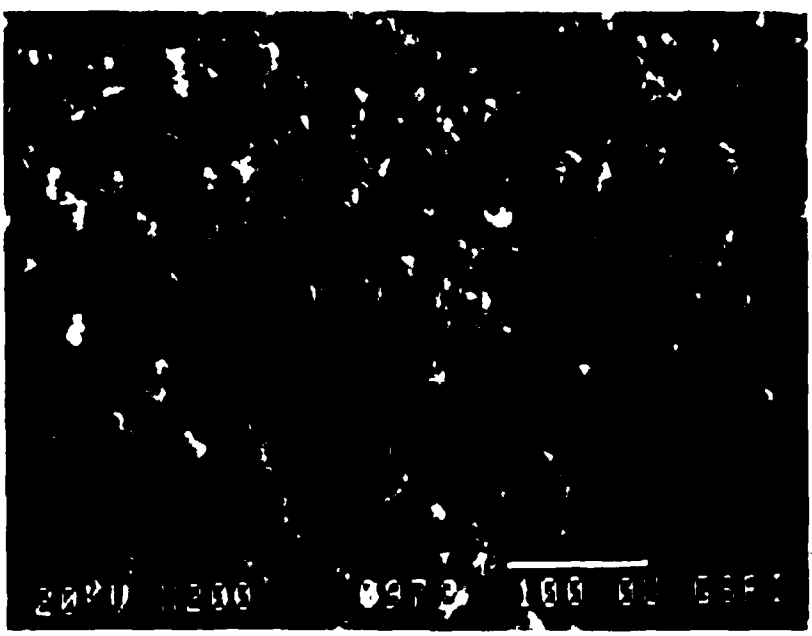

(B)

Figure 107. SEM photomicrographs of (A) 619-70, (b) 619-74 and (C) 619-81. Scale bar in A and B is 100 μm, 10 μm in C. (Figure continued on following page).

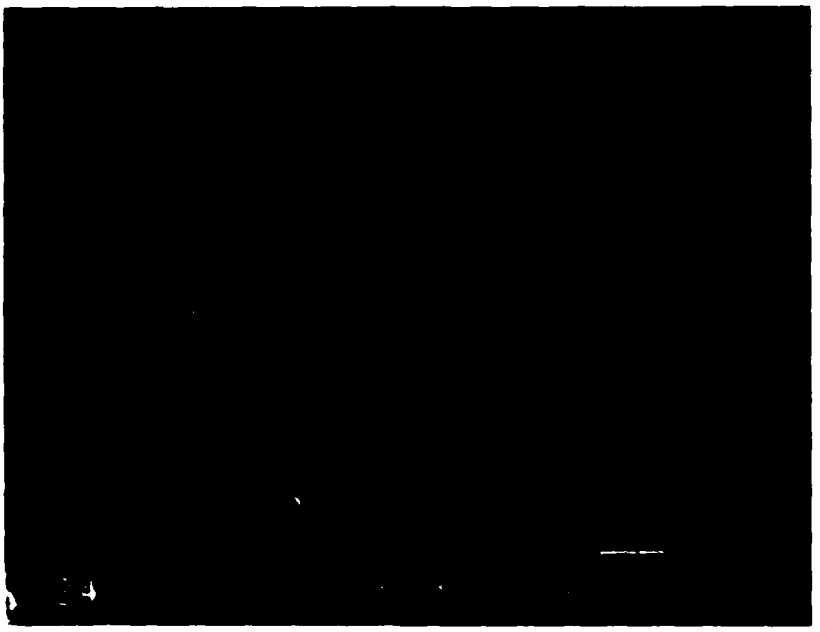

Figure 107. (continued from previous page).

(A)

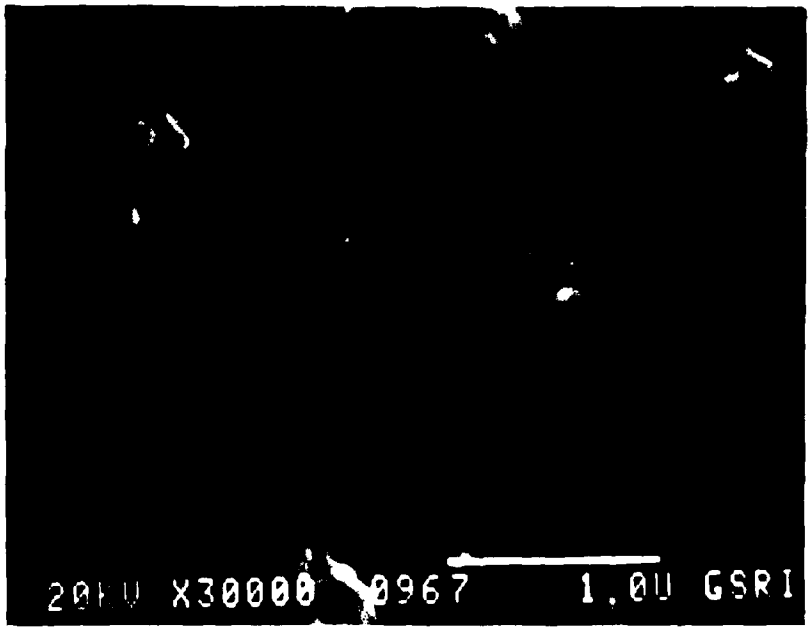

(B)

Figure 108. SEM photomicrographs of (A) 619-70, (B) 619-74 and (C) 619-18. Scale bar is 1.0 μm. (Figure continued on following page).

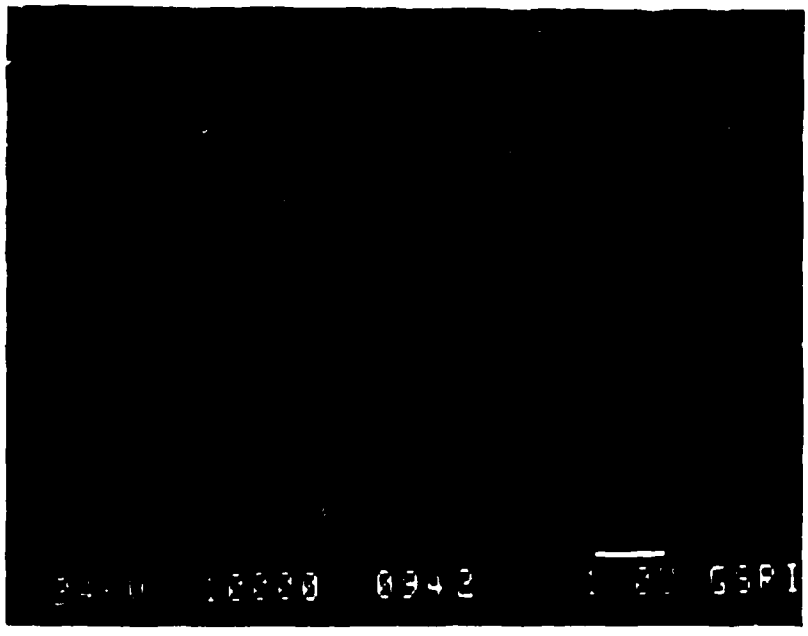

(C)

Figure 108. (continued from the previous page).

optical microscopy sample 619-70, the control, appears to be similar to earlier samples such as 619-45, which was free of irregularities and agglomeration.

Since changes in the ionic strength of the aqueous phase may have reduced the effectiveness of the surfactant in the emulsion stage, attempts were made to eliminate the agglomeration problem through the use of higher levels of surfactant. Table 27 presents a formulation (619-95) in which the amount of organic phase surfactant (Brij 72) was increased by 50% over the control (619-81) which represented a 70% increase in polymer mass compared to (619-70). SEM evaluation of the microcapsule morphology indicated a similar agglomeration and amorphous structure, as was found in 619-81 (Figure 109). However, evaluation of the degree of dispersion and microcapsule size and morphology by optical microscopy indicated that 619-95 was more similar in characteristics to 619-70 than to 619-74 or 619-81. The release data for 619-95 (Figure 110) support this trend, in that shorter release times were obtained which may suggest a change in wall thickness or the degree of amorphous polymer embedment.

In order to determine whether or not increases in polymer/aqueous phase ratio resulted in increased wall thickness, microcapsule fracture studies were conducted as a means of monitoring the extent of wall thickness. The samples were prepared by dispersing a microcapsule/cyclohexane mixture in an epoxy embedding compound, and freeze-fracturing the resulting samples in liquid nitrogen (see Table 28).

SEM characterization of the resulting fractured microcapsules (Sample 619-70) revealed some interesting structural occurrences:

a) The microcapsules possess a cavity which constitutes approximately 80% of the overall diameter. Thus, the microcapsule wall thickness constitutes approximately 10% of the overall diameter (Figure 111).

b) The microcapsules may be single or multicavitied (Figure 112).

c) The walls of the microcapsules may be somewhat porous. The reticulate structure may arise from foam entrapment, a non-uniform accretion process, or entrapment of smaller aqueous droplets. Obviously, microcapsules possessing a reticulated wall structure would provide greatly reduced release times (Figure 113).

TABLE 27. POLYUREA MICROCAPSULE (619-95) PROCEDURE FOR 50% ORGANIC PHASE SURFACTANT INCREASE (OVER 619-81)

Solution Preparation

1. 6.76 g hexane-1,6-diamine + 0.5 g Brij 58 + 3.0 g $Na_2B_4O_7 \cdot 10H_2O$ + 50.0 ml D.I.H_2O.

2. 3.0 g Brij 72 + 0.5 g of 4.73% (w/w) DBTDL/cyclohexane + 125 ml of 2.2/1 (v/v) cyclohexane/chloroform.

3. 10.31 g toluene-2,4-diisocyanate + 25.0 ml of 2.2/1 (v/v) cyclohexane/chloroform.

Reaction Procedure

1. Temperature = 40°C.

2. Add solution (1) to the blender at 16,500 rpm.

3. Add solution (2) to the blender at 16,500 rpm.

4. Add solution (3) to the blender, dropwise, over a 3.0 min period at 16,500 rpm.

5. Remove product.

Purification/Storage

1. Pour the reaction product into a 1.0 l Erlenmeyer flask.

2. Extract the microcapsules with 300-400 ml of pure cyclohexane x 3.

3. Store the product in the Erlenmeyer flask, under pure cyclohexane, in suspension form.

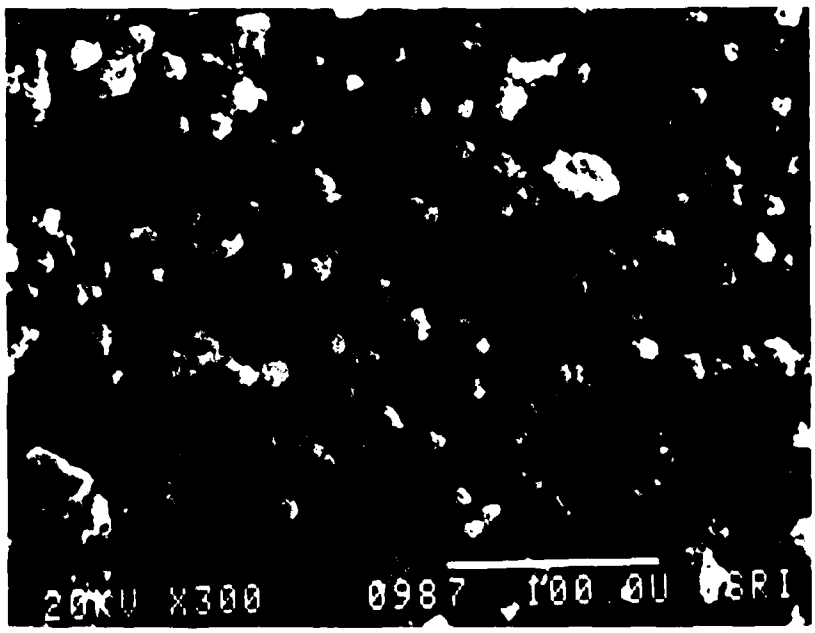

(A)

(B)

Figure 109. SEM photomicrographs of sample 619-95 (A, scale bar is 100 μm) and (B, 1.0 μm scale bar).

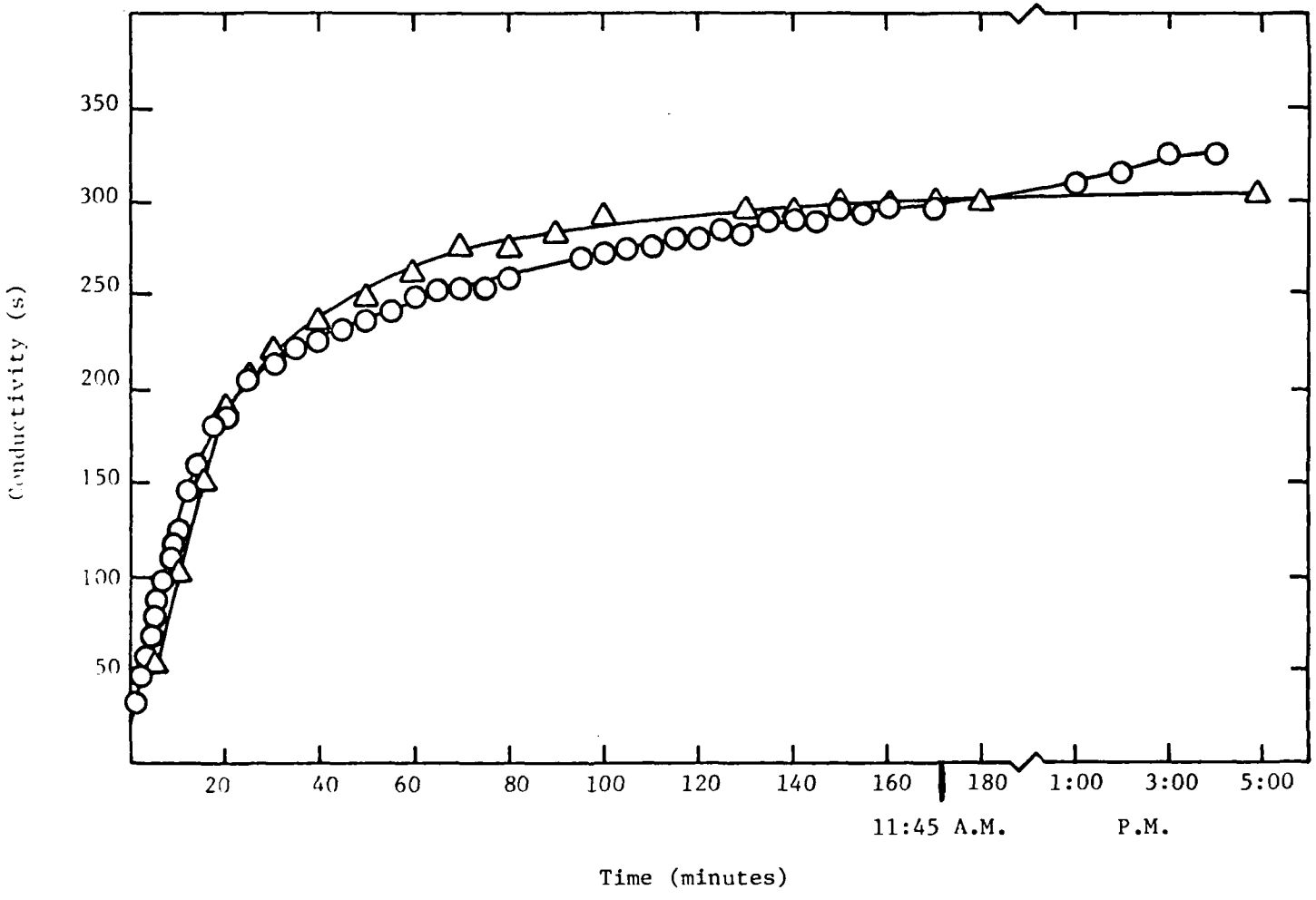

Figure 110. Release test of 619-95.

TABLE 28. EMBEDDING PROCEDURE FOR SEM FREEZE-FRACTURE ANALYSIS OF MICROCAPSULES

1. Weigh out 15.0 g of Buehler Met-A-Test epoxy.

2. Blend in microcapsules in cyclohexane suspension, to obtain ~10% microcapsules by (dry) weight. Microcapsules were concentrated prior to blending by solvent evaporation.

3. Blend the microcapsules, cyclohexane, and epoxy well by magnetic stirrer; allow to sit ~10 min to displace air bubbles.

4. Add 2.0 g Buehler Met-A-Test hardener; blend in via magnetic stirrer; allow to stand for ~5.0 min to displace air.

5. Add 2 drops DMP-30 catalyst; mix rapidly; allow to stand ~5 min.

6. Pipet the mixture into molds; allow to harden overnight.

7. Perform SEM freeze fracture analysis, using liquid N_2.

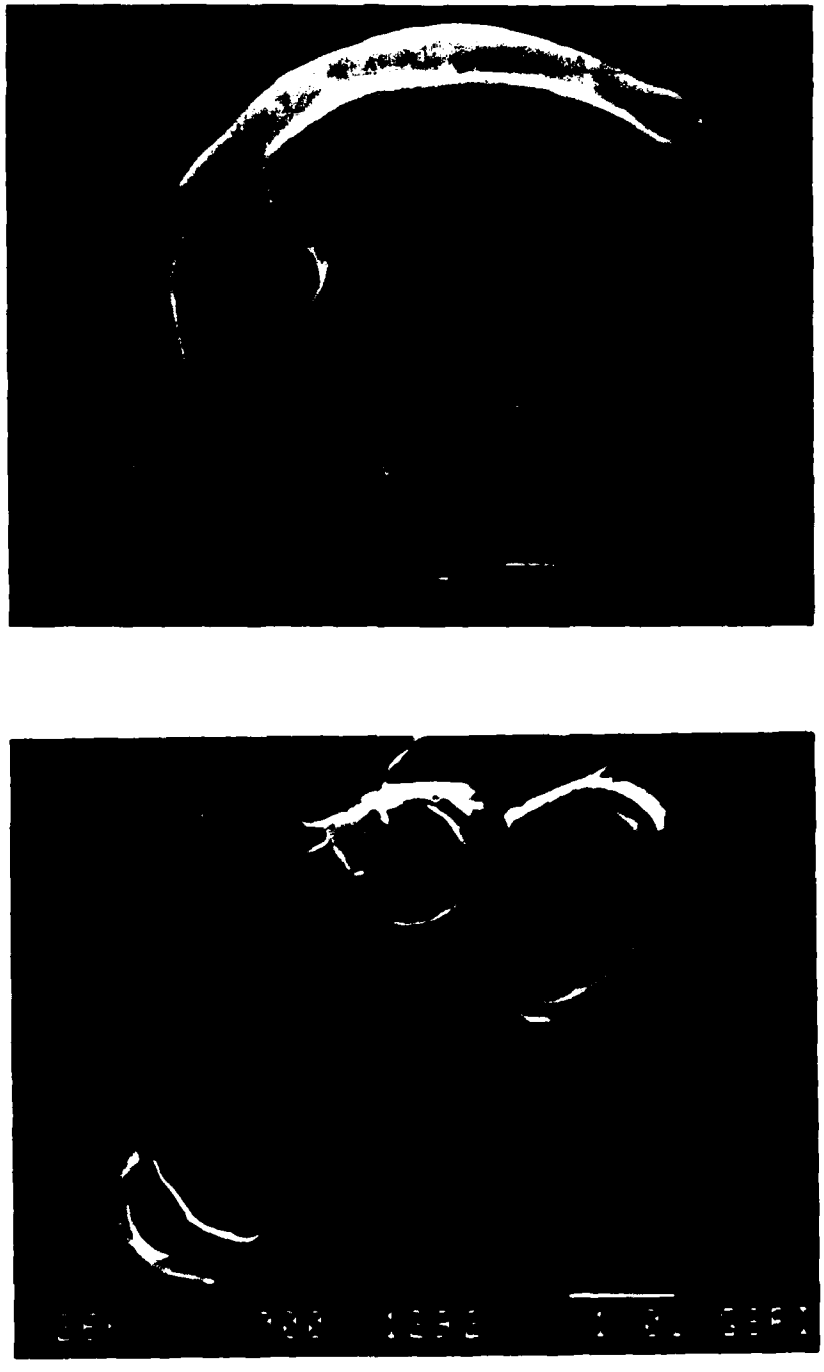

Figure 111. SEM photomicrograph of freeze-fracture analysis of 619-70 microcapsules, displaying dimensions.

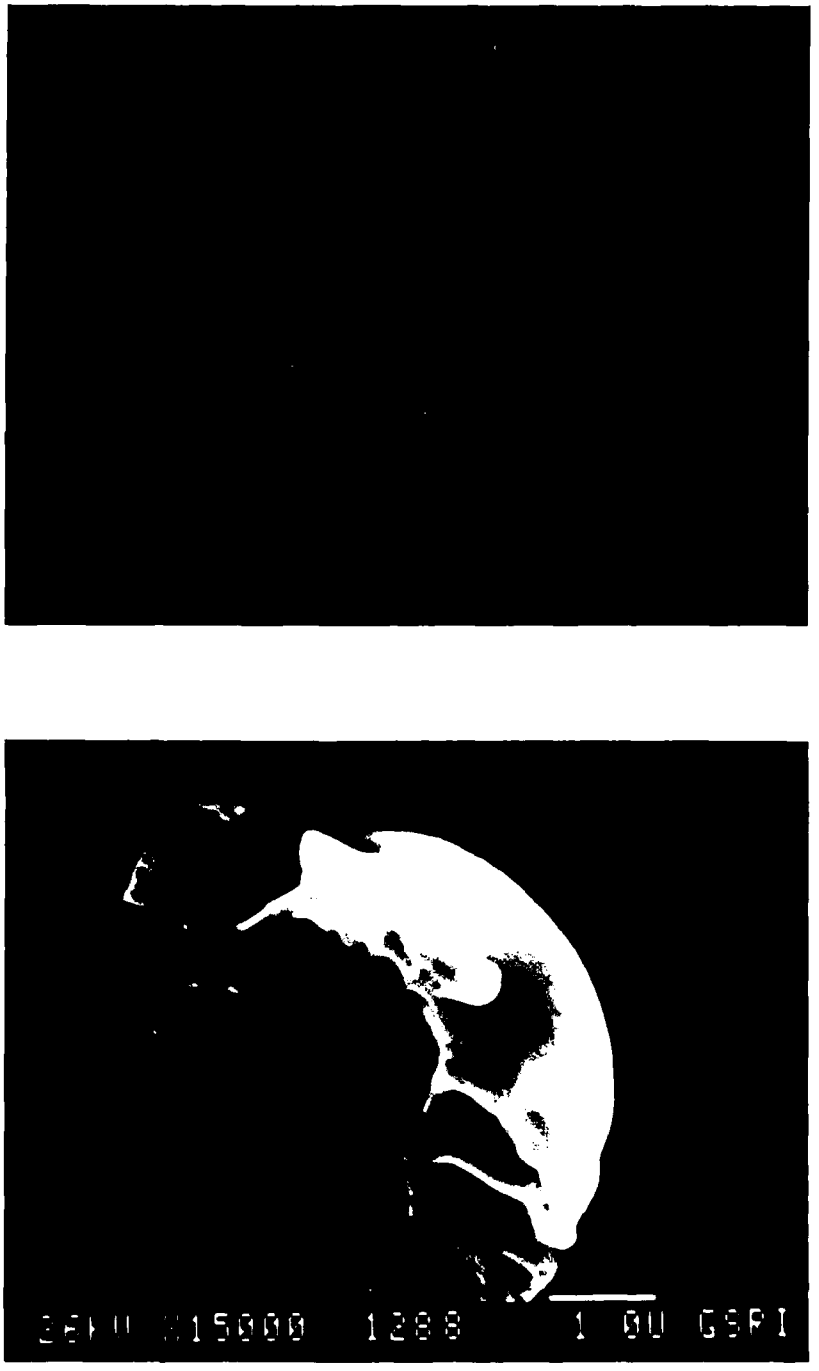

Figure 112. SEM photomicrograph of freeze-fracture analysis of 619-70 microcapsules, showing the various cavity configurations.

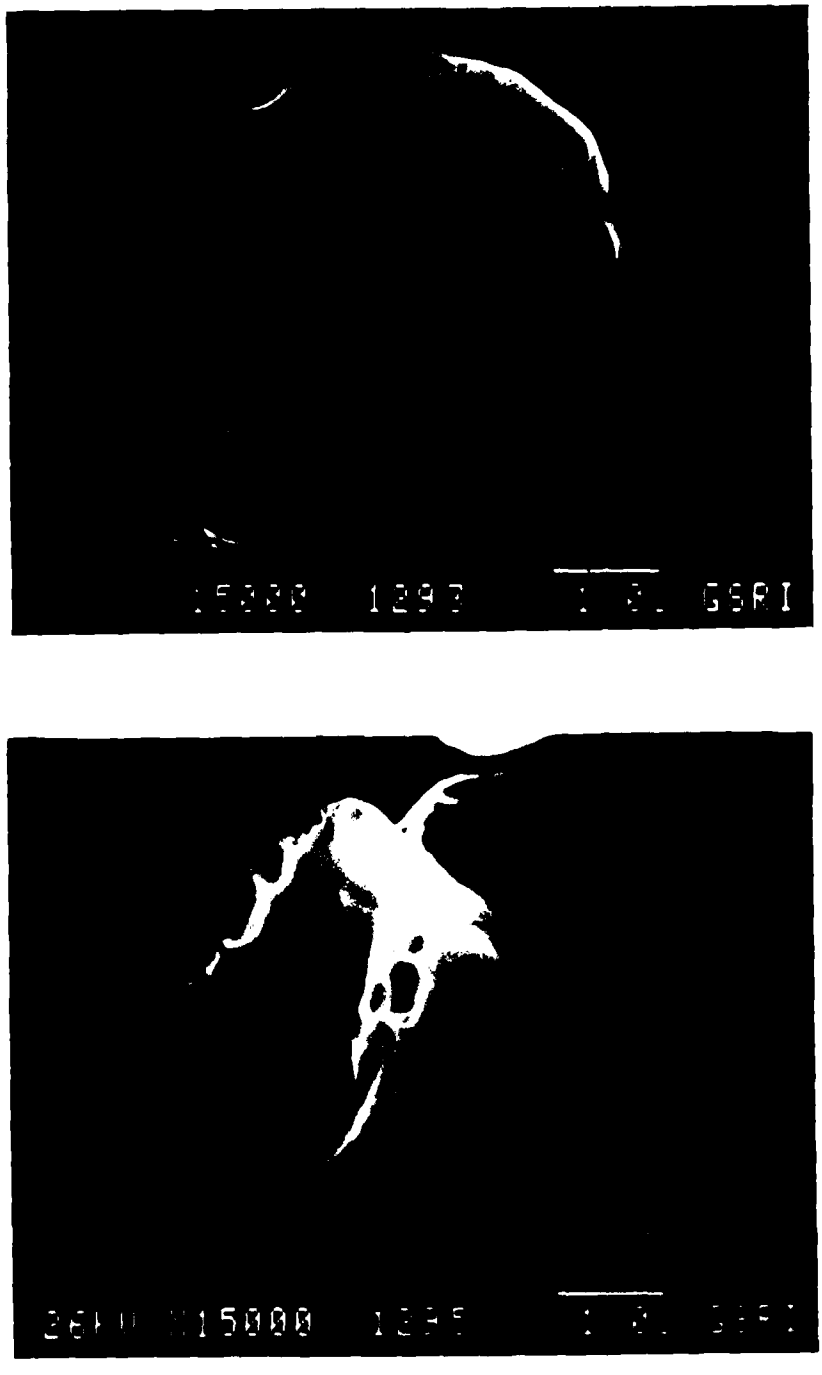

Figure 113. SEM photomicrograph of freeze-fracture analysis of 619-70 microcapsules, revealing the membrane wall porosity.

While considerable effort was expended in generating freeze-fractured SEM's of the thicker-walled microcapsule samples, the results obtained were not comparable to those of the control. Although certain deficiencies, such as the reticulated structure and the formation of amorphous structure, were associated with this last generation of microcapsules, the use of an enhanced wall accretion process to gain sustained release significantly improved performance characteristics as compared to the initial approach. The encouraging results were that AFIF-containing microcapsules could be prepared in the 1 to 10 μm range which displayed controlled release over a 3-4 hr period. These microcapsules were judged suitable for subsequent studies to evaluate the effectiveness of the microencapsulation approach in achieving sustained release.

4. Loading Determination of Polyurea Microcapsules

In studies relating to the development of AFIF-containing microcapsules, the AFIF loading value of the microcapsules is of theoretical and practical importance. The degree of loading may be defined as:

$$\text{loading} = \frac{\text{amount inhibitor}}{\text{amount microcapsules}} \times 100$$

Since the AFIF mixture is encapsulated as a 10% aqueous solution, the loading parameter is very sensitive to variation in water content. The state of hydration is an intrinsic factor which affects the loading parameter. In the "stored" state (i.e., slurry in cyclohexane), the organic phase surrounding the microcapsules acts as a transport barrier to retain water in the product. Since variable water contact can dramatically alter the results of loading value determinations, an experiment was performed to establish the water loss as a function of time to obtain the initial water content through extrapolation. Additionally, dry loading values were obtained by subsequently removing all the water from the samples by vacuum drying at temperatures less than the T_g of the polymer.

A simple model for the dry loading value may be given which is reasonable from the aspect of material balance. Consider Table 29, which lists all the main components for the samples prepared using the established preparation method, excluding the organic phase solvent and DBTDL catalyst. In this simple model, assume all the H_2O can be removed, and that the Brij 72 may or may not be "locked" into the membrane wall as it is deposited. Furthermore, assuming that no competing side reactions occur, the dry loading value is given as follows:

$$\text{Dry Loading (Theoretical)} = \frac{C}{A+B+C+D+E} \times 100,$$

with all quantities in grams.

The results of the theoretical "dry" loading calculations, with both $E = 0$, $E \neq 0$, are given in Table 30, along with the experimental values for the loading, as determined by atomic absorption analysis of boron.

The experimental procedure utilized in the boron atomic absorption spectrometric determination of the loading is given in Table 31. The results obtained using this procedure indicate that the experimental loading values are in the general range of the theoretical values (16 to 26%). However, the considerable variability in the results of the various samples precludes quantitative conclusions. Such variability may be inherent in the procedure selected for the determination. This variability was also found to be prevalent in studies to determine the rate of water loss from the sample.

The procedure used to determine the water release time was identical to that presented in Table 31; the microcapsule suspension was placed in an evaporating dish and weight loss was monitored as a function of time. Obviously, the initial component to be lost should be the cyclohexane phase followed by the water phase. The results of the study for samples 619-70, 74, 81 and 95 are presented in Figures 114, 115, 116, 117, respectively. Due to the variability in the dry loading results, interpretation of the drying curve data is of little value in calculating the actual amount of H_2O contained in the microcapsule samples. However, the observed rapidity with which the H_2O left the samples was unforseen. Within 20-40 min after the bulk of the cyclohexane phase evaporated, all the H_2O had evaporated. This effect may be associated with the reticulated wall structure or the nature

TABLE 29. COMPOSITION OF MICROCAPSULE SAMPLES

Designator	Component	Component amounts (in grams) 619-70	619-74	619-81	619-95
A	hexane-1,6-diamine	4.0	5.2	6.76	6.76
B	toluene-2,4-diisocyanate	6.1	7.93	10.31	10.31
C	$Na_2B_4O_7 \cdot 10H_2O$	3.0	3.0	3.0	3.0
D	Brij 58	0.5	0.5	0.5	0.5
E	Brij 72	2.0	2.0	2.0	3.0
	H_2O	50.0	50.0	50.0	50.0

TABLE 30. COMPARISON OF THEORETICAL AND EXPERIMENTAL LOADING DETERMINATION

Sample	Theoretical Dry Loading (E = 0)	Theoretical Dry Loading (E ≠ 0)	Loading by Atomic Absorption Trial 1	Trial 2	Avg. AA Loading	%Δ **
619-70	22.0	19.2	49.7*	17.8	17.8	24
619-74	18.0	16.1	26.0	17.9	21.9	18
619-81	14.6	13.3	16.1	14.4	15.2	4
619-95	14.6	12.7	16.0	7.1	11.6	26

* Discard this point as spurious

** $\frac{[\text{Avg. AA Loading} - \text{Theor. Dry Loading (E=0)}] \times 100}{\text{Avg. AA Loading}}$

TABLE 31. PROCEDURE FOR DRYING CURVE AND LOADING ANALYSIS

1. Pour 10.0 ml of suspension of the microcapsule sample into a drying dish.
2. Take weight (g) vs time (min) data until $\frac{d\,(\text{mass})}{dt} \sim 0$.
3. Dry the dish and sample in vacuum drying oven for 3-4 hrs.
4. Take final mass reading; calculate dry mass of wall and salt.
5. Collect known amount of the solid into a container; add 30.0 ml of 0.1% Brij 58/H_2O to the solid; triturate and then stir, closed, for 6-8 hrs.
6. Filter the suspension, collect the filtrate; measure the volume of the filtrate.
7. Determine boron by AA analysis

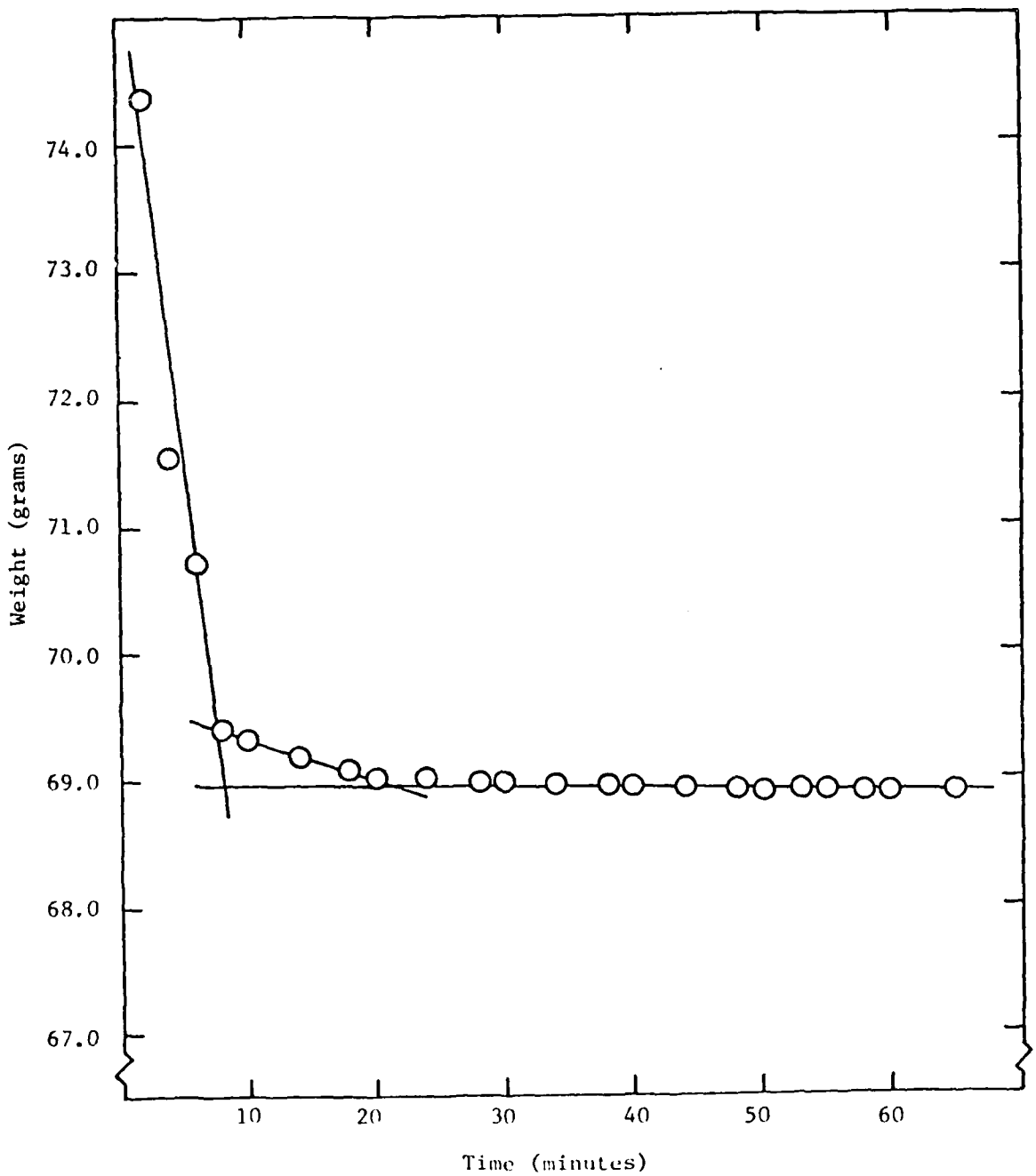

Figure 114. Drying curve for 619-70.

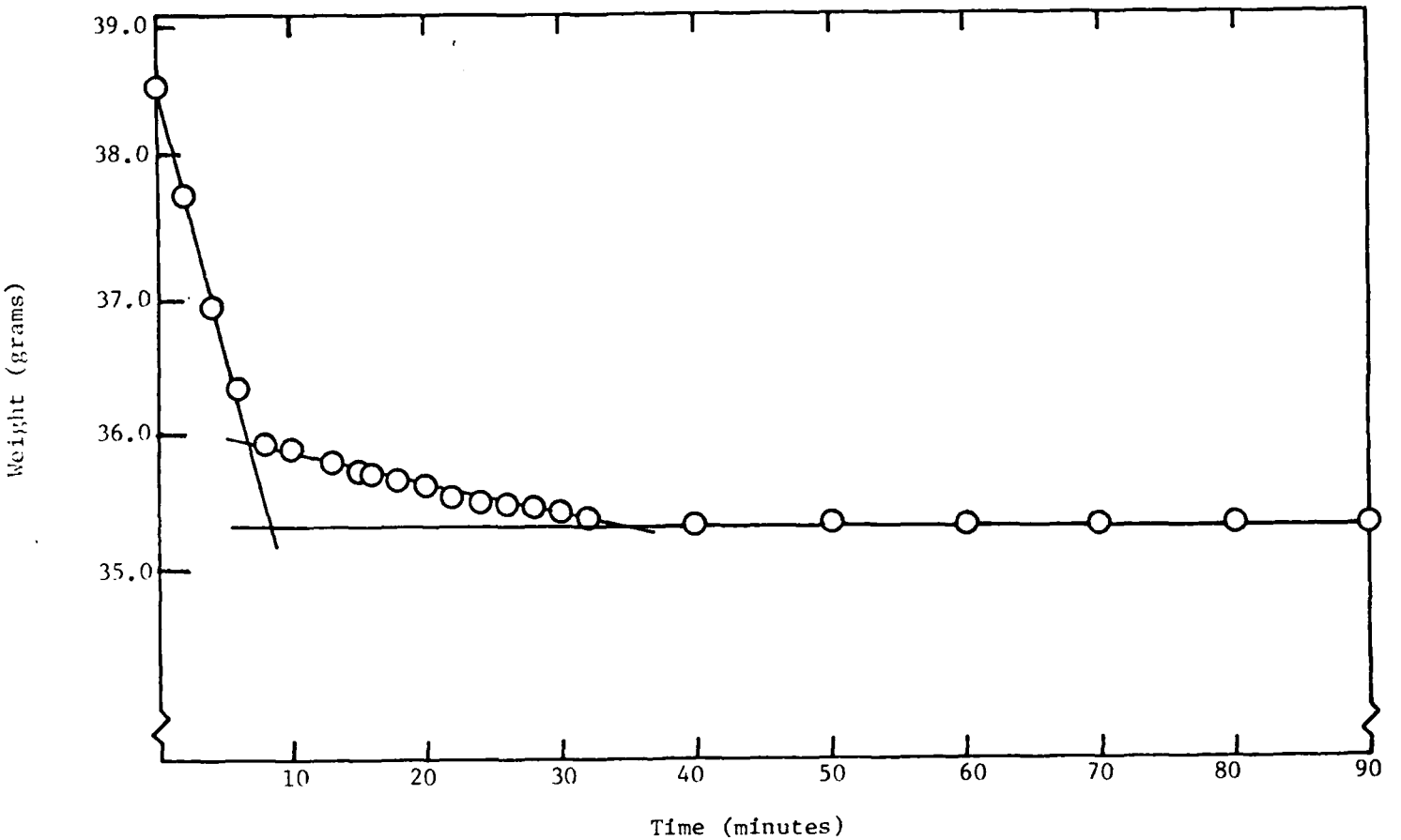

Figure 115. Drying curve for 619-74.

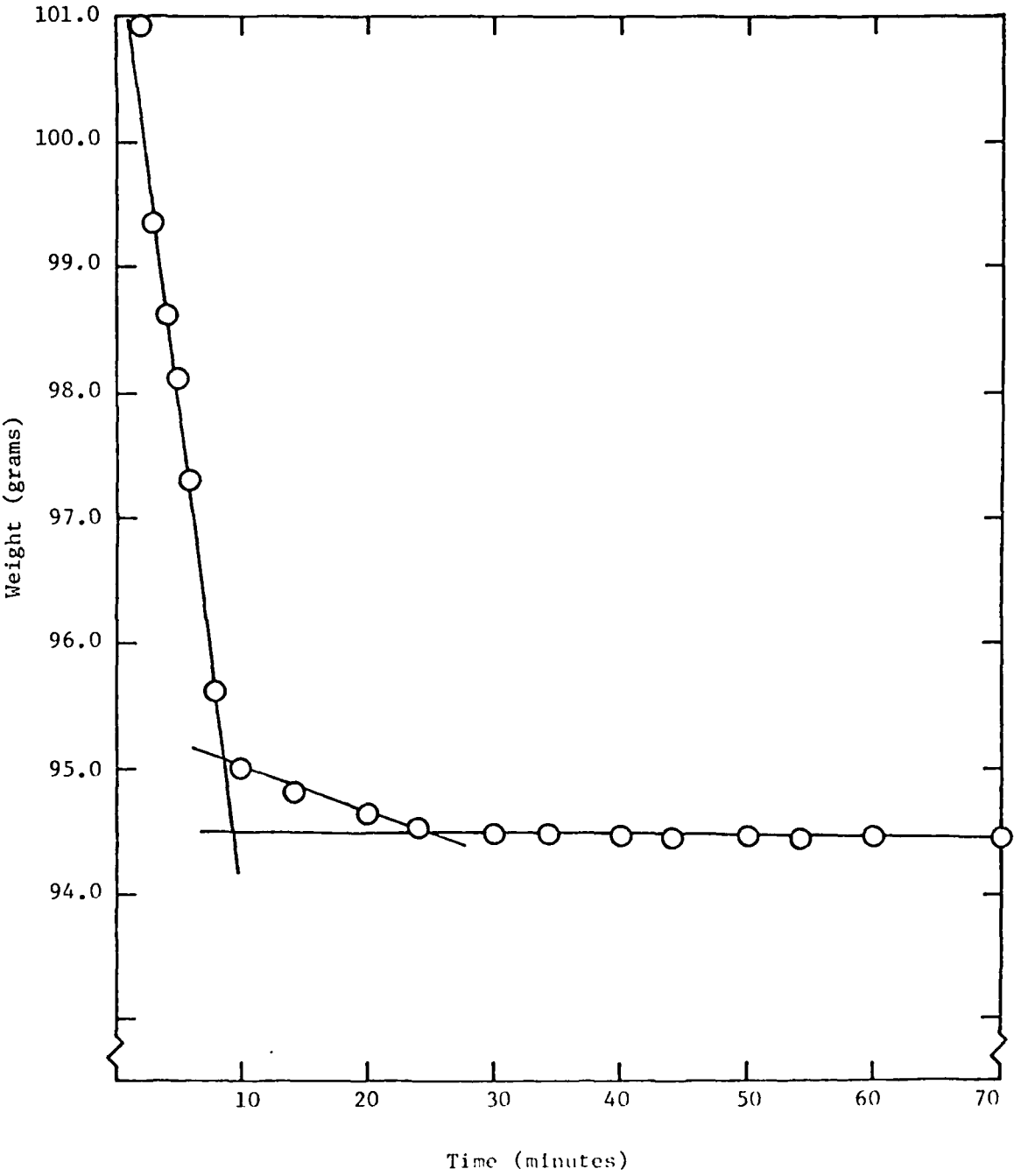

Figure 116. Drying curve for 619-81.

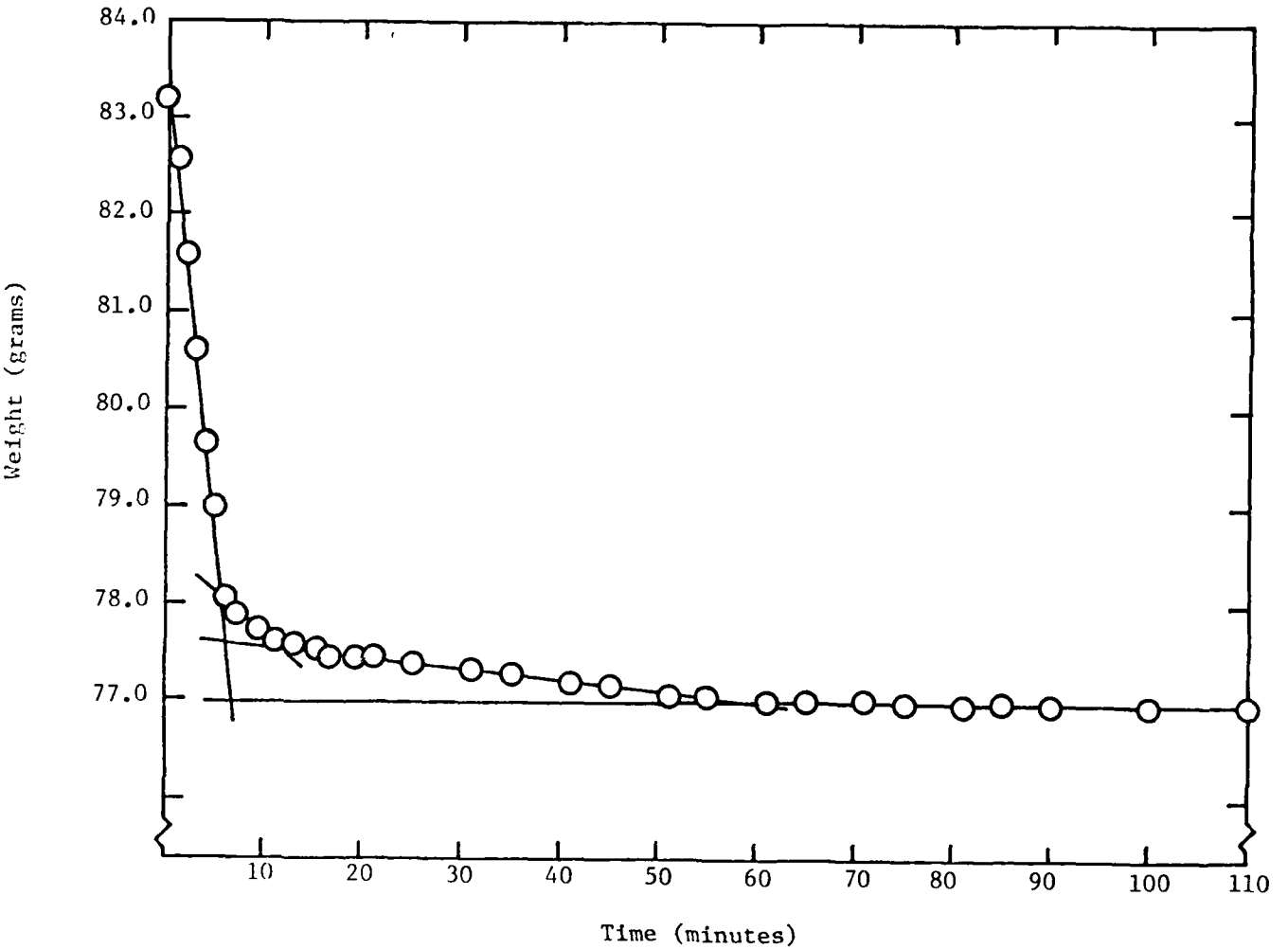

Figure 117. Drying curve for 619-95.

of the polymer which makes up the membrane wall. Obviously, rapid dehydration of the microcapsule, in either the paint formulation or the coating, could greatly alter the release characteristics.

V. POLYMERICALLY-BOUND, TIME-RELEASABLE CORROSION INHIBITORS

A. Background

The chemical modification of carrier polymers with pendant, or chelated, corrosion-inhibiting functional groups was investigated as a method of extending corrosion protection via controlled release rates. By binding inhibiting pendant moieties directly to a polymer, several fundamental problems surrounding the application and consumption of the inhibitor are addressed.

a) In conventional applications, initial inhibitor concentrations necessary to achieve protection may cause undesirable effects (e.g., blistering or loss or adhesion), while inhibitor erosion, consumption or deterioration with time eventually lowers the concentration below its threshold of effectiveness. A consistent release profile may theoretically be achieved by binding the inhibitor to a polymer, minimizing the initial stability shock to the system and providing an improved source of inhibitor for long-term protection.

b) Release of the bound inhibitor is controlled by contact with a corrosive environment, i.e., the penetration of water through the polymer-primer matrix, solution pH, etc., creating a site-specific inhibitor system.

c) Release rates and the level of inhibitor may also be controlled by varying the degree of polymer substitution.

A requirement for the preparation of polymerically-bound inhibitors is that the polymer and inhibitor each contain accessible and mutually reactive functional groups. Subsequently, the bond created in the reaction must degrade under environmental conditions to release the active component. The degree of substitution and accessibility of the bond to the hydrolyzing environment will influence the release rate. Ultimately, the degree of controlled release attainable with this type of approach is dependent on several factors, including water sensitivity of the polymeric salt, compatibility of the modified polymer with the primer system, water permeability of the primer matrix and mass transfer boundary layer conditions.

Attachment to the polymer may be achieved through several bonding mechanisms. The strongest or highest energy bond is a covalent bond, which would be expected to provide the longest sustained released through the time-dependent hydrolysis of the bond. As a general rule, the rate of release is inversely related to the strength of the inhibitor-polymer bond. Bond energies (ΔH) range from greater than 50 Kcal/mol for covalent bonds to approximately 1 Kcal/mol for Van der Waals type forces. Bonds of intermediate strength are chelates ($\Delta H \sim 50$ Kcal/mol), ionic ($\Delta H \sim 10$ to 15 Kcal/mol) and hydrogen bonds (1 to 10 Kcal/mol).

Two types of polymerically-bound inhibitor systems were investigated. The first approach involved crosslinking poly(vinyl alcohol) (PVA) or methyl cellulose chains via borate anions, while the second method introduced pendant phosphonic acid moieties onto the methyl side groups of poly(2,6-dimethylphenylene oxide). The selection of borate anion as an inhibitor in this particular study was based on earlier evaluations of soluble salts, in which sodium borate exhibited promising corrosion inhibitor characteristics for steel. Sodium borate was bonded to the -OH functional groups of poly (vinyl alcohol) or methyl cellulose, yielding a chelated borate anion with a slow release rate. The probable crosslink structure obtained is illustrated using PVA as a model (47):

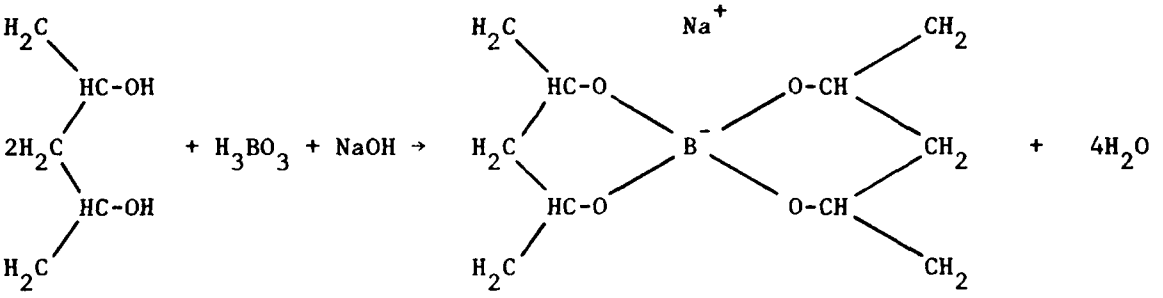

Since borate ester bonds are hydrolyzed in aqueous solutions, the polymers may release borate ions. The borate polymers synthesized by the above design may not be suitable for solvent base paints because of their hydrophilic character leading to possible nonuniform dispersion in solvent base coating systems; however, they were useful as model compounds to test the feasibility of this approach.

Polymers containing phosphate or phosphonate ester functional groups can be hydrolyzed to obtain the phosphonic acid. Besides providing an

anodically protective coating, these polymers are compatible with a large variety of polymer systems. The structures of poly(phenylene oxide phosphonate) (48) and poly(styrene phosphonate) (49) are shown below:

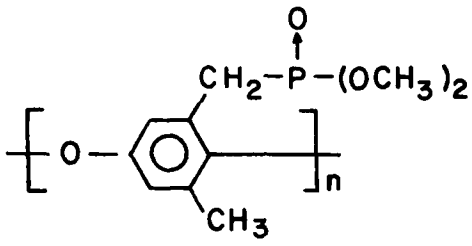

poly(phenyleneoxide hydroquinone phosphate)

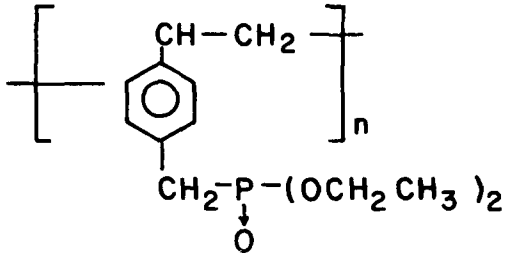

poly(styrene phosphonate)

B. Experimental

1. Borate Inhibitors Bound to Poly(Vinyl Alcohol)

The following procedures were employed in preparing the borate polymers. A 10 g sample of PVA (<99 percent hydrolyzed) obtained from Polysciences was dissolved in 40 ml dimethylformamide (DMF) at 60°C, and 1.0 g boric acid was added after the mixture was cooled to room temperature. After filtration, the polymer was washed with methanol to neutralize the acid. The polymer was precipitated by the addition of methanol and was dried under vacuum. This polymer was crosslinked and would not dissolve completely in water. The adjustment of the amount of PVA and boric acid to 3.0 g and 10 g, respectively, did not solve this problem.

The control of the cation to borate ratio is essential in obtaining a stable, crosslinked gel and water solubility. Improved stability and water solubility were achieved by the alkaline hydrolysis of poly(vinylacetate) to obtain the sodium alcoholate. Hydrolysis of the acetate was carried out by

slowly adding 10 ml of 5 percent NaOH in methanol to 25 g of poly(vinyl-acetate) in 400 ml of CH_3OH at 30°C. After stirring for 25 min, the viscous solution was poured into 400 ml methanol to precipitate the polymer. After the polymer was washed with CH_3OH and dried under vacuum, it was soluble in DMF.

A 4 g sample of poly(vinyl alcoholate) in 300 ml DMF was mixed with 10 g boric acid in 200 ml of DMF. The mixture was heated to 50°C for 1 hr. After cooling to room temperature, the polymer was precipitated by adding acetone. After filtration the polymer was washed with CH_3OH and vacuum dried yielding 1.7 g polymer. Atomic absorption analysis of 0.25 g polymer in 20 g distilled water showed a concentration of 650 ppm boron (i.e., the equivalent of 0.3 g of Na_2BO_2 in 1 g of polymer).

2. Borate Inhibitor Bound to Methyl Cellulose

Methyl cellulose borate was prepared by placing 1 g methyl cellulose in 20 ml chloroform and adding to 4 g boric acid in 25 ml DMF at 30°C. After stirring the polymer for 1 hr, it precipitated during the reaction. After filtration, the polymer was washed with methanol, 5 percent NaOH in CH_3OH solution, and then acetone. The polymer was dried under vacuum. The polymer yield was 1.1 g. Atomic absorption analysis revealed the equivalent of 0.16 g of Na_2BO_2 in 1 g polymer.

3. Chemical Modificiation of PPO

Poly(2,6-dimethy-p-phenylene oxide) (PPO, General Electric) was chemically modified to introduce pendant phosphonate groups on the methyl groups of the polymer, and the ester was then hydrolyzed to yield the phosphonic acid. Prior to phosphonation, the successive brominations of the phenylene backbone and the methyl substituents were carried out. Phenylene bromination was achieved at low temperatures (electrophilic substitution), and bromination of the methyl groups was achieved at reflux (radical substitution).

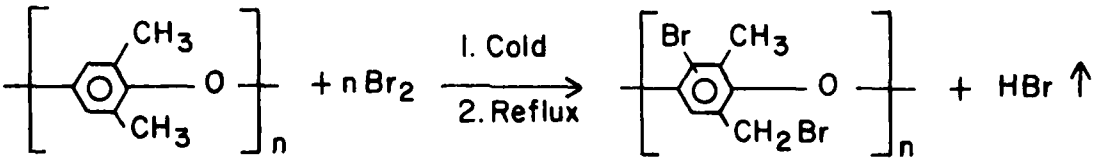

Bromination

The methyl bromine of the polymer was replaced according to the Arbusov reaction by trimethyl phosphite and yields a pandent phosphonate group.

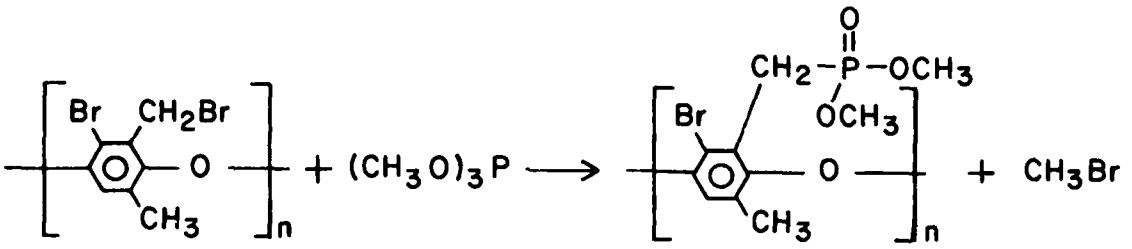

Phosphonylation

The polymer was then hydrolyzed with NaOH in the presence of water:

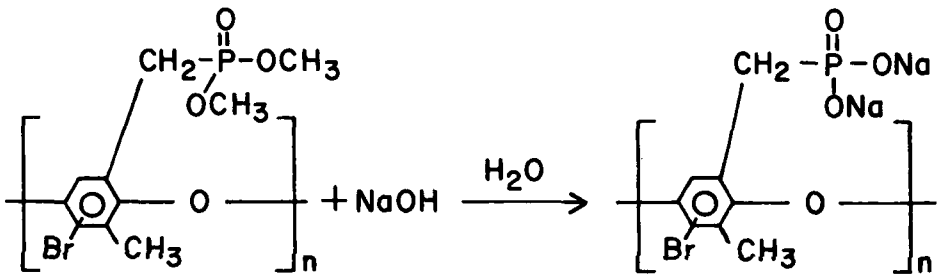

4. Release Rates of PVA-Borate and Methyl Cellulose-Borate

Release rates of each of the polymers were determined by addition of 0.45 g of polymers to 50 g distilled water and measuring the conductivity of the solution at given intervals with a Yellow Springs Instrument Company Model 31 conductivity bridge.

5. Potentiodynamic Corrosion Resistance Test

Aqueous solutions of the polymers (0.1%) were prepared, and salt was added to obtain a concentration of 5% NaCl. The pH was adjusted by adding 1N NaOH or 10% acetic acid. Potentiodynamic polarization experiments were run under the conditions described in Section III.

6. NMR Analysis of Phosphonic Acid Polymers

A 60 megacycle proton NMR (nuclear magnetic resonance) spectrometer was used to prepare spectra of the unmodified PPO and the phosphony-

lated PPO polymers before and after hydroylsis.

C. Results and Discussion

1. Release Rates of PVA-Borate and Methyl Cellulose-Borate

Release rates of borate ion from poly(vinyl alcoholate)-borate and methyl cellulose-borate are shown in Figure 118. These data indicate a zero order release rate. The release rate from polyvinyl alchohol is slower than that of the methyl cellulose-borate due to a higher crosslink density of PVA. The principle of polymerically binding corrosion inhibitor to provide controlled release of the inhibitor on demand (when exposed to moisture) is validated by these studies.

2. Potentiodynamic Corrosion Resistance Test

The corrosion protection potential of boric acid is reported in Figures 119-121. Potentiodynamic polarization evaluation of 2024 aluminum alloy in 5 percent NaCl solution containing 0.1 percent boric acid is shown in Figure 119. Under acidic (pH<7) conditions, extensive cathodic protection of the metal with cathodic current densities $\sim 10^{6}$-10^{4} nA/cm^{2} is noted. The equilibrium potential is $\sim$-0.65V, and no anodic passivation exists. When the concentration of boric acid in solution is increased to 1 percent (Figure 120) at neutral or acidic ($pH \leq 7$) conditions, aluminum shows an extensive cathodic region with low current densities. Similar experiments with steel (Figure 121) and 1 percent boric acid show anodic passivation at near neutral or alkaline ($pH \leq 7$) conditions. Hence, to be effective on both steel and aluminum, the borate-containing polymer should have a pH which is near-neutral and a sufficient borate release rate.

Figure 122 shows the potentiodynamic polarization of 2024 aluminum alloy with 0.1 percent PVA (pH 6.4) as compared to 0.1 percent PVA-borate (polymer) adjusted to pH values of 7.6 and 3.9. The substituted polymer has an equilibrium corrosion potential of $\sim$-1.05V and an anodic passivation region between -1.05 and -0.7V with passive current density $\sim 7 \times 10^{3}$ nA/cm^{2}. The pH of the substituted polymer does not show any appreciable effect on the corrosion behavior of the metal. The equilibrium potential shifts to a more negative value of $\sim$-1.18V, and the passivation region extends to -0.6V. The passive current density is higher by an order of magnitude. An apparent

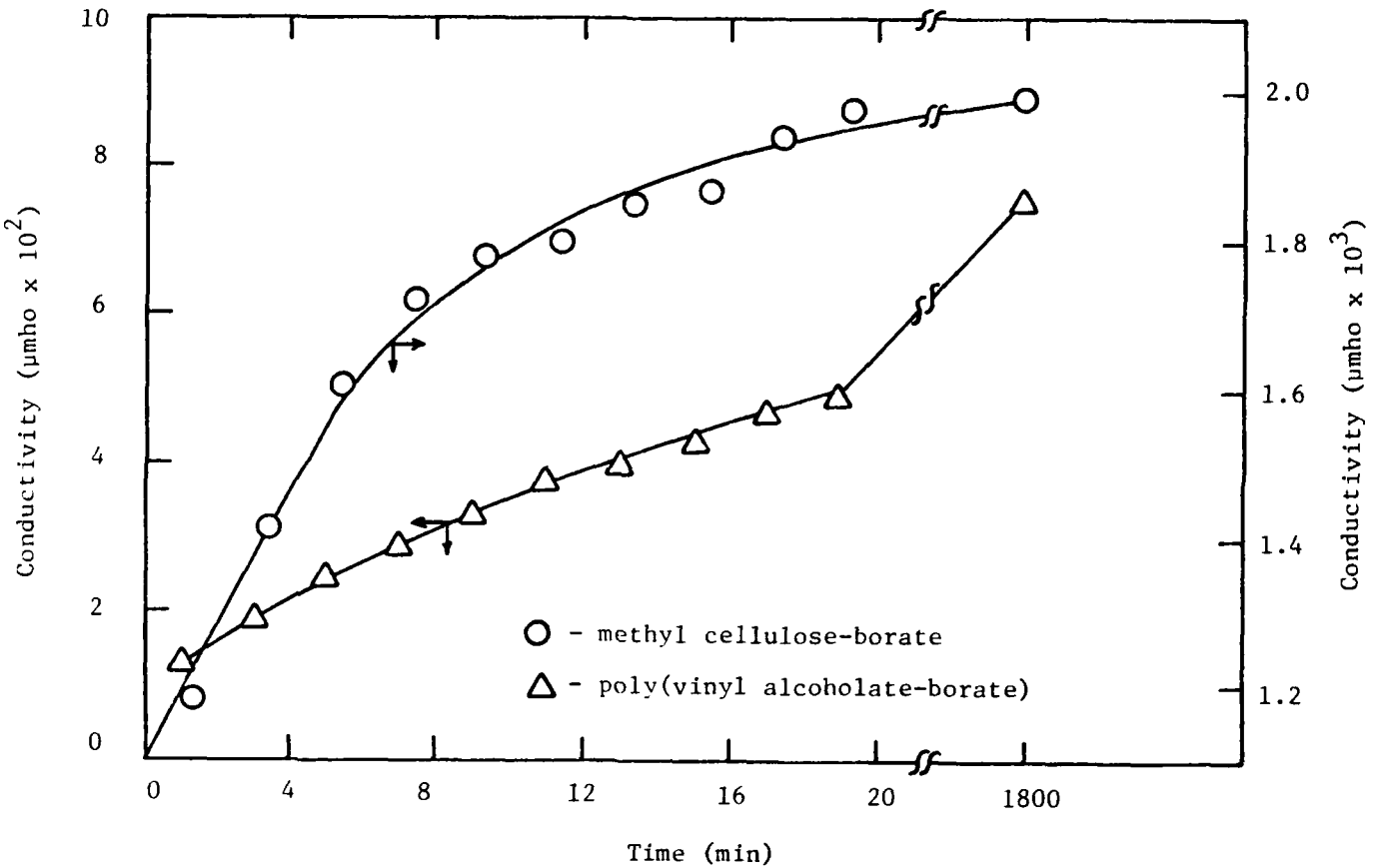

Figure 118. Release rate of borate from poly(vinyl alcoholate-borate) and methyl cellulose-borate.

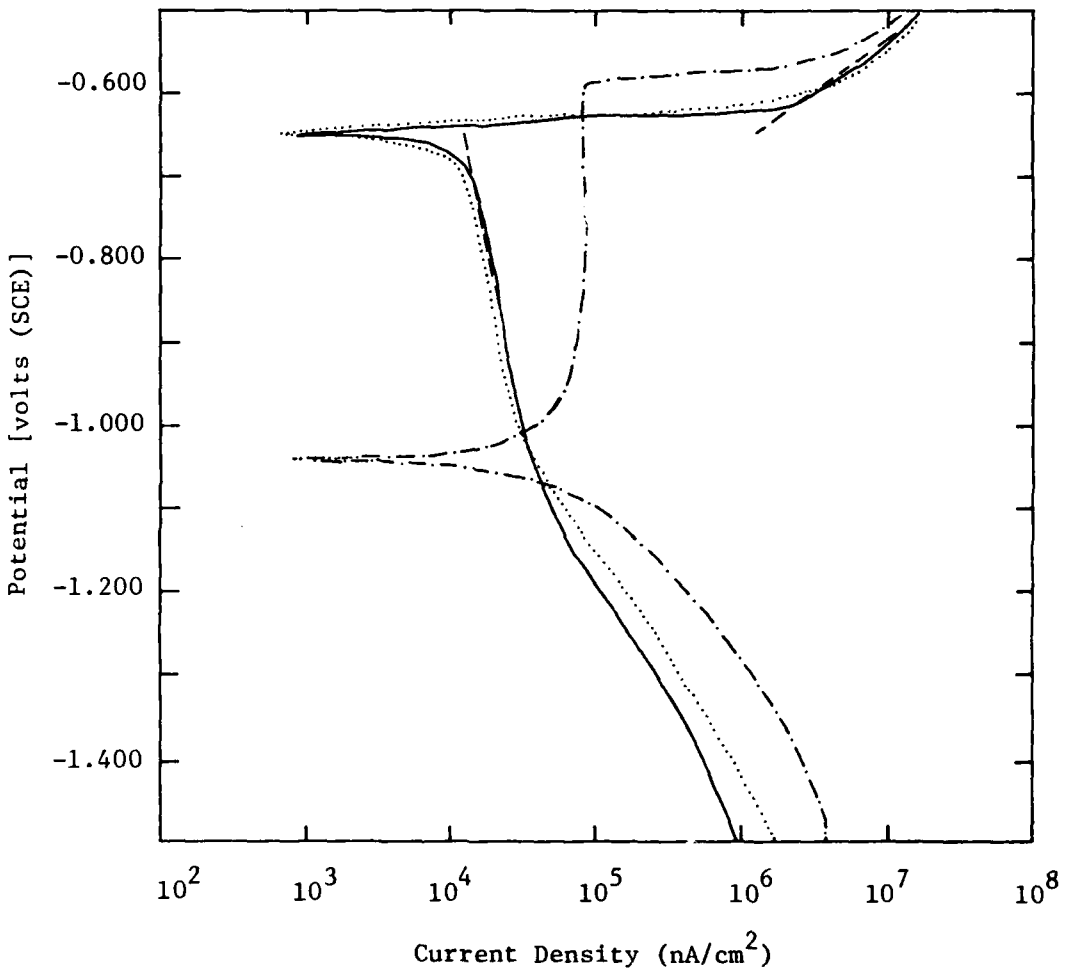

Figure 119. Potential vs. current density for potentiodynamic polarization experiment with aluminum alloy 2024-T3 in 5% NaCl containing 0.1% boric acid at pH 8.5 (—— ·), 5.8 (····), and 5.1 (——).

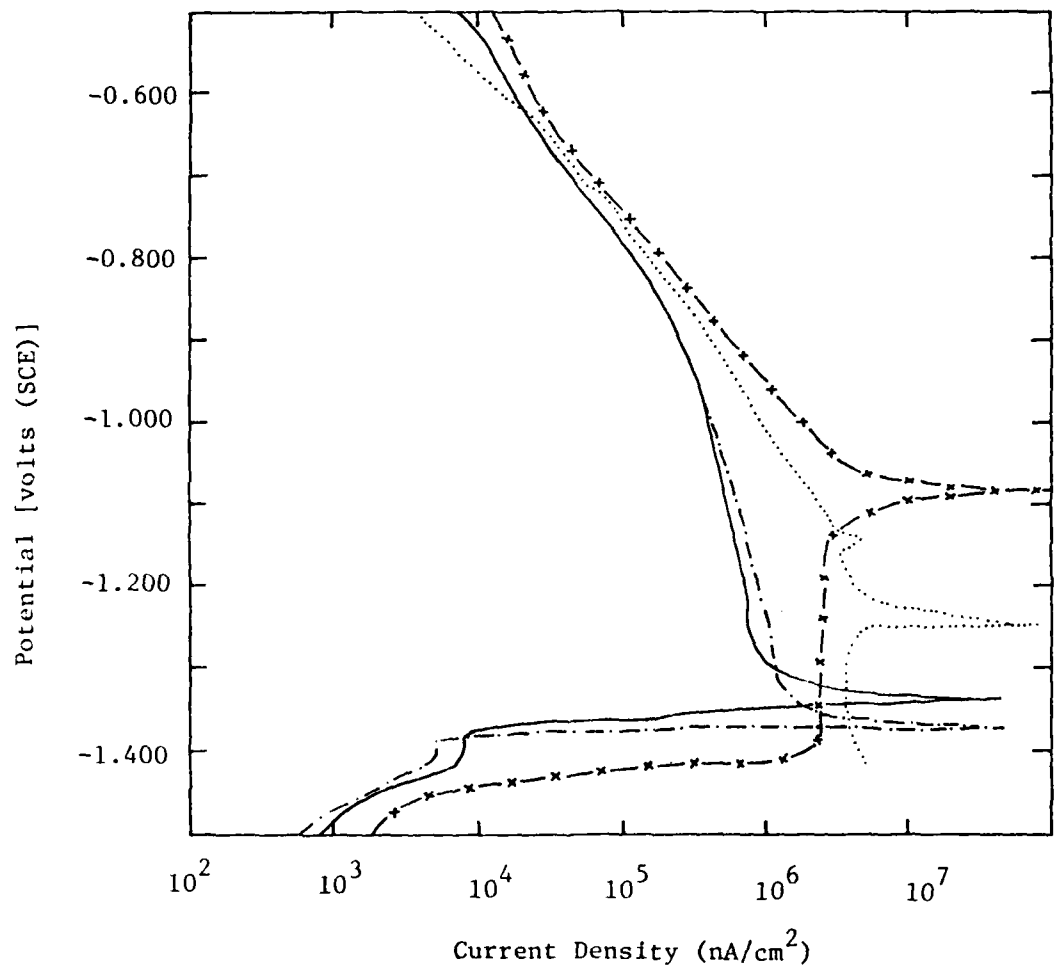

Figure 120. Potential vs. current density for potentiodynamic polarization experiment with aluminum alloy 2024-T3 in 5% NaCl containing 1% boric acid at pH 9.0 (x ——), 8.5 (····), 7.5 (—— ·), and 5.2 (——).

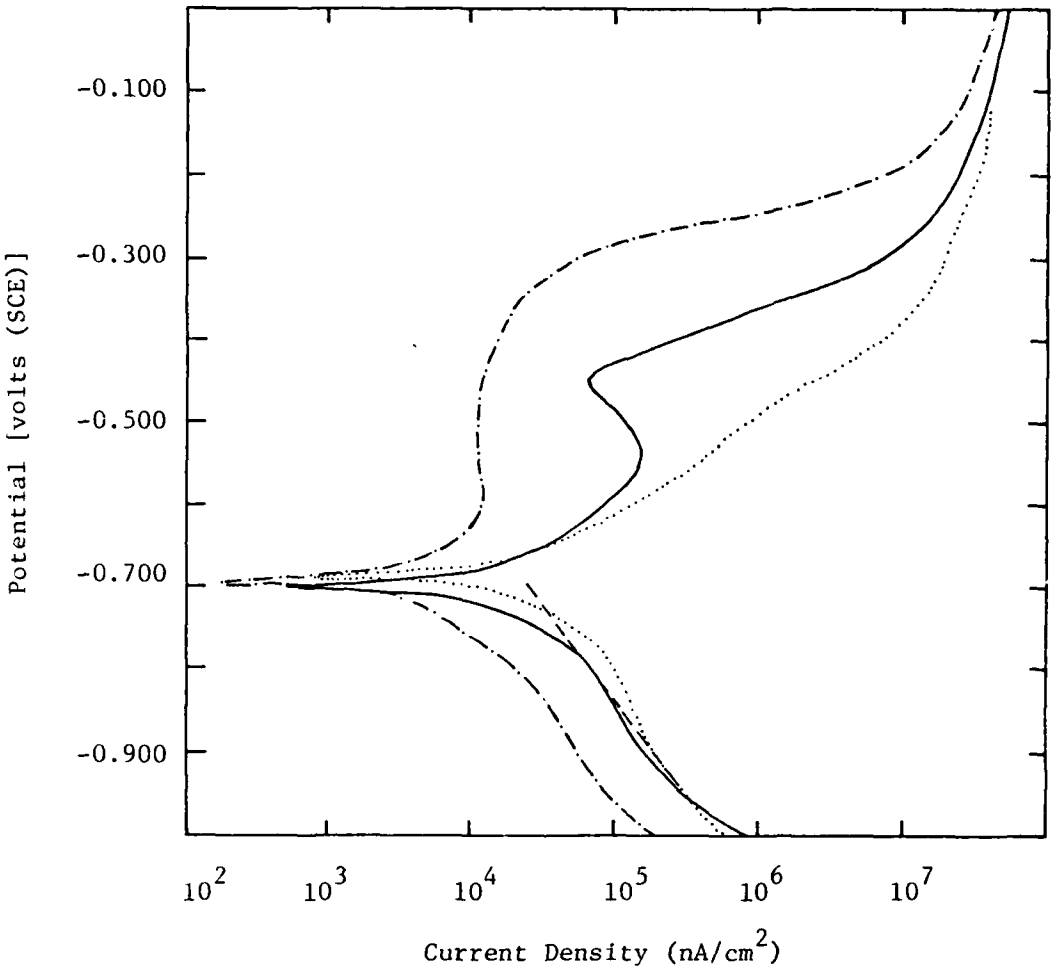

Figure 121. Potential vs. current density to potentiodynamic polarization experiment with 4340 steel in 5% NaCl solution containing 1% boric acid at pH 8.5 (—— ·), 7.5 (——), and 5.1 (···).

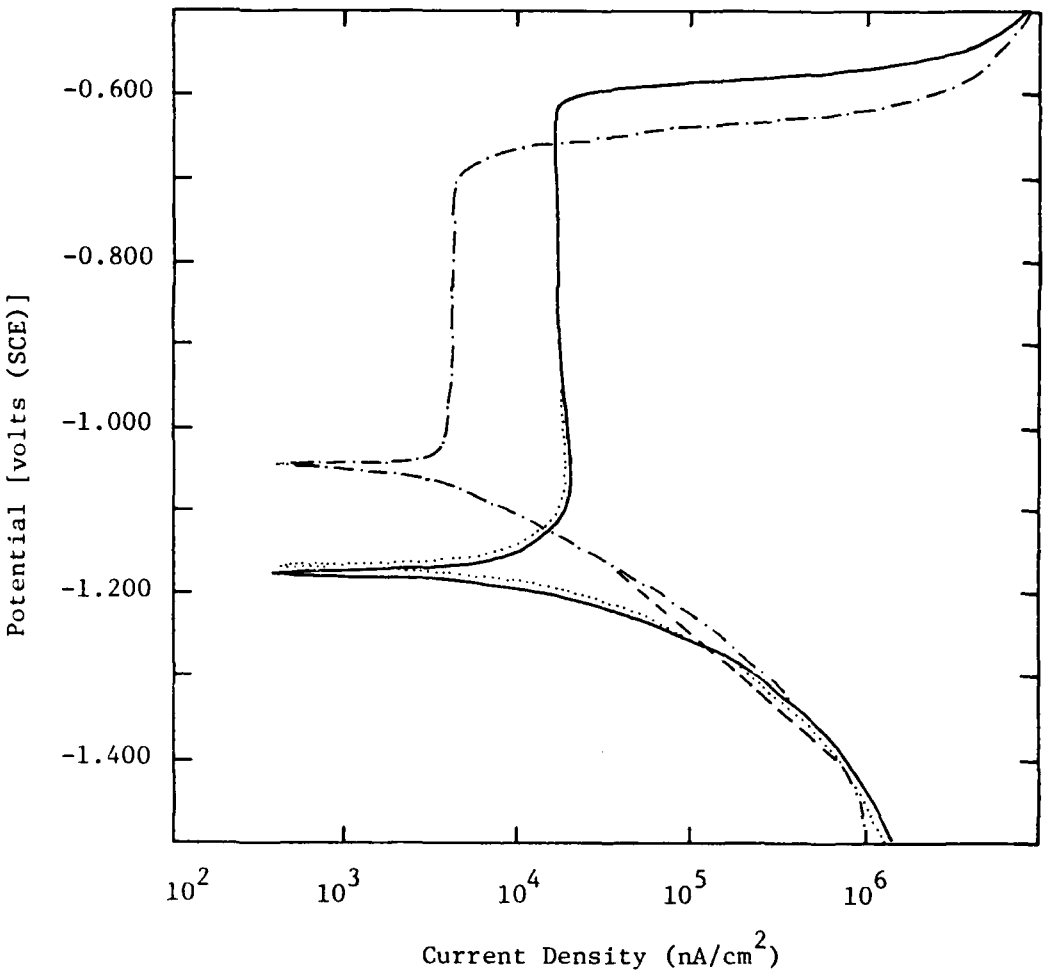

Figure 122. Potential vs. current density for potentiodynamic polarization experiment with aluminum alloy 2025-T3 in 5% NaCl solution with 0.1% PVA with pH 6.4 (—— ·), 0.1% PVA-borate (7-7) with pH 7.6 (····), and 0.1% PVA-borate (7-7) with pH 3.9 (——).

improvement in protection may be attributed to the polymer coating on the surface rather than the action of the borate, since borate concentration is relatively low. In the coating application, water penetration into the film will be low as compared to the PVA film and the borate concentration in aqueous phase may be higher due to the lower volume of water. Higher concentrations of the borate at the metal surface should provide additional cathodic protection.

Similar potentiodynamic polarization results are seen when 4340 steel is evaluated in the presence of 0.1% PVA (99.8% hydrolyzed), 0.1% PVA with lower degree of hydrolysis (7-1, 0.1% PVA-borate and 5% methyl cellulose-borate) (Figure 123). The preparation of the hydrolized PVA has a significant effect on corrosion inhibition behavior. The lower hydrolyzed polymer (7-1) offers both anodic and cathodic protection (with equilibrium potential ~-0.27V and cathodic current density $\sim 10^4$ -5 x 10^5 nA/cm^2; anodic passive current density $\sim 10^4$ -5 x 10^4 nA/cm^2). The anodic passivation region is effective since no transpassive region could be detected within the experimental potential limit. However, with 99.8% hydrolyzed PVA, the anodic protection is limited, and substituted polymers show effects similar to those found with the inorganic borate (Figure 122).

The hydrolyzed phosphonylated polymer (PPOP) was evaluated for corrosion inhibition with both 4340 steel and 2024 aluminum alloy in the presence of 5% NaCl. The effect of polymer concentration was studied by varying the hydrolyzed PPOP concentration between 0.1 percent and 10 percent. Further studies on 4340 steel using 1 percent hydrolyzed PPOP and NaOH mixtures were carried out.

The potentiodynamic polarization of 4340 steel in 5% NaCl solutions containing 5% and 10% concentrations of hydrolyzed PPOP is shown in Figure 124. The addition of the polymer results in a shift of the corrosion potential to a more negative value of -745 mV from -650 mV (control). However, no passivation occurs, and the metal corrodes actively. With the addition of NaOH to form the sodium salt of the polymer (pH of the resultant solution is ~10), the polymer passivates steel between -700 and -470 mV, with a passivation current density of 3.55 x 10^{-2} A/m^2 (Figures 125 and 126). The corrosion potential in the solution is -750 mV, which is more negative than the potential obtained with the AFIF. The passivation current density is lower than that obtained with AFIF.

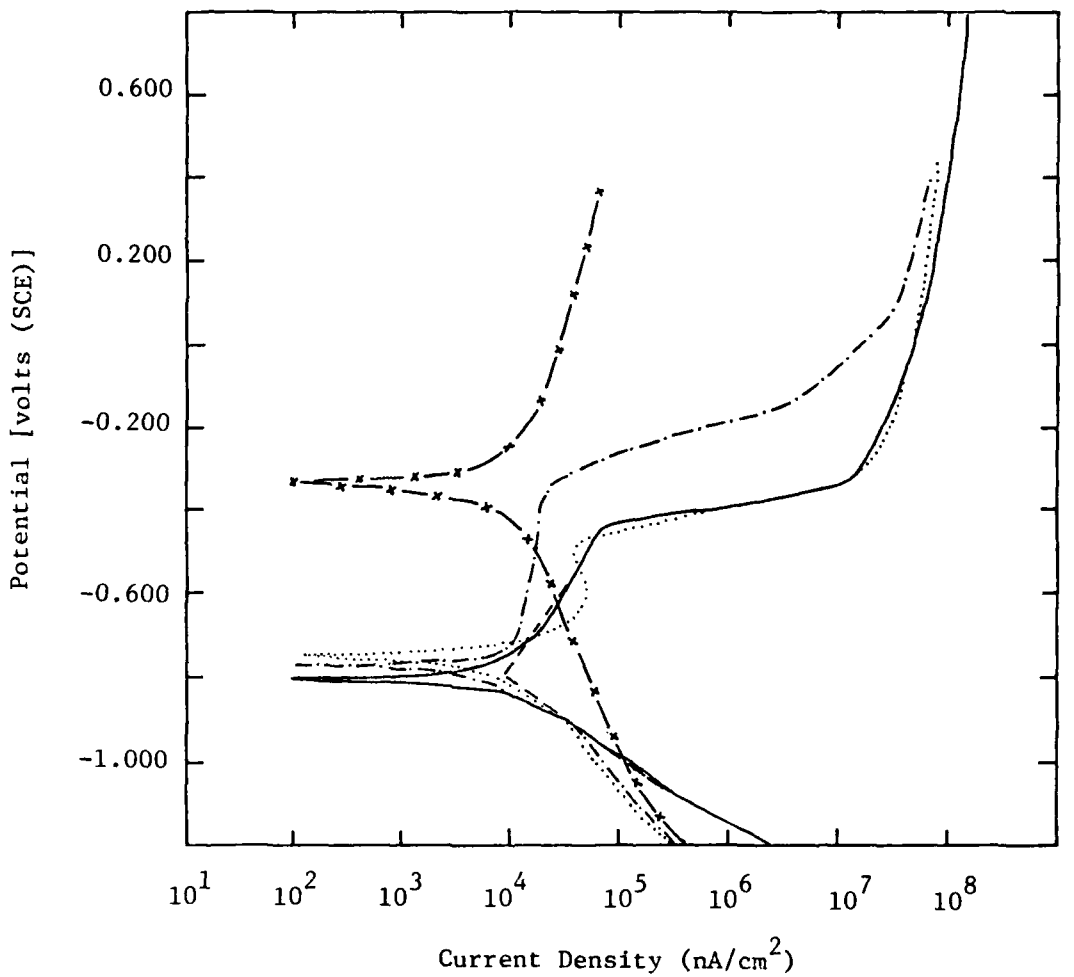

Figure 123. Potential vs. current density for potentiodynamic polarization experiment with 4340 steel in 5% NaCl containing 0.1% PVA (7-1) at pH 6.8 (x——x), 0.1% PVA (99.8% hydrolysis) at pH 6.3 (——·——), 0.1% PVA-borate (7-7) at pH 7.6 (····), and 5% cellulose-borate at pH 7.6 (——).

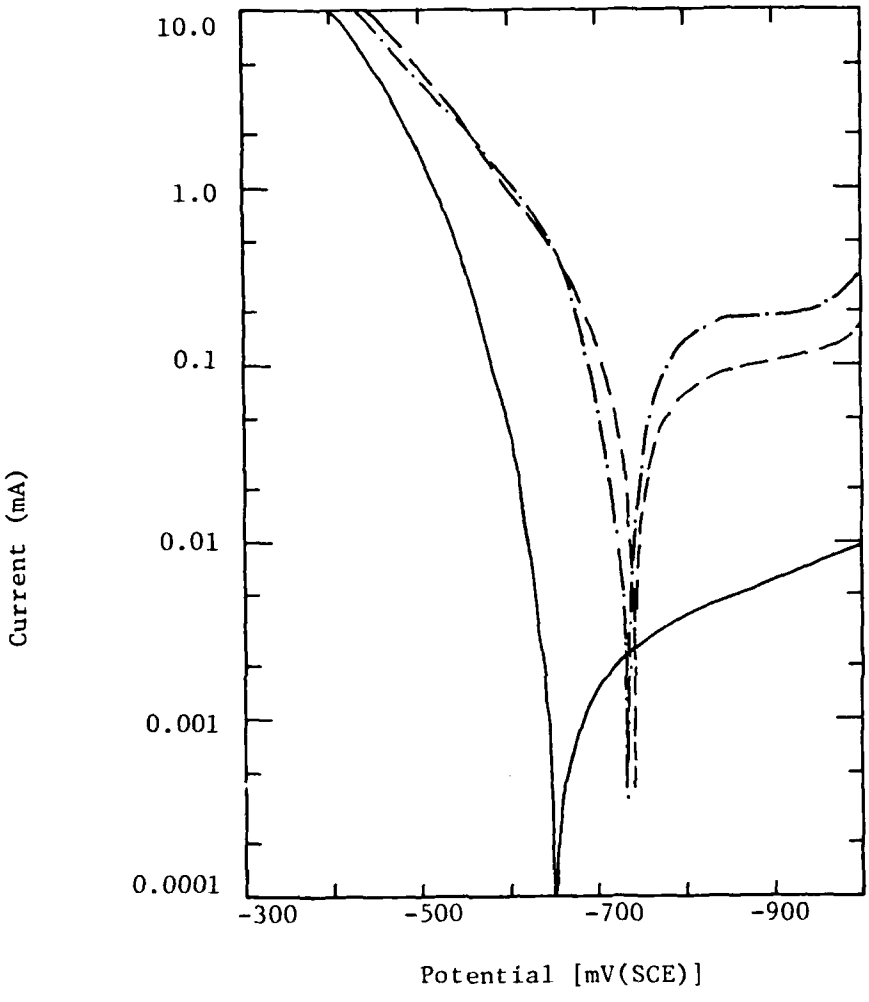

Figure 124. Current vs. potential for potentiodynamic polarization experiment with 4340 steel of 1.267 cm^2 surface area in 5% NaCl electrolyte solution: ____ control; - - - with 5% hydrolyzed PPOP; —— · —— with 10% hydrolyzed PPOP.

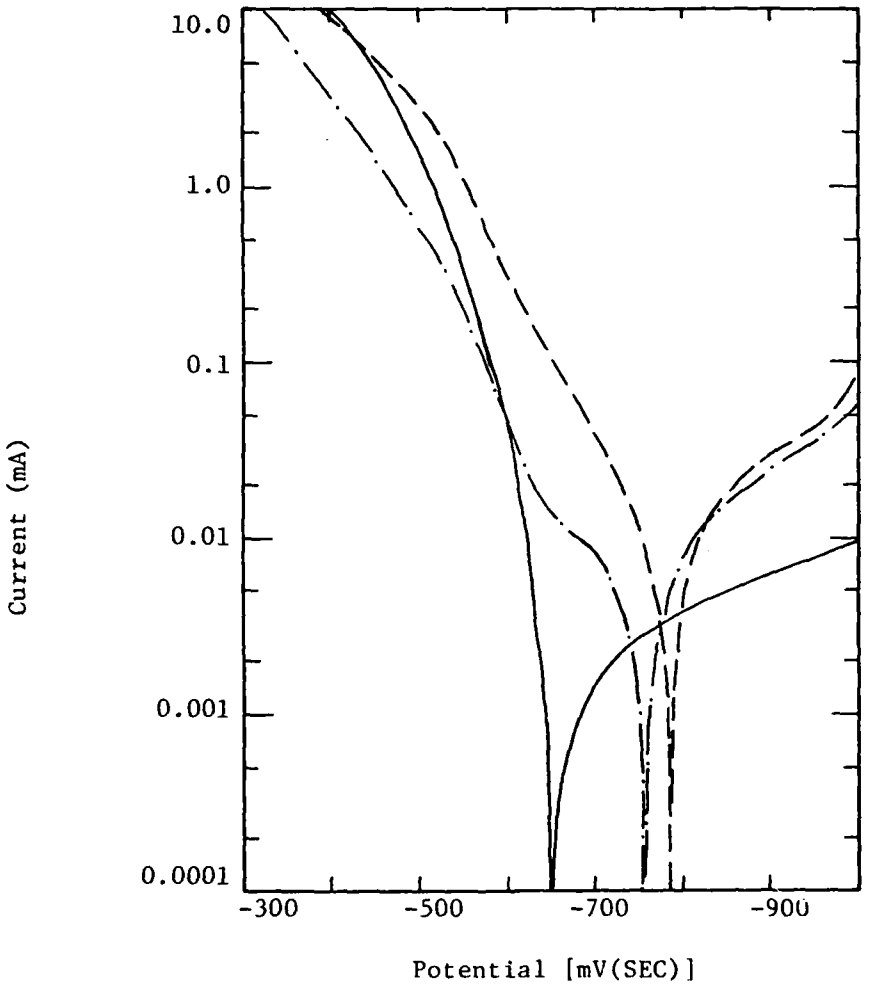

Figure 125. Current vs. potential for potentiodynamic polarization experiment with 4340 steel of 1.267 cm^2 surface area in 5% NaCl electrolyte solution: ___ · ___ with 1% hydrolyzed PPOP and 0.0044% NaOH (pH = 9.28).

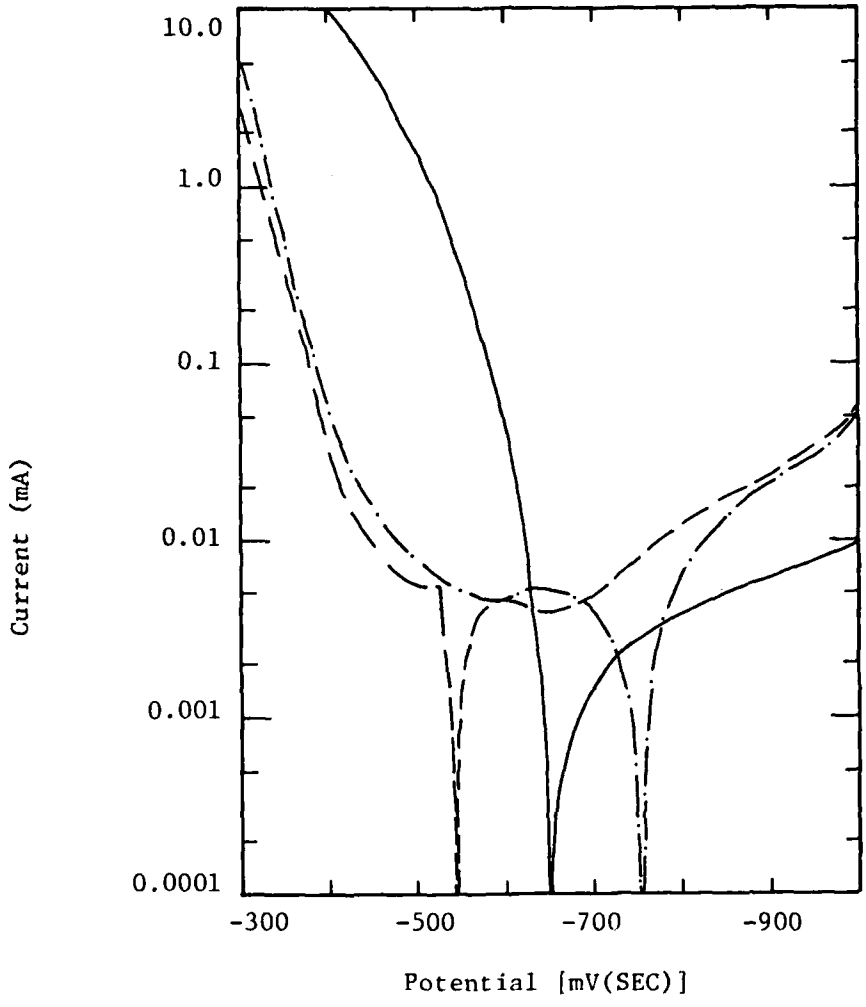

Figure 126. Current vs. potential for potentiodynamic polarization experiment with 4340 steel of 1.267 cm^2 surface area in 5% NaCl electrolyte solution: ——— control; - - - with 1% hydrolyzed PPOP and 0.022% NaOH (pH = 10.9); —— · —— with 1% hydrolyzed PPOP and 0.008% NaOH (pH = 10.0).

Hydrolyzed PPOP was electrochemically evaluated as a corrosion inhibitor for 2024 aluminum alloy. Figures 127 and 128 show the potential-current behavior of 2024 aluminum in the presence of 5% NaCl solution with 10%, 5%, 1%, or 0.1% hydrolyzed PPOP. Addition of polymer shifted the corrosion potential to values near the breakdown potential (∿-700 mV), disrupting formation of a protective Al-oxide film and resulting in loss of anodic passivation. However, the polymer shifts the equilibrium potential to values in the passive region of the alloy and also to overvoltage values conducive to enhancement of the cathodic process. The scan with 0.1 percent polymer concentration gives an equilibrium potential value just lower than the transpassive potential. Thus, concentrations below 0.1 percent are expected to enhance corrosion protection of the alloy. In summary, hydrolyzed PPOP at a concentration of 1% and pH 10 offers anodic inhibition to 4340 steel comparable to the AFIF. Much lower concentrations (<0.1 percent) of the polymer are required to enhance cathodic protection of 2024 aluminum alloy.

3. NMR Analysis of Polymer Modification

The probable structure of the phosphonated polymer (PPOP) was determined to be:

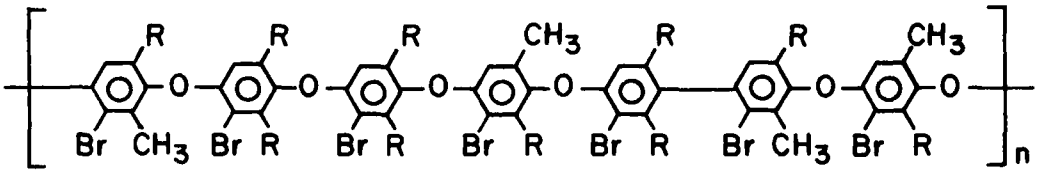

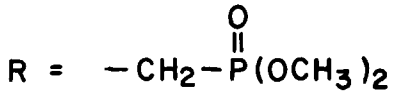

Controlled hydrolysis with 10 percent NaOH removed a portion of the methoxy groups to yield phosphonic acid moieties. NMR spectra (60 megacycle proton) of unmodified PPO and the PPOP polymers before and after hydrolysis were prepared as shown in Figures 129-131. The NMR spectrum of the PPOP polymer had the following characteristic peaks: δ 2.05, 2.30 [12H, p- and o- ph(CH_3)], δ 3.67, 3.82 [60H, p- and o- $(OCH_3)_2PO$], δ 4.20 [20H, $CH_2(OHC_3)_2PO$], δ 6.35 (7H, phH). The hydrolyzed polymer had the following

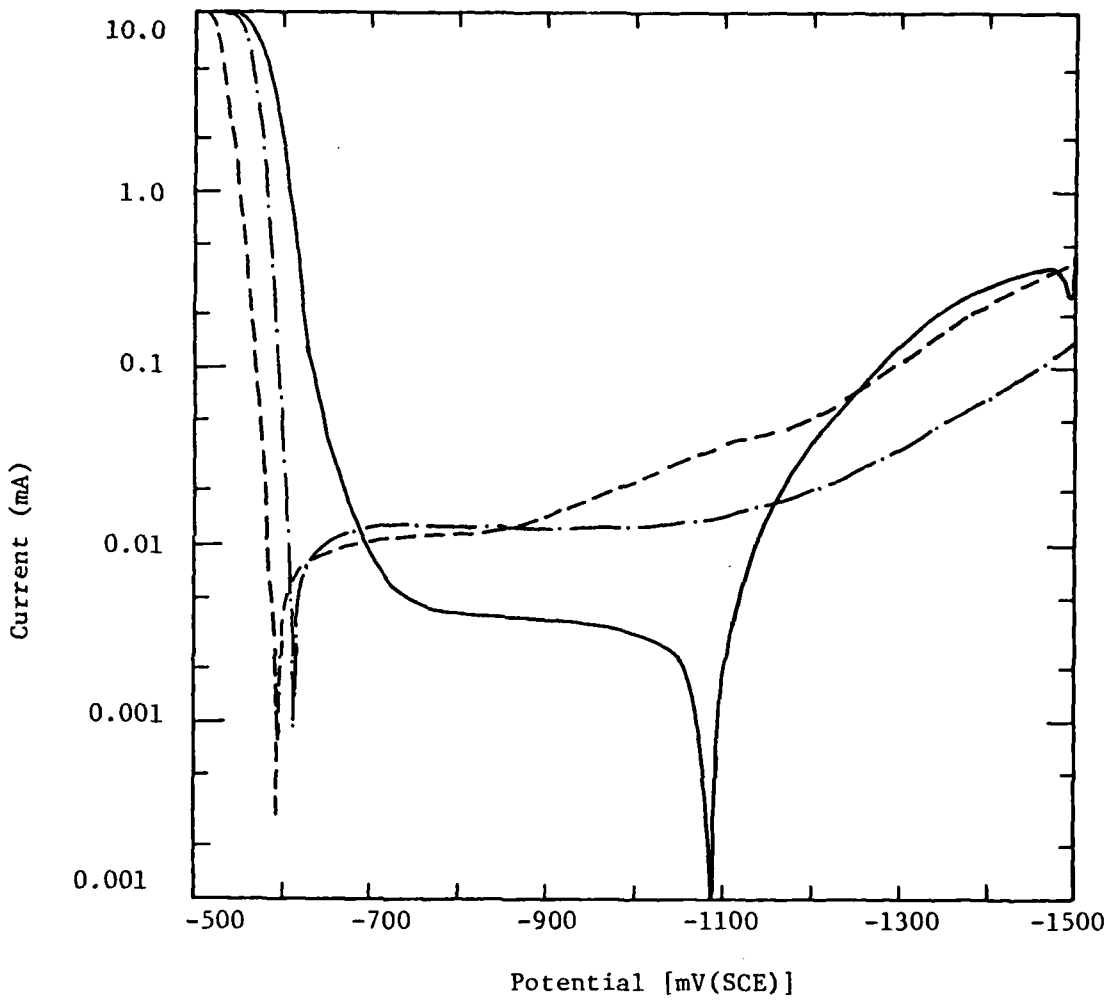

Figure 127. Current vs. potential for potentiodynamic polarization experiment with alloy 2024 of 1.267 cm^2 surface area in 5% NaCl electrolyte solution: ____ control; - - - with 10% hydrolyzed PPOP; ___ · ___ with hydrolyzed PPOP.

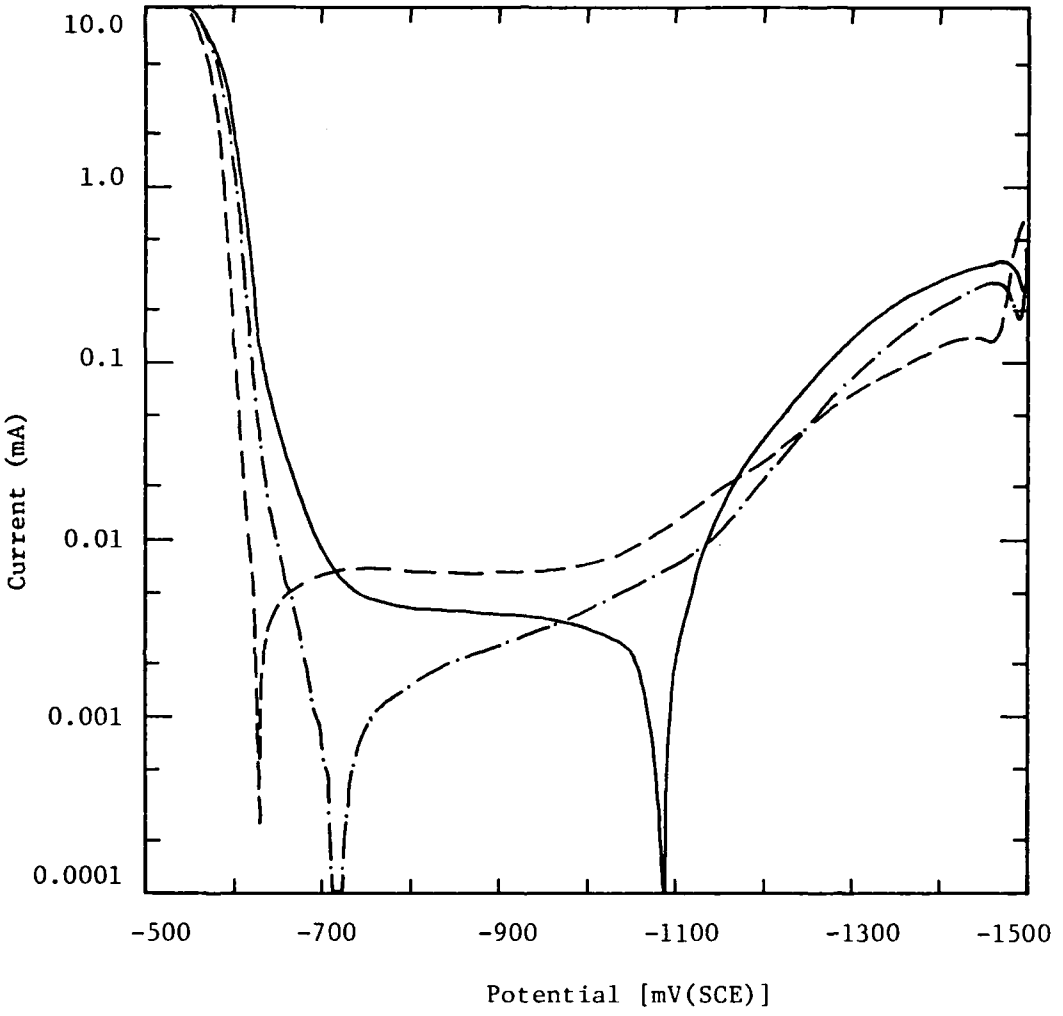

Figure 128. Current vs. potential for potentiodynamic polarization experiments with alloy 2024 of 1.267 cm^2 surface area in 5% NaCl electrolyte solution: ——— control; - - - with 1% hydrolyzed PPOP; ——— · ——— with 0.1% hydrolyzed PPOP.

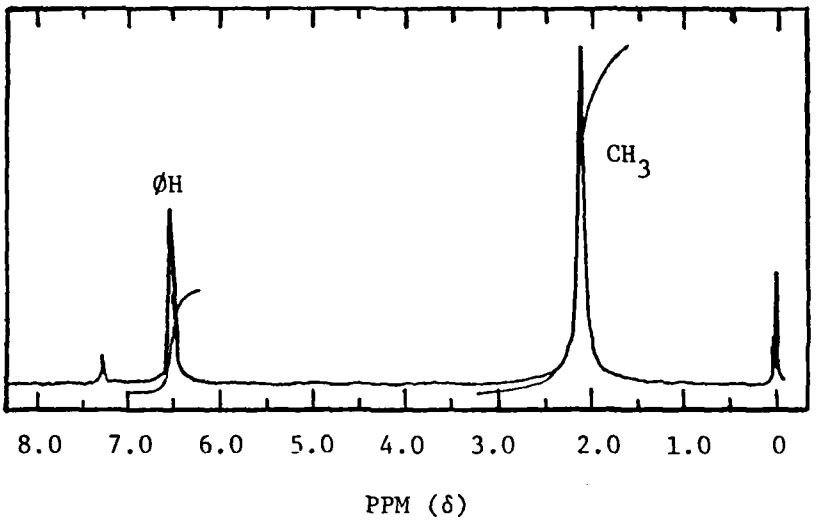

Figure 129. NMR spectrum of PPO.

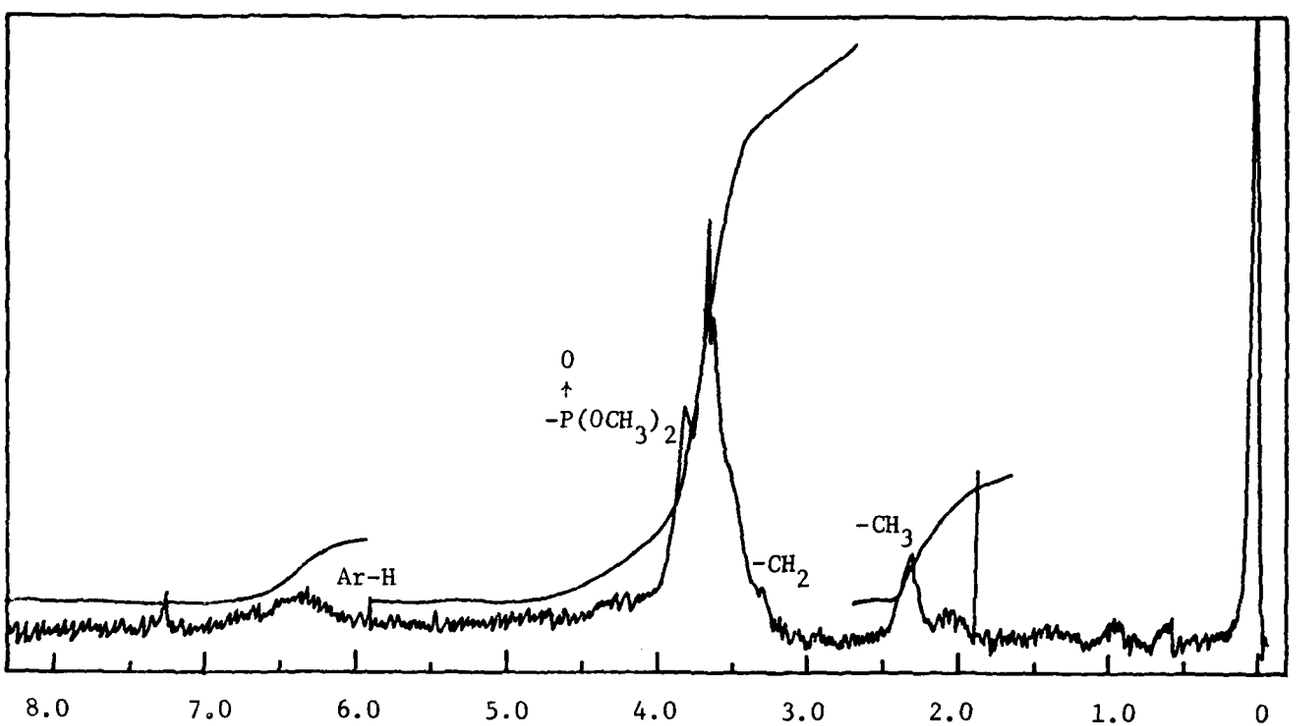

Figure 130. NMR spectrum of PPOP before hydrolysis.

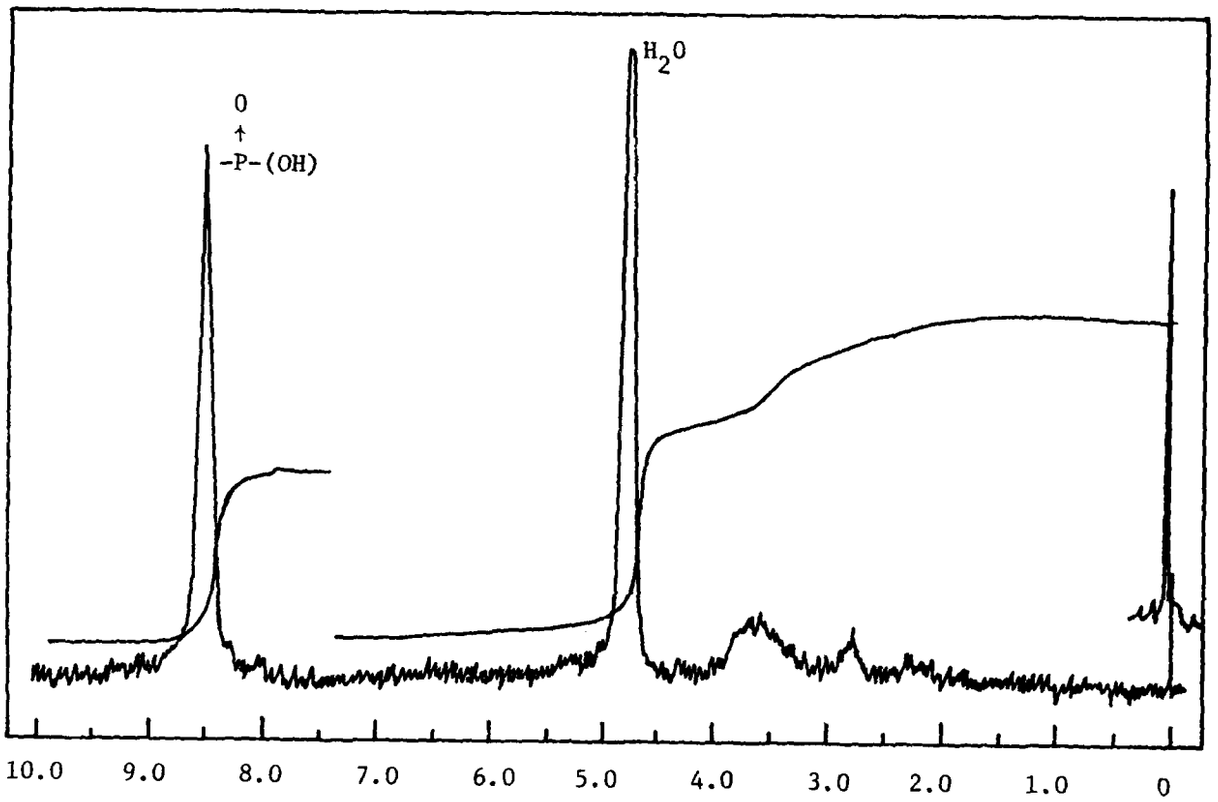

Figure 131. NMR spectrum of hydrolyzed PPOP.

characteristic peaks: δ 2.25, 2.75 [12H, p- and o- ph(CH_3)], δ 3.55, 3.70 [30H, p- and o- $(OCH_3)_2PO$], δ 6.5 [7H, phH), δ 8.50 (10H, P(O)OH]. The peak area ratio of the methoxy protons to the methyl proton changed from an original ratio of 5:1 to 2.5:1 in the hydrolyzed polymer, indicating that one-half of the methoxy groups had been removed. Thus, the probable structure of the hydrolyzed polymer becomes:

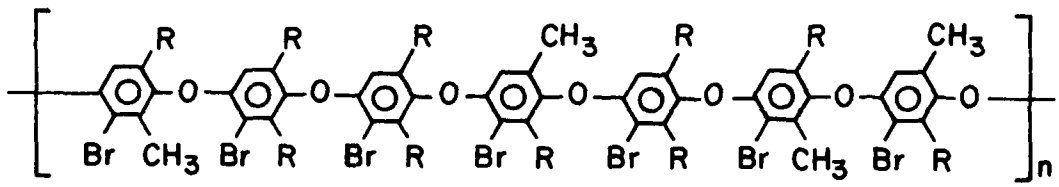

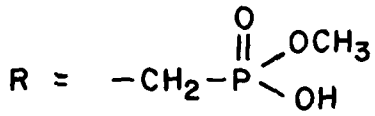

VI. PHYSICAL ENTRAPMENT OF THE AIR FORCE INHIBITOR FORMULATION (AFIF)

A. Background

Historically, the coatings industry has avoided the use of corrosion inhibiting pigments which possess water solubilities greater than 2.0 g/liter (5), since the resulting coatings usually display such property disadvantages as higher leaching rates, blistering, or loss of adhesion. Additionally, considerable research time and effort are required to develop the technology needed to produce a product which would be suitable under varied environmental conditions. However, if a viable system is to be developed using the AFIF mixture, an in-depth investigation is required to isolate the controlling parameters and optimize the system for the maximum performance characteristics. The principal variables investigated in a suitably designed study are described in the following sections.

1. Surface Treatment

The anchor pattern and metal surface treatment greatly affect the adhesive strength of primer coatings. For example, an Epon 828/methylenedianiline primer coating gave bond shear strengths of > 9000 psi when the aluminum substrate was chromate treated, but displayed adhesive failure on untreated aluminum (50). While surface treatment in accord with MIL-A-03625 is an established practice, newer approaches have evolved which may provide improved corrosion resistance and adhesion with the AFIF primer formulation (51).

Studies related to conversion coating science are quite complex, involving the quantitative elucidation of such parameters as the mechanism of formation and barrier properties of the passivating layer, the repassivation ability of the AFIF mixture in cases of barrier violation, nature and strength of interaction between the primer vehicle and barrier coat, and ability of the conversion coating to disperse osmotic forces. Obviously, an in-depth study of conversion coatings is beyond the scope of this program, yet an evaluation of the performance properties of several prime candidates may provide encouraging results.

2. Particle Size

One of the goals of the program was to develop a coatings system which would provide up to 5 years of corrosion protection. Conceivably, to achieve this degree of longevity, a combined approach of inhibitor entrapment and encapsulation may be required to obtain an optimum leaching rate. From the data presented in Figure 132, it is apparent that leaching rate is a function of pigment particle size. Thus, empirical work was required to provide insight into the following parameters and properties.

a) Property
   i. leaching rate
   ii. corrosion resistance
   iii. wet and dry adhesion
   iv. blister resistance

b) Parameters
   i. method of particle size reduction (high speed dispersion, ball mill, etc.)
   ii. milling composition (nature of vehicle, i.e. polyamide versus epoxy resin; solvent environment, i.e. effects of dielectric constant, hydrogen bonding, acid-base interaction, etc.; shearing rheology, such as Daniel flow point versus empirical methods; grinding aids such as urea resins; and presence of water in solvents and absorption from air.)
   iii. sensitivity to flocculation of AFIF (storage stability, pigment shock resistance when combined with extender pigments, epoxy resin, spray retarders, etc.)

The methodology used to achieve the correct particle size has a profound effect on the interaction between the pigment surface and the continuous phase. For example, under the mechanical stress resulting from milling, adsorption isotherms of epoxy resin on sodium chloride particles indicate the formation of a monolayer containing packed, unfolded epoxy molecules and a second, 2-fold larger monolayer. At higher shear rates the thickness of the adsorbed layers increased 3-4 fold, caused by the deposition of molecular aggregates (52).

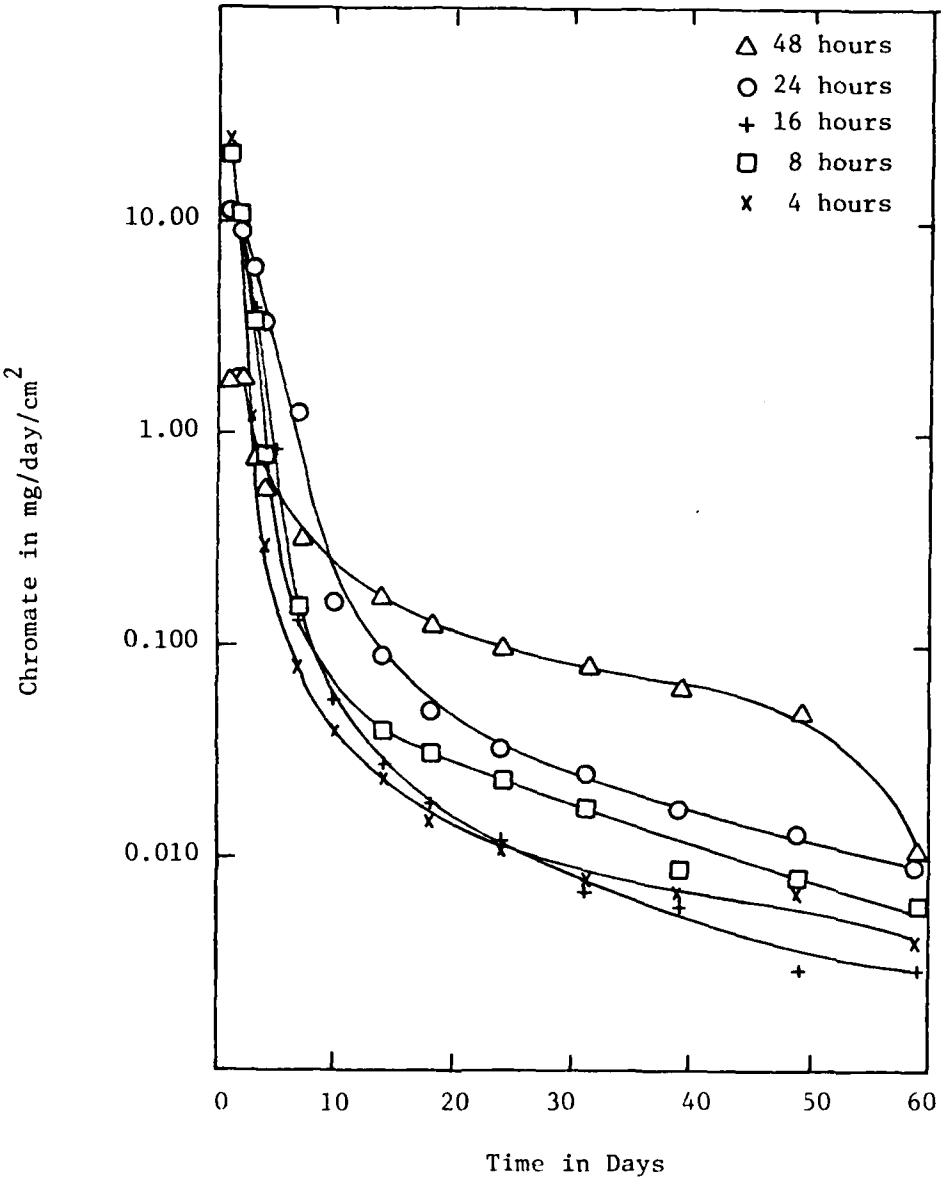

Figure 132. Milling times directly correlate with particle size. The longer the milling time, the finer the particle size.

Thus, since an in situ adsorption encapsulation process occurs during milling, optimization of the controlling parameters can greatly contribute to improvements in leaching rate, water adsorption, and blister resistance.

3. Modified Inhibitor Formulations

While field and laboratory testing have demonstrated that the AFIF mixture provides a satisfactory level of corrosion protection for aluminum and steel alloys, some results indicate that other combinations of inhibitors may provide superior protection. In fact, certain combinations may be more effective in reducing stress corrosion due to the action of nascent hydrogen. Possible candidates would include the following:

a) substituting piperizine for borax in the AFIF mix.
b) formulation 471-8 consisting of 0.5% potassium cinnamate, 0.1% $NaNO_2$, 0.02% $(NaPO_3)_6$.
c) formulation 471-9, consisting of 0.5% potassium cinnamate, 0.15% $NaNO_2$, 0.05% $Na_2MoO_4 \cdot 2H_2O$, 0.1% 3,5-dimethyl-1-hexynol, 0.02% $(NaPO_3)_6$.
d) other chelating agents such as gallic acid or protocatechuic acid, which provide improved salt spray and water resistance in water-based epoxy/polyamide coatings (53).
e) other nonchromate-containing inhibitors (discussed under extender pigments).

Higher loadings of the inhibitor pigmentation can be achieved by incorporating candidates which possess lower water solubilities. Since a wide range of inhibiting mixtures is available, selections can be made from candidates which offer the greatest possibility of success.

4. Concentration of Inhibitors

The osmotic pressure at the metal surface-primer interface is directly dependent upon the concentration of water-soluble salt present in the polymer matrix. As the concentration of inhibitor increases, a point is reached where the osmotic pressure exceeds the forces of adhesion, and delamination of the coating occurs. The limiting concentration of inhibitor

which provides the best balance among such properties as corrosion resistance, adhesion and blister resistance must be established empirically. This level will serve as a control for optimization studies designed to achieve adequate adhesion and blister resistance at higher loadings of inhibitor.

5. Pigment Volume Concentration (PVC)

The critical pigment volume concentration (CPVC) represents that state in which the minimum amount of binder is present to provide an adsorbed layer on the pigment particles and still fill the interstices between the wetted particles. As shown in Figure 133, blister resistance and corrosion resistance vary oppositely with respect to PVC. Thus, coatings formulated below the CPVC possess relatively closed structures with low permeability and corrosion tendencies, but also tend to blister.

At PVC levels above the CPVC, the structure is open and osmotic forces are dispersed. Open structures are usually preferred for corrosion resistance since mobility of the inhibitor increases (54). However, as illustrated in Figure 134, the leaching rate of the inhibitor is directly related to the PVC level. An optimum value for the PVC must be established to obtain the balance required between adhesion and corrosion resistance.

6. Nature of the Extender Pigments

a) Extender Pigment Type. The type of extender pigment used in the primer formulation has been found to greatly affect such properties as adhesion and water absorption (55). For example, several studies have shown that amorphous silica improves cathodic disbonding resistance (56) and adhesion (57). Silica has a low oil absorption (15-25 g oil/100 g pigment) and allows a greater interaction between the resin and substrate. Silica also contributes to the water resistance of the coating (58).

b) Pigment Surface Treatment. Amorphous silica can be surface-treated with silane coupling agents that chemically interact with the epoxy resin. Two commercially-available amorphous silicas possess surfaces treated with gamma-aminopropyltriethoxysilane and gamma-glycidoxypropyltrimethoxysilane. These treatments provide a modulus continuum at the polymer-pigment interface. The property improvements obtained by using surface-treated silica can be seen in Table 32.

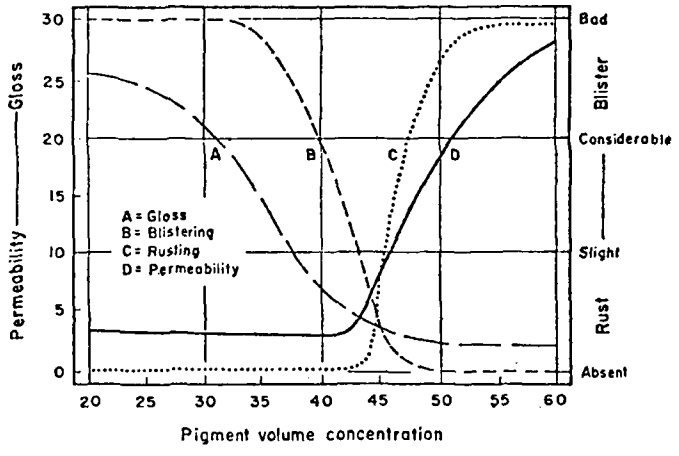

Figure 133. Effect of the critical pigment volume concentration on paint properties.

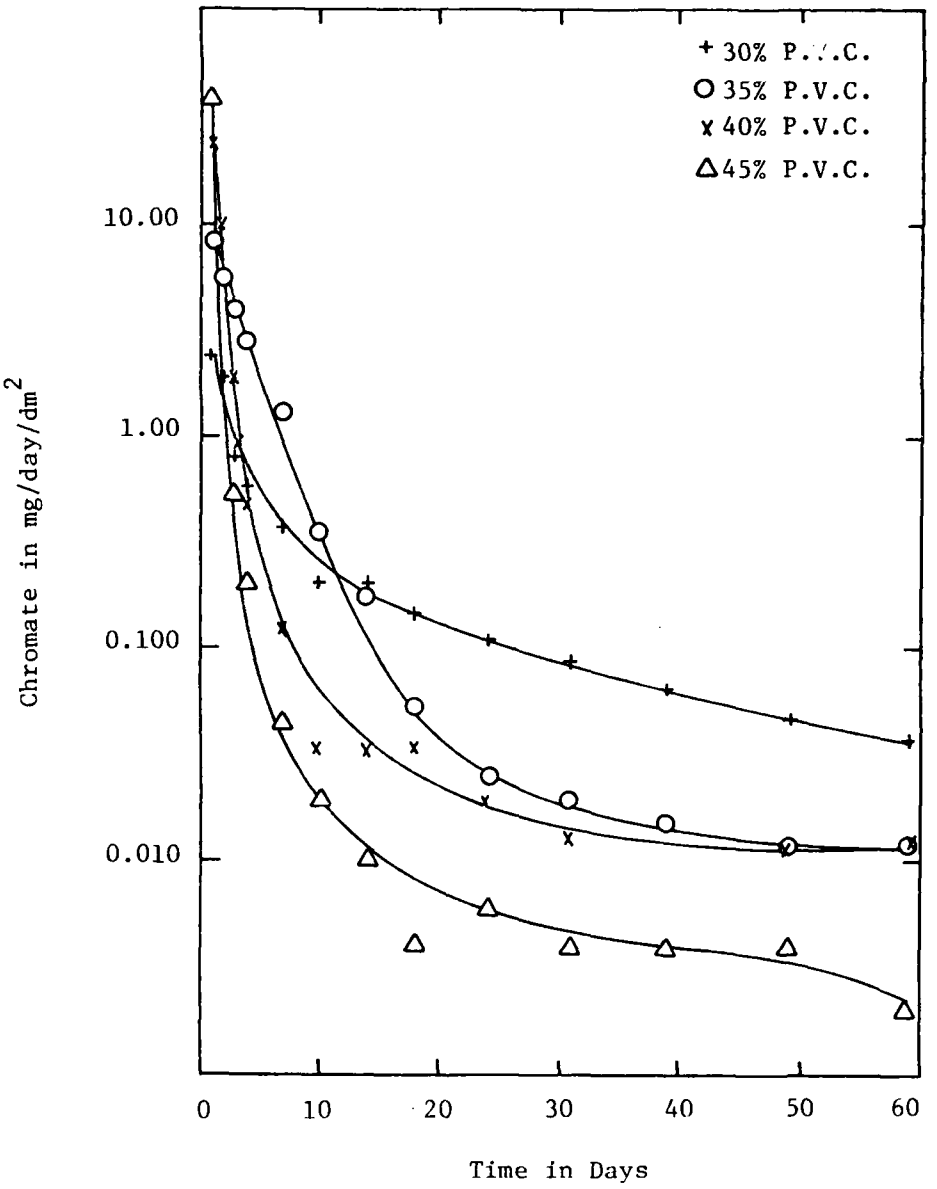

Figure 134. Leach rates of primers having varying pigment volume concentrations.

TABLE 32. PHYSICAL PROPERTIES OF A SILICA-FILLED NYLON

Filler	Unnotched (ft-lb/ inch)	Notched (ft-lb/ inch)	Reverse (ft-lb/ inch)	Flexural Strength Initial (psi)	Flexural Strength Boiled* (psi)
untreated silica	4.27	.31	2.27	10,300	8,600
treated	11.62	.71	7.78	17,700	14,600

*immersion in boiling water for 8 hours.

Other performance improvements which result from the use of surface-treated silica include weatherability, chemical resistance, salt spray and corrosion resistance, and reduced wicking from vapor transmission.

For pigmented systems in which there is a strong interaction between the pigment surface and binder, the permeability coefficient decreases linearly with an increase in the pigment volume fraction. However, when the pigment particles are incompletely wetted by the binder, pigment aggregates including air are formed in the film and, as a consequence, permeability to water increases (59).

c) Pigment Shape. In addition to the type of pigment and surface treatment, pigment shape markedly affects corrosion resistance, adhesion, and water permeability. For example, leafing aluminum and mica, which are commonly used in primer formulations containing fibrous Zn powder (length 20-100 μm, diameter 2-3 μm), provided superior impact and salt spray resistance compared to an identical formulation containing nodular Zn pigment with a diameter of 5 μm (60).

d) Other "Extender" Pigments. To obtain greater synergism between the AFIF mixture and the extender pigments, a portion of the extender pigment combination may be substituted with calcium borosilicates or calcium barium phosphosilicate. The salt fog corrosion resistance data for calcium borosilicate as a function of PVC are presented in Table 33. Other possible candidates include Busan 11-M1 (61), zinc phosphate, and zinc phospho-oxide complexes. Through such combinations, it may be possible to achieve significantly greater corrosion resistance while avoiding the problems arising at higher loadings of AFIF.

TABLE 33. PERFORMANCE OF CALCIUM BOROSILICATE IN SALT FOG RESISTANCE

PVC	General Panel* Corrosion (hrs)				Corrosion at* Scribe (hrs)				Blistering (hrs)		
	262	526	886	886†	262	526	886	886†	262	526	886
47.30	10	9	8	8-9	10	10	9	10	10/10	10/10	9/7
43.91	9	0	9	9	10	10	9	10	10/10	10/10	10/10
40.67	9	8	8	8	10	10	9	10	10/10	10/10	10/10
37.35	9	8	8	7	10	10	9	9	10/10	10/10	9/7
23.65	7	6	7 3/16	6-7	10	9	8	9	10/10	10/10	10/10
18.67	7	6	6 3/8	5	10	10	8	7	10/10	10/10	4/8

*Panels are rated 0 to 10. 10 is the highest rating, 0 indicates failures (stripped panels).
†Panels were stripped and evaluated for corrosion.

7. Effect of Solvents

The degree of interaction achieved between a coating and a metal substrate is greatly dependent upon the rheological and wetting properties and the thermodynamic state of the polymer/solvent/pigment system. The condition for wetting to occur is given by

$$\gamma_{LV} - (\gamma_{SV}^{D} \gamma_{LV}^{D})^{\frac{1}{2}} - (\gamma_{SV}^{P} \gamma_{LV}^{P})^{\frac{1}{2}} = 0$$

where D and P indicate dispersion and polar components, respectively.

The thermodynamic work of adhesion, W_A, may be related to the surface free energies by the Dupre equation, which may be modified to the following form:

$$W_A = 2(\gamma_a^{D} \gamma_b^{D})^{\frac{1}{2}} + 2(\gamma_a^{P} \gamma_b^{P})^{\frac{1}{2}}$$

where γ represents the surface free energy in terms of dispersion and polar components.

Obviously, to achieve the requisite polymer-substrate interactions requires deposition of the macromolecule in such a manner that the secondary

forces are maximized. The mole fraction of effective contact sites will depend upon the nature of the deposited coil, which can also be related to Flory's expansion factor, α. The expansion factor is a thermodynamic property which is calculated from the ratio of the root-mean-square end-to-end distance of a molecule in a good solvent to the corresponding distance in a θ solvent. The thermodynamic "goodness" of a solvent is dependent upon the interaction parameter, χ, which is related to the solubility parameter δ:

$$\chi = V_1/RT\ (\delta_1 - \delta_2)^2$$

Figure 135 illustrates the effect of varying the solubility parameter and fractional polarity (measure of the relative contribution of the polar forces involved) on the solubility of epoxy resins. The phase boundary lines represent those conditions where χ is greater than 0.5 and precipitation occurs. Note that isopropyl alcohol, acetone, and MIBK are poor solvents for the given system.

In multicomponent solvent systems the evaporation rate is a complex phenomenon (Figure 136), and in improperly designed systems, a very poor solvent could be the last component to evaporate. Figure 137 shows the development of internal stress in epoxy films as a function of time. The lower internal stress displayed by the thicker film results from the presence of contained solvents and their effectiveness in providing chain mobility. Obviously, the thermodynamic nature of the solvent and its evaporation rate markedly influence the degree of internal stress exhibited by a given formulation.

Solvent combinations which provide low degrees of internal stress and greater adhesive strength can be designed using computer programs containing solubility parameter and evaporation rate data. One recommended solvent combination for Epon 1001 may be found in Table 34.

8. Type of Curing Agent

Epoxy resins cured with polyamide amines are noted for developing excellent adhesion to poorly prepared, even moist, surfaces in addition to providing good corrosion resistance (when prepared from dimeric linoleic acid and ethylenediamine) (62). In applications requiring maximum resistance to solvents, acids, and other corrosive chemicals, amine adducts are preferred to polyamide amine curing agents. Table 35 indicates the batch

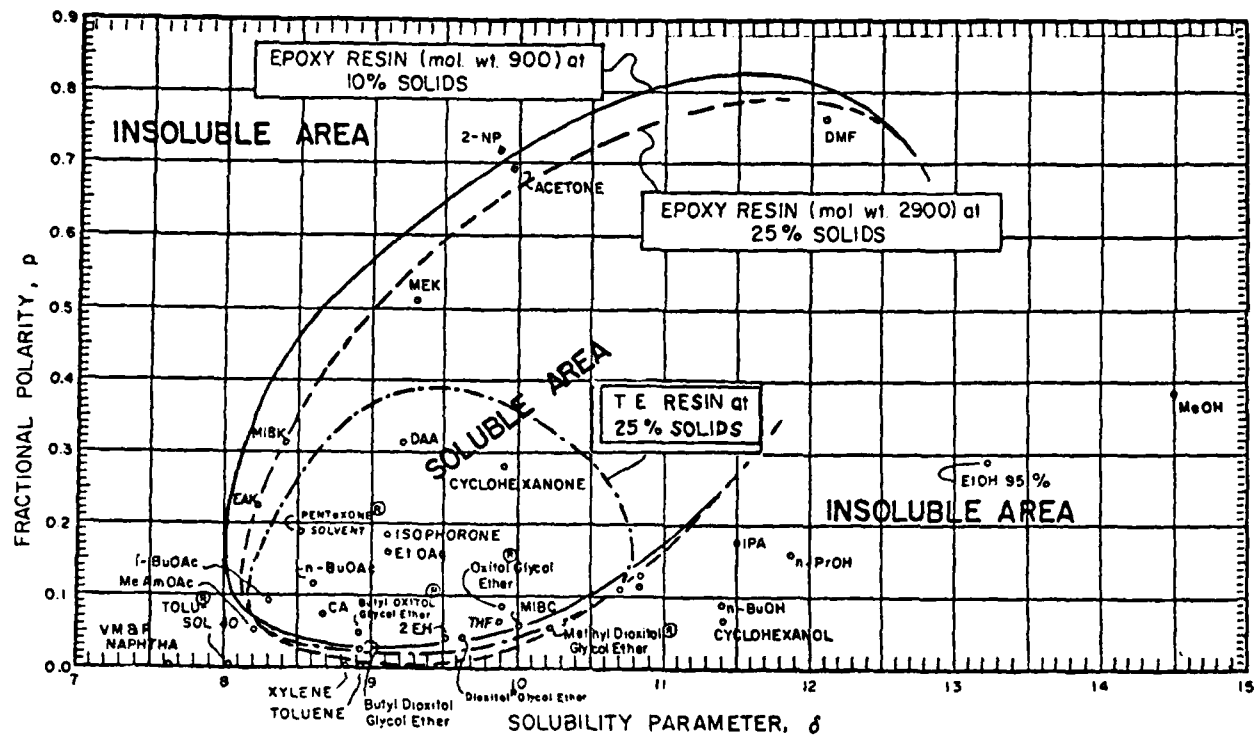

Figure 135. Solubility map for Epon resins at 25°C.

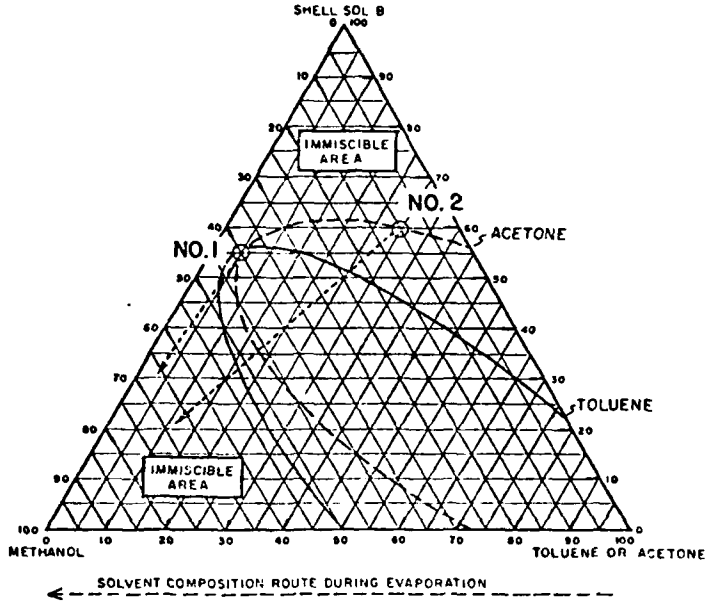

Figure 136. Epoxy resin solubility map. 40 vol% solids; acetone or toluene with Shell Sol B and methanol.

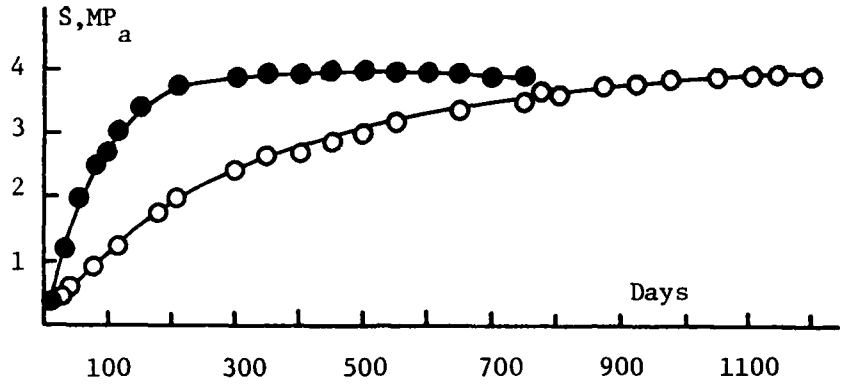

Method for Measuring Internal Stress

Figure 137. Epoxy resin. Development of internal stress, S(MPa) for two thicknesses of coating (●, c = 66 μm; ○, c = 110 μm) as a function of time (days) at T(°C) = 21 ± 0.8 and RH(%) = 52 ± 1; t (substrate thickness) = 0.209 mm; H (substrate width) = 12.7 mm.

TABLE 34. SOLVENT SYSTEM FOR SPRAY APPLICATION

Component	Weight Percent
Diacetone alcohol	10.0
Methyl isobutyl carbinol	12.5
Isopropyl alcohol	12.5
Methyl ethyl ketone	5.0
Xylene	60.0

TABLE 35. AMINE ADDUCT FORMULATION BASED ON EPON 1001

Material	Batch Change (% w)
Diethylenetriamine	12.6
Epon 1001-K-75	46.7
Toluene	10.7
n-Butyl alcohol	27.4
Oxitol glycol ether	2.6

charge used for the preparation of a typical amine adduct curing agent. Approximately 50-55 parts by weight of the above adduct are required to react completely with 100 parts by weight of Epon 1001.

Various classes of epoxy curing agents have been developed in recent years which offer distinct advantages over the polyamide amines. The importance in selecting the proper curing agent to obtain maximum adhesion can be seen in the following: Epoxy coatings cured with 1,3-bis-(carboxyethyl) isocyanurate and 1,3,5-tris-(carboxyethyl)isocyanurate displayed initial adhesive strengths of 94.5 and 291.5 kg/cm^2, respectively. Upon exposure to an aggressive medium for 21 weeks, the adhesive strength decreased to 30-60 kg/cm^2 for the former and 56-122 kg/cm^2 for the latter (63). Thus, even after 21 weeks exposure, the trifunctional curing agent at times provided greater adhesion than the initial values for the difunctional curing agent. Other possible candidates and their property advantages are listed in Table 36.

TABLE 36. ALTERNATE CURING AGENTS FOR THE POLYAMIDE AMINE

Compound	Property Advantage	Reference
m-Phenylenediamine	low internal stress, high adhesion to metals	64
Azelaic dihydrazide	no adhesive loss after 1 yr in boiling water; cathodic detachment 14 mm	65
Aromatic amine (Epicure 8494, 849)	superior corrosion resistance	66
Polyethyleneamine adduct	6 yrs exposure to salt water line exposure	67
1/1/-Triethylenetetramine/Epirez 5012/ Epirez 5011 adduct	underwater surface curing agent	68

Conductance studies in NaCl solutions indicate that the nature of the polymer structure governs the permeation ability of chloride ions through the matrix (69). Thus, certain curing agents may provide advantages in adhesion and corrosion resistance.

9. Other Epoxy Resins

In addition to the bisphenol A-based epoxy resin, other room-temperature curable epoxy systems are available which offer specific advantages in adhesion and corrosion resistance. After 1000 hours of salt spray, Shell's new generation epoxy resin Eponex resin/acrylic curing agent demonstrated superior resistance properties as compared to conventional systems (Figure 138). An adhesion-promoting composition consisting of a diglycidyl isocyanurate/hexamethylenetetramine formulation demonstrated excellent adhesion to steel, giving peel strengths of 6.6 to 8.8 lb/linear inch (70). A variety of alternatives to bisphenol-A epoxy resins can be investigated as a means of achieving property improvements.

10. Use of Additives

Additives represent perhaps the largest and most diversified class of materials which are used to alter specific properties of coatings. The ability of a given additive to impart a specific property change can be seen in the following example. 2-Mercaptobenzothiazole derivatives have been found to improve the adhesive strength of epoxy coatings to metals. A bisphenol-A epoxy resin cured with 24 phr 2-mercaptobenzothiazole zinc salt displayed adhesive strengths of >1000 (mold steel), 817 (stainless steel), 690 (brass), and 552 kg/cm^2 (copper) compared with 605, 595, 478, and 218 kg/cm^2, respectively, for the same resin cured with 20 phr m-phenylenediamine (71).

While several classes of compounds have demonstrated varying abilities to improve the adhesive strength of epoxy coatings, perhaps the most widely accepted and investigated compounds for promoting adhesion are the organo silanes. Table 37 illustrates the benefits gained when organosilanes are used in an epoxy paint formulation. As an extension of this study, X-ray photoelectron spectroscopy (XPS) was used to determine the nature of the adhesive site failure. Both the metal surface after fracture and the underside of the film removed during the adhesion test were examined. These data are presented in Table 38.

These data indicate that the paint film failed cohesively (aluminum was not detected within the first 20-50 Å of the surface) and that failure occurred within an unpigmented boundary layer at the paint/metal interface (no titanium was detected at the surface of film underside). The presence

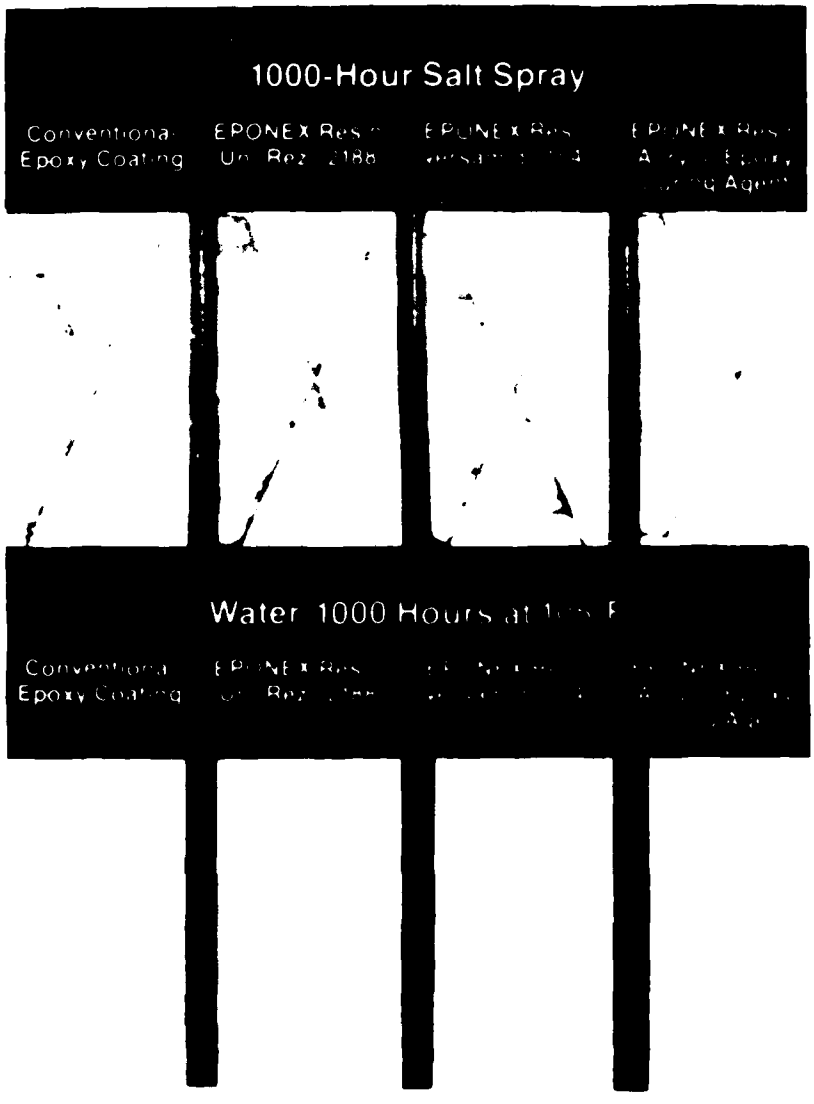

Figure 138. Photograph of test panels of the entire family of ambient cure formulations show EPONEX Resins' performance.

TABLE 37. WET AND RECOVERED ADHESION VALUES - DIRECT PULL-OFF ON ALUMINUM

Silane*/treatment	Control (psi/area of detachment)	Wet Adhesion (psi/area of detachment)	Recovered Adhesion (psi/area of detachment)
Degreased only	2050/100	320/100	1880/180
0.2% A-189/degreased	4000/0	3820/0	3960/20
0.2% A-1120/degreased	4590/0	3680/0	3910/0
sandblasted only	3050/10	1070/100	3230/20
0.2% A-189/sandblasted	4530/0	3640/0	3870/5
0.4% A-1120/sandblasted	4090/0	4090/0	4160/0

*A-189 = α-mercaptopropyltrimethoxysilane
A-1120 = n-beta aminoethylaminopropyltrimethoxysilane

TABLE 38. XPS DATA ON FRACTURE SURFACES OF EPOXIDE PAINT

System	Storage Condition	Metal Surface							Paint Surface						
		C^1	C^2	N	O^1	O^2	Si	Al	C^1	C^2	N	O^1	O^2	Si	Al
Epoxide paint (nonfracture surface)	In air								0.68	--	0.11	0.16	--	0.03	--
A1120 Empirical formula		0.57	--	0.14	0.21	--	0.071								
Al/Epoxide	In air	0.50	0.15	0.10	0.06	0.18	--	--	0.50	0.19	0.10	0.17	--	0.010	--
Al/Epoxide	In water	0.50	0.19	0.13	0.16	--	0.008		0.51	0.17	0.12	0.17	--	0.016	--
Al/A1120/Epoxide	In air	0.51	0.19	0.11	0.17	--	0.002	--	0.51	0.18	0.11	0.18	--	0.003	--
Al/A1120/Epoxide	In water	0.50	0.20	0.12	0.18	--	0.005	--	0.52	0.17	0.12	0.18	--	0.016	--

of silicone was established at the surface of each fracture site (72). Besides serving as an adhesion promoter, the silane coupling agents may be used to surface treat the AFIF salts as another means of generating microencapsulated, controlled-release behavior.

Other types of additives which have provided an increase in adhesion when formulated with epoxy resin are listed in Table 39.

TABLE 39. ADHESION PROMOTERS FOR EPOXY RESIN COATINGS

Compound	Property Imparted	Reference
Furfuryl acetone polymer	3 years immersion in salt water	73,74
Aromatic compound containing OH, amino and imino groups	anticorrosive coating with good water resistance	75
Dimethyl terephthalate by-products, coke distillate	high adhesive strength in corrosive media residues	76
Cresol novolak resin	highly resistant to water, NH_3, acetic acid, H_2SO_4 and HCl	77
Styrene-maleic anhydride copolymer	adhesion remained at 8 MPa for 150 days immersion	78
Urea sulfonate	salt water immersion protection	79

11. Overview

Besides providing an introduction and rationale for the empirical work, the previous discussion also illustrates the numerous parameters which may affect the performance of a primer system. While a systematic optimization of each parameter could undoubtedly enhance the chances of developing a viable system, such an undertaking was beyond the scope of the project. Consequently, the empirical work which follows functions: a) to illustrate the advantages and limitations associated with AFIF-containing primers, and b) to identify the parameters which control the performance characteristics of the system.

B. The Preliminary Empirical Study

Prior to evaluating those formulation parameters needed to maximize the performance characteristics of films containing physically entrapped AFIF, a study was conducted to a) optimize the method of particle size reduction, b) characterize possible reaction inhibition due to interaction with AFIF, c) establish the CPVC of the base formulation, and d) optimize the method of application in order to eliminate complications arising from variations in these fundamental parameters.

1. Method of Particle Size Reduction

To achieve a mill-paste mixture which would allow for controlled particle size reduction, a study was conducted to evaluate suitable grinding solvent/resin combinations. While certain polar solvents normally yield good milling results, the combinations listed in Table 40 were found to be inadequate for achieving the desired degree of fineness.

TABLE 40. INITIAL ATTEMPTS TO DETERMINE A SUITABLE MILL PASTE COMBINATION FOR THE AFIF INHIBITOR MIXTURE

138 g AFIF + 425 g of the following solvent mix: 9.9% xylene, 39.7% toluene, 25.3% IPA, and 25.3% butanol (MIL-P-23377D solvent combination)
138 g AFIF + 425 g isopropyl alcohol
138 g AFIF + 425 g n-butanol
138 g AFIF + 425 g cyclohexane
138 g AFIF + 425 g toluene
138 g AFIF + 6.27 g polyamide (enough to form a monolayer around the AFIF pigment) + 276 g hexane to cyclohexane
138 g AFIF + 138 g polyamide resin + 276 g of the above MIL-P-23377D solvent combination

Additionally, the milling formulation outlined in MIL-P-23377D in which the milling vehicle is the epoxy resin was found to be unsuitable for obtaining fine particle size pastes. In commercially-available two-component

epoxy paints, the usual procedure is to grind the pigments in the polyamide resin phase, since interaction occurs between the pigment agglomerates and the polar amine groups.

The effectiveness of using the polyamide resin as a grinding medium was investigated using the following mill charge (which is a modification of MIL-P-23377D). In a Norton size 0 jar mill the following ingredients were charged: 69.01 g AFIF, 99.44 g polyamide, 42.62 g xylene, 171.25 g toluene, 108.85 g isopropanol, and 108.85 g n-butanol. The milling medium consisted of 34 burundum balls, and the fineness of grind was measured as a function of time. The data presented in Table 41 indicate that the above polyamide/solvent combination provided the proper wetting and shear characteristics to obtain an acceptable fineness of grind after 24 hours of milling.

TABLE 41. EFFECTIVENESS OF A POLYAMIDE/SOLVENT COMBINATION TO FINELY GRIND THE AFIF MIXTURE

Time	Hegman Value
10 min	3.5
4 hours	5.0
8 hours	6.0
12 hours	6.5
16 hours	7.0
20 hours	7.2
24 hours	7.3

A Daniel "flow point" determination was conducted to establish a near-optimum mill paste composition. The solvent combination used for this procedure consisted of 9.53% xylene, 38.48% toluene, 25.77% isopropanol, and 26.21% n-butanol (from MIL-P-23377D). The results from the determination indicated that a mill paste consisting of 50/50 polyamide/solvent provided the best rheological properties for generating high shear values (Figure 139).

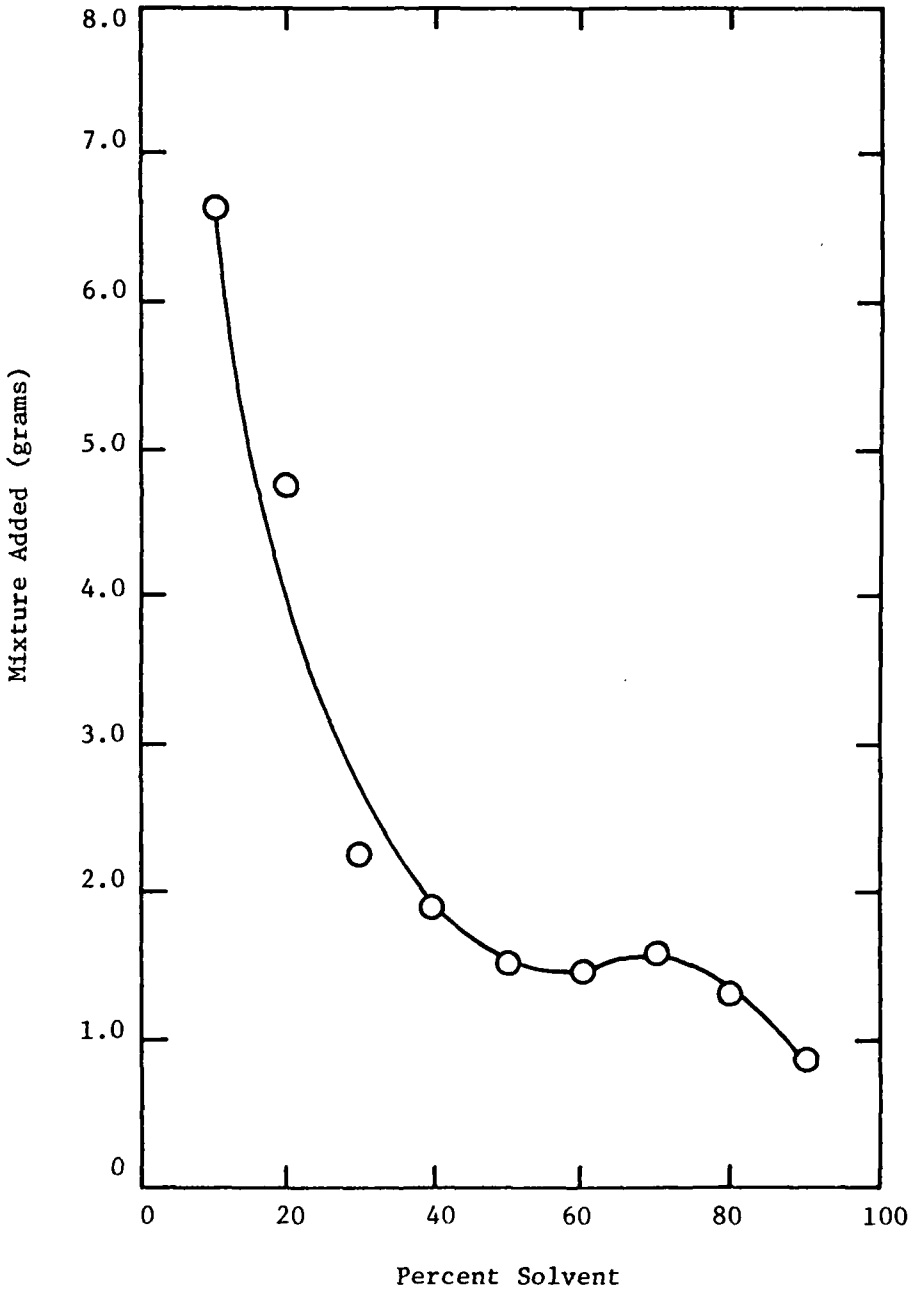

Figure 139. "Flow point" method of Daniel.

The effectiveness of using the Daniel "flow point" composition to achieve fine particle size grinds was examined by comparing its grinding efficiency against that obtained with the above MIL-P-23377D modification. The Daniel composition and MIL-P-23377D modification mill pastes were jar milled for 32 hr, and the particle sizes of the resulting mill pastes were characterized by means of Coulter counter (Figures 140 and 141). While the Daniel method did provide some advantage over the arbitrary MIL-P-23377D modification (3.43 μ versus 4.33 μ, respectively) in achieving fineness of grind, the similarity of the results attests to the overwhelming effectiveness of the polyamide resin to disperse the AFIF mixture.

2. Crosslinking Inhibition Due to the AFIF Mixture

Incorporation of the AFIF mixture (11% by weight of the nonvolatile components) into a commercial two-component epoxy/polyamide paint (Sherwin William's Tile Clad) resulted in markedly increasing (doubling) the gel time (Table 42). As a result, an in-depth study ensued in which the rate of crosslinking was monitored for films of Epon 1001/Ancamide 220 (MIL-P-23377D formulation void of pigmentation) which contained 1, 3, 7, and 11 percent by weight of AFIF. The degree of crosslinking was followed through infrared analysis (unsuccessfully), Brookfield viscosity, swelling ratio, and percent MEK insolubles. All measurements indicated that the AFIF mixture did not inhibit crosslinking and that films of very high crosslink density developed after 24 hrs of reaction, irrespective of the level of AFIF. The results are presented in Tables 43, 44, 45.

3. Determining the Critical Pigment Volume Concentration

Coatings properties such as inhibitor mobility and leaching rate, moisture permeability, blister resistance, and adhesion are greatly dependent upon the accessible free volume of the polymer matrix. Thus, prior to investigating such parameters as the level of inhibitor, nature of the formulation, type of curing agent, etc., a study was conducted to determine the critical pigment volume concentration (CPVC) of a formulation which would serve as a "base" control for subsequent studies. The formulation was a modification of that specified in MIL-P-23377D. The modification involved substituting strontium chromate and diatomaceous silica with an equal volume of amorphous silica (Imsil A-10 with a fineness of grind of 7 on the Hegman

CE #4322 Date: 12-8-81
Organization: Gulf South Research Institute
Sample: Inorganic Salts, Polyamide Ground in Ball Jar Mill
Electrolyte: 7% LiCl/ 1:5 Acetone:IPA
Dispersant: 30 secs. of ultrasonics
Equipment: TAII.....#2
Operator: Glen Fun
Apertures: 70 microns

Vol.%

SIZE	CUM	DIF
1.	100.	6.6
1.26	93.4	8.6
1.59	84.8	10.5
2.	74.3	10.3
2.52	64.	10.6
3.17	53.4	12.2
4.	41.2	11.9
5.04	29.4	10.3
6.35	19.1	7.6
8.	11.5	5.3
10.08	6.1	3.3
12.7	2.9	1.
16.	1.9	.7
20.16	1.2	1.2
25.4	0.	0.
32	0.	0.

Vol.Geo Mean 3.43 Standard Dev. 1.99

Median 3.39 Mode 3.86

Figure 140. Particle size distribution of the AFIF mixture ground according to the Daniel flow point method.

CE #4301 Date: 12-8-81
Organization: Gulf South Research Inst.
Sample: Polyamide Resin
Electrolyte: 7% LiCl/1:5 Acetone:IPA
Dispersant: 30 secs of ultrasonics
Equipment: TA II.....#2
Operator: Glen Fun
Apertures: 70 microns

Vol.%

SIZE	CUM	DIF
1.	100.	2.5
1.26	97.5	4.4
1.59	93.	6.2
2.	86.9	7.9
2.52	78.9	10.3
3.17	68.6	13.9
4.	54.7	14.3
5.04	40.4	11.9
6.35	28.5	9.4
8.	19.1	8.5
10.08	10.6	6.1
12.7	4.5	3.5
16.	1.	.8
20.16	.2	.2
25.4	0.	0.
32.	0.	0.

Vol.Geo Mean 4.33 Standard Dev. 1.9

Median 4.32 Mode 4.13

Figure 141. Particle size distribution of the AFIF mixture ground using a modification of MIL-P-23377D mill paste.

TABLE 42. EFFECT OF ADDING AFIF MIXTURE TO EPOXY/POLYAMIDE PAINT

Viscosity (cps)	Time (hrs)								
	1	4	6	8	10	22	27	35	48
with AFIF	80	80	100	156	297	632	1000	1030	gelled
without AFIF	140	120	120	243	290	7680	gelled		

TABLE 43. VISCOSITY AS A FUNCTION OF TIME FOR A CURING PRIMER

Time (hours)	AFIF Milled in Polyamide					Milled in Epoxy
	11% AFIF	7% AFIF	3% AFIF	1% AFIF	0% AFIF	11%
0.5	80	52	56	64	50	28
17.0	400	142	278	440	116	108
18.0	1230	145	440	540	120	108
19.0	2160	152	580	640	132	112
20.0	3920	180	760	890	136	112
21.0	24000	216	800	1140	140	116
22.0	48000	248	900	49500	152	126
23.0	solidified	300	980	∞ (100000)	170	136
24.0		300	1030	∞ (1200000)	196	14
27.0		3200	29600	solidified	240	220
28.0		∞ (6080000)	solidified		260	240
29.0		solidified			264	250
30.0					solidified	solidified

TABLE 44. SWELLING RATIO DATA AFTER CURING FOR 24 HOURS

AFIF Level	Dry Film Weight (mg)	Swollen Weight† (mg)	Z^*	$P_p{}^*$	$P_s{}^*$	$Q_m{}^*$
11% milled in polyamide	1.908	2.054	1.08	1.1	0.80	1.11
7% milled in polyamide	1.991	2.085	1.05	1.1	0.80	1.07
3% milled in polyamide	1.929	2.067	1.07	1.1	0.80	1.10
1% milled in polyamide	1.953	1.994	1.02	1.1	0.80	1.03
0% + polyamide	1.942	2.048	1.05	1.1	0.80	1.08
11% milled in epoxy	1.981	2.123	1.07	1.1	0.80	1.10

† after 24 hours in MEK

* $Z = \left(\frac{\text{swollen weight}}{\text{dry weight}} \right)$

P_p = polymer density (d/ml)

P_s = solvent density (g/ml)

Q_m = swelling ratio = $1 + (Z - 1) \left(\frac{P_p}{P_s} \right)$

TABLE 45. PERCENT INSOLUBLES AFTER CURING FOR 12 HOURS

AFIF Level	Sample Weight Before Extraction (mg)	Sample Weight After Extraction (mg)	Insolubles* (%)
11% milled in polyamide	2.3868	1.3529	56.68
7% milled in polyamide	2.0537	1.2955	63.08
3% milled in polyamide	1.3352	0.7668	57.43
1% milled in polyamide	2.6506	1.4733	55.58
0% in polyamide	0.9305	0.5393	57.96
11% milled in epoxy	1.4709	0.9126	62.05

* $\%\ \text{Insolubles} = \frac{(\text{sample weight after extraction}) \times 100}{(\text{sample weight before extraction})}$

TABLE 46. BASE FORMULATION FOR USE WITH THE AFIF MIXTURE

MIL-P-23377D (approximate)			Base Formulation		
	lbs	gal		lbs	gal
Mill Paste					
$SrCrO_4$	110.18	3.39	Imsil A-10	105.49	4.78
TiO_2	21.12	0.62	TiO_2	21.12	0.62
Talc	5050	2.12	Talc	50.50	2.12
Diatomaceous Silica	26.63	1.39	--	--	--
Polyamide	68.78	8.49	Polyamide	68.78	8.49
Xylene	29.48	4.08	Xylene	24.48	4.08
Toluene	118.45	16.36	Toluene	118.45	16.36
Isopropanol	75.29	11.15	Isopropanol	75.29	11.67
Butanol	75.29	11.15	Butanol	75.29	11.15
	575.72	59.27		544.40	59.27
"B" Component					
Epoxy Resin	125.34	12.66	Epoxy Resin	125.34	12.66
Toluene	101.45	14.01	Toluene	101.45	14.01
MIBK	115.69	17.32	MIBK	115.69	17.32
	342.48	43.99		342.48	43.99

PVC = 26.23

Amine/epoxy ratio = 0.549

gauge). Table 46 presents the ingredients used in the "base" formulation. The pigment volume concentration of the epoxy/polyamide coatings can be conveniently varied by adjusting the amount of amorphous silica used in the formulation.

The CPVC for the formulation was determined by monitoring the tensile strength of cured films as a function of PVC [the method of Becker and Howell; Official Digest, 28 (1956), 775]. The formulation for the mill pastes used in the determination are given in Table 47. Each formulation contained an arbitrary level of AFIF mix (5%, based on nonvolatile content, for the 35 PVC formulation only), and test samples were applied by means of conventional and airless spray. The results of the study are presented in Figure 142.

These data indicate that a marked disparity exists in the tensile response of films applied through the two methods. Presumably, this difference arises from variations in void space resulting from air entrapment and rheological changes. Coatings prepared by means of conventional spray apparatus (Binks #18 siphon gun) displayed the classical behavior (CPVC at 40 PVC) while those prepared by means of the airless spray yielded atypical results.

4. Determining the Optimum Application Method

Since the extent of void space can markedly affect the results of subsequent studies, the film properties and close packed nature of coatings applied through the two methods were investigated further. To ensure more rapid release of entrapped air, and increased flow and annealment of the drying film, the solvent mixture used in the epoxy component and as a spray retarder for the formulation was modified. Thus, a 61.9% Epon 1000 epoxy solution was prepared as a "B" component using the following mixture of solvents: 10% MIBK, 12.5% IPA, 12.5% methyl isobutyl carbinol, 15% diacetone alcohol, and 50% xylene. The epoxy resin solution (24.4 g) was blended with 75.6 g of a polyamide mill paste (35 PVC "base" formulation) to produce a composite mixture with a viscosity of 360 cps. The above spray retarder (4 g) was added to the paint to achieve spray viscosity (110 cps at ~40% solids). The mixture was applied by means of conventional and airless spray and hand casting to release paper at 2 mils dry film thickness and onto brushed 1010 steel panels at 2 mils dry film thickness. The extent of void content was monitored through the following tests:

TABLE 47. MILL PASTE FORMULATIONS USED IN ESTABLISHING THE CPVC FOR THE "BASE" FORMULATION

Pigment Volume Concentration	35	40	42.5	45	50
Mill Paste Ingredients*					
Imsil A-10	172.36	232.17	265.88	303.01	387.76
AFIF	18.64	18.64	18.64	18.64	18.64
TiO_2	21.12	21.12	21.12	21.12	21.12
Talc	50.50	50.50	50.50	50.50	50.50
Polyamide	68.78	68.78	68.78	68.78	68.78
Xylene	29.48	29.48	29.48	29.48	29.48
Toluene	118.45	118.45	118.45	118.45	118.45
Isopropanol	75.29	75.29	75.29	75.29	75.29
Butanol	75.29	75.29	75.29	75.29	75.29

*Each mill paste was let down with the ingredients specified in Table 34.

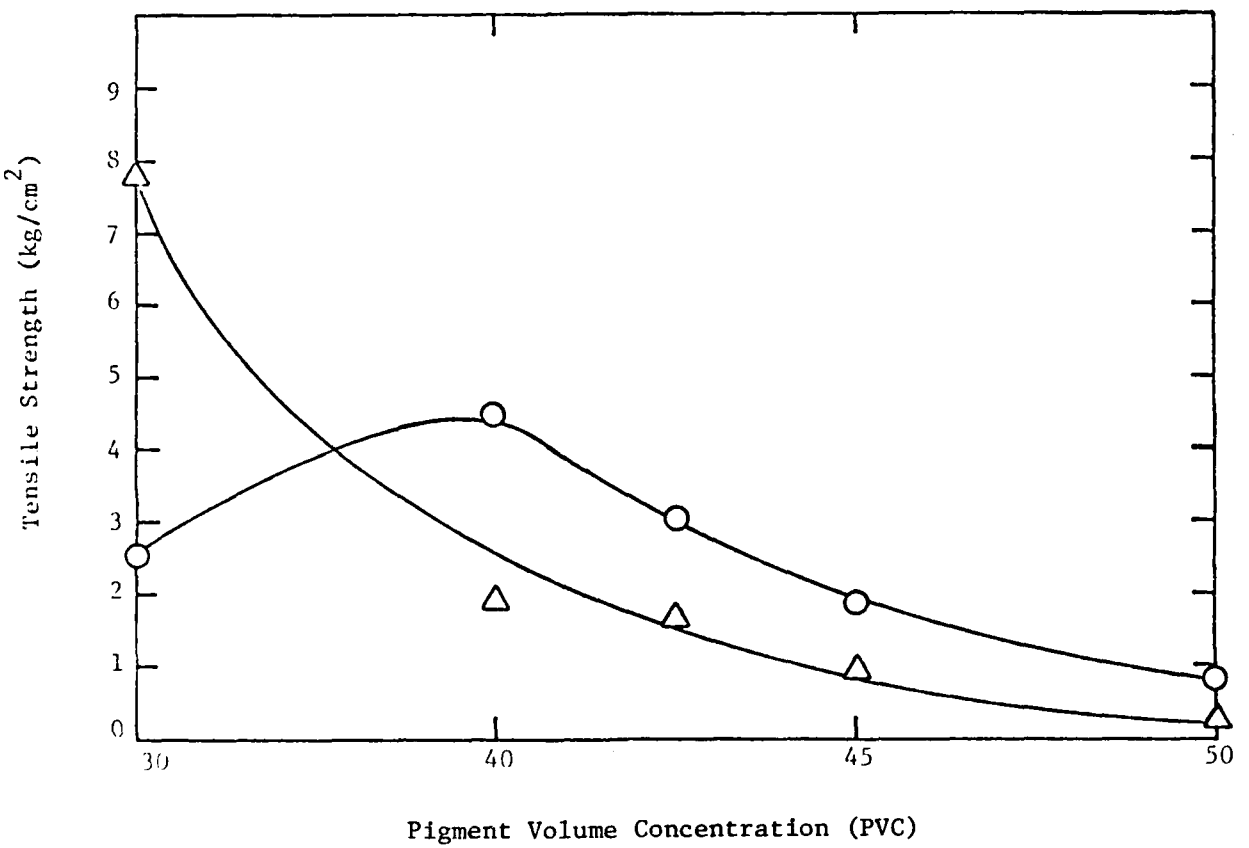

Figure 142. Determination of the CPVC.

AD-A144 311 ENCAPSULATED MULTIFUNCTION CORROSION INHIBITIVE PRIMER 4/4
(U) GULF SOUTH RESEARCH INST NEW ORLEANS LA
D V GUPTA ET AL. NOV 83 AFWAL-TR-83-4123
UNCLASSIFIED F33615-79-C-5061 F/G 11/3 NL

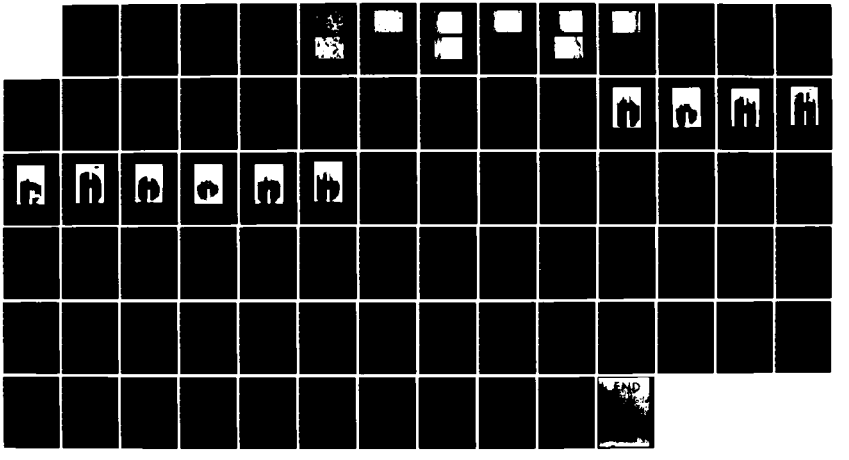

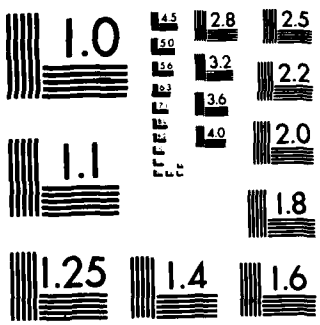

a. Tensile Strength. Film continuity and internal cohesive energy as measured by tensile strength data (6.74 kg/cm^2 for films applied by airless spray versus 2.48 kg/cm^2 for conventionally applied films) indicate some advantage for films generated through airless spray application.

b. Surface Corrosion Breakthrough. The extent of film porosity may be monitored directly from the extent of surface corrosion breakthrough on samples subjected to salt fog exposure. After 400 hours of exposure (Figure 143), little differentiation could be made among the corrosion resistance of films applied by the three methods. However, those samples applied by means of airless spray seem to exhibit slightly superior properties.

c. Water Vapor Transmission Rate. The water vapor transmission rate data for the three methods of application indicate that the film porosity decreases according to the following order (Figure 144):

Airless spray $\cong$ hand cast > conventional spray.

d. SEM Surface Analysis. The degree of surface discontinuity and porosity as evaluated from SEM surface analysis was found to increase according to the following order (Figure 145):

Airless spray < hand cast < conventional spray.

e. SEM Cross-sectional Analysis. The degree of internal coarseness and void content as evaluated from SEM cross-sectional analysis was estimated to increase according to the following order (Figure 146):

Airless spray < conventional < hand cast.

In addition, films applied by means of airless spray or hand casting appeared to be more continuous with the substrate than films applied by means of conventional spray (Figure 147). While no overt differences exist among these collective data, coatings applied by means of airless spray application may provide a slight property advantage over those applied by means of conventional spray.

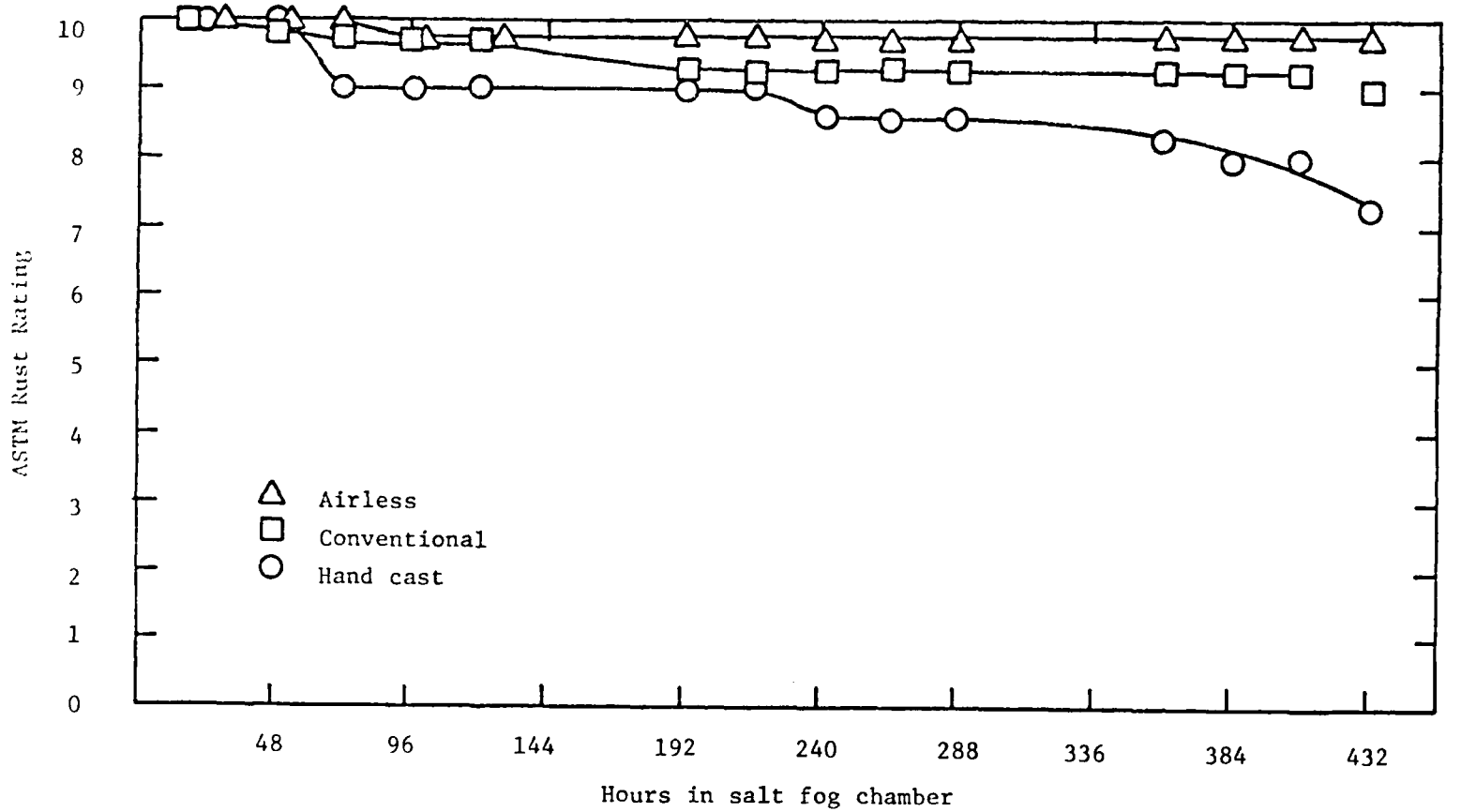

Figure 143. Surface corrosion breakthrough results for films applied via conventional and airless spray and hand casting.

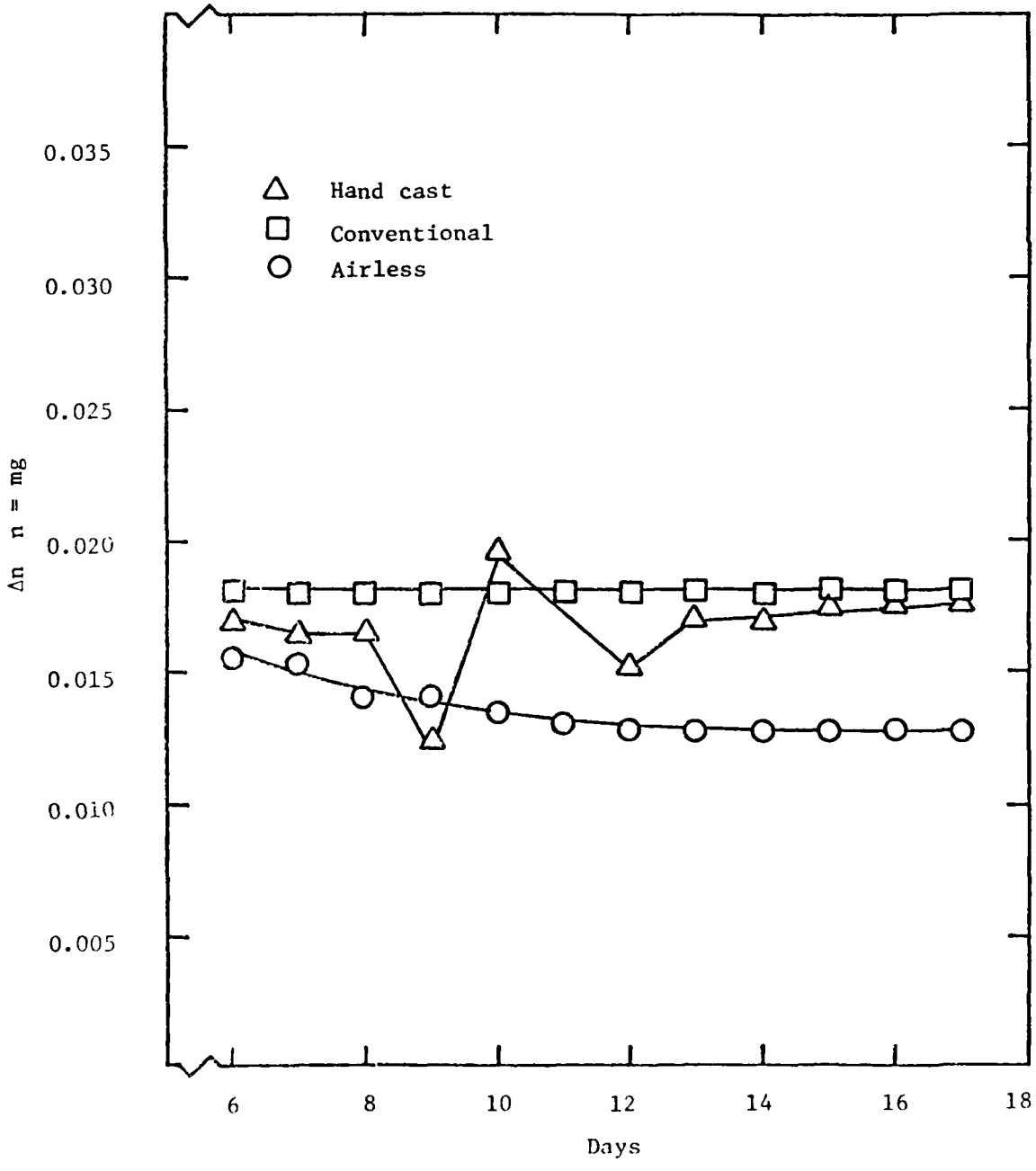

Figure 144. Water vapor permeability for films applied through conventional and airless spray and hand casting.

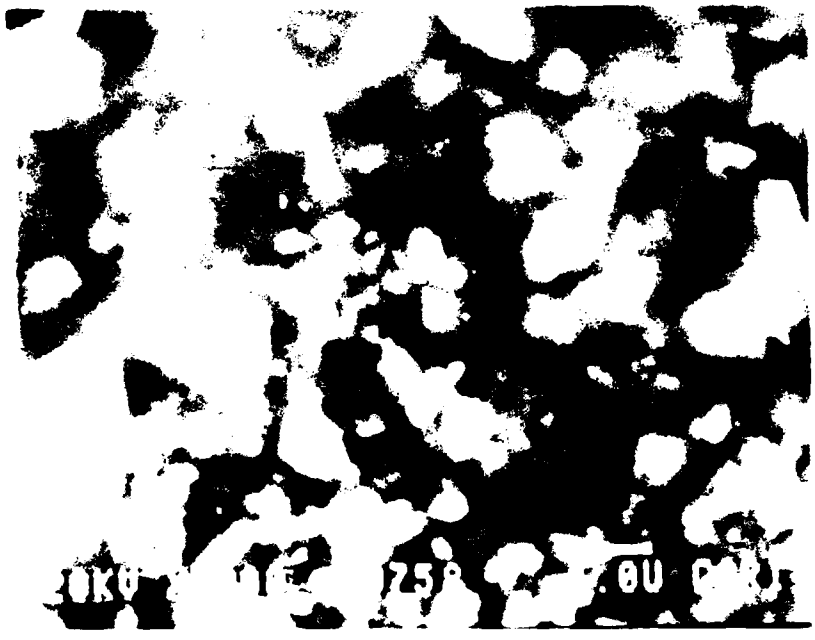

(A)

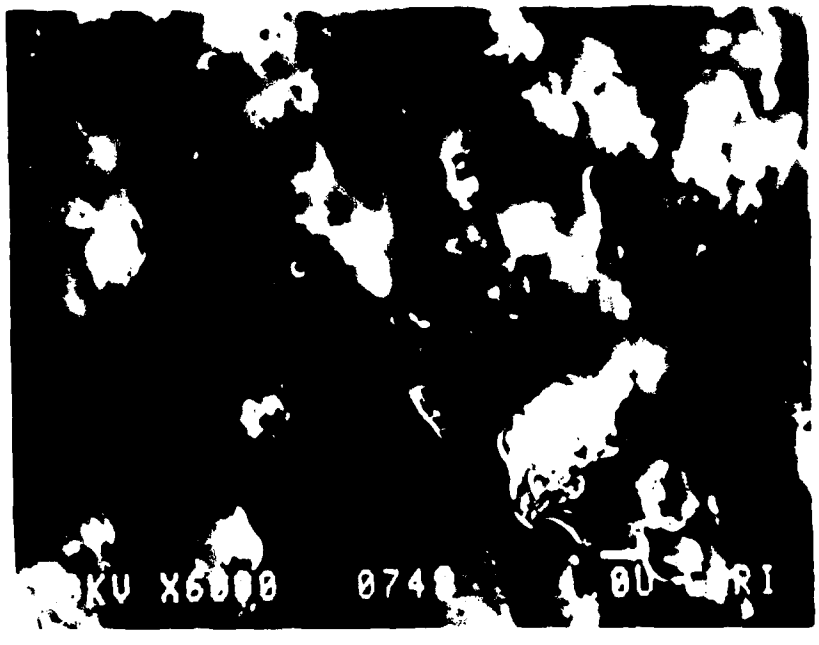

(B)

Figure 145. SEM surface analysis of coating deposited by airless spray (A), hand cast coating (B), conventional spray (C). (Figure continued on the following page).

(C)

Figure 145. (Figure continued from the previous page).

(A)

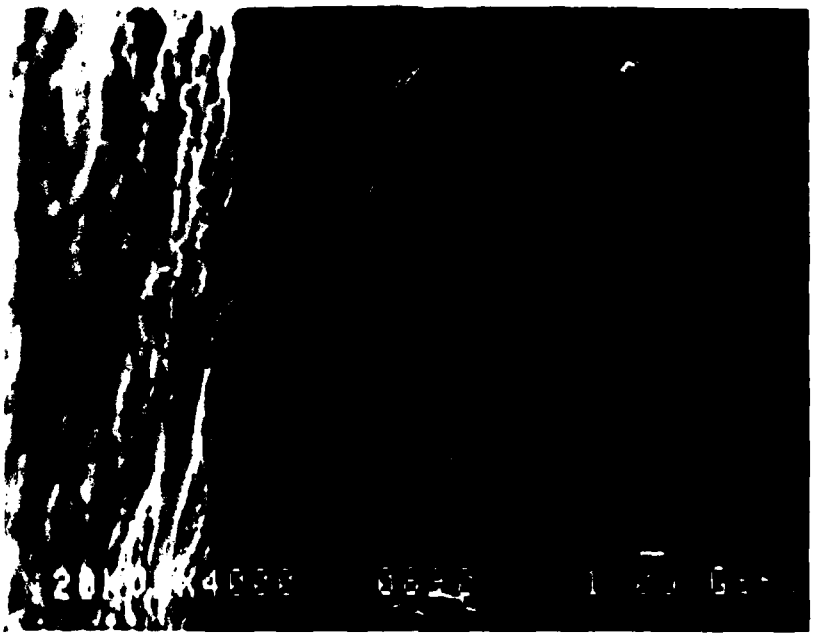

(B)

Figure 146. Cross-sectional structures of films obtained through airless spray (A), conventional (B), and hand cast methods (C). (Figure continued on the following page).

(C)

Figure 146. (Continued from previous page).

(A)

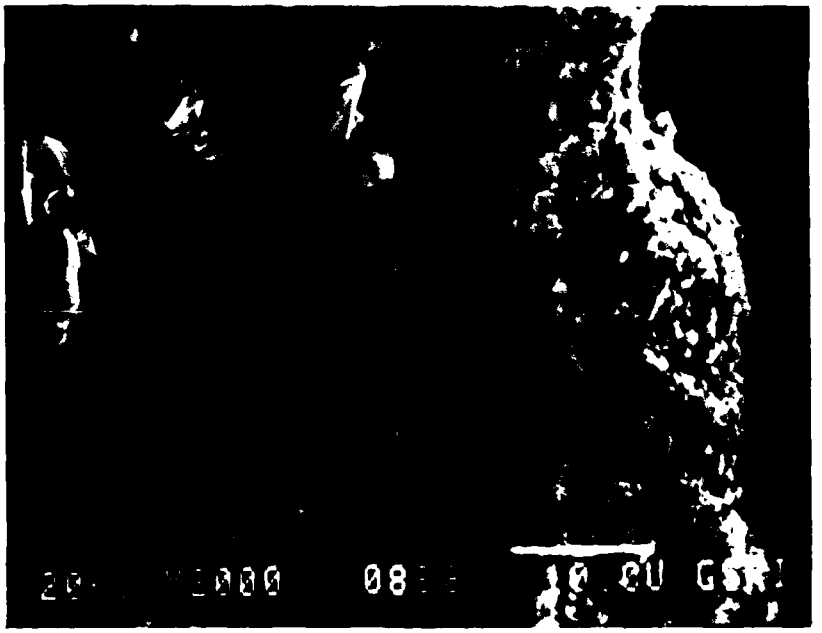

(B)

Figure 147. Interfacial structure of films obtained through airless spray (A), hand cast methods (B), and conventional spray (C). (Figure continued on the following page).

(C)

Figure 147. (Figure continued from previous page).

5. Release Studies Using Films Containing Microcapsules

An approach for obtaining semi-applied release data involved using films containing dispersed microcapsules. This approach would eliminate complications associated with the presence of cyclohexane, and filtration of the microcapsules from the release medium, and would improve duplication of "field performance" conditions.

Because of possible rupture of the polyurea membrane due to interaction with polar solvents (alcohols and ketones) or amine end-groups (polyamide curing agent), a 100% solids, long-oil linseed alkyd resin (Aroplaz 1271) was selected as the vehicle for the initial evaluations. In comparison with other classes of vehicles, alkyd resins provide an environment which more closely approximates that displayed by an alkane (cyclohexane), thereby minimizing the chances of polymer-membrane wall interaction and premature rupture of the capsules. Also, solvent and end-group interactions arising from the components used in the epoxy/polyamide formulation can be evaluated by singly introducing each of the polar solvents into the alkyd/microcapsule mixture and monitoring the release data from the resulting films.

To evaluate the feasibility of this approach, a study was conducted to determine the release properties of the following three systems:

1. coatings on aluminum of Aroplaz 1271 and driers;
2. coatings on aluminum of Aroplaz 1271 and driers and AFIF mixture;
3. coatings on aluminum of Aroplaz 1271 and driers and AFIF-filled microcapsules (619-45).

The formulations for each system are listed in Table 48. Release testing was accomplished by immersing known weights of each sample in 100 ml deionized water. The film weights (grams) for the various samples were: control 0.34025, milled AFIF = 0.34163, AFIF-filled microcapsules = 0.38248. The results of the release data are presented in Figure 148. The film with the physically entrapped AFIF showed a higher release rate than the film with the AFIF-containing polyurea microcapsules (619-45), over much of the time course of the release profile. Since the AFIF levels in both trials were the same, it was anticipated that the final equilibrium conductometric release values would be equivalent, and this was borne out in the experiment. There does appear to be a definite quantitative difference between

TABLE 48. AROPLAZ 1271/AFIF FORMULATIONS USED FOR RELEASE STUDIES

Control	Aroplaz 1271/AFIF Blend	Aroplaz 1271/AFIF-filled Microcapsules
Aroplaz 1271 - 400 g	Aroplaz 1271 - 192.72 g	Aroplaz 1271 - 15 g
Toluene* - 100 g	Toluene - 48.18 g	Toluene - 3.75 g
6% Cobalt naphthenate - 2.0 g	6% Cobalt naphthenate - .96 g	6% Cobalt naphthenate - 0.075 g
8% Zinc naphthenate - 5.12 g	8% Zinc naphthenate - 2.47 g	8% Zinc naphthenate - 0.192 g
4% Calcium naphthenate - 11.76 g	4% Calcium naphthenate - 5.67 g	4% Calcium naphthenate - 0.441 g
	AFIF mix** - 0.77088 g (Grind in ball mill to Hegman grind of 7+)	AFIF-filled microcapsules - **, † 19.4 g (619-45)

* Toluene was included in the formulation for viscosity reduction during milling.

** Each film contained 0.4% by weight AFIF mix.

† 1.5 g of microcapsules (approximately 4% by weight AFIF) dispersed in 17.9 g cyclohexane.

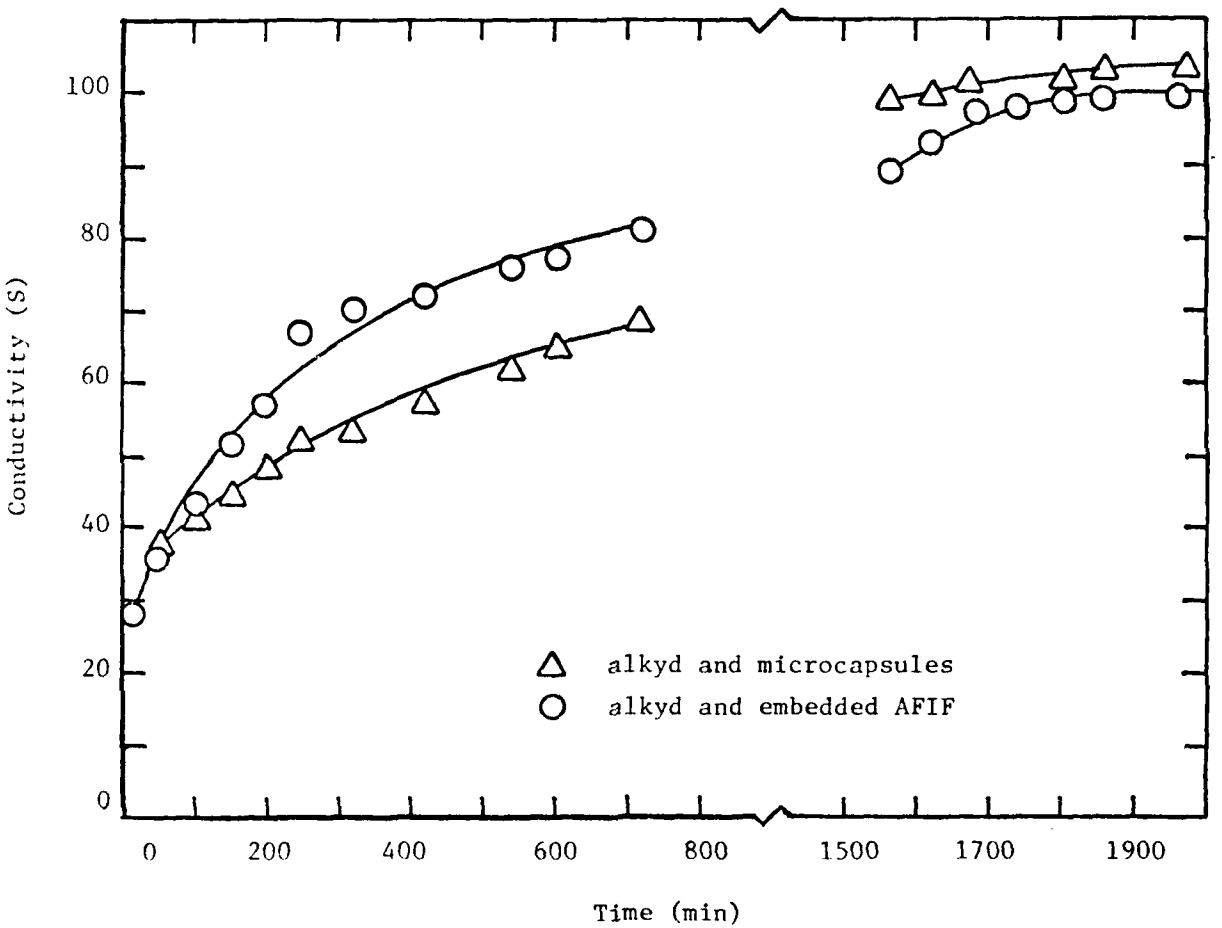

Figure 148. Time versus conductivity for alkyd and microcapsules containing AFIF, and alkyd and embedded AFIF.

the release of AFIF in the physically entrapped state as opposed to the microencapsulated state.

C. Physical Entrapment Studies of the AFIF Inhibitor in the Primer Matrix

Examination of the parameters which control the development and subsequent performance of coatings containing entrapped AFIF was important for several reasons:

1. Coatings containing entrapped AFIF would serve as a control for determining the advantages and limitations of coatings containing microencapsulated AFIF.
2. The potential for the AFIF mixture to provide corrosion resistance in films could be examined.
3. The establishment of the deficiencies which arise from premature release of the AFIF and incorporation of approaches designed to overcome the weaknesses. Coatings containing low levels of AFIF may simulate those which undergo premature release of microencapsulated AFIF.

The experimental design developed to formulate AFIF within the basic MIL-P-23377D epoxy-polyamide primer may be resolved into five coatings studies: (1) PVC and AFIF concentration determination, (2) AFIF concentration optimization, (3) corrosion protection optimization, (4) coatings optimization, and (5) comparative study: entrapped vs encapsulated AFIF.

PVC and AFIF Concentration Study - The purpose of this study was to semi-quantitatively determine the optimal PVC and AFIF concentration level for our formulation work. The PVC study was a two level design, utilizing high (50) and low (30) PVC values which bracket the CPVC value established earlier for the modified MIL-P-23377D formulation.

The AFIF concentration study was designed to screen a large range of concentration values, in order to establish the effects of varying AFIF concentration on several physical and chemical parameters. Two controls were run (0% AFIF: 0% AFIF + $SrCrO_4$) for each PVC value studied, to get an indication of the relative response between the two systems.

This preliminary formulation work also served as a variables refinement period, where our techniques of coatings formulation were tested and modified as needed. The base formulations obtained from this work were used in our next optimization studies.

AFIF Concentration Study - The purpose of this study was to further optimize the AFIF concentration level around the most acceptable value found in the previous study, and at a specified PVC. The objective was to obtain coatings containing the highest levels of AFIF which still displayed acceptable performance characteristics.

Corrosion Protection Optimization - Several nonchromate corrosion inhibitors were tested for synergistic corrosion protection when combined with AFIF in the primer matrix. The AFIF concentration and PVC values were those determined in previous studies. Thus, any weaknesses of AFIF as a corrosion inhibitor may be compensated for by the addition of another inhibitor.

Coatings Optimization - Any performance deficiencies with the AFIF-containing coatings, such as adhesion loss, blistering, application problems, etc., were addressed at this stage of the experimental design. Approaches targeted those deficiencies which arose from the presence of AFIF and its affect on system variables. With this stage completed, a model formulation was available, containing AFIF with perhaps one or more commercial corrosion inhibitors. This model served as a control for studies designed to establish the usefulness of the microencapsulated AFIF approach.

Comparative Study: Entrapped vs Encapsulated AFIF - Testing at this stage determined the feasibility and any selective advantages for corrosion control by either the entrapped or encapsulated AFIF.

1. PVC and AFIF Concentration Determination

This study represented the first stage of our investigative plan to establish the controlling parameters and their range of variability for the direct incorporation of AFIF in the modified MIL-P-23377D formulation.

The purpose of this first study was to establish the following system parameters:

1. The optimal pigment volume concentration (PVC) for our model primer formulations.
2. The approximate effective concentration range of AFIF needed in the primer.
3. A general indication of the feasibility of entrapped AFIF as an anti-corrosion agent, and for its suitability as a primer system component (e.g., whether or not it is a "good" paint material, in spite of its water solubility).

a. General Procedure. The initial study on the entrapped AFIF is outlined below.

1. Ten different primers were formulated for use in this study (Tables 49 and 50).
2. Thirty AL7075 panels were pretreated, primed, and topcoated (one half of panel) for each of the ten primer formulations, in accordance with MIL-C-83286B, MIL-P-23377D, and MIL-T-81772. The eight best panels for each formulation were chosen for testing (see 3, 4, and 5 below).
3. Three panels from each formulation were tested for salt fog spray resistance, in accordance with ANSI/ASTM B117-73 (Reapp. 1979).
4. Three panels for each formulation were tested for 100% relative humidity resistance, in accordance with ASTM D2247-68.
5. Two panels for each formulation were tested for wet adhesion, in accordance with FED. TEST METHOD STD. No. 141B, Method 6301, February 1, 1979.

In regard to the salt fog spray and 100% relative humidity tests, the test panels were evaluated formally in accordance with ASTM D 1654-79a, and results reported as specified (Figure 149).

b. Primer Formulation. The ten primer formulations used in this study fall within the general requirements of MIL-P-23377D in regard to composition. Except where specified, the AFIF was used as a replacement for the strontium chromate. Two different PVCs were used, 30 and 50. The PVC was adjusted by adding appropriate amounts of amorphous silica. Two controls were used for each PVC, one with 0% AFIF and one with $SrCrO_4$. All primers

TABLE 49. PRIMER FORMULATIONS FOR INITIAL STUDY OF ENTRAPPED AFIF

Formulation #	PVC	Milled AFIF Inhibitor (%)
1	30	0%
2	30	0%; $SrCrO_4$ at MIL-P-23377D level
3	30	1%
4	30	5%
5	30	10%
6	50	0%
7	50	0%; $SrCrO_4$ at MIL-P-23377D level
8	50	1%
9	50	5%
10	50	10%

TABLE 50. COMPOSITIONS OF AFIF-CONTAINING MILL PASTES WITH CONTROLS

Formulation Number	1		2		3		4		5	
	Control		Strontium		1% AFIF		5% AFIF		10% AFIF	
Ingredients	lb	gal	lb	gal	lb	gal	lb	gal	lb	gal
Imsil A-10	139.83	6.34	64.82	2.94	133.15	6.03	106.41	4.82	73.00	3.31
TiO_2	21.14	0.62	21.14	0.62	21.14	0.62	21.14	0.62	21.14	0.62
Talc	50.56	2.13	50.56	2.13	50.56	2.13	50.56	2.13	50.56	2.13
$SrCrO_4$			110.11	3.39						
AFIF					4.69	0.31	23.46	1.51	46.91	3.02
Polyamide	68.73	8.49	68.73	8.49	68.73	8.49	68.73	8.49	68.73	8.49
Xylene	29.63	4.10	29.63	4.10	29.63	4.10	29.63	4.10	29.63	4.10
Toluene	120.14	16.59	120.14	16.59	120.14	16.59	120.14	16.59	120.14	16.59
Isopropanol	75.04	11.46	75.04	11.46	75.04	11.46	75.04	11.46	75.04	11.46
Butanol	75.33	11.15	75.33	11.15	75.33	11.15	75.33	11.15	75.33	11.15
Diacetone Alcohol	12.58	1.62	12.58	1.62	12.58	1.62	12.58	1.62	12.58	1.62
Methyl Isobutyl Carbinol	10.48	1.57	10.48	1.57	10.48	1.57	10.48	1.57	10.48	1.57
Isopropanol	10.48	1.60	10.48	1.60	10.48	1.60	10.48	1.60	10.48	1.60
Methyl Isobutyl Ketone	8.38	1.25	8.38	1.25	8.38	1.25	8.38	1.25	8.38	1.25
Xylene	41.92	5.81	41.92	5.81	41.92	5.81	41.92	5.81	41.92	5.81
Epoxy Resin	125.76	12.71	125.76	12.71	125.76	12.71	125.76	12.71	125.76	12.71
PVC		30		30		30		30		30
Total Pigment		9.09		9.08		9.09		9.08		9.08
Total Resin		21.20		21.20		21.20		21.20		21.20
Total		30.29		30.28		30.29		30.28		30.28
Hegman Grind		8.0		7.4		7.8		7.6		7.5
Viscosity of mill paste (centipoise)		248		290		270		298		340

(continued)

TABLE 50. (continued).

Ingredients	6 Control		7 Strontium		8 1% AFIF		9 5% AFIF		10 10% AFIF	
	lb	gal	lb	gal	lb	gal	lb	gal	lb	gal
Imsil A-10	401.62	18.20	326.49	14.79	392.21	17.77	354.92	16.08	308.13	13.96
TiO_2	21.14	0.62	21.14	0.62	21.14	0.62	21.14	0.62	21.14	0.62
Talc	50.56	2.13	50.56	2.13	50.56	2.13	50.56	2.13	50.56	2.13
$SrCrO_4$			110.11	3.39						
AFIF					6.60	0.42	32.84	2.11	65.68	4.22
Polyamide	68.73	8.49	68.73	8.49	68.73	8.49	68.73	8.49	68.73	8.49
Xylene	29.63	4.10	29.63	4.10	29.63	4.10	29.63	4.10	29.63	4.10
Toluene	120.14	16.59	120.14	16.59	120.14	16.59	120.14	16.59	120.14	16.59
Isopropanol	75.04	11.46	75.04	11.46	75.04	11.46	75.04	11.46	75.04	11.46
Butanol	75.33	11.15	75.33	11.15	75.33	11.15	75.33	11.15	75.33	11.15
Diacetone Alcohol	12.58	1.62	12.58	1.62	12.58	1.62	12.58	1.62	12.58	1.62
Methyl Isobutyl Carbinol	10.48	1.57	10.48	1.57	10.48	1.57	10.48	1.57	10.48	1.57
Isopropanol	10.48	1.60	10.48	1.60	10.48	1.60	10.48	1.60	10.48	1.60
Methyl Isobutyl Ketone	8.38	1.25	8.38	1.25	8.38	1.25	8.38	1.25	8.38	1.25
Xylene	41.92	5.81	41.92	5.81	41.92	5.81	41.92	5.81	41.92	5.81
Epoxy Resin	125.76	12.71	125.76	12.71	125.76	12.71	125.76	12.71	125.76	12.71
PVC		50		50		50		50		50
Total Pigment		20.95		20.93		20.94		20.94		20.93
Total Resin		21.20		21.20		21.20		21.20		21.20
Total		42.15		42.13		42.14		42.14		42.13
Hegman Grind		8.0		7.5		7.7		7.5		7.5
Viscosity of mill paste (centipoise)		725		742		771		769		785

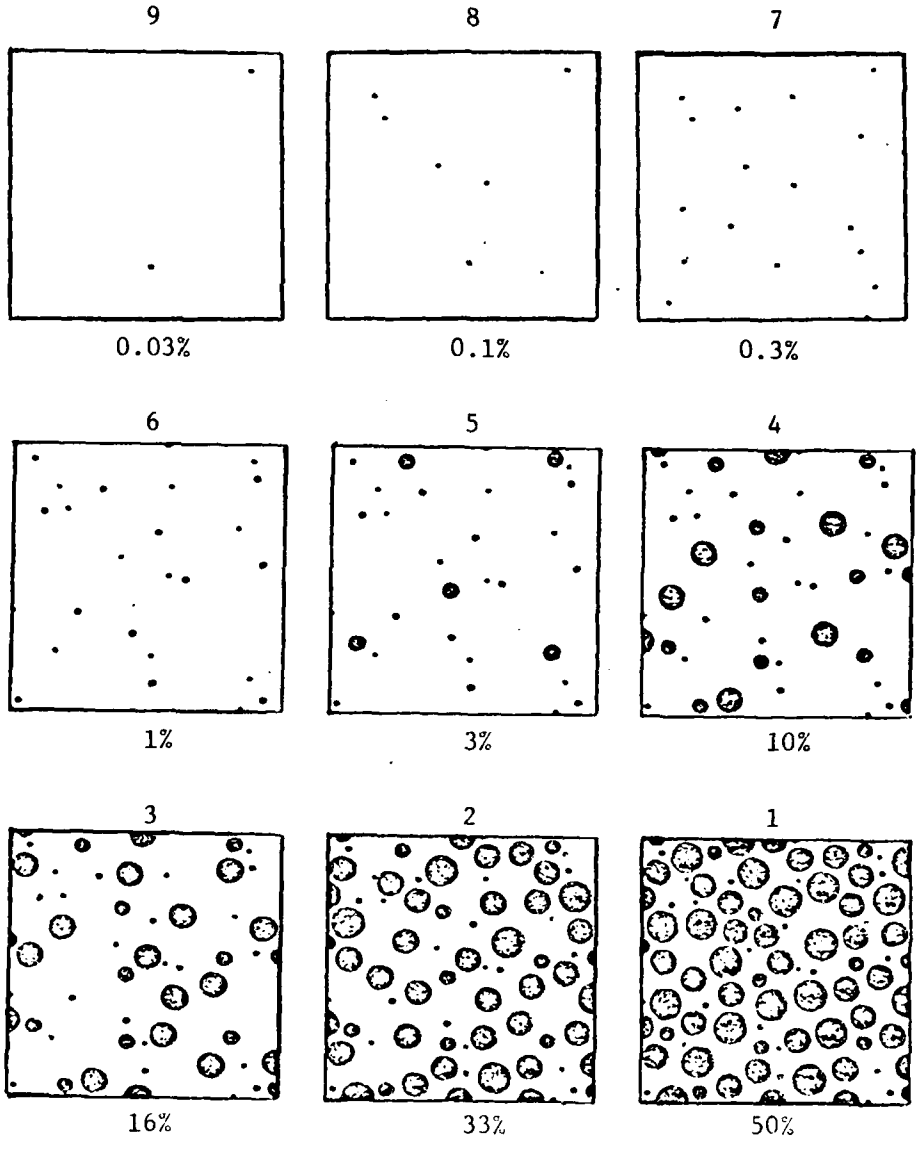

Figure 149. ASTM rust ratings corresponding to percent of area rusted.

were ground on a roller mill to Hegman grind ~7 or 8 (Table 50).

c. Panel Pretreatment. The metal panels used in this testing series were of Al 7075 alloy, 3x12x0.04 inches. The panel pretreatment procedure is given in Table 51, in accordance with MIL-C-25769J, MIL-C-5541C, and MIL-C-81706.

d. Primer and Topcoat Application. Approximately two hours after the panel pretreatment was completed, 30 panels were sprayed over their entire length in accordance with MIL-P-23377D, such that the dry film thickness is between 0.6 mil and 0.9 mil.

After these primed panels had dried for three to four hours, a one mil thick coating of the DeSoto two-component Super Desothane aliphatic polyurethane enamel (MIL-P-83286B) was applied to each panel. Again, after waiting 45 minutes to one hour, another one mil thick application of the topcoat was applied. Topcoat application is over only half the surface area of the primed panels, and is otherwise in accordance with MIL-C-83286B. A Binks Model 18 spray gun, driven by a Dayton Speedaire air compressor, was used for both the primer and topcoat applications. Coating thickness measurements were made with an Elcometer Instrument, Ltd. Minitector 150 electronic thickness gauge.

e. Testing Regime Period. After the application step, the primed, topcoated panels were allowed to cure for 168 hours, and then the following test procedures were carried out:

1. The wet tape adhesion test was performed on two panels from each formulation, in accordance with Fed. Test Method Std. No. 141B, Method 6301, February 1, 1979.
2. The salt fog spray test was performed on three panels from each primer formulation, in accordance with ANSI/ASTM B 117-73 (Reapp. 1979), for a period of 500 hours.
3. The 100% relative humidity test was performed on three panels from each formulation, in accordance with ASTM D2247-68, for a duration of 500 hours.

f. Test Results. The results of the wet (tape) adhesion test are given in Table 52. Two panels were tested for each primer formulation, with very

TABLE 51. METHOD FOR SURFACE TREATMENT OF ALUMINUM PANELS

PROCEDURE:

1. MEK wash for degreasing.
2. Soak for 20-35 minutes in Turco Air-Tec #19 (alkaline detergent), scrubbed vigorously with cheese cloth, then perform R.I.A. drop test for cleanliness (ASTM 7.1.6.22) (Turco Air Tec # 19 meets MIL-C-25769).
3. Rinse thoroughly with deionized H_2O.
4. Deoxidation step: Soak panels for approximately 5 minutes in a solution of the following:

components	volume by %
butyl alchohol	35
isopropyl alchohol	25
distilled deionized H_2O	22
85% phosphoric acid	18
	100

5. Give panel a fresh deionized H_2O rinse.
6. While the panel is still wet, chromate conversion process is initiated (Turcoat Accelagold, i.e., chromate conversion solution prepared to yield a concentration of 0.5 oz per gallon. 4.83 g of part 1 are added to 9.66 g of part 2 and enough water is added to give a one gallon solution. 20 drops of nitric acid are added to achieve a pH of 2.0. pH must range between 1.5 and 2.1. If pH is too low, add ammonium hydroxide. The above formulation meets MIL-C-81706 and was applied in accordance with MIL-C-5541.) Dip panels into the formulation for 3 to 5 minutes at ambient temperature. (When rinsed with deionized H_2O, the panels assumed a straw color.)
7. After the H_2O rinse, the panels are allowed to dry and are coated within 8 hours.
8. Test area on the aluminum 7075 panels is 74 mm by 149 mm.

TABLE 52. WET ADHESION TAPE TEST RESULTS

Formulation	Panel 1		Panel 2	
	Adhesion Loss	Blistering	Adhesion Loss	Blistering
1	no	10	no	10
2	no	10	no	10
3	yes	0	yes	10
4	yes	0	yes	0
5	yes	0	yes	0
6	no	10	no	10
7	no	10	no	10
8	no	10	no	10
9	yes	0	yes	0
10	yes	0	yes	0

consistent results for the two trials in all cases. Figures 150-159 are the photographic prints taken of each panel set after the wet adhesion test was performed. All four of the control formulations (1, 2, 6, and 7) performed well, thus providing an unambiguous set of standards for comparison of the AFIF formulations. The only AFIF primer formulation which performed well was formulation 8 (1% AFIF at 50 PVC), while all other AFIF primers (3, 4, 5, 9, and 10) definitely failed. The results indicate that the incorporation of AFIF into the coating matrix had a deleterious effect on adhesion and blistering properties. Obviously, extreme osmotic pressures occur at the coating-metal interface for systems containing greater than 1% AFIF and PVC values of less than 50%. These data indicate that the 1% AFIF level formulated at 50 PVC is the starting point for subsequent exploratory studies.

The results given above on wet adhesion all refer to the topcoated portion of the aluminum panels. Considering response of the non-topcoated, primed panel to the wet adhesion test, all passed except those from the formulations 3, 4, and 5, which again illustrates the deleterious effects of high osmotic pressures. The AFIF formulations at the 50 PVC value all performed well, apparently because of their open structure. The disparity between the topcoated and non-topcoated primer formulations is ample evidence that inferences about the topcoated system cannot be made solely on the response of the non-topcoated primed samples.

No appreciable oxidation was observed on any of the panels tested. This is reasonable, since the wet adhesion test calls for only 24 hr immersion in distilled water at 25°C.

The salt fog spray test was run for 500 hr on all samples, and the results are reported in Table 53. Evaluation of the scribed and unscribed portions of the test panels was done in accordance with ASTM D 1654-79a.

The PVC value apparently had no effect upon the extent of corrosion creepage at the scribed region. However, surprisingly, the creepage was approximately proportional to the AFIF inhibitor concentration level; e.g., as the AFIF concentration increased, the extent of creepage also increased. This effect may be due to rapid leaching of inhibitor as a result of channelling or from high concentration gradients.

On the other hand, interpretation of results was unambiguous for the unscribed areas of the test panels. All four control formulations (1, 2, 6, and 7) passed the 500 hr exposure period, along with the 1% AFIF formula-

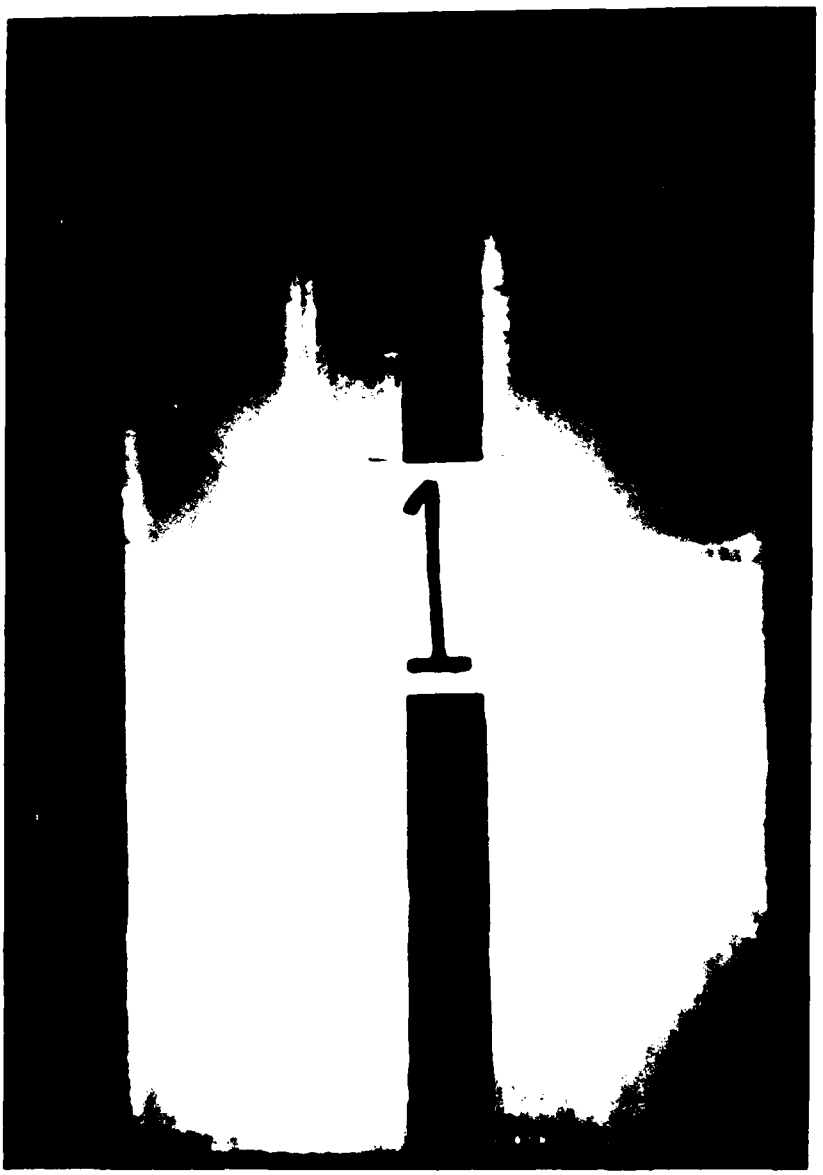

Figure 150. Wet adhesion test results for 30 PVC at 0% AFIF.

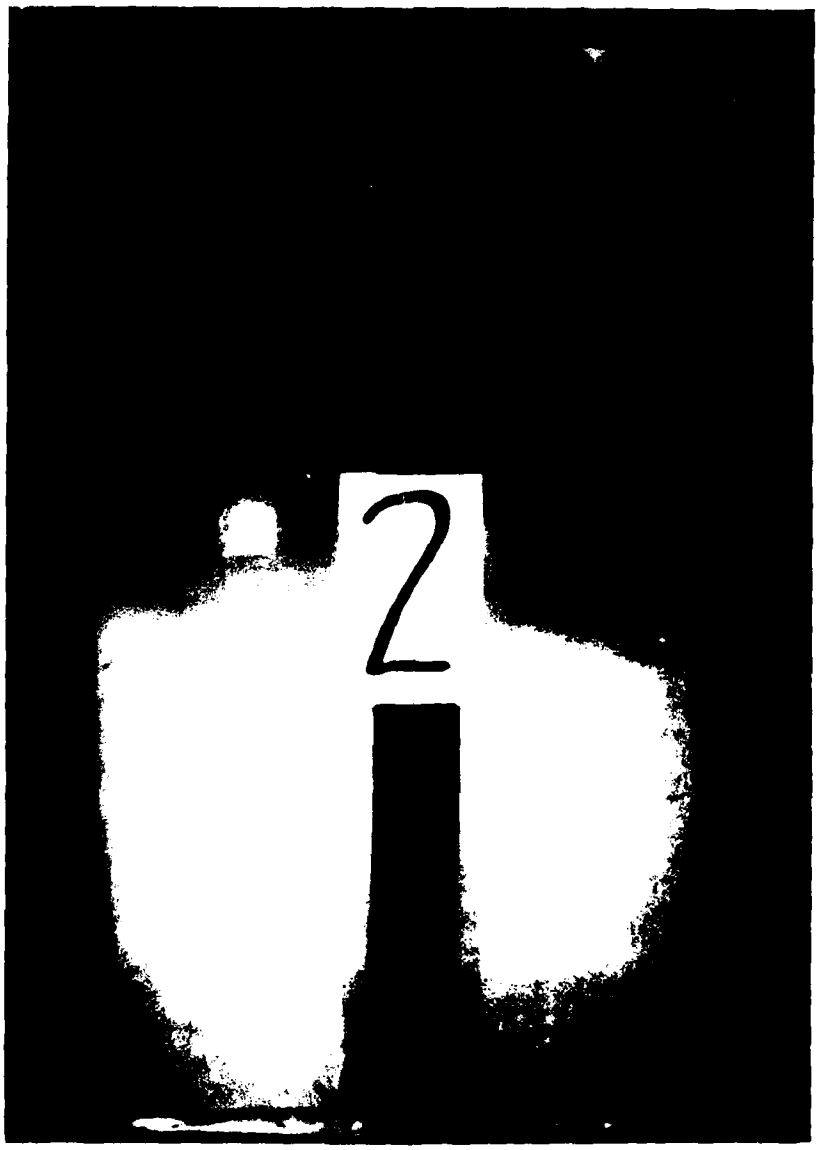

Figure 151. Wet adhesion test results for 30 PVC at 0% AFIF, plus $SrCrO_4$.

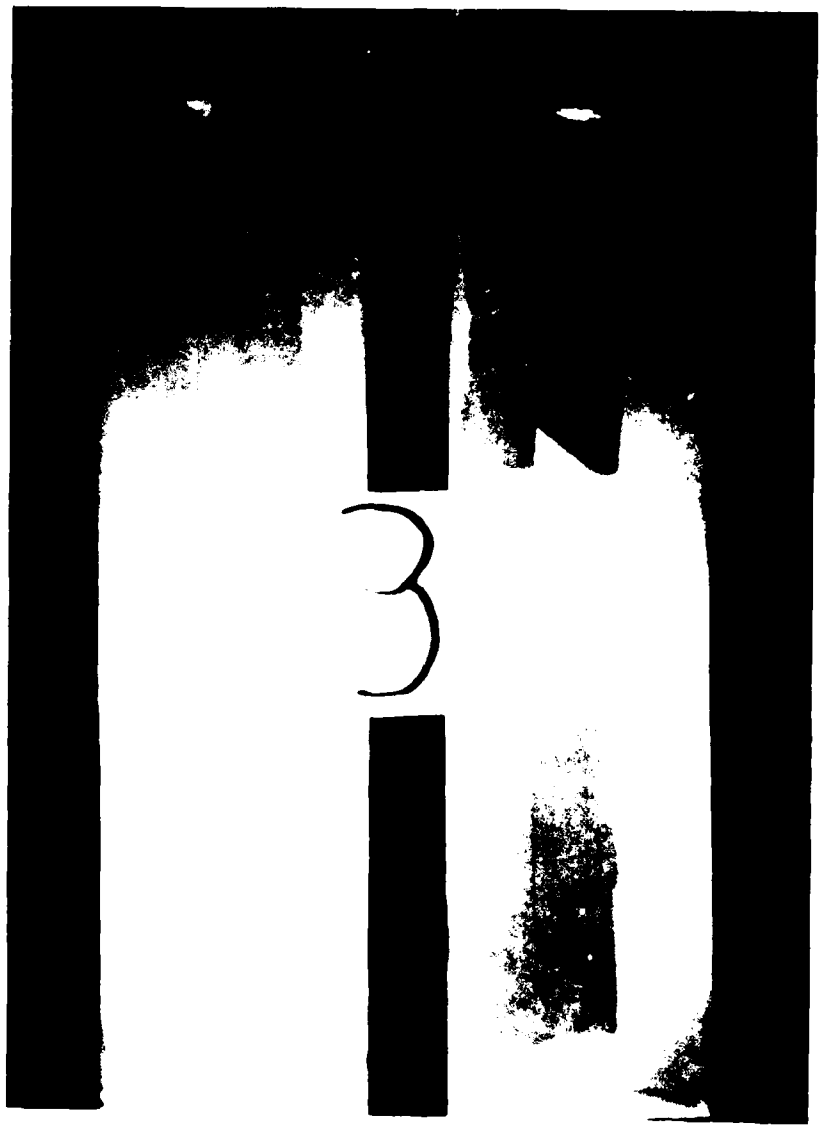

Figure 152. Wet adhesion test results for 30 PVC at 1% AFIF.

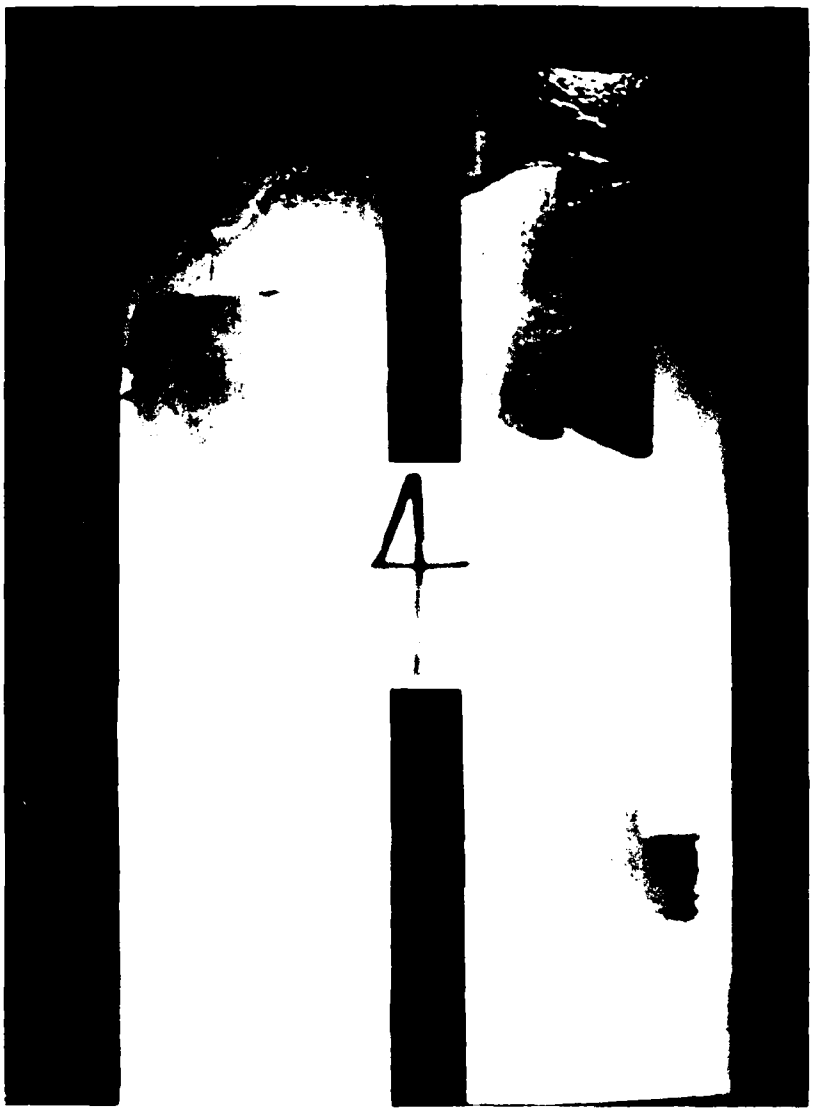

Figure 153. Wet adhesion test results for 30 PVC at 5% AFIF.

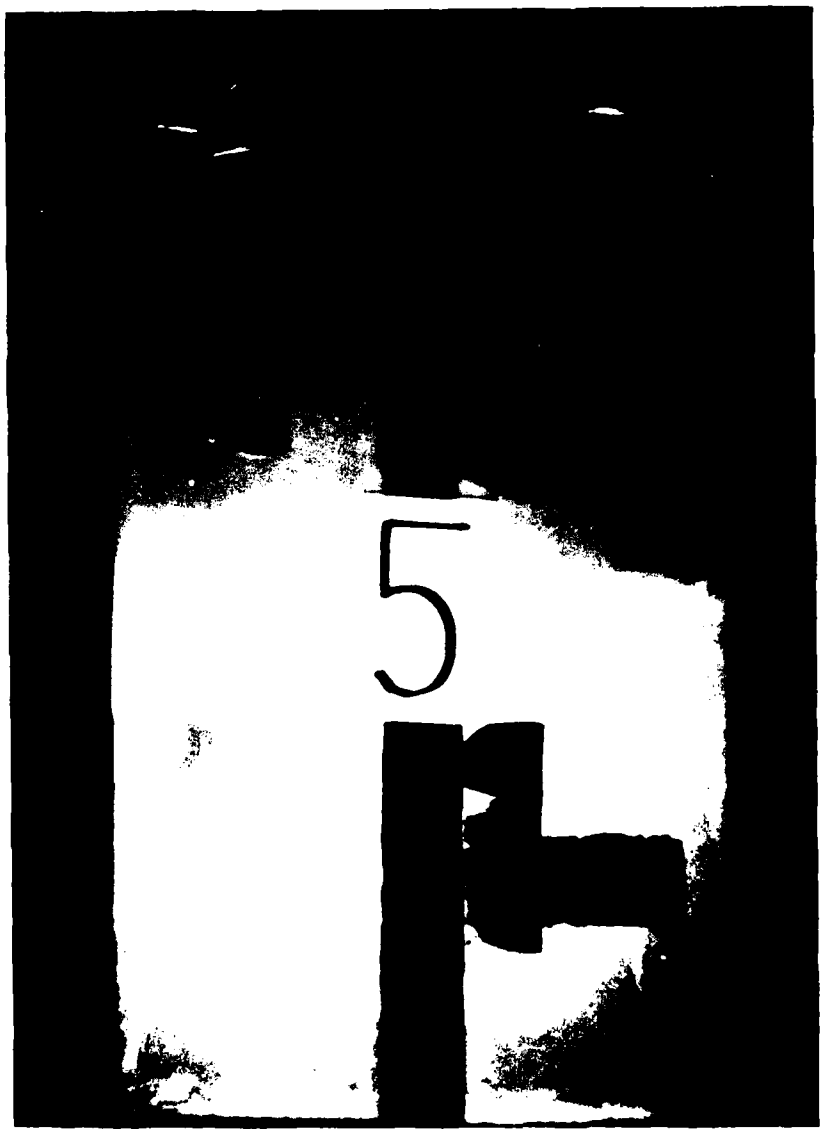

Figure 154. Wet adhesion test results for 30 PVC at 10% AFIF.

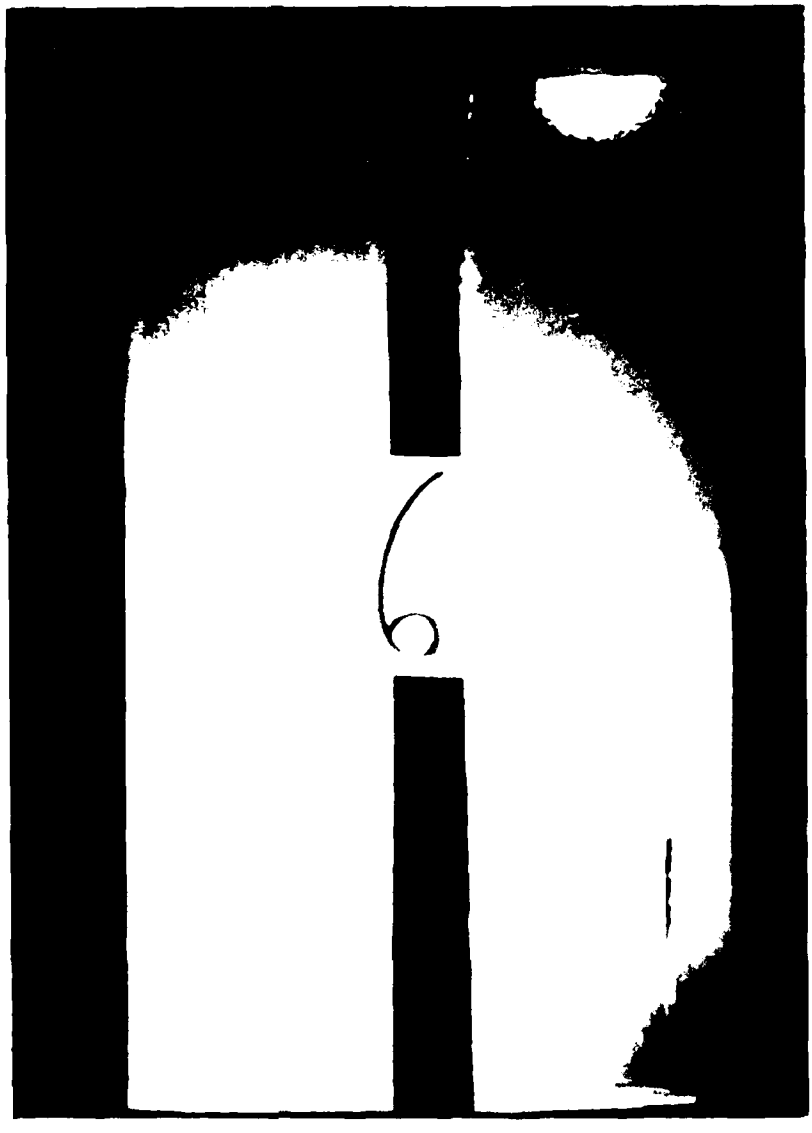

Figure 155. Wet adhesion test results for 50 PVC at 0% AFIF.

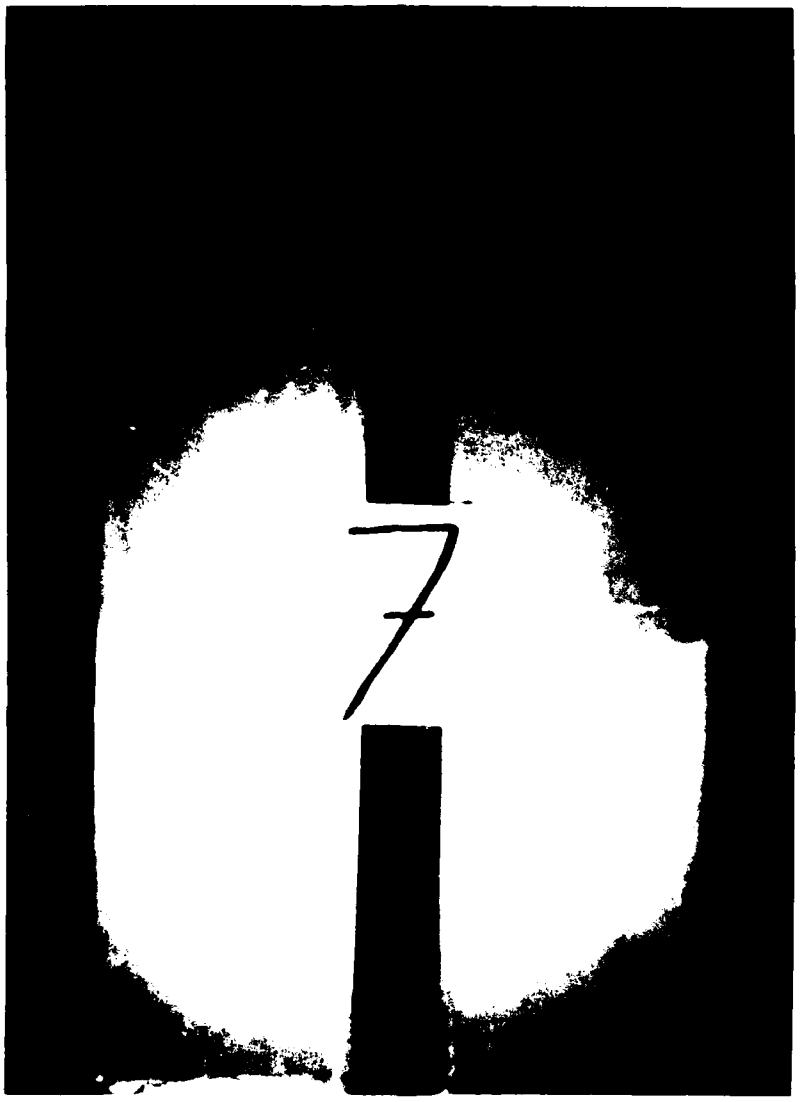

Figure 156. Wet adhesion test results for 50 PVC at 0% AFIF, plus $SrCrO_4$.

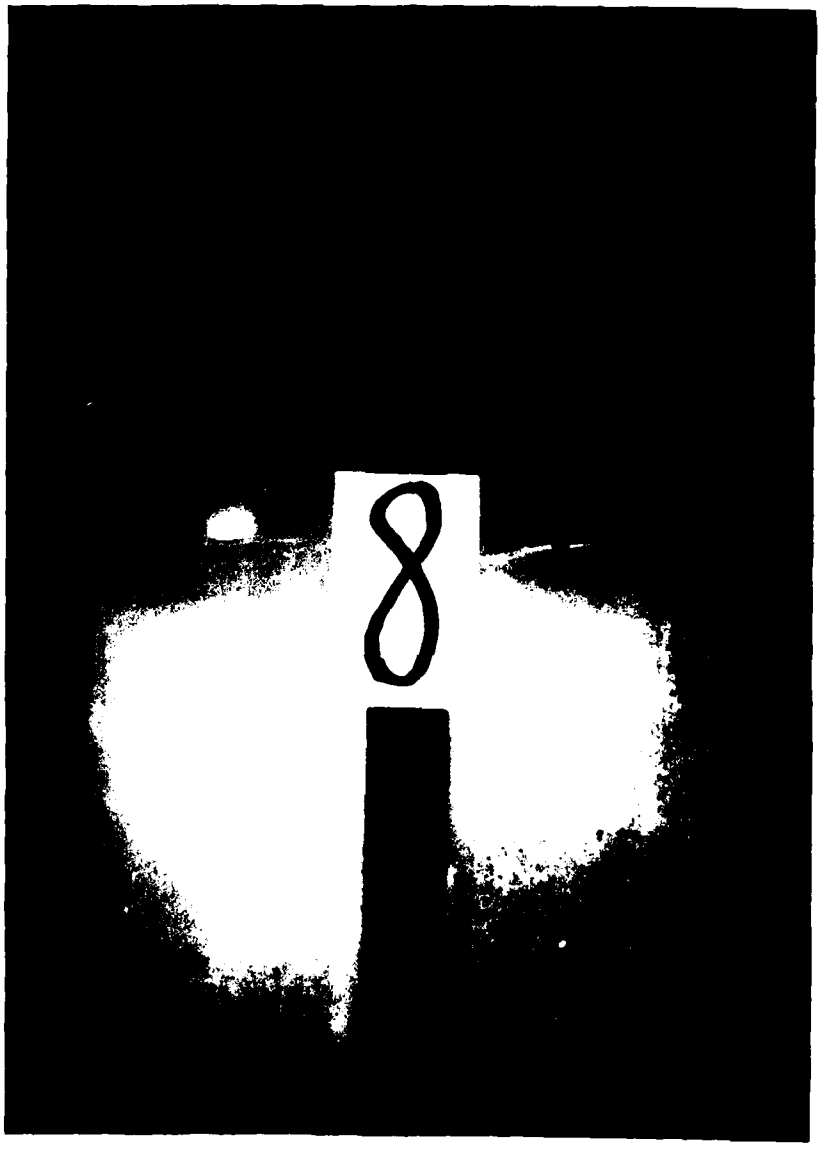

Figure 157. Wet adhesion test results for 50 PVC at 1% AFIF.

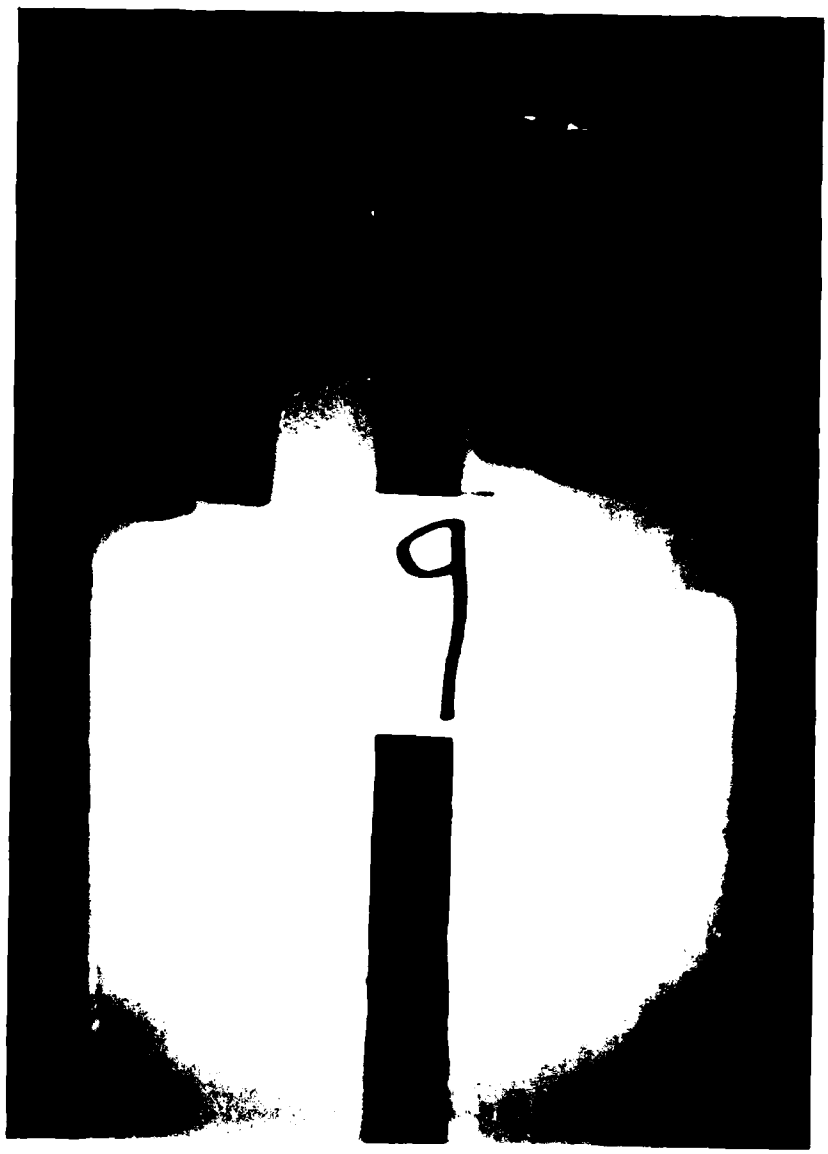

Figure 158. Wet adhesion test results for 50 PVC at 5% AFIF.

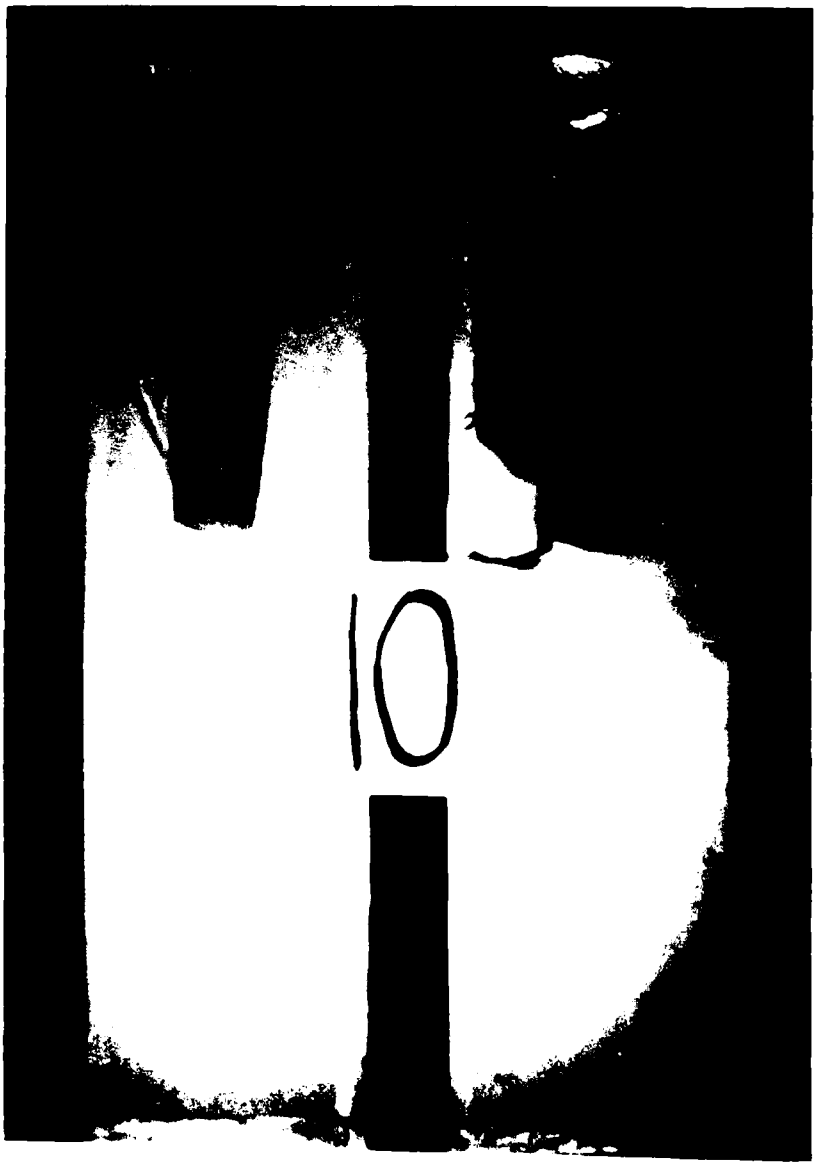

Figure 159. Wet adhesion test results for 50 PVC at 10% AFIF.

TABLE 53. SALT FOG SPRAY TEST RESULTS (ASTM D 1654-79a RATING)

Formulation	Scribed Area			Unscribed Area		
	Panel 1	Panel 2	Panel 3	Panel 1	Panel 2	Panel 3
1	9	9	9	9	9	10
2	10	10	10	10	10	10
3	9	8	7	9	9	9
4	3	7	7	0	0	0
5	7	7	5	0	0	0
6	8	9	9	9	9	9
7	10	10	10	10	10	10
8	9	9	9	8	8	8
9	7	7	7	0	0	0
10	7	8	7	0	0	0

tions (3 and 8) at both 30 and 50 PVC. Some of these samples did display a sort of crenation of the topcoat surface, but there was no blistering. The other AFIF formulations (4, 5, 9, and 10) suffered serious blistering, corresponding to 100% surface area involvement in all cases, e.g., total failure.

The 100% relative humidity test was run on three panels from each primer formulation for 500 hr, and the results are given in Table 54. Evaluation of the surface involvement was performed in accordance with ASTM D 1654-79a. As may be observed in Table 54, formulations 1, 2, 3, 6, 7, and 8 passed the test, while formulations 4, 5, 9, and 10 failed completely. These test results correlate extremely well with those of the salt fog test. Another similarity of the 100% relative humidity test to the salt fog spray test is the presence of a crenated topcoat, but which is apparently not related to blistering. The coating on these crenated specimens still remained intact and performed well under test conditions.

2. AFIF Concentration Optimization

a. General Procedure. Based upon the results obtained in the study, a further optimization study was planned which specifically involved optimization of the AFIF concentration for the 50 PVC primer formulation. In this present study, the PVC was held constant at 50, while the AFIF concentration was varied over the following values: 0.0%, 0.5%, 1.0%, 1.5%, 2.0%, and 3.0% AFIF based on total weight of solids. The only two primer

TABLE 54. 100% RELATIVE HUMIDITY RESULTS (ASTM D 1654-79a RATING)

Formulation	Panel 1	Panel 2	Panel 3
1	9	9	9
2	10	10	10
3	9	9	9
4	0	0	0
5	0	0	0
6	9	9	9
7	10	10	10
8	9	10	9
9	0	0	0
10	0	0	0

components affected were the AFIF and Imsil A-10 concentrations, where for each primer formulation an increase in AFIF level resulted in a corresponding reduction in the Imsil A-10 level. All other primer components were held at constant composition values. Test panels were 1010 steel instead of aluminum since the degree of corrosion is more quantifiable on steel panels.

b. Primer Formulation. The calculated composition values for the six primer formulations used in this study are given in Tables 55 and 56.

c. Panel Pretreatment. Steel (low carbon 1010) panels were substituted for the aluminum panels used previously. Panel pretreatment was in accordance with ASTM D609-61, Section 4(a), Solvent Spray Cleaning of Steel Panels.

d. Primer and Topcoat Application. The methodology used for application of the primer and topcoat were the same as that previously specified in Section C.1.d.

e. Testing Regime. The testing regime used is the same described in Section C.1.e.

f. Test Results. The experimental results for the salt fog spray, 100% relative humidity, and wet (tape) adhesion tests are reported in Table 57. The results for the 100% relative humidity indicated that levels of AFIF above 1% were not feasible, as excessive blistering occurred. The results from the salt spray and wet adhesion tests showed some variability, but again higher levels of AFIF consistently displayed poor adhesion and excessive blistering. When considered together, the tests indicate that the

TABLE 55. COMPONENT COMPOSITION VALUES: CONSTANT VALUES

Component	lb	gal
Imsil A-10	y	y
TiO_2	21.14	0.62
Talc	50.56	2.13
AFIF	x	x
Ancamide 220	68.73	8.49
Xylene	29.63	4.10
Toluene	120.14	16.59
Isopropyl Alcohol	75.04	11.46
Butanol	75.33	11.15
EPON 1001F	201.97	20.41
Diacetone Alcohol	20.20	2.60
Methyl Isobutyl Carbinol	16.83	2.52
Isopropyl Alcohol	16.83	2.57
Methyl Isobutyl Ketone	13.46	2.01
Xylene	67.32	9.33

TABLE 56. COMPONENT COMPOSITION VALUE: VARIABLES

	AFIF		Imsil A-10	
% AFIF	lb	gal	lb	gal
0.0	0.00	0.00	578.62	26.22
0.5	4.59	0.29	572.15	25.92
1.0	9.16	0.58	565.70	25.63
1.5	13.71	0.87	559.28	25.34
2.0	18.24	1.16	552.89	25.05
3.0	27.26	1.74	540.17	24.48

TABLE 57. RESULTS OF SALT FOG SPRAY, 100% RELATIVE HUMIDITY, AND WET ADHESION TESTS

Panel	Salt Fog Spray			100% RH*		Wet Adhesion
	Scribed*	Unscribed*				
0.0	2	0	blisters	10	blisters	passed
0.0	2	6	blisters	10	no blisters	passed
0.0	3	10	no blisters	10	no blisters	-
0.5	1	6	blisters	10	no blisters	passed
0.5	3	10	no blisters	10	no blisters	passed
0.5	3	7	blisters	10	no blisters	-
1.0	4	0	blisters	10	no blisters	failed
1.0	4	10	no blisters	10	no blisters	passed
1.0	3	10	no blisters	10	no blisters	-
1.5	9	0	blisters	10	no blisters	failed
1.5	5	0	blisters	10	no blisters	failed
1.5	5	10	no blisters	2	blisters	-
2.0	8	0	blisters	0	blisters	failed
2.0	0	10	no blisters	0	blisters	failed
2.0	0	10	no blisters	0	blisters	-
3.0	7	0	blisters	0	blisters	failed
3.0	9	0	blisters	0	blisters	failed
3.0	7	0	blisters	0	blisters	-

*Rating scales used are from ASTM D1654-79a.

optimal AFIF concentration level is 1.0% based on the weight of total solids in the dry film, for PVC = 50.

3. Corrosion Protection Optimization Using Commercial Corrosion Inhibitive Pigments

a. General Procedure. The previous studies revealed that the 1% level of AFIF was the maximum level of corrosion inhibitor which could be incorporated into the primer system. Since 1% inhibitor represents only a fraction of the level normally used to afford adequate and long-term protection, a co-inhibitor study was designed with the objective of discovering a synergistic inhibitor combination which would provide high levels of extended protection.

This study utilized commercially available nonchromate corrosion-inhibitive pigments in combination with the optimal 1% AFIF level. As before, the pigment volume concentration for all primers tested was held at PVC = 50. Each of the commercial pigments was tested at concentration levels of 1%, 5%, and 10%, and was milled with the polyamide component, as was done for the AFIF, to a final Hegman gauge reading of ~7-8. The commercial corrosion-inhibitive pigments used were:

1. NICHEM #7 Zinc Phosphate
2. Heubach Heucophos ZPA (basic aluminum zinc phosphate)
3. Halox BW-191 (calcium barium phosphosilicate)
4. Sherwin Williams Moly White 101 (zinc molybdate)

b. Primer Formulation. Tables 58 and 59 give the composition values for the primers used in this study.

c. Panel Pretreatment. Steel alloy 1010 panels were used, and the panel pretreatment method corresponded to that described in Section C.2.c.

d. Primer and Topcoat Application. The methodology used for application of the primer and topcoat were the same as that previously specified in Section C.1.d.

e. Testing Regime. The testing regime used was the same as that specified in Section C.1.e.

TABLE 58. PRIMER COMPONENT COMPOSITION: CONSTANT VALUES

Component	lb	gal
Polyamide Component		
Imsil A-10	Y_m	Y_v
TiO_2	21.14	0.62
Talc	50.56	2.13
AFIF	X_m	X_v
Ancamide 220	68.73	8.49
Xylene	29.63	4.10
Toluene	120.14	16.59
Isopropyl Alcohol	75.04	11.46
Butanol	75.33	11.15
Commercial Corrosion Inhibitor	Z_m	Z_v
Epoxy Component		
Epon 1001 F	201.97	20.41
Diacetone Alcohol	20.20	2.60
Methyl Isobutyl Carbinol	16.83	2.52
Isopropyl Alcohol	16.83	2.57
Methyl Isobutyl Ketone	13.46	2.01
Xylene	67.32	9.33

TABLE 59. PRIMER COMPONENT COMPOSITION: VARIABLE QUANTITIES

Primer	Corrosion Inhibitor	Corrosion Inhibitor (wt %)	AFIF X_m (lb)	Imsil A-10 Y_m (lb)	Corrosion Inhibitor Z_m (lb)
C	None	0	9.16	564.20	0.00
1	NICHEM	1	9.19	558.11	9.19
2	NICHEM	5	9.31	533.08	46.56
3	NICHEM	10	9.47	500.82	94.73
4	Heucophos	1	8.91	530.93	8.91
5	Heucophos	5	8.04	413.82	40.22
6	Heucophos	10	7.17	295.98	71.72
7	Halox	1	9.16	555.76	9.16
8	Halox	5	9.19	521.62	45.95
9	Halox	10	9.22	478.66	92.24
10	Moly White	1	9.20	559.37	9.20
11	Moly White	5	9.38	539.32	46.90
12	Moly White	10	9.61	513.14	96.12

f. Test Results. The results for this experiment are given in Table 60. The best responses to our test battery were given by primers 2, 3, and 8. These correspond to the NICHEM #7 Zinc Phosphate (primers 2 and 3) and the Halox BW-191 (primer 8). The NICHEM appeared to be the most consistent product of all those tested, demonstrating good resistance to salt spray, moderate blister resistance, but poor adhesion. It should be noted that these formulations performed noticeably better than the control.

Considering the overall response of these systems, based on salt fog spray, 100% humidity, and wet adhesion, the following order of decreasing performance was obtained:

2,3 > 8 > 6,7,9 > C,1,4,5,10,11,12

The commercial nonchromate corrosion inhibitors could be ranked in the following manner, based on their overall performance.

NICHEM > Halox > Heucophos > Moly White

The NICHEM #7 Zinc Phosphate was chosen for further testing in the final comparative coatings study.

4. Adhesion Promoter Study.

Five primers were prepared based on the control formulation. Two epoxy-compatible organosilane adhesion promoters were added at two concentration levels, producing four test formulations. The adhesion promoters were added directly to the polyamide portion of the primer, and formulations were jar milled in the usual fashion. After spraying and the 168 hour ambient temperature cure, the wet tape adhesion test was performed on these samples. Four panels were tested for each primer formulation. As may be seen in Table 61, all panels failed this test. Thus, there was no observed improvement with the organosilane adhesion promoters.

5. Comparative Study: Entrapped vs. Encapsulated AFIF

a. General Procedure. This experimental design was the final stage of work on coatings and physical entrapment. The purpose of this study was to compare the corrosion protection and coatings performance of

TABLE 60. RESULTS OF SALT FOG SPRAY, 100% RELATIVE HUMIDITY, AND WET ADHESION TESTS*

Formulation	Salt Fog Spray			100% Relative Humidity		Wet Adhesion	
	Scribed	Unscribed	Blisters?		Blisters?		Blisters?
C	7	0	+	10	-	fail	+
C	2	0	+	10	-	fail	+
C	5	0	+	10	-		
1	5	0	+	10	-	fail	-
1	7	0	+	10	-	fail	-
1	8	0	+	10	-		
2	8	10	-	10	-	fail	-
2	7	10	-	10	-	fail	-
2	5	10	-	10	-		
3	7	10	-	10	-	fail	+
3	6	10	-	10	-	fail	-
3	7	10	-	10	-		
4	5	1	+	10	-	fail	+
4	7	0	+	10	-	fail	+
4	5	0	+	10	-		
5	4	1	+	10	-	fail	-
5	7	2	+	10	-	fail	-
5	5	0	+	10	-		
6	7	4	+	10	-	fail	-
6	7	7	+	10	-	fail	-
6	3	10	-	10	-		

*Rating scale as in ASTM D 1654-79a.

(continued)

TABLE 60. Continued*

Formulation	Salt Fog Spray			100% Relative Humidity		Wet Adhesion	
	Scribed	Unscribed	Blisters?		Blisters?		Blisters?
7	6	10	-	10	-	fail	+
7	5	4	+	10	-	fail	+
7	6	1	+	10	-		
8	7	5	+	10	-	fail	+
8	7	9	-	10	-	fail	+
8	7	10	-	10	-		
9	3	4	+	10	-	fail	+
9	3	7	+	10	-	fail	+
9	6	8	+	10	-		
10	7	0	+	10	-	fail	+
10	5	0	+	10	-	fail	+
10	4	0	+	10	-		
11	7	0	+	10	-	fail	+
11	7	0	+	10	-	fail	+
11	6	0	+	10	-		
12	8	2	+	10	-	fail	+
12	8	0	+	10	-	fail	+
12	7	0	+	10	-		

*Rating scale as in ASTM D 1654-79a.

Table 61. Adhesion Promoter Study

Formulation	Adhesion Promoter	Adhesion Promoter (wt %)	Wet Adhesion
13	None	0.0	failed
13	None	0.0	failed
13	None	0.0	failed
13	None	0.0	failed
14	β-(3,4 epoxycyclohexyl)ethyl-trimethoxysilane	1.0	failed
14	β-(3,4 epoxycyclohexyl)ethyl-trimethoxysilane	1.0	failed
14	β-(3,4 epoxycyclohexyl)ethyl-trimethoxysilane	1.0	failed
14	β-(3,4 epoxycyclohexyl)ethyl-trimethoxysilane	1.0	failed
15	β-(3,4 epoxycyclohexyl)ethyl-trimethoxysilane	2.0	failed
15	β-(3,4 epoxycyclohexyl)ethyl-trimethoxysilane	2.0	failed
15	β-(3,4 epoxycyclohexyl)ethyl-trimethoxysilane	2.0	failed
15	β-(3,4 epoxycyclohexyl)ethyl-trimethoxysilane	2.0	failed
16	n-Beta aminoethyl-aminopropyltrimethoxysilane	1.0	failed
16	n-Beta aminoethyl-aminopropyltrimethoxysilane	1.0	failed
16	n-Beta aminoethyl-aminopropyltrimethoxysilane	1.0	failed
16	n-Beta aminoethyl-aminopropyltrimethoxysilane	1.0	failed
17	n-Beta aminoethyl-aminopropyltrimethoxysilane	2.0	failed
17	n-Beta aminoethyl-aminopropyltrimethoxysilane	2.0	failed
17	n-Beta aminoethyl-aminopropyltrimethoxysilane	2.0	failed
17	n-Beta aminoethyl-aminopropyltrimethoxysilane	2.0	failed

the primers formulated with entrapped AFIF vs. the primers formulated with microencapsulated AFIF. Also, an attempt was made to provide a basis for evaluation of these systems within the context of a number of other primers, mainly those containing $SrCrO_4$ and NICHEM #7 Zinc Phosphate.

Three controls were run in this study: 1) 1% AFIF, 2) 1% $SrCrO_4$, and 3) 20% $SrCrO_4$ (all values as weight per dry film). An attempt was made to prepare a primer with $SrCrO_4$ at the MIL-P-23377D level (42% $SrCrO_4$ per weight pigment), but problems were encountered in the jar milling stage. The 20% $SrCrO_4$ per weight solids which was tested instead is equivalent to 28% $SrCrO_4$ per weight pigment. No problems were observed with this formulation.

With primers 4 and 5, an attempt was made to alleviate the poor adhesion performance observed for most of the previously formulated compositions. This was a carry-over from the adhesion promoter study described earlier. Union Carbide Organofunctional Silane A-186 [beta-(3,4-epoxycyclohexyl) ethyl-trimethoxysilane] was the adhesion promoter of choice. In primer 4, the A-186 was added directly to the polyamide component prior to jar milling, at the 1% (per solids content) level (recommended level by the manufacturer). For primer 5, a 10% A-186 solution in toluene was prepared. This solution was sprayed on the panels directly after the panel pretreatment stage, and the solvent was allowed to evaporate before priming. This must be considered a basically qualitative test, since the A-186 concentration at the metal surface-coating interface is not equivalent for the two systems. This approach was considered a spot test to evaluate the effect of surface modification.

Primers 6 and 7 contained 1% AFIF with 10% and 15% of NICHEM #7 zinc phosphate, respectively. This was an extension of the work described earlier in Section VI.C.3. The 10% level was selected based on the results of previous work, and 15% was included as a means of providing additional information.

Primers 8 and 9 represented the key formulations in this study. These were the formulations which contained the microencapsulated AFIF. The objective was to add enough microcapsules to provide the 1% AFIF level (per weight solid dry film) which was utilized in the physical entrapment studies, but achieving this level of loading was not possible. Problems were encountered when the toluene suspensions of microcapsules were blended

into the polyamide component. The low loading values of AFIF, coupled with the large volume of material (solvent plus polymeric microcapsules), resulted in an adverse response of the primer base, manifested by apparent solvent shock and incompatibility when a certain addition level was reached. The AFIF levels that were attainable by this method were significantly lower than the 1.0% level (approx. 0.1%).

Primer 10 was an attempt to add sodium molybdate-containing polyurea microcapsules to the organic coating. The key feature of the $NaMbO_4$ is its relatively higher water solubility compared to the AFIF. The microcapsules were prepared by substituting the $NaMbO_4$ for AFIF in the encapsulation procedure, with no other alterations in procedure.

b. Primer Formulation. Tables 62 and 63 give the formulation compositions for the primer components used in this study. Table 64 describes the characteristics of the microcapsules utilized in primers 8, 9, and 10. Encapsulation Procedure 619-74 (Table 25, microencapsulation) was used for microcapsule preparation.

c. Panel Pretreatment. Steel alloy 1010 panels were used, and the panel pre-treatment method corresponds to that described in section C.2.c. The exception was primer 5, which was pretreated as described in C.5.a.

d. Primer and Topcoat Application. This procedure was the same as specified earlier in section C.1.d.

e. Testing Regime. This procedure was the same as specified earlier in section C.1.e.

f. Test Results. The results for this experimental design are given in Table 65.

Primers 1, 2, and 3 were the control formulations for physically entrapped AFIF (1%) and $SrCrO_4$ (1% and 20%), respectively. These formulations performed very well in all three test procedures. There was a slight amount of corrosion breakthrough on the unscribed region of the 1% $SrCrO_4$; this was attributed to the presence of film defects, which were formed most likely during the film application stage. The control primers may be ranked as follows, based on decreasing order of performance: $3 > 1 \sim 2$. Primer formulation 3 was found to provide the best balance of properties and contained the highest level of $SrCrO_4$. Primers 1 and 2 are essentially equivalent in response. These results suggest that at low inhibitor levels, the AFIF may perform in a similar fashion to the $SrCrO_4$. At higher AFIF levels,

TABLE 62. PRIMER COMPONENT COMPOSITION: CONSTANT VALUES

Component	lb	gal
Polyamide Component		
Imsil A-10	Y_m	Y_v
TiO_2	21.14	0.62
Talc	50.56	2.13
AFIF	X_m	X_v
Other Corrosion Inhibitor	Z_m	Z_v
Ancamide 220	68.73	8.49
Xylene	29.63	4.10
Toluene	120.14	16.59
Isopropyl Alcohol	75.04	11.46
Butanol	75.33	11.15
Epoxy Component		
Epon 1001F	201.97	20.41
Diacetone Alcohol	20.20	2.60
Methyl Isobutyl Carbinol	16.83	2.52
Isopropyl Alcohol	16.83	2.57
Methyl Isobutyl Ketone	13.46	2.01
Xylene	67.32	9.33

TABLE 63. PRIMER COMPONENT COMPOSITION: VARIABLES

Primer	AFIF wt% DF*	AFIF #lb	Imsil A-10 #lb	Other Inhibitor wt% DF	Other Inhibitor #lb	Other Material wt% or #lb
1	1.00	9.16	564.26	---	---	---
2	0.00	0.00	570.86	$SrCrO_4$ 1%	9.22	---
3	0.00	0.00	443.61	$SrCrO_4$ 20%	196.48	---
4	1.00	9.16	564.26	---	---	A-186 1%
5	1.00	9.16	564.26	---	---	---
6	1.00	9.47	500.82	NICHEM 10.0%	94.73	---
7	1.00	9.64	467.42	NICHEM 15.0%	144.60	---
8	0.09	0.241	564.26	---	---	microcapsules 4.725
9	0.15	0.404	564.26	---	---	microcapsules 7.080
10	0.00	0.00	564.26	$NaMbO_4$ 0.13%	0.366	microcapsules 5.550

* Dry film

TABLE 64. MICROCAPSULE† CHARACTERISTICS FOR PRIMER FORMULATION

Primer	Inhibitor Encapsulated	Dry Loading*	Maximum Release Time (min)	Solids Added (g)	Inhibitor Added (g)	Wt% Inhibitor in Dry Film
8	AFIF	5.1%	72	4.725	0.241	0.09
9	AFIF	5.7%	58	7.080	0.404	0.15
10	$NaMbO_4$	6.6%	29	5.550	0.366	0.13

* Determined by oven drying, weighing, and an appropriate conductometric calibration curve for both AFIF and $NaMbO_4$

† Encapsulation procedure given in Table 25.

TABLE 65. SALT FOG SPRAY AND 100% RELATIVE HUMIDITY TEST RESULTS

Primer Formulation	Salt Fog Spray Scribed	Salt Fog Spray Unscribed	100% Relative Humidity	Blister	Wet Adhesion	Blister
1	8	10	10	-	pass	-
1	6	10	10	-	pass	-
1	8	10	10	-	--	
2	8	9	10	-	pass	-
2	8	9	10	-	pass	-
2	9	10	10	-	--	
3	9	10	10	-	pass	-
3	9	10	10	-	pass	-
3	9	10	10	-	--	
4	5	10	10	-	fail	+
4	6	7	10	-	fail	+
4	6	9	10	-	--	
5	5	0	10	-	fail	+
5	8	0	10	-	fail	+
5	6	0	10	-	--	
6	6	9	10	-	pass	-
6	7	10	10	-	fail	+
6	7	10	10	-	--	
7	9	10	10	-	pass	-
7	9	9	10	-	pass	-
7	3	9	10	-	--	
8	7	10	10	-	fail	+
8	5	9	10	-	fail	+
8	7	9	10	-	--	
9	6	9	10	-	fail	+
9	5	8	10	-	fail	+
9	6	8	10	-	--	
10	2	0	10	-	fail	+
10	4	0	10	-	fail	+
10	1	0	10	-	--	

previous results indicated that the water solubility problem became a dominant problem, thus reducing the desirability of using higher concentrations of AFIF in coating formulations.

Primers 4 and 5 were formulations in which the Union Carbide organosilane adhesion promoter A-186 was used in an attempt to improve the adhesion properties of the AFIF primers. No improvement in adhesion was observed, and the responses to the salt fog spray test appeared to be adversely affected. Note that primer 1 (without A-186) passed the wet adhesion test. In primer 4, where the A-186 was added directly to the primer, the test response was much better than for primer 5, where the A-186 was sprayed directly onto the metal panels prior to coating. The relative primer ranking here was as follows, in decreasing order of performance: 1 > 4 > 5. These results are not consistent with studies in the literature where the organosilanes apparently increase coating adhesion on a metal substrate in a significant manner.

Primers 6 and 7 were formulated at 1% AFIF and 10% and 15% NICHEM #7 Zinc Phosphate, respectively. The only significant difference in response appeared to lie in the wet adhesion results, where the higher NICHEM level provided better adhesion.

Primers 8 and 9 tested for the utility of microencapsulated AFIF for corrosion control, while primer 10 studied microencapsulated $NaMbO_4$. Primer 10 provided very poor test responses in every category. Since there was not really a significant difference in the amount (wt%) of $NaMbO_4$ in the dry film compared to the AFIF encapsulation levels, the poor performance must be attributed to the increased water solubility of the molybdate compound, which caused serious osmotic pressure gradients across the film layer.

Formulations 8 and 9 showed basically similar response levels to the test regime. The salt fog spray and 100% humidity test results were only marginally less favorable relative to the primer 1 control, while the wet adhesion test results were inferior. The wet adhesion results suggest that the polyurea microcapsules tend to disrupt the adhesive bonding at the metal surface. This is reasonable, since in the MIL-P-23377D specification, the primer is an epoxy-polyamide, which is applied under the polyurethane topcoat. The polyurea microcapsules are more similar in their chemical properties to the topcoat material, so a loss of adhesion could occur if poly-

mer-polymer incompatibility disrupted the homogeneity which augments adhesion qualities.

The similarity of the salt fog spray and 100% relative humidity results of primers 8 and 9 to primer 1 is encouraging, based upon the level of AFIF contained in formulations 8 and 9. Surprisingly, concentrations of AFIF as low as 0.09% based on total weight of dry film appear to be sufficient to provide a reasonable measure of corrosion control. Whether or not microencapsulation was effective in prolonging corrosion resistance would require more quantitative testing conditions and alleviation of deficiencies inherent in the model formulation.

VII. DISCUSSION

A. Evaluation of Corrosion Inhibitors

1. Summary of Inhibitor Screening for 4340 Steel

An examination of the results from the potentiodynamic anodic polarization screening of corrosion inhibitor candidates for 4340 steel reveals three categories of response: (1) candidates that do not provide any form of corrosion protection, (2) candidates that reduce the metal dissolution process significantly over a certain potential range, and may possibly serve as effective corrosion inhibitors, and (3) candidates that form passive film barriers on the metal surface over a fairly wide potential range, often with a significant reduction in current density relative to the control.

The passive film formers are most likely to serve as effective corrosion inhibitors for the intended application. However, several qualifying statements must be made concerning the reliability of the potentiodynamic anodic polarization screening results.

The potentiodynamic polarization method is an artificially induced, accelerated corrosion testing method, with the sample suspended within a bulk aqueous phase, to which the inhibitor candidate is added. In those cases where a passive film is not present the metal surface is in direct contact with the water. Extrapolation of the activity of a corrosion inhibitive pigment candidate in this environment to the activity of the same material within a primer matrix is a complex process that would require further evaluation. The lack of reliable long term field correlations for potentiodynamic anodic polarization behavior of corrosion inhibitors attests to the challenge of this situation.

At the present state of the art, the method can serve as a comparative screening technique for a relative ranking of corrosion inhibitors in a given service environment. Such a relative assessment can be quite informative if the service environment closely matches the test environment; if not, long term predictions must be considered with caution.

Most of the corrosion inhibitor candidates studied for the protection of 4340 steel had some protective function (Table 1). Three did not function as inhibitors; β-mercaptobenzothiazole, $MgSiF_6 \cdot 6H_2O$, and sarcosine.

Eight of the compounds afforded some protection against the metal oxidation and dissolution process, mainly by reducing the activity of the metal in the environment. Some of these compounds were "almost" passivators, though the potential range of passivation effects was usually very narrow. Those inhibitors providing corrosion protection, but not necessarily passivation, were: $(NaPO_3)_6$, $NaNO_3$, $Na_2SiO_3 \cdot 9H_2O$, $(NH_4)_2MoO_4$, 1-ethynyl-1-cyclohexanol, 3,5-dimethyl-1-hexyne-3-ol, alizarin red S, and sodium sarcosine. The function of these inhibitors is interesting, yet they do not provide quite the type of protection of interest for the intended application. These materials would probably be most useful when used in conjunction with passivating corrosion inhibitors.

The passivating corrosion inhibitors represented the largest class of compounds studied by potentiodynamic anodic polarization of 4340 steel. They were: AFIF, $Na_2B_4O_7 \cdot 10H_2O$, $NaNO_2$, hydroxyquinoline, 2-propyn-1-ol, NH_4NO_2, $NH_4HB_4O_7 \cdot 3H_2O$, sodium cinnamate, potassium cinnamate, mercaptoacetic acid, $Na_2MoO_4 \cdot 2H_2O$ and 471-1, 2, 5, 6, 8, and 9.

The AFIF mixture of interest in this program contains two components which provide the passivating function for this inhibitor, $Na_2B_4O_7 \cdot 10H_2O$ and $NaNO_2$. All other AFIF components provide some protection, except β-mercaptobenzothiazole, which has no inhibitor activity. The AFIF polarization behavior was generally characteristic for the passivating inhibitors studied. For this reason, and because of its intrinsic interest as an effective wash primer for aircraft, AFIF was chosen among all of these inhibitors for further study in microencapsulation and coatings entrapment. The AFIF inhibitor was considered a representative passivator of all the inhibitors studied.

For the conditions of potentiodynamic anodic polarization in our studies, the aqueous electrolyte (5% NaCl) solutions used for testing were not deaerated, to provide a realistic, antagonistic environment. An increase in the rate of the cathodic reaction may occur due to dissolved O_2 in the electrolyte. Thus, the anodic oxidation and dissolution phenomena are probably rate-limited by diffusion-controlled transport of O_2 to the cathodic sites on the sample surface from the bulk electrolyte.

Most of the materials tested for corrosion protection had pH > 7. As

is well known, in basic aqueous solutions, the ferrous oxide ($FeO \cdot nH_2O$) or ferrous hydroxide [$Fe(OH)_2$] would be the primary constituent species of the passive oxide layer. The complicating effects of Cl^- in the electrolyte cannot be assessed in terms of its effect on the corrosion rate, oxygen transport, or on passive film formation. A great deal of effort would be necessary, involving many different types of experimental designs, to elucidate the mechanistic and kinetic aspects of these complex systems. A better definition of these phenomena may contribute to future improvements in corrosion protection.

2. Summary of Inhibitor Screening for 2024 Aluminum

The results of the potentiodynamic anodic polarization studies sort the corrosion inhibitor candidates for 2024 aluminum into three general categories: (1) passivators, (2) those which provide some protection, but do not passivate, and (3) those which provide no protection. The same general statements concerning the validity and use of potentiodynamic anodic polarization for 4340 steel are also applicable to 2024 aluminum.

Three of the inhibitor candidates tested provided passivation of the metal surface. These were $NaNO_2$, potassium cinnamate, and sodium molybdate.

Five of the inhibitor candidates provided some corrosion protection, yet were not passivators. These were NH_4NO_2, 1-ethynyl-1-cyclohexanol, 3,5-dimethyl-1-hexyne-3-ol, sarcosine, and sodium cinnamate.

The remaining 21 inhibitor candidate formulations or compounds did not provide any corrosion protection at all. In some cases, the rate of the anodic dissolution was significantly increased by the addition of the test material. Care should be exercised in the application of multicomponent mixtures such as the AFIF system. If the multicomponent formulation is incorporated into a primer in a system where differential migration occurs, it may promote corrosion rather than provide protection.

In coatings formulation work on the physical entrapment and microencapsulation of corrosion inhibitor, steel 1010 panels were primarily used, mainly because the extent of corrosion and other degradative phenomena could be detected and followed more easily, since steel is generally more observably active in salt fog spray and other testing.

The most obvious feature of the potentiodynamic anodic polarization inhibitor studies is the passivation of the 2024 aluminum by the 5% NaCl

electrolyte. This is a generally known characteristic of aluminum in water, either aerated or deaerated. The presence of O_2 in solution also tends to promote oxide formation on aluminum.

Additionally, in the evaluation of different concentrations of corrosion inhibitors, the pH of the test solution may vary considerably for different inhibitors. The corrosion of aluminum is very sensitive to this parameter, with high rates being observed in acidic and basic solutions. Around neutral pH, corrosion may still occur, but at a more reduced rate. Almost all of the inhibitor candidate solutions had measured pH values > 7, and this is the reason most of these compounds were ineffective. Systems that provide a buffering or control of pH may prove advantageous for aluminum protection.

B. Microencapsulation of Corrosion Inhibitors

1. Approach Evaluation

The microencapsulation study was designed to test the feasibility, utility, and performance of the corrosion inhibitors when blended into an organic coating. The use of relatively water-soluble inorganic salts as pigments and extenders in organic coatings is atypical of industry practice, since their water solubility increases the affinity of the coating for water uptake. This in turn causes blistering, adhesion loss, pigment loss through leaching, and general disruption of the coatings integrity, with subsequent corrosion and oxidation of the underlying metal.

Clearly, within the traditional boundaries of coatings formulation for corrosion protection, water-soluble salts as pigments and inhibitors are not considered to be the material of choice for any coating application. The use of heavy metal inorganic salts ($SrCrO_4$, $ZnCrO_4$, red lead, etc.), with, marginal water solubility, as corrosion inhibitors has been widespread for many years, and from the standpoint of coating performance and cost effectiveness are considered the advantageous choices.

However, recent concern by government agencies about the toxicity and environmental impact of chromate salts has initiated a search for nontoxic corrosion inhibitive pigments to replace chromate. The nontoxic AFIF mixture had displayed good anticorrosion properties when used as a wash primer for aircraft. Also, its many components with a range of responses to dif-

ferent metals implied that its multifunctional nature might hold great promise for corrosion protection, if only the material could be formulated into the coating in a manner that circumvented the class of problems its water solubility would cause.

Thus, out of the need to find a nontoxic chromate replacement arose the impetus to develop techniques or processes that would minimize the problems of the water-soluble material while providing a reservoir for the inhibitor. Careful consideration of the design specifications needed to formulate an organic coating which contained a water-soluble corrosion inhibitor yielded microencapsulation as the most promising process.

A variety of methods are available for forming microcapsules. The interfacial polymerization method for microencapsulation appeared advantageous for several reasons. The method could be adapted easily for encapsulation of water-soluble core materials, simply by using a water-in-oil emulsion system. The very small particle size distribution needed for the coatings application (<5-10 μm) could be obtained through conventional emulsion techniques. Also, many different polymer types were accessible with this method; any addition or condensation polymer whose monomers had the correct solubility and kinetic relationship could be used. A wide range of polymers with widely different property relationships was available, many of which are used extensively in current membrane research.

2. Nylon 6,10

The nylon 6,10 was selected as the polymer system for microencapsulation work through the initial investigative stage; the initial investigation was directed to isolating and defining the responses of the major controlling variables of microencapsulation. Once microcapsules were formed, further work was spent in evaluating the parameters which govern the formation of a viable system.

Through all the microencapsulation work, there were two dominant themes which served to direct our experimentation. These were (1) the particle size distribution of the microcapsule product and (2) the release time and profile of diffusion-controlled release of the corrosion inhibitor across the microcapsule membrane wall.

When the first successful microcapsule product was formed, SEM and light microscopic analysis placed the range of the product distribution at diameters from 1.0 μm to 20.0 μm, with the average in the 5.0 μm to 10.0 μm

region. There was a significant aggregation phenomenon evident with the dried product. The release time of this material usually fell in the 5-20 minute range. At this stage of the research work, the nylon 6,10 capsules were always air-dried before being resuspended in water for release testing.

Thus, with this incipient microcapsule product, it was felt that further fine tuning with the surfactant type and ratio would narrow the microcapsule particle size distribution, and possibly reduce the average particle diameter. However, the release times of the nylon 6,10 microcapsules were considered to be less than that required for the ultimate corrosion-control coatings application. Since the target period for corrosion protection was $\sim$ 5 years, the 5-20 minute release data did not seem adequate. Granted, correlation of the release data in pure water to that obtained with microcapsules dispersed within a topcoated epoxy-polyamide primer may not be practical in the present study. A justification for this attitude is the contention that the nylon 6,10 membrane wall should function in diffusion-controlled release with selective retention of the corrosion inhibitor in a characteristic fashion, irrespective of the volume of water carrier permeating the membrane wall at any exchange rate. The selective release profile observed with copius amounts of water should become even more favorable within the coating environment, where the amount of water penetrating into the capsule-coating matrix would be lessened. Increased inhibitor release times in our release tests should be reflected by a similar time increase within the primer.

With these considerations in mind, a study was designed to optimize the major parameters for the microencapsulation process. The goal at that stage was a significant, preferably dramatic, increase in the diffusion-controlled inhibitor release time. As a target, release times of hours were sought (as compared to seconds or minutes) for the microencapsulated inhibitor incorporated into the primer.

An extensive portion of the parameter optimization study dealt with variations in aqueous and organic phase surfactant type, concentration, and ratio. The studies where the release time was measured as a function of the type and concentration of the aqueous phase surfactant indicated that Brij 58 was the best surface active agent for aqueous emulsification. A similar study for the organic phase surfactant tested the following nonionic

surfactants: Brij 52, Igepal RC-520, Igepal CO-430, and Brij 72. The release data did not show any significant variation of release time behavior when plotted against this variable. However, when the organic/aqueous phase surfactant ratio (wt/wt) was varied over a wide range, the Igepal CO-430 and the Brij 72 were found to provide somewhat longer release times. The Brij 58 (aqueous)/Brij 72 (organic) surfactant system was used in the later microencapsulation work.

Hypothetically, release time should be independent of the relative surfactant concentration. The primary function of the surfactants for this process is to form a water/oil emulsion with the correct particle size range for a period of time long enough for the interfacial polymerization reaction to go to completion. As long as a stable emulsion is formed, and the surfactants are chemically unreactive with the two monomers, there should not be a significant surfactant effect upon the second stage of the microencapsulation process, which is the diffusion-controlled polymerization reaction at the interface which deposits the encapsulating polymer around each emulsion particle. This relatively insensitive release time behavior as a function of surfactant composition is thus seen to be consistent with the model for the microencapsulation process.

The studies performed to evaluate the effect of monomer reactant ratio (amount diacid chloride/amount diamine) on the inhibitor release time were typical of many of the experiments performed during this project. Fairly wide variations in monomer ratio were studied for several surfactant systems. The release times appeared to be proportional to the (diacid chloride/diamine) ratio for the Brij 58/Igepal CO-430 surfactant pair, especially for the higher values. There was no detectable trend for the Brij 58/Igepal RC-520 and Brij 58/Brij 72 systems. However, the release times for the Brij 58/Brij 72 system were all consistently larger than for the other surfactant combinations as the reactant ratio was varied. These results corroborate to our findings about the Brij 58/Brij 72 surfactant pair in other studies.

A possible explanation of the variability of these results lies in the nature of the diffusion-controlled transport of diamine from the aqueous core to the particle surface, which in turn reacts with a diacid chloride that has diffused to the surface from the bulk continuous phase, and across any unstirred boundary layer at the surface. It has been established that

the optimal reactant stoichiometry for interfacial reactions is not necessarily 1:1. This may be due to the differing rates at which the diamine and diacid chloride reach the reaction site. The rate of diamine transfer across the interface, the monomer partition coefficient for the particular solvent system, and the initial concentrations and diffusion constants of diamine and diacid chloride must all be considered to affect the optimum reactant ratio. Since diffusion in the microencapsulation process may be considered essentially a first order kinetic process, the rate of diffusion is thus dependent upon the initial concentration of monomers. Hence, there is an appropriate balance of initial concentrations to achieve a compact membrane wall of high molecular weight polymer; the release characteristics of the membrane wall should be fairly sensitive to this parameter. The test results suggest that the surfactant composition also mediates the wall formation and release characteristics of the system. This would not be expected to be of such significance in the classical non-emulsified interfacial synthesis; however, in the emulsified system, with the tremendous increase in interfacial surface area, the surfactant effects are more far-reaching.

The studies designed to find the optimal organic solvent composition with respect to the release time observable did not show any significant trend. The primary effects of organic solvent on the microencapsulation process would be on the reaction kinetics and the molecular weight distribution of the polymer. It is doubtful if the release time would show very sensitive behavior as a function of this variable. The solvent composition used in our later studies (2.2/1 cyclohexane/chloroform) corresponds generally to that typically used for classical interfacial synthesis of polyamides. We found its greatest effect to lie in density matching of the organic phase to that of the aqueous phase; the emulsions thus formed were very stable for our application.

The studies on the variation of release time with reaction temperature can be interpreted similarly to the organic solvent composition studies, and for the same general reason. Thermal effects on chemical reactions primarily influence the kinetics of the process. The release time behavior of microcapsule delivery would not be expected to show drastic dependence on this variable. For classical interfacial synthesis, optimal temperatures for condensation and addition polymer formation usually fall within the

0°-50°C range, which is much lower than for the usual step and bulk condensation processes. The temperature range we used in our studies (25°-40°C) did not appear to have a significant effect upon the microencapsulation product's properties.

Towards the conclusion of the parameter optimization studies of nylon 6,10 microencapsulation of corrosion inhibitors, it became obvious that there was a problem with the system. For all of our nylon 6,10 work, the release tests of every formulation had displayed anomalously high initial rates of release of conducting species; this was termed the burst effect in the earlier work. The general rationalization used to explain this was that part of the inhibitor salt was trapped within the nylon membrane wall, near the surface, and was released into water all at once, before the AFIF within the aqueous core had diffused through the wall. It was presumed that this problem would be minimized as the overall system was optimized for wall properties and release characteristics. However, no improvements were realized in eliminating this phenomenon.

Since HCl is a well known by-product of interfacial synthesis of polyamides, the suspicion grew that a significant amount of HCl might be partitioned within the aqueous core during the polymerization reaction. Experiments were designed which tested the acidity of core release of the microcapsules, via pH studies, and of the core chloride content, via chloride meter.

The test data supported the speculation that high HCl levels were present within the nylon 6,10 microcapsules. Neither acidic release nor chloride release could be tolerated for a product designed as a corrosion protection system. No method of removing the HCl could be devised that would not also affect the inhibitor salt mixture. There was no choice but to change the wall membrane polymer, preferably to some system without deleterious reaction by-products. The omnipresent burst effect was now thought to be due entirely to HCl trapped in-situ within the membrane wall during the interfacial polymerization process.

A significant amount of work was done on nylon 6,10 microencapsulation study before the need arose to abandon the polyamide wall material for a more desirable system. In general, the parameter optimization resulted in a narrower particle size distribution, with the average diameter $\sim$ 6 μm as a

more well-defined quantity (SEM results). Microcapsules which contained the inhibitor mixture were prepared.

Also, the parameter optimization gradually provided somewhat higher values of the diffusion controlled inhibitor release time (from 10-20 minutes initially to 30-50 minutes later in the study). However, this increase was not consistent with our goal for this value - the target release time being estimated between 2 and 4 weeks.

Finally, the dry loading values for the corrosion inhibitor mixture of the optimized nylon 6,10 microcapsules was 18-24% (wt%); the average range of the weight% of chloride anion was 5.6-11.0%. The inhibitor loading value is dependent on the water solubility of the inhibitor mixture. There was little promise for improving this parameter. It was at this stage that the decision was made to investigate the suitability of polyurea microencapsulation systems.

3. Polyurea

The choice of polyurea as a replacement for nylon 6,10 evolved from several fundamental considerations. A polymer was sought which could be adapted to the basic nylon 6,10 procedure without disrupting the established technology. The nature of the reaction is such that there are no by-products to contaminate the system;

toluene-2,4-diisocyanate + hexane-1,6-diamine → polyurea

The organic phase solubility of the TDI rendered it a perfect replacement for the sebacyl chloride; in the first experiments with TDI, the only variation on the nylon 6,10 procedure was the substitution of TDI for sebacyl chloride. Furthermore, the physical properties of the polyurea formed from these reactants were not too different from the nylon 6,10, considering the role as membrane wall material that it was designed for.

Most of the initial problems encountered in the adaptation of the nylon procedure to polyurea involved the kinetics of the polymerization reaction. Since polyurea formation is somewhat slower than the nylon reaction, a dibutyltin dilaurate catalyst for addition to the organic continuous phase was tested and found to give adequate results. Polyurea microcapsules were formed, as observed from SEM studies. Coulter counter particle size dis-

tribution analysis was run on the product, and the average particle size (volume%) equalled 6.17 ± 1.39 μm. The release times of representative microcapsule preparations at this stage were within the range of 60-90 minutes; no burst effect was observed with the polyurea microcapsules at any time. Further work on optimization yielded a procedure with a volume phase ratio of 50:150 (aqueous:organic), a TDI solution addition rate of 3.0 minutes, and 2% TDI stoichiometric excess as favorable to forming relatively non-aggregated product (Table 24).

A further alteration in the capsule testing program related to changes introduced into the release testing. For the nylon 6,10 microcapsules, the product was air-dryed and stored in solid form until release testing was performed. The material was always difficult to disperse; many times the agglomeration observed was just too great to provide reliable results.

A variation was introduced for the polyurea microcapsules (Table 24). The product was not isolated, but after repeated extractions with cyclohexane, the material was stored in suspension until testing or use. For release testing, a given volume of suspension was dispersed into 0.1% Brij 58 in water. Excellent dispersions were obtained with stirring, and much more uniform release results were obtained. It was clear that if these microcapsules were to be of use, a procedure was needed to retard the irreversible aggregation observed upon drying. This became a routine procedure in all later work.

At this stage of the polyurea microencapsulation work, a preparation had been developed with a particle size distribution considered adequate for use in coatings formulation. The requisite property of long diffusion-controlled inhibitor release times had yet to be developed. Although increases in release time up to 90 minutes had been observed, longer times were considered desirable. An investigation of the membrane wall was then undertaken to seek further improvements in this area.

Several experiments were designed to provide direct or indirect information about the membrane wall structure and characteristics. They were (1) comparative study of borate vs. AFIF release, (2) wall thickness increase of microcapsules, (3) freeze-fracture study of microcapsule wall, and (4) water drying curves.

The comparative release study of sodium borate vs. AFIF was designed to detect the phenomenon of selective release among any of the inhibitor com-

ponents. Borate release from microcapsules was followed by atomic absorption analysis, while AFIF release was measured by the usual conductometric method. The release curves of the two methods were very superimposable, implying that no membrane selectivity exists for any of the AFIF components. The inference was that the microcapsule wall was relatively macroporous with respect to the inhibitor components; selective retention or retardation of diffusion through the membrane due to charge, molecular weight, or volume effects was not observed. Although diffusion-controlled release does occur, no selectivity amoung the AFIF components may be inferred.

The wall thickness studies were designed to increase the release times of the inhibitor, since thicker walls would give longer diffusion paths. Increases of 30% and 70% of wall-forming material over a control formulation of microcapsules were prepared, and release times were measured (control ~100 minutes, 30% ~70% ~200 minutes). Increased release times were observed for both of the wall increase formulations over the control. Thus, a significant increase in release time could be obtained by this method. The equivalence of release times for the 30% and 70% wall increase preparations may be explained in terms of the self-limiting nature of the interfacial polymerization reaction. The polymer membrane wall formed in-situ around each emulsion particle is deposited until the membrane itself becomes a barrier to further diamine diffusion to the capsule surface. The polymerization reaction is effectively over at this point. The self-limiting amount of polymer wall formation may be considered to lie somewhere between that of the control and the 30% wall increase preparation.

The freeze-fracture studies of the polyurea wall membrane revealed some interesting features. The microcapsules may be either single or multi-cavitied, and in some cases void areas were observed within the membrane wall. In general, the wall thickness is approximately 1/10 of the overall particle diameter for the single cell microcapsules. The multi-cavity capsules could be formed in the first stages of emulsion flocculation, or perhaps the polymerization reaction time is comparable to the collision time of nearest-neighbor emulsion particles. The apparent void areas within the capsule wall are of unknown origin, and could be a very serious problem if this phenomenon were widespread. Release times would certainly be shorter for such microcapsules.

The water drying curves were obtained to get a relative idea concerning the water retention of the polyurea. Weight loss vs. time data were taken for a sample of microcapsules in cyclohexane which were allowed to air-dry in a glass dish. The microcapsules were completely dry within 20-40 minutes. The polyurea membrane wall was found to be fairly permeable to water. This was surprising at the time; however, considering the bulk of the previous work, in retrospect this observation was not altogether unexpected, and corroborated the growing realization that the polyurea microcapsule wall as formed in our procedure was relatively macroporous to the core material, in varying degrees.

In general terms, the polyurea microencapsulation process yielded considerably better results than the nylon 6,10 system. The particle size distribution was narrower, with the most probable volume fraction lying at the ~6.0 μm diameter. This was well within the tolerances needed for addition of this material to a primer. The dry loading of the inhibitor fell within 11.0-22.0% (wt%). Although this range was somewhat broad, it was still of comparable magnitude to the nylon values (18-24%). There was no problem with HCl contamination of the polyurea, nor was a burst effect observed at any time. The release times of inhibitor from polyurea microcapsules were much better than for nylon 6,10. The observed release times for the optimized polyurea system all fell within the 90-200 minute range, with the release curve profile of the shape expected for diffusive release. The wall thickness was found to be approximately 1/10 of the particle diameter, and both single and multi-cavitied capsules were observed. Voids were observed in some of the fractured walls, which could be a serious problem affecting the capsule release profiles.

Finally, the nature of the polyurea microcapsule wall may be inferred from a number of experiments performed to ascertain the permeability and selectivity of the polymer membrane. The membrane is fairly permeable to H_2O, which probably accounts for the absence of osmotic pressure rupturing of the microcapsules. Free exchange of solvent across the wall would dissipate the powerful osmotic pressure gradients that could have occurred. There is some diffusion-controlled release of the inhibitor salt components, although it is not a selective process. The transport rates of all the salt components appear to be essentially equivalent. In this respect, the membrane wall must be considered a non-selective, macroporous diffusion barrier

to the inhibitor mixture. Solutes with larger molecular weights or hydration radii would most likely experience more significant selectivity and diffusion-controlled transport than the inhibitor salt components, all of which are under 200 daltons. This view is corroborated in the patent literature, the most notable instance being the work of Lim (U.S. Patent 4,251,387). The molecular weight ranges for similar types of microcapsule formation which show differences in permeability have values from 200-30,000 daltons. The AFIF components are all at the lower end of this range. Within the scope of the compositions investigated in this work, the interfacial polymerization mechanism of microcapsule membrane wall formation was insufficient to provide really long diffusion-controlled release times and selectivity when the core material was in the molecular weight range of the AFIF components. Further research may develop procedures to decrease the membrane wall permeability of microcapsules formed by interfacial polymerization to such low molecular weight core components, and provide a better data base for the definition of the potential of the system.

C. Polymerically Bound, Time-Releasable Corrosion Inhibitors

Another approach to providing a more stable reservoir of inhibitor over extended times is by chemical modification of carrier polymers with pendant or chelated corrosion-inhibiting functional groups. Two types of polymerically-bound systems were studied to demonstrate feasibility. The binding of inhibiting pendant moieties directly to the polymer backbone has the potential of (1) reducing the initial shock to the primer system and minimizing undesirable side effects such as blistering and loss of adhesion, (2) providing a site specific inhibitor system as the water penetrating into the primer coat contacts the bound inhibitor, and (3) a controlled release rate through polymer selection and degree of substitution.

The models chosen to study the feasibility of this approach were cross-linking of poly(vinyl alcohol) or methyl cellulose with borate anions and the introduction of phosphonic acid onto the methyl groups of poly(2,6-dimethylphenylene oxide). The anions chosen (borate and phosphonic acid) were selected based on the potentiodynamic corrosion test. Water-soluble polymer systems were chosen for the study so comparisons could be obtained with earlier studies. The systems selected were (1) poly(vinyl alcohol), which

chelated with the borate anion; the borate ester bond was hydrolyzed in aqueous solutions, releasing the borate ion, and (2) a phosphonylated PPO was also hydrolyzed in an aqueous environment.

Release rates of each polymer were determined by addition of 0.45% of polymer to 50 g distilled water and measuring the conductivity of the solution. The poly(vinyl alcohol) release of borate ion was first order and continued for more than 30 hours. The potentiodynamic corrosion resistance measurements indicated an apparent improvement in both anodic and cathodic protection for aluminum and steel. However, this protection may be attributed to the polymer coating on the surface rather than the action of the borate, since the borate concentration in solution is relatively low. In the coating application, water penetration into the film will be low compared to the PVA film, leading to higher net concentration in solution due to the small volume of water. Higher concentrations should provide additional cathodic protection.

Hydrolysis of the PPOP at a 1% concentration and pH 10 offers anodic inhibition of 4340 steel comparable to the AFIF mixture. However, much lower concentrations (< 0.1%) and neutral pH are required to enhance cathodic protection of 2024 aluminum alloy. These systems were not suited for primer applications in the study. However, data confirms the concept and provides a basis for further evaluation.

D. Physical Entrapment of AFIF

The experimental work performed on the development and formulation of a primer coating containing a nontoxic, nonchromate corrosion inhibitive pigment was an integral part of the project design. The formulation was designed (1) to determine the feasibility of adding AFIF directly to the paint, and (2) to provide the background and control work necessary to test inhibitor-containing microcapsules. Also of interest were observations pertaining to the differential test responses of a coating formulated with and without a chromate pigment. The limitations of water-soluble corrosion inhibitors compared to the chromate pigment were obvious in every performance category; the use of water-soluble inhibitors in coatings formulation represents a true frontier of research.

The coatings formulation work may be divided into two stages. The initial stage was the preliminary empirical study designed to prepare a primer within the latitude allowed by the MIL-P-23377D specification, and to provide for the development and standardization of the routine formulation and handling techniques required in coatings work.

The second stage was the coatings optimization study; variations of interest were the PVC of the primer, AFIF concentration level, other non-chromate inhibitors, adhesion promoters, and comparative studies of the use of AFIF-containing microcapsules, tested against several controls.

A brief summary of the preliminary empirical study follows. Particle size reduction was achieved through use of jar milling; a mill paste with good shear properties was obtained by the Daniel flow point method, which utilized the polyamide primer component as a grinding medium. The possible inhibition of the epoxy-polyamide curing reaction by AFIF was examined; no inhibition of the cross-linking process was observed. Tensile strength of the primer was monitored as a function of PVC, and an estimate of the critical PVC made, which corresponded closely with the classical expectation for this parameter ($\sim$40). The coating application method was examined for relative void content among films prepared by hand casting, airless spray, and conventional spray; the conventional spray method was used in all later work.

Other preliminary work was the formulation and release testing of entrapped and microencapsulated AFIF added to a long-oil linseed alkyd resin. The objective of the study was to determine the compatibility, mechanical properties, and release characteristics of microcapsules added to an epoxy-polyamide primer. The polarity of the epoxy-polyamide primer matrix could seriously interact with the microcapsule wall, and the internal film stress caused by solvent evaporation, curing reaction, and the close-packing of microcapsules in an increasingly crowded micro-environment could overcome the mechanical properties of the capsules. The alkyd resin was thought less likely to cause environmental shock with the microcapsule wall, and the absence of other pigments and extenders should have relieved some of the internal stress effects. These preliminary alkyd studies were performed to obtain a general idea of the response of microcapsules dispersed within a coating matrix. The results indicated that there was an advantage in release characteristics for the AFIF-containing microcapsules over the entrapped AFIF.

The coatings optimization design was a five-stage experimental study; the best primer formulation from each stage was carried over into the next for further testing.

In general, all $SrCrO_4$ control primer formulations passed our battery of environmental tests; the concentration (wt%) ranged from 1.0-20.0% (dry film). Corrosion breakthrough was rarely observed, and neither adhesion loss nor blistering was ever observed. This pigment was superior to any alternative tested in our program, thus corroborating an industry fact.

The estimated critical PVC of our basic primer formulation was ~40. The best value for our application and material constraints was PVC = 50. This PVC should have alleviated much of the tendency toward blistering, due to the relative openness of the matrix. The trade-off between inhibitor mobility and corrosion resistance for the water-soluble AFIF is questionable. Clearly, too many factors were involved to expect the classical coating behavior.

AFIF primer concentrations ranging from 0.5% to 10.0% (wt% dry film) were tested. The best value of this parameter which could be tolerated within the primer, and still pass the requisite coatings tests, was the 1.0% level. The lower values studied (0%, 0.5%) usually performed in a comparable fashion to the 1.0% value, while the higher concentration levels performed to a lesser extent. In one of our later studies, the 1.0% AFIF was run against a 1.0% $SrCrO_4$, and little variation in test response was observed.

Several nonchromate corrosion inhibitors were studied in conjunction with the 1.0% AFIF (dry film) at PVC = 50. These inhibitors were: NICHEM #7 zinc phosphate, Heubach Heucophos ZPA, Halox BW-191, and Sherwin Williams Moly White 101. Concentrations of 1.0%, 5.0%, and 10.0% were run. The best primers within this series were the 5% and 10% NICHEM with 1.0% AFIF. A 15.0% NICHEM (wt% dry film) was run in a later study, and outperformed the other members of the series. This pigment inhibitor appears to have some potential for corrosion control in this type of primer.

An adhesion promoter study was performed, in an attempt to improve the generally poor adhesion performance of the AFIF primers. These compounds were:

β - (3,4-epoxycyclohexyl)ethyltrimethoxysilane
(Union Carbide A-186)

N-β - (aminoethyl)-gamma-aminopropyl-trimethoxysilane
(Union Carbide A-1120)

No improvement in adhesion properties was observed with the use of these organosilane adhesion promoters. In one of these studies, both the A-186 and A-1120 were added directly to the polyamide mill paste prior to grinding, at both 1% and 2% (wt% DF). In another study with A-186, a comparison between jar milled and direct spray application to the metal surface (10% A-186 in toluene) was performed. In neither case were positive results observed. Either the organosilane was tied up in the coating through adsorption, or some other phenomenon, and thus unable to interact with the substrate; or perhaps the material was reactive with some primer component which renders it inactive. Possibly the toluene was the problem, in the case of the spray application experiment.

A comparative evaluation between entrapped AFIF and microencapsulated AFIF was performed. An absolute basis for comparison could not be obtained, due to certain physical constraints which exist concerning the microencapsulated material. The entrapped AFIF concentration in the dry film was 1.0% (wt.%). The highest value of microencapsulated AFIF that could be added to the primer without the occurrence of solvent shock and incompatibility was $\leq$0.15%. This was due primarily to the large volume of material (microcapsule plus a minimum amount of organic solvent) that had to be added to obtain the desired loading. The volume had already been reduced as much as possible, down to the level where essentially irreversible aggregation of the microcapsules usually occurred. This volume could not be minimized further, since dispersability of the product within the primer was of utmost importance. We used the highest loading values we could get in each case. The limitation here was the amount of AFIF that could be incorporated within the microcapsules. The maximum attainable microcapsule loading value corresponds to the solubility limit of the material in the core aqueous phase; this was the value at which we always encapsulated the AFIF.

The results of the salt fog spray and 100% relative humidity tests were somewhat better for the entrapped AFIF (1.0%) primer than for the encapsu-

lated AFIF ($\leq$0.15%), although not by any significant margin. The wet adhesion test for the microencapsulated AFIF was definitely much worse than for the entrapped material. However, the wet adhesion test is relatively crude in nature, being dependent on many factors relating to coating application. There may not be significance to these results, especially when the other two tests go against it.

Several general conclusions may be reached. The AFIF levels obtainable for both the entrapped and microencapsulated system are too low to provide corrosion protection similar to the chromate system. The water solubility of the material is a liability when it is used as a physically entrapped pigment. Ironically, the level of water solubility that is so damaging in the entrapped system is too low to allow proper loading in the microencapsulated system. Higher loadings may be obtained for inhibitor systems with greater solubility or by microencapsulation of solid materials. These data indicate a potential for the microencapsulation of soluble inhibitors. However, significant improvements must be achieved to provide corrosion protection similar to that obtained with the chromate systems.

VIII. CONCLUSIONS AND RECOMMENDATIONS

Based on data provided by these studies, the following observations and recommendations can be made:

1. Potentiodynamic anodic polarization provides useful information in screening corrosion inhibitors, defining their limits of effectiveness, and understanding the mechanisms of action.
2. Three compounds were identified by potentiodynamic polarization as passivating corrosion inhibitors for both steel and aluminum: sodium nitrite, potassium cinnamate and sodium molybdate.
3. The AFIF demonstrated passivating corrosion protection in screening studies for steel, but not for aluminum. Of the seven components formulated in the mixture, six provided some protection for steel. The seventh (β-mercaptobenzothiazole) appeared to be inert. However, only one of the AFIF components ($NaNO_2$) functioned as a corrosion inhibitor for the aluminum. The others had no significant effect on the system, except $Na_2B_4O_7 \cdot {}_{10}H_2O$, which accelerated the anodic process.
4. Microcapsules containing water-soluble corrosion inhibitors can be prepared and incorporated into primer formulations. More efficient inhibitors and/or higher capsule inhibitor loadings are needed to extend the concept to practical applications.
5. The feasibility of microcapsule formation was demonstrated using interfacial polymerization methods for microencapsulation with a nylon 6,10 and polyurea polymer system. An examination of microcapsule morphology using SEM fracture techniques and studies of diffusion release times indicates that further developments are desirable to achieve best performance.
6. Inorganic corrosion inhibitors bound in a polymeric matrix demonstrated the potential for incorporation into primer formulations in which the inhibitor would be released by hydrolysis with water permeation into the primer.
7. Release rates of inorganic inhibitors bound in polymeric matrices may be controlled through the type of bonds formed, degree of substitution and permeation characteristics of the binding polymer and coating matrix.

8. Evaluation of inhibitors incorporated in epoxy-polyamide formulations indicated that a) the best inhibitor was $SrCrO_4$, b) the AFIF was marginally acceptable when included as an entrapped solid or within microcapsules, based on definitions of MIL-P-23377D, c) concentrations of the AFIF mixture that could be incorporated into the primer as entrapped solid or in microcapsules were too low to be as effective as the chromate inhibitor, and d) of several commercial inhibitors evaluated the best performance was observed with NICHEM No. 7 Zinc Phosphate.

A potential for several systems is indicated; therefore, the following recommendations are suggested.

1. Potentiodynamic screening may be used to develop a multicomponent inhibitor system which may be more effective for steel and aluminum. If the system is to be encapsulated, greater water solubility on solid encapsulation would be desirable.
2. Operational problems in the incorporation of microcapsules must be optimized so the system can be fully evaluated. For example, increased loadings can be achieved if a method is developed for drying and redispersion of the microcapsules without agglomeration. A better definition of the desired release time as it relates to performance in the primer formulation is needed before optimization of the microcapsule wall structure is studied.
3. A review of possible polymeric systems for binding inorganic inhibitors is needed. Polymeric systems compatible with primer formulations must be evaluated.
4. A more quantitative response system must be considered in the evaluation of primer coatings. Development work may be necessary to achieve this objective.
5. Further experimentation would be required to develop the interfacially polymerized membrane walls of the microcapsules such that diffusion-controlled release of very low molecular weight (<200 daltons) inhibitor molecules could be obtained.

REFERENCES

1. McCafferty, E., Mechanism of Corrosion Control, Corrosion Control by Coatings, pp. 279, H. Leidheiser, Jr. (Ed.) Science Press, Princeton, NJ (1979).

2. Kehler, G.L., Localized Corrosion, pp. 117, NACE, Houston, TX (1974).

3. Suboda, M. and Mleziva, J., Prog. Org. Coatings 2 207 (1972).

4. Leidheiser, J.R. and Kenchig, M.W., Corrosion 32 69 (1976).

5. Uhlig, H.H., Corrosion and Corrosion Control, 2nd ed., John Wiley & Sons Inc., New York, N.Y. (1971).

6. Tomashov, N.D. and Chernova, G.P., Passivity and Protection of Metals Against Corrosion, Plenum Press, New York (1967).

7. Kolotyrkin, YaM. and Bune, N.Y., J. Phys. Chem. (Russian) 35:7 1542 (1961).

8. Franck, U.F. and Weil, K., J. Electro. Chem 56 814 (1952).

9. Tomashov, N.D., Sinelshichikova, G.P. and Vedeneeva, M.A., Proc. Acac. Sci. USSR 62:1 105 (1948).

10. Weissfuch, A., Carter, D.A. and Nathan, C.C., Mater. Prop. Per. 10 11 (1971).

11. Zecher, D.C., Mat. Per. 15 33 (1976).

12. LeRoy, R.L., Corrosion 34 98 (1978).

13. Rajan, K.S. and Ase, P.K., "Development of Corrosion Inhibitors and Adhesion Promoters," NTIS Report No. AD-770-627 (1973).

14. Tirbound, F. and Fiand, L., Corrosion Sci. 18 139 (1978).

15. Kallfass, H., Rasp, C. and Schliebe, R., U.S. patent 4,026815 (1977).

16. Bohnsack, G., Geffers, H. and Radt, W., U.S. Patent 4,057,511 (1977).

17. Cook, B., Dingwall, J.G. and Thomas, B.K., U.S. Patent 4,052,160 (1977).

18. Graupp, R.H. and Nygren, J.A. Jr., U.S. Patent 3,992,318 (1976).

19. Sexsmith, D.R., U.S. Patent 4,105,581 (1978).

20. Mitchell, R.S. and King, T.M., U.S. Patent 4,033,896 (1977).

21. Foroulis, Z.A., U.S. Patent 4,108,790 (1978).

22. Liu, C.T., U.S. Patent 4,085,063 (1978).

23. Murray, W.B., U.S. Patent 4,105,406 (1978).

24. Frenier, W.W. and Settineri, W.J., U.S. Patent 3,969,414 (1976).

25. Settineri, W.J., Freneir, W.W. and Oswald, J.H., U.S. Patent 3,996,147 (1976).

26. Settineri, W.J., Frenier, W.W. and Oswald, J.H., U.S. Patent 4,101,438 (1978).

27. Kudo, N. and Ibe, H. U.S. Patent 3,976,494 (1976).

28. Kerpot, D.G.E., U.S. Patent 4,132,667 (1979).

29. Robitaille, D.F., Vukasovich, M.S. and Barry, H.F., U.S. Patent 3,969,127 (1976).

30. Vukasovich, M.S. and Sullivan, F.J., U.S. Patent 4,017,315 (1977).

31. Hosiguchi, S. and Nakamura, M., U.S. Patent 4,066,462 (1978).

32. Hoshino, M., Shinchara, T., Kawahara, Y., Takase, K., Tsuju, T. and Fukuda, J., U.S. Patent 4,098,749 (1978).

33. Traister, A. and Troup, G., U.S. Patent 4,049,596 (1977).

34. Higgins, J.F., U.S. Patent 4,046,589 (1977).

35. Conner, A.J. Sr., U.S. Patent 4,116,701 (1978).

36. Rowe, L.C., Corrosion Inhibitors, NACE, 173 (1973).

37. Humphries, T.S. and DeRamus, G.E. Jr., Corrosion Inhibitors for Solar Heating and Cooling Systems, NASA TND-8409 (1977).

38. Humphries, T.S., Corrosion Inhibitors for Solar Heating and Cooling Systems, DOE/NASA TM-78180 (1978).

39. Gouda, V.K. and Shater, M.A., Corrosion Sci. 15 199 (1975).

40. Controlled release, Pesticide Symposium

41. Brandrup, Polymer Handbook, V-15

42. Diffusion in Polymers, Crank and Park

43. Encyclo. of Polymer Science and Tech., Vol. 10

44. Davies, J.T., Proc. Intern. Cong. Surface Activity, 2nd, London 1957, 1, 42G

45. Kondo, A., and J.W. Valkenburg, "Microcapsule Processing & Tech.", Delcher, N.Y. H_2

46. Morgan, P.W., "Condensation Polymers by Interfacial and Solution Methods," No X in Polymer Review Series, Interscience, N.Y., 1965.

47. Cheng, A.T.Y., and F. Rodriguez, J. App. Pol. Sci. 26, 761, 1981.

48. Cabasso, I., J. Jagur-Grodzinski, and D. Vofsi, J. Pol. Sci., 12, 1141, (1974).

49. Cabasso, I., J. Jagur-Grodzinski, and D. Vofsi, J. Pol. Sci. 18 1969 (1974).

50. Lin, C.J. and Bell, J.P., J. Appl. Polym. Sci., (1972) 16(7), 1721-33.

51. Zvendt, R.F., et al., U.S. 4,225,351; CA 93:241299e.

52. Bogomolova, E.P., et al., Kolloidn. Zh. 1975, 37(2), 224-9.

53. Hayashi, Masaaki, et al., Ger. Offen. 2,606,117; CA 85:162075K.

54. Kresse, Peter, Farbe-Lack (1970), 76(11), 1099-1104 (12), 1209-20.

55. Sekerina, N.V., et al., LaKokras. Mater. IKh Primen 1975, (1), 10-11.

56. Moore, R.J. and Allen, R.A., U.S. Patent 3,578,615; CA 75:380332.

57. Yanakiev, Ya. Stroit Mater. Silikat Prom., 1968, 9(6), 9-13.

58. Podgorski, D. Syn. Resins Bldg. Constr., Pap. BILEM Symp. 1967, 1, 431-42.

59. Peiera, D.Y. and Heertjes, P.M., J. Oil Colour Chem. Ass., 1971, 54(8) 774-94.

60. Nippon Steel Corp. Japanese, 80,155,066; CA 94:123248k.

61. Salas, Viv, Colares Pinturas, 19968, 17(113), 11-13.

62. Schwartz, L. et al., Rev. Coroz., 1971, 1(1), 33-7.

63. Fedorenko, V.P. and Lysobyk, S.E.; Sin. Fiz. Khim. Polim., 1974, 13, 41-3.

64. Shaposhnik, S. and Chapurin, V.I., Lakokrasoh. Mater. Ikh. Primen. 1973, (4); 23-4.

65. Kehr, J.A., Ger. Offen. 2,428,531; CA 83:207681.

66. Shimp, D., et al., SPI Plast./Comps. Div., Proc. 24th, 1969, 9-B-1-8.

67. Gadzhieva, R.G., and Siwitsyna, Yu.E., Epoksidnye, Monomery Epoksidnye Smoly., 1975, 269-76.

68. Kinneman, W.P., U.S. Patent 3,639,344; CA 76:142494g.

69. Von Fraunhofer, J.A., et al., Paint Technoloby, 1971, 35(1), 5-11.

70. Sexsmith, F.H. and Hornaman, E.C., U.S. Patent 4,195,140; CA 93:151788j.

71. Yanamoto, M., Japanese Patent 7239,500; CA 78:114423y.

72. Walker, P., J.C.T., 1980, 52(670), p. 49.

73. Romanova, V.I., Tr. Vses. Proekt.-Izyskatel'skii, Nauch.-Issled. Inst. Gidroproekt., 1972, No. 74, 169-72.

74. Koziw, V.M., et al., U.S.S.R. 478,046; CA 84:6638v.

75. Sato, T. Japan Kokai, 75,151,222; CA 84:123570c.

76. Murafa, A.V., et al., Lakokras. Mater. Ikh. Primen., 1981 (1) 33-5.

77. Schneider, W., et al., Ger. offen. 3,027,140; CA 94:210434.

78. Dorofeev, A.G., et al., Korroz. Zashch. Neftegazov. Prom-sti., 1980, (10), 17-18.

79. Khanlarova, A.G., Korroz. Zashch. Neftegazov. Prom-sti., 1975 (9), 20-3.

AD-A150 [illegible]

END

FILMED

DTIC